TEMPERATURE CONTROL OF HANDHELD ELECTRONIC DEVICES
USING LATENT HEAT ENERGY STORAGE

by

Benjamin Sponagle

Submitted in partial fulfillment of the requirements
for the degree of Doctor of Philosophy

at

Dalhousie University
Halifax, Nova Scotia
February 2018

TABLE OF CONTENTS

LIST OF TABLES

LIST OF FIGURES

ABSTRACT

The processing power of handheld electronic devices, has increased rapidly over the last decade. Modern handheld devices are thin (<9 mm) and utilize passive temperature control strategies. The combination of these three factors has resulted in temperature control becoming a major obstacle to continued development.

This work investigates the use of latent heat thermal energy storage (LHTES) modules to improve the temperature control of tablet computers. LHTES modules, utilizing solid-liquid phase change materials (PCM), were designed and tested. Modules of this type store energy during periods of high heat dissipation and release it at a later time when the device is less active. Numerical and experimental studies were used to investigate the design requirements for LHTES temperature control modules as well as the magnitude of performance improvement which they can provide.

A key aspect of designing these systems is identifying the appropriate PCM, more specifically, what transition temperature is optimum. A numerical model of a tablet computer was created. Simulations with LHTES modules having transition temperatures between 35 and 47°C, showed that PCMs with lower transition temperatures allowed the tablet computer to operate longer without overheating. Phase change materials with transition temperatures between 35 and 40°C were found to be optimal. Two organic PCMs, n-eicosane (T_m=35.6 °C) and PT37 (T_m=36.4 °C), were selected.

A simplified experimental setup was used to both investigate the thermal characteristics of LHTES temperature control modules, and validate the techniques used in the numerical model. These experiments compared the performance of LHTES modules using n-eicosane and dodecanoic acid (T_m=43 °C). It was found that n-eicosane was superior. The experiments also confirmed that the numerical techniques were effective.

An experimental platform which simulated a tablet computer was built and used to test the effectiveness of an LHTES module based on n-eicosane. It was found that the module improved the temperature control of the simulated tablet computer, increasing the operational time before overheating by 30% and better controlling the temperature of the heat source.

LIST OF ABBREVIATIONS AND SYMBOLS USED

TES	thermal energy storage
LHTES	latent heat thermal energy storage
PCM	phase change material
CPU	central processing unit
SOC	system on a chip
LED	light emitting diode
PMIC	power management integrated circuit
COG	chip on glass
T_m	transition temperature
T_s	surface temperature
T_i	initial temperature
T_f	final temperature
T_∞	ambient temperature
T_{lim}	temperature limit
Ra	Rayleigh number
Nu	Nusselt number
Pr	Prandtl number
k	thermal conductivity coefficient
h	convection coefficient
α	thermal diffusivity
β	volumetric thermal expansion coefficient
v	kinematic viscosity
ρ	density

ACKNOWLEDGMENTS

I would like to thank the members of my committee for their support and guidance during this project. With special thanks going to my supervisor Dr. Dominic Groulx. Your support, advice and patients have been invaluable to me.

I would also like to thank all of the graduate students whom I have had the pleasure of working with over my many years at Dalhousie University. With special thanks going to Mr. Simon Maranda and Mr. Tousif Ahmed. Working with such a diverse and exceptional group of professionals has been a pleasure.

Last but not least, I would like to thank my family. It is from you that I derive my energy and strength.

Melissa, this wouldn't have happened without you. Thank you for the love, support and understanding it took to get me here.

CHAPTER 1 INTRODUCTION

1.1 Project Overview

This thesis is the culmination of a 4-year project investigating temperature control of handheld electronics. Project funding was provided by Intel Corporation and included work performed in the Lab of Applied Multiphase Thermal Engineering (LAMTE) under Dr. Dominic Groulx and in the chemistry department under Dr. Mary Anne White, both at Dalhousie University. The engineering branch of the project, carried out by the LAMTE, included a MASc project by Mr. Tousif Ahmed, and a doctoral project, which is presented in this thesis. Mr. Ahmed's masters project and the author's doctoral project have run in parallel, each informing and impacting the other. Mr. Ahmed's work is summarized in Chapter 4. A portion of the author's doctoral work was done in collaboration with Mr. Simon Maranda. Mr. Maranda worked with an experimental setup, designed by the author, as a part of his Master's project done as an intern at Dalhousie University and awarded by the University of Lucerne in Switzerland. This work was co-supervised by the author and is summarized in Chapter 3.

The goal of this project was to investigate the use of solid-liquid phase change material (PCM) based latent heat thermal energy storage (LHTES) modules to improve temperature control of handheld electronic devices. The original research proposal to Intel included seven research questions.

1. What type of inexpensive and easily obtainable PCM will best fulfill the requirements for the optimal thermal energy storage (TES) platform?
2. What is the effect of the phase change temperature (melting temperature) on the thermal and energetic behavior of a TES PCM platform?
3. For a selected PCM, what is the impact of the heat sink design and geometry on the overall thermal and energetic behavior of the TES PCM platform?
4. Which method of encapsulation should be used for this specific application? From a point of view of design, thermal behavior, compatibility with the PCM and the electronic device, cost, and manufacturability?
5. What are the best tools to study and model the "real-life" behavior of the developed platform from a thermal and energetic point of view?

6. How do those PCMs react with typical heat sink and electronics materials (Al, Cu, Graphite, Carbon fiber, Si, Li-ion battery materials)?
7. For the considered PCM, what are their hysteresis effect and their long term cyclability?

The first research question is the core of the project and has been addressed, in part, by all participants. While phrased in terms of material selection in the research proposal, PCM selection is intimately coupled with the design and encapsulation of the LHTES module. Therefore, the primary goal of the project is to design the optimum LHTES module for temperature control of handheld electronic devices, which includes selection of the optimum PCM.

Question 2 and 3 are coupled together and encompass the fundamental engineering focused questions. How do LHTES modules behave in a modern handheld electronic device and what impact does PCM transition temperature have on this behaviour? This question forms the fundamental impetus to Mr. Ahmed's work as well as the work presented in this thesis.

Design of the encapsulation (question 4) is an important aspect of any system containing PCM. Encapsulation is dealt with throughout this thesis work and that of Mr. Ahmed's. A method for effectively encapsulating the PCM was found. However, a comprehensive comparative study of different encapsulation methods was not conducted and will be discussed in future work.

An important aspect of this project has been to develop effective methods for investigating the temperature control of handheld electronic systems (question 5). Both numerical and experimental platforms were developed and used. The results of these studies represent much of the work presented in this thesis.

As acknowledged in question 6 and 7, the appropriateness of a PCM for use in an LHTES module is not solely a function of its thermo-physical properties but also its material compatibility and long term cyclability. These questions have been the focus of extensive work by Dr. Kahwaji, a post-doctoral researcher working under Dr. Mary Anne White. An experimental setup for cycling PCM's was developed at LAMTE by Ali Kheirabadi (Kheirabadi and Groulx, 2014) and was used to study the stability of several PCMs which are of interest to LHTES systems (Kahwaji *et al.*, 2017).

1.2 Background

Recent discoveries in microelectronics and battery technology have allowed rapid advancement in handheld electronic systems. Specifically, handheld computing devices with fast processor speeds, high quality displays and high aspect ratio designs such as: smart phones and tablet computers have become common place. Historically, it has been battery capacity and CPU size which have limited the design of handheld systems. However, modern processor and lithium ion battery technology have alleviated many of these constraints. In modern devices, temperature control is an important limiting factor. Faster processors (more transistors, higher clock speed, or multi-core processors) use more electrical power and therefore dissipate more heat to the environment. Other microelectronic components, like memory and network devices, also contribute to a lesser degree. Barring drastic advances in the technology used in microprocessors, as the capabilities of handheld systems evolve, the heat they dissipate will continue to increase. Therefore, innovative temperature control strategies will be required for future handheld computing devices.

1.2.1 Introduction to Temperature Control in Portable Electronics

The primary role of the temperature control system is to keep the main components temperature below their critical design limit during times of heavy use and to control mean system operating temperatures. Exceeding components design temperature will result in immediate device failure. Higher mean temperatures will not cause a critical failure, but consistently elevated temperatures are closely correlated with premature failure of computer systems (Yeh, 1995). Handheld devices have additional constraints due to ergonomic concerns associated with people holding the devices during use. This section offers an introduction to temperature control systems and the strategies commonly employed.

In this thesis, temperature control strategies will be divided into three categories. These strategies overlap and rely on one another, but the distinction will be useful moving forward. The simplest and most recognizable temperature control strategy is "cooling". Cooling systems reduce resistance to heat dissipation from major components to the environment. An example of a common cooling system is the fan and heat sink assembly used in many stationary computing systems. Cooling systems are delineated into two types: active and passive. Active cooling systems expend energy to further decrease cooling system resistance, often through forced convection from a fan or pump. Passive cooling systems do not require any source of energy and

have no moving parts, an example would be a free convection heat sink. Often cooling is directly correlated with temperature control but there are several other strategies which are also important to portable electronic systems.

Heat spreading encompasses a variety of engineering techniques that aim to increase the surface area over which heat is transferred. While the concept of heat spreading is closely coupled with cooling (extended surfaces, and heat sinks) it also has added meaning in temperature control systems, namely controlling the cover temperature of handheld electronics by dissipating internal energy over a larger area.

The third strategy which will be critical to this discussion is thermal storage. Thermal storage is often overlooked, possibly because it is only applicable to systems which operate transiently. At steady state, thermal storage is meaningless, but in systems where the heat generation rate is variable (such as computing systems), it can be important.

1.2.2 Current Methods of Temperature Control

Handheld portable electronic systems suffer the same thermal challenges experienced by stationary systems but also have several additional complicating factors. The first of these is available space. Handheld portable electronics are thin and have little room for a dedicated temperature control system. Thickness or perhaps "thinness" of these devices has long been a heavily promoted feature. Manufacturers are skeptical of increasing package thickness, even if it benefits performance. This lack of space means the temperature control system is directly competing with critical components for space. A larger temperature control system will require sacrificing critical components or more likely battery capacity. This is one of the factors which has led to modern devices having very limited temperature control systems. Heat spreading films are common but are the extent of temperature control in these systems. Heat generated in the components is transferred through the body of the tablet to the surface of the device where it is expelled to the surroundings by natural convection.

Second, handheld devices are handled directly by the user so ergonomic concerns are important. Chiefly, maintaining the external device package at a temperature which is comfortable for the user. As with many issues dealing with user perception determining a precise limit is challenging. Following discussions with engineers at Intel the author has chosen to use 40°C as a reasonable

and conservative limit. This is slightly lower than the limits found in literature (42-45°C) (Greenspan *et al.*, 2003; Patapoutian *et al.*, 2003). In a real system the goal is to avoid throttling the processor, which would be done in advance of the user becoming uncomfortable.

The requirement to remove heat from the device and maintain a low surface temperature are in direct opposition. An idealized maximum heat transfer rate can be calculated. These calculations use the dimensions of a Samsung Galaxy Tab E (L = 241.9 mm, W = 149.5 mm, t = 8.5 mm), any device could have been chosen, but this tablet was current at the time of writing and is quite large. Assuming the tablet has a perfect heat spreading system (the surface is at constant temperature) and is held vertically in air at 25°C, a conservative value of maximum heat transfer can be calculated. Table 1.1 gives the properties that were used. Using empirical correlations for Nusselt number (Eq. (1.1)) an average heat transfer coefficient and total heat transfer rate can be determined (Eqs. (1.1) to (1.3)) (Incropera *et al.*, 2007).

Table 1.1. Properties used to calculate the idealized maximum heat transfer rate.

β	0.00327 K^{-1}
α	2.25×10^{-5} m^2/s
ν	1.59×10^{-5} m^2/s
k	2.63×10^{-2} W/mK
T_s	40 °C
T_∞	25 °C
Ra_L	1.97×10^7

$$\overline{Nu}_L = 0.59\,(Ra_L)^{\left(\frac{1}{4}\right)} = 39.0 \tag{1.1}$$

$$\bar{h} = \frac{\overline{Nu}_L k}{L} = 4.24 \text{ W/m}^2\text{K} \tag{1.2}$$

$$q_{max} = \bar{h}A(T_s - T_\infty) = 4.6 \text{ W} \tag{1.3}$$

In modern tablet computers, it is common for the peak electronics heat dissipation to be greater than 5 W. This simple calculation serves to illustrate how maintaining a low surface temperature sets a hard limit on the rate of heat transfer which can be dissipated. This calculation also shows that heat spreading, no matter how advanced, will not be sufficient. However, heat spreading is critical to reducing the impact of hot spots.

Cooling systems are often separated into active and passive system. Active systems consume energy to increase heat transfer rates. This often involves circulating a heat transfer fluid using a fan or pump. Passive systems do not consume additional energy and rely solely on the available temperature difference in the system. Cooling systems are additionally classified based on the heat transfer fluid used (liquid or air cooling systems) (C. Kheirabadi and Groulx, 2016).

Indirect, active, liquid cooling strategies are common. In these systems, a liquid passes through a heat sink which is in thermal contact with the heat source. The flow of liquid transports heat from the source to an external cooling system where it is dissipated to the environment. There has been much research regarding the design of the liquid cooled heatsink with much of the state of the art focused on micro channel heat sink designs (Asadi *et al.*, 2014; Kadam and Kumar, 2014). Direct liquid cooling systems, where the heat transfer fluid comes into direct contact with the heat source, have also been proposed. These systems include spray cooling (Kim, 2007) and jet impingement (Bar-Cohen *et al.*, 2006) techniques. Each of these systems efficiently transfers heat from a source to a liquid heat transfer fluid which then needs to be cooled and cycled back to the heat source. This is problematic in handheld devices. In addition to the equipment needed to implement the cooling loop, a system to dissipate the heat from the heat transfer fluid to the environment is also required.

A special type of indirect liquid cooling is the heat pipe. A heat pipe is a passive two-phase cooling system where the flow of heat transfer fluid is driven by the available temperature difference. In a heat pipe, the heat transfer fluid is vaporized by the heat source. This vapor is transported to a condenser via pressure driven advection. Condensate is then transported back to the evaporator via capillary action or gravity. Many heat pipe designs have been proposed and investigated in the literature and could have applications in handheld devices. As with other liquid cooling strategies, these devices excel at transferring heat from one place to another, but a system to dissipate that heat from the device to the environment is also required (Maydanik *et al.*, 2014; Siedel *et al.*, 2015).

The most practical active cooling system for handheld electronics is an air cooling system. A fan is used to draw cool air from the environment, through a heatsink where it absorbs heat from the source. Hot air is then expelled back to the environment. The author could not find any publications examining the use of active cooling solutions in modern handheld electronics. However, Grimes

et al. (2010) studied the use of a low-profile fan in the cooling of an older model cell phone (Nokia 3120). This older model phone was thick (20 mm) compared to modern devices. The fan was only 7mm thick which could conceivably be placed into the case of modern devices, though it would occupy the entire thickness of the device. Grimes *et al.* (2010) found that the inclusion of the fan increased the allowable heat dissipation by 40 to 60% when compared to the phone with no fan. In this study, the fan ingested air through a vent in the back of the phone and blew it through the length of the phone and out a vent at the far end. This method could be troublesome for modern electronics as the cases of modern devices are nearly completely filled with components and would represent a large flow blockage. Singh *et al.* (2013) studied the use of a piezoelectric fan coupled with a heat spreader. In this study, the cooling device was not tested in a handheld device and the results appear to be preliminary. However, the piezo electric fan was only 2 mm thick, so could feasibly be placed in a modern handheld device.

Both solutions presented above would require the device case be thoroughly vented. This could be problematic for modern devices as many users place their devices in cases or other situations with blocked air flow. Work on active solutions in modern portable electronics is non-existent and the author could not find any published results (numerical or experimental) explaining what the major barriers are. The author would speculate that it is a combination of the size of the fans and that inducing internal air flow in modern devices will be challenging.

Another potential option is to integrate a thermal storage system into the handheld device. This concept takes advantage of the fact that computer systems are inherently transient. Throughout the course of running an application, the power usage profile is transient, fluctuating up and down and only peaking for short periods. Also, handheld electronics are often used intermittently, beings used for a short period of time (10s of minutes) and then being left idle. This offers up the possibility of a temperature control strategy very similar to peak shaving. By introducing thermal storage, at peak power dissipation the thermal storage will absorb and store a portion of the heat supplementing the cooling system, if sufficient storage is available the temperature of the heat source can be controlled until power dissipation levels drop. When power dissipation rates fall, the stored heat is expelled to the surroundings. An isothermal heat storage technology, like latent heat thermal energy storage (LHTES), is theoretically ideal for this type of system. LHTES systems store heat using the phase transition of a phase change material (PCM). A solid-liquid

phase transition is most commonly used. This concept has been researched for many years in relation to larger systems.

1.3 Stationary Electronics

Much of the published research on temperature control of electronics via LHTES has been focused on what are referred to as hybrid heat sinks. Hybrid heat sink systems typically consist of a finned heat sink with PCM placed between the fins. Some researchers have specified how their hybrid heat sink would be coupled with a cooling system, others have not. Figure 1.1 shows a basic schematic of the hybrid heat sink concept.
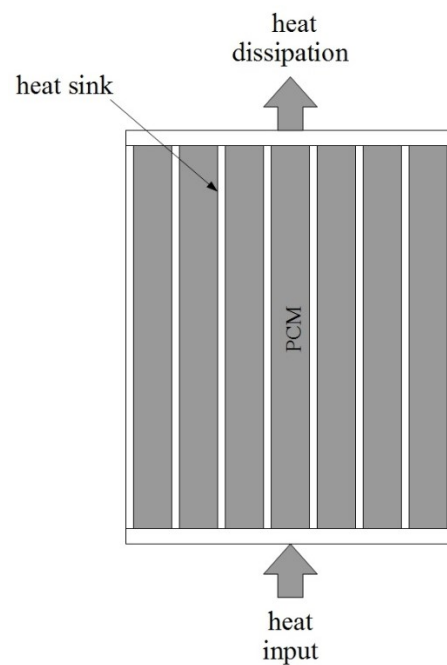
Fig. 1.1 Basic schematic of a hybrid heat sink system represented here as a plate fin heat sink for simplicity

This type of system was investigated by Zheng and Wirtz (2004), they developed a semi empirical finite volume model, and built and tested a prototype (see Fig. 1.2). The prototype consisted of a plate fin aluminum heat sink filled with pentaglycerine ($T_m = 83°C$) with a base which was 100 mm by 100 mm and fins which were 50.8 mm long.
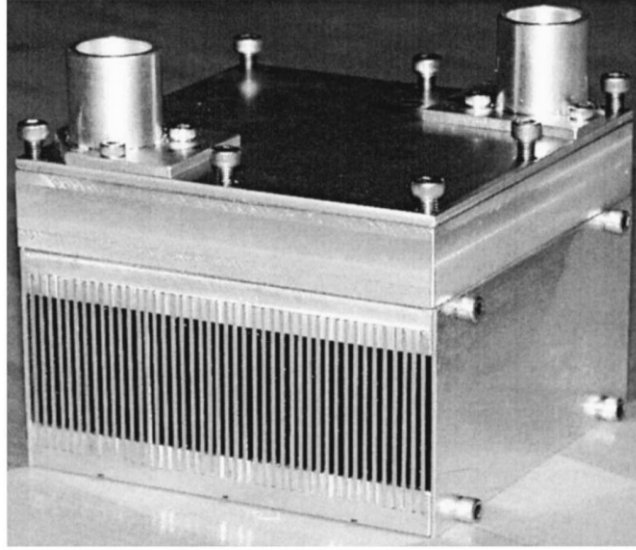
Fig. 1.2 Photograph of hybrid heat sink used by Zheng and Wirtz (2004)

Heat was applied with an electric heater and removed with a liquid cooled cold plate. During testing, the system was brought to steady state with a constant heat input of 100 W (giving a steady state temperature just below the melting temperature) and then the heat input was increased to 130 W. The transient temperature history of the prototype was compared to their simulation and was found to be in good agreement. Zheng and Wirtz (2004) remarked that the response of the system was very sensitive to the properties of the PCM selected but did not make any recommendations on PCM selection. The nature of the prototype and the power input demonstrated this setup was not intended for typical computing applications, portable or stationary. Kozak *et al.* (2013) performed a similar analysis with a device which was strikingly like Zheng and Wirtz. The device tested was a plate fin heat exchanger filled with PCM, however an air-cooled heat sink was used in place of a liquid cooled cold plate. The heat sink had a base 150 mm by 150 mm and a total height of 107 mm. *n*-eicosane was used as the PCM, having a transition temperature of $T_m =$ 35.6°C. Similar steady power input experiments were conducted, however, the setup started at room temperature and then the transient temperature history was examined as it was heated. In addition, the cooling phase was examined after the heating element was turned off and the setup was allowed to return to room temperature. The power input was very high (100 to 300 W). Kozak *et al.* (2003) found their numerical model matched with their experimental results and attempted to non-dimensionalize their results. However, they did not make any practical conclusions which are relevant to portable electronics applications. Both Zheng and Wirtz (2004) and Kozak *et al.*

9

(2013) used an engineered cooling device (cold plate, or fanned heat sink) to increase the heat transfer on the heat dissipation side of the hybrid heat sink. Other authors have used a simpler approach.

Fan *et al.* (2013) investigated a hybrid heat sink with an 80 mm by 80 mm base which was 30 mm tall. Heat inputs between 60 W and 120 W were applied to the heat sink. A fan was used to blow air across the top of the hybrid heat sink. Two different PCMs were tested: *n*-eicosane ($T_m =$ 35.6°C) and 1-hexadecanol ($T_m = 46.8$°C). Fan *et al.* (2013) concluded that using a PCM with a transition temperature closer to the temperature limit of the source will allow it to operate for longer before reaching its limit and therefore was superior. Lu *et al.* (2014) used the same experimental setup modified to operate at precise inclination angles. Experiments were run at a steady 20 and 40 W using 1-hexadecanol. Comparing the time which it took for the setup to reach a set point of 75°C, they found that for a heat dissipation of 40 W, an inclination angle of 75° was optimal resulting in an increase of 66.7% over the horizontal orientation. For a heat dissipation of 20 W, an inclination angle of 60° was optimal and offered an increase of 3.7%. The experiments of Fan *et al.* (2013) and Lu *et al.* (2014) cannot be used to make conclusions about portable electronics but do offer a few points which are interesting. First, using a PCM which has a higher transition temperature (closer to the high temperature limit of the source) offers better protection to the source. Secondly, the inclination angle of the LHTES may be important.

Several other publications have not included a cooling system at all. Baby and Balaji (2012) tested a hybrid heat sink with an 80 mm by 62 mm base which was 25 mm tall with plate fins. Steady melting experiments at a power dissipation rate between 2 and 7 W were carried out with *n*-eicosane. In these experiments, the top of the heat sink was sealed with a clear plastic cover. Two other papers use a similar setup for the investigation of a pin fin heat sink (Baby and Balaji, 2013) and the investigation of unsteady heat inputs (Baby and Balaji, 2014) . The unsteady power profiles appear to have been invented by the authors and are quite complex. The authors struggled to draw useful conclusions from their experiments. However, intermittent operation is fundamental to the concept of using LHTES for temperature control and therefore deserves to be investigated. Fok *et al.* (2010) did a very similar set of experiments including a set of intermittent heating experiments. They used several plate fin heat exchangers, the smallest of which had a base which was 85 mm by 72 mm and was 21 mm tall which was filled with *n*-eicosane.
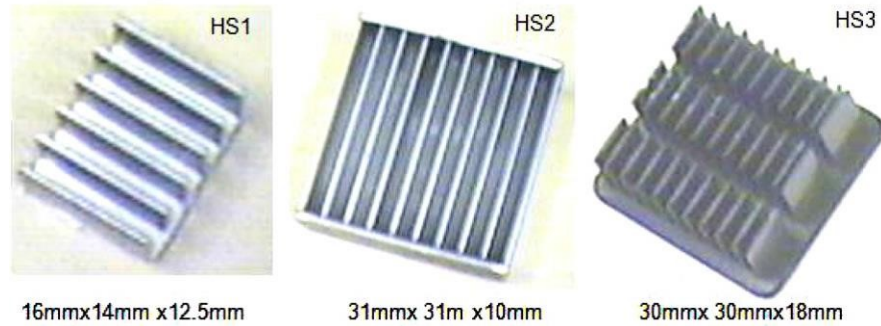
Fig. 1.3 Photographs of hybrid heat sinks used by Kandasamy *et al.* (2008)

Kandasamy *et al.* (2008) left the top of the hybrid heat sink open to the atmosphere. The hybrid heat sink was not completely filled with PCM therefore a portion of the fins' length was available for natural convection. Three different sizes of plate fin hybrid heat sink were tested, the thinnest having a base which was 31 mm by 31 mm and being 10 mm tall (see Fig. 1.3). This is one of the thinnest "traditional" hybrid heat sinks found in the literature. Steady melting experiments were done at 2 and 4 W using paraffin wax (T_m = 46–48°C). They found the heat sink controlled the temperature better with PCM than without for 4 W and had little impact at 2 W. Saha *et al.* (2008) used a pin fin (square cross section on the pins) hybrid heat sink which had a base which was 42 mm by 42 mm and was 30 mm tall. The heat sink seems to have been filled entirely but was left open to the atmosphere at the top surface. Melting experiments were done at 4 and 8 W of heat dissipation. They were primarily investigating what the optimum volume ratio between the fins and the PCM is, finding that a heat sink with 8% by volume fins was superior. Mahmoud *et al.* (2013) investigated several different orientations of fins in a hybrid heat sink which had a base which was 50 mm by 50 mm and 25 mm tall. They performed several heating and cooling experiments at 3 to 5 W. Uniquely, they compared the use of 6 different PCMs with transition temperatures ranging from 29 to 58°C. They concluded that the PCM with the lowest melting temperature was superior.

Several authors have investigated more exotic variations on this concept. Weinstein *et al.* (2008) investigated the use of graphene nano-fiber filled paraffin wax. Essentially they replaced the aluminum heat sink of previous works with a high conductivity nano-particle. Sanusi *et al.* (2010) investigated a similar technique. Jaworski (2012) investigated putting the PCM inside of hollow pin fins on a heat exchanger.

11

Quite a bit of work has been done on the hybrid heat sink concept. It has been thoroughly shown that the concept of integrating LHTES into a heat sink is a feasible way to improve the temperature control of intermittently heated systems. However, due to the complexity of PCM modeling and the differences in design and size of heat sinks, it is very difficult to distill many overarching conclusions from this work and even more difficult to extrapolate it to include modern handheld systems. Many of these authors claim their work is intended for use in portable electronics but all of these temperature control solutions are far too large to work with modern handheld devices. The thinnest of the hybrid heat sink devices is 10 mm thick; modern devices often have a total thickness smaller than 9 mm.

There is no consensus on the optimal transition temperature. Fan *et al.* (2013) found that a PCM with a transition temperature closer to the sources high temperature limit afforded better temperature control. Mahmoud *et al.* (2013) found the opposite, lower temperature PCMs were superior. The experiment done by Mahmoud *et al.* (2013) was far from being representative of a portable electronic system but their system was cooled by natural convection and had a heat dissipation in a range more realistic for modern handheld devices making it more relevant. More work is required to resolve this issue.

1.4 Portable Electronics

A few authors have investigated using LHTES for the temperature control of handheld electronic devices. Several of these authors did experimental and numerical work with LHTES systems integrated into mock devices. These studies are well executed and interesting but are quite old and dealt with devices which have a form factor different from modern handheld electronics.

1.4.1 Older Studies

Hodes *et al.* (2002) investigated the use an LHTES module installed in a mock phone handset. The mock phone was 12.7 cm by 5.1 cm by 1.9 cm and consisted of a simulated printed circuit board, source, and an ABS case. The actual LHTES module was 5.1 cm by 3.2 cm by 1.0 cm and consisted of a rectangular aluminum container. Steady heating and cooling tests were conducted with 3 W of heat dissipation. Two different PCMs were used: *n*-tricosane ($T_m = 48°C$) and a commercial micro-encapsulated PCM, Thermasorb-122 ($T_m = 50°C$). They found the addition of PCM increased the time that the handset could be used before the surface temperature reached an

"unbearable temperature" of 62°C by 3 times for the Thermasorb-122 and 5 times for the *n*-tricosane. This difference was due mainly to *n*-tricosane having a larger latent heat of fusion.

Alawadhi and Amon (2003) investigated the use an LHTES module for the temperature control of a "wearable computer". Their work was mainly numerical but was validated using an experimental mock computer. They used an expanded aluminum foam filled with *n*-eicosane. From their numerical and experimental studies, they concluded the inclusion of the LHTES module improved the temperature control of the device.

These two studies are of more interest than the studies which looked at hybrid heat sinks. They showed that one of the few ways to analyze the effectiveness of an LHTES module is to place it in a mock device, either numerically or experimentally. They do not however, offer any insights into optimal PCM selection or LHTES design as the systems are too large, and old, to be comparable to modern devices.
.

1.4.2 Recent Studies

Tomizawa *et al.* (2016) studied the integration of an LHTES unit into the temperature control system of a mock handheld computing device which was close to the size of a modern device (122 mm by 62 mm by 14 mm). This mock device consisted of a case made from 1 mm sheets of acrylic (rear case) and 1 mm polycarbonate sheet (front and side of the case). An electric ceramic heater was mounted to a simulated printed circuit board (PCB). The LHTES unit consisted of a microencapsulated paraffin powder which was mixed (50% by weight) with polyethylene (PE). This mixture of microencapsulated PCM and PE was cast into sheets which were 25 mm by 25 mm by 4 mm and 50 mm by 50 mm by 1 mm. Melting experiments were completed with a steady power input of 2 W. The use of a mock handheld device and LHTES module which could believably fit into a modern handheld device make this work relevant. Tomizawa *et al.* (2016) found that the sheets delayed the system temperature rise and reduced the system steady state temperature. Another, aspect which was investigated by Tomizawa *et al.* (2016) was the inclusion of a heat spreader. In addition to testing the two sizes, LHTES units with a copper sheet attached were tested. It was found that the maximum steady state temperature change in the system was smallest for the thinnest LHTES unit with a copper sheet.

Moore *et al.* (2015) present a numerical analysis of a large tablet computer which utilizes a forced convection cooling system. They simulated the system numerically with a commercial PCM (Outlast LHS 90G, T_m=42 to 45°C) placed near the CPU. The transition temperature of the PCM was varied from 32 to 47°C. Transient temperature profiles on the CPU heat spreader were presented showing that the PCMs delayed the temperature increase in this heat spreader. Simulations which used a lower transition temperature showed a larger delay. However, this work is lacking in many details. The exact location, and dimensions of the PCM are not given. Description of the PCM modeling technique and mesh study are missing or lacking. The exact location where the temperature is measured is not given making a comparison to other work difficult.

Two of the authors, who have published on this topic, conducted their research at the LAMTE as a part of the same research contract as the work presented in this thesis. Ahmed (2016) and Maranda (2017) conducted research as a part of this research contract, their work is summarized here but is discussed in more detail in chapters 4 and 3 respectively.

Ahmed (2016) studied the use of LHTES units for the temperature control of handheld electronic devices. Specifically, tablet computers were examined. Other published studies have used "mock" handheld electronic devices. However, these did not capture key aspects of modern tablets, mainly the thermal mass or conduction paths. These two aspects are impacted by two components of the tablet which are challenging to simulate: the display and the battery.

The display of handheld computing devices is an assembly of parts which generally consists of a steel frame and several layers of plastics and glass. The display assembly is important as it represents nearly half of the tablet heat transfer area and has unique conductive and heat spreading properties that are difficult to represent with a simpler structure. Lithium ion batteries consist of many layers of thin material, some of which are toxic, and are challenging to simulate with a simpler structure. Ahmed (2016) employed the simplest approach to solving this problem and used a real tablet display and battery in his experiments. A Dell Venue 8 Pro tablet computer was disassembled, and a mock PCB cut from a piece of copper clad FR4 was used to replace the existing PCB. A 1" by 1" polyimide heater was used to simulate the heat dissipated by the main source.

Ahmed (2016) conducted several experiments where the heat generation rate was held constant for a heating phase and was then shut off for a cooling phase. Cyclic heat generation experiments were also conducted, in these studies the heat source was activate and shut off in a cycle. Ahmed (2016) tested LHTES modules which utilize two PCMs: *n*-eicosane and a commercial material called PT37 (T_m=36.3 °C). These LHTES modules were encapsulated with heat sealable laminated film.

Ahmed (2016) concluded that the LHTES module tested aided in controlling the temperatures of both the main heat source and the tablet computers surface with a variety of heat generation rates and orientation angles.

Maranda (2017) conducted an experimental investigation of the performance of LHTES temperature control modules in a simplified experimental setup. The transient heat transfer in a mock device (like that used by Ahmed (2016)) are complex and difficult to understand given the limited data which is available from experimental studies. To better understand how LHTES modules charge and discharge, a simpler more controlled experimental setup was used to study two different LHTES modules. These modules were similar to those tested by Ahmed (2016) but were thinner and an improved LHTES construction process enhanced the precision with which their thickness was controlled. The two LHTES modules tested used *n*-eicosane and dodecanoic acid (T_m=43.6 °C) as the PCM.

Mr. Maranda found the performance of the LHTES module using *n*-eicosane combined with an aluminum heat spreader was superior, offering better temperature control when compared to only a heat spreader, and no spreader or module. However, the difference between the two LHTES modules were relatively small.

1.5 Encapsulation

Published work studying the use of LHTES modules for the temperature control of electronic devices largely deals with hybrid heat sinks, therefore, the PCM was encapsulated in a metallic heat sink. Older studies which use a mock device and more realistic LHTES module (Alawadhi and Amon, 2003; Hodes *et al.*, 2002) had more space to work with than modern devices and encapsulated their PCM in a rigid aluminum container. Tomizawa *et al.* (2016) used microencapsulated paraffin powder which was mixed (50% by weight) with polyethylene (PE).

This mixture of microencapsulated PCM and PE was cast into sheets. This method resulted in a shape stabilized, leak proof LHTES module which would be easy to handle. However, less than half of the LHTES module is composed of PCM so it has a relatively poor storage density.

Work by Desgrosseilliers (2016) has shown heat sealable laminated films are an effective method of encapsulating PCMs. This method was adapted by Ahmed (2016) and the author for the manufacture of thin packets of PCM suitable for use in the temperature control of handheld electronics.

1.6 Scope of the Thesis

The primary research questions this thesis work will answer are:

- What are the key design requirements for an LHTES temperature control module for use in a tablet computer?
- What is the magnitude of temperature control improvements which can be gained by utilizing an LHTES module?
- What PCMs are most suited for use in an LHTES temperature control module?

The work presented in this thesis can be split into two parts. First, an initial numerical study was conducted to inform the selection of the most appropriate PCM. A three-dimensional, transient, finite element model of a modern tablet computer was constructed and used to investigate the general heat transfer behaviour of an LHTES temperature control module. This work focuses on investigating the impact of transition temperature on the behaviour of the LHTES module and informed Mr. Ahmed, Mr. Maranda, and the author's experimental work. The second phase of this thesis work was a definitive experimental study of the use of an *n*-eicosane based LHTES temperature control module in a mock tablet computer. These studies implemented an improved experimental platform, a more controlled LHTES module construction method, and an investigation of the effect of heat spreading on LHTES performance. These studies are sufficiently similar to modern handheld electronic devices to definitively assess the viability of using LHTES modules to improve the temperature control of modern handheld electronic systems.

CHAPTER 2 : NUMERICAL STUDY AND MATERIAL SELECTION

2.1 Background PCM information

One of the key unresolved questions in designing an LHTES system for use in the temperature control of handheld electronics is PCM selection. Several PCMs have been proposed for use in temperature control of electronics. However, most of the research was performed in hybrid heat sinks and not systems which are representative of handheld electronics. A series of numerical simulations using COMSOL Multiphysics 5.3 were performed to give direction to the PCM selection for this work.

Material selection is challenging due to the complex interaction of a PCMs major thermo-physical properties: latent heat, specific heat, thermal conductivity, density, and transition temperature. Using a PCM with a larger latent heat of fusion will increase the storage capacity of the LHTES unit and will have a positive effect on its performance. A larger specific heat will increase the sensible storage of the LHTES which will also have a positive, if less significant, impact on its performance. The volumes available to place the LHTES in handheld devices are tiny, this restriction on the size of the LHTES unit makes a higher density attractive as it will increase the storage capacity per unit volume. For PCMs with exceptionally high densities (low melting temperature metallic alloys for example) the increase in the devices weight may need to be considered.

The ideal thermal conductivity is more complex to determine. A PCM with a high thermal conductivity will allow heat to transfer from the source to the PCM more easily and will likely increase the rate and extent of melting, which will have a positive impact on performance. However, increasing thermal conductivity will also improve the sources coupling to the devices outer case and will negatively impact the outer surface temperature. Thermal conductivity does not typically change significantly within a family of PCM. Cost, material compatibility, super cooling, etc. also impact the choice of PCM family and largely overrides the selection for thermal conductivity. This thesis only considers pure PCMs, thermal conductivity enhancement techniques are not considered.

Transition temperature is the key thermo-physical property for which there is little selection guidance in the literature. The upper limit of possible transition temperatures is bounded by the high temperature limit of the heat source, which will be taken as 80°C in this work, and the lower limit is bounded by the ambient temperature and the user's body temperature. If the PCM transition temperature is not sufficiently higher than its surroundings it will not solidify at a sufficient rate, if at all. Body temperature is of interest mainly in the context of phones, which may spend a significant amount of time stored near the user's body.

2.1.1 Organic vs Inorganic

Phase change materials can be categorized into two groups: organic and inorganic. There are many types of organic compounds which can be utilized as phase change materials, these include: paraffins, fatty acids, esters, and alcohols. Inorganic phase change materials generally refer to low melting temperature metals/metal alloys and salt hydrates. This thesis will only consider organic PCMs. Organic PCMs have been shown to be compatible with the materials used in handheld electronics and to be stable under multiple phase transition cycles (Kahwaji *et al.*, 2017).

Some commonly used salt hydrates have been shown to exhibit both incongruent melting and super cooling. Also, both salt hydrates and low melting temperature metal alloys are electrically conductive. Even a small leak or contamination on the PCB of a handheld electronic device could lead to a short circuit and device failure.

This work and the work of Maranda (2017) and Ahmed (2016) have shown organic PCMs to be viable for the temperature control of handheld electronics. They are available, non-toxic and generally easy to use. However, a comprehensive comparative study comparing the performance of organic PCMs to inorganic alternatives is not presented here.

2.2 Numerical Simulation

A numerical simulation of a tablet computer with an LHTES temperature control unit was created in the commercial finite element software COMSOL Multiphysics 5.3. This model was not intended to be an exact simulation of an existing tablet but a numerical platform for doing comparative studies. Current numerical modeling techniques still struggle to accurately simulate a number of phenomenon which will play a part in this model. Examples include the natural convection on the cover of the tablet and the contact resistances between components in the tablet.

This set of simulations looks at the comparative performance of different LHTES modules in a representative numerical model. The goal was to investigate the key heat transfer characteristic of these systems and to give direction on PCM selection, specifically regarding transition temperature.

2.2.1 Geometry

The geometry is based on a model supplied by our industrial partners at Intel. Four orthographic views are shown in Figs. 2.1 to 2.4. The full model consists of >250 parts and is not included in full, however, partial engineering drawings are included in Appendix A. The major components of this tablet model can be placed into five groups: display assembly, stiffener, battery, motherboard, and external cover. The full model contains a large number of very thin layers and proved difficult to implement with a reasonable sized mesh. The geometry consists entirely of rectangular features which are all aligned with a Cartesian grid. Therefore, it is possible to mesh the entire domain using a structured rectangular mesh. In COMSOL Multiphysics, the simulation domain was formed by slicing the full domain into rectangular regions (>10,000) and then grouping them into the features of the tablet (see Fig. 2.5). Several of the features in the full model were neglected or simplified in the numerical simulation. Each of the major components is discussed in detail below.
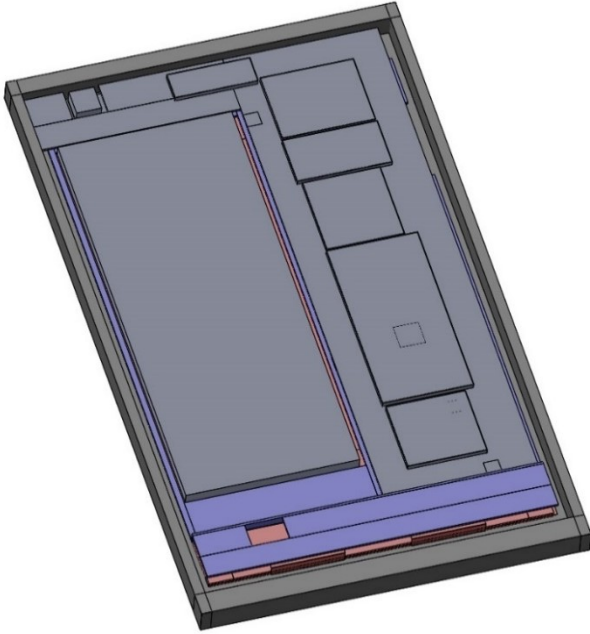
Fig. 2.1 Orthographic view of the tablet model with back cover removed.
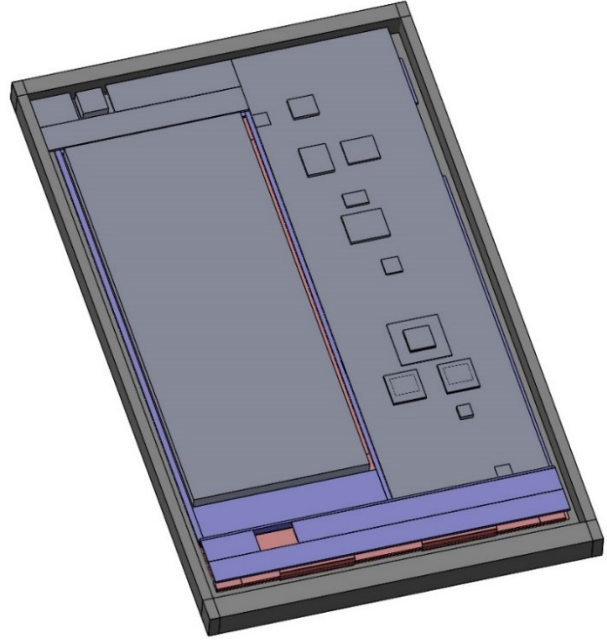
Fig. 2.2 Orthographic view of the tablet model with back cover, and EMI shields removed.
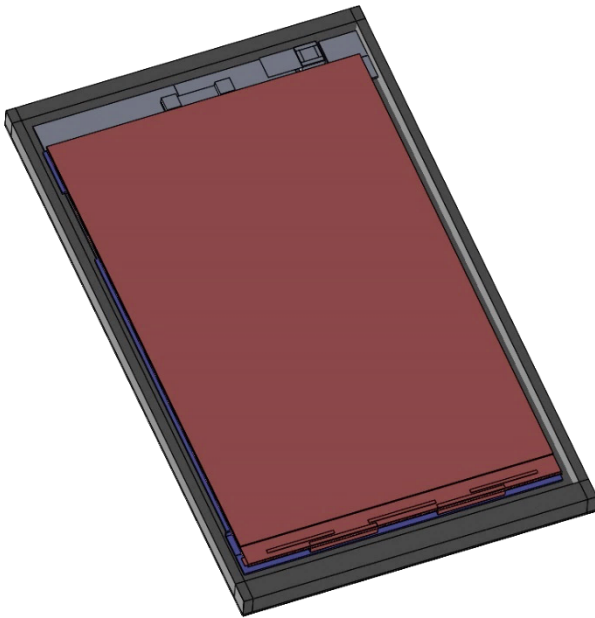
Fig. 2.3 Orthographic view of the tablet model with front touch glass removed.
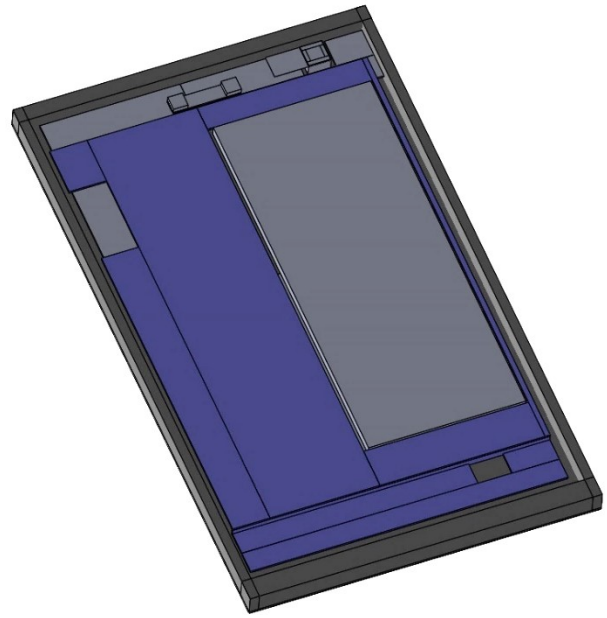
Fig. 2.4 Orthographic view of the tablet model with display assembly removed.
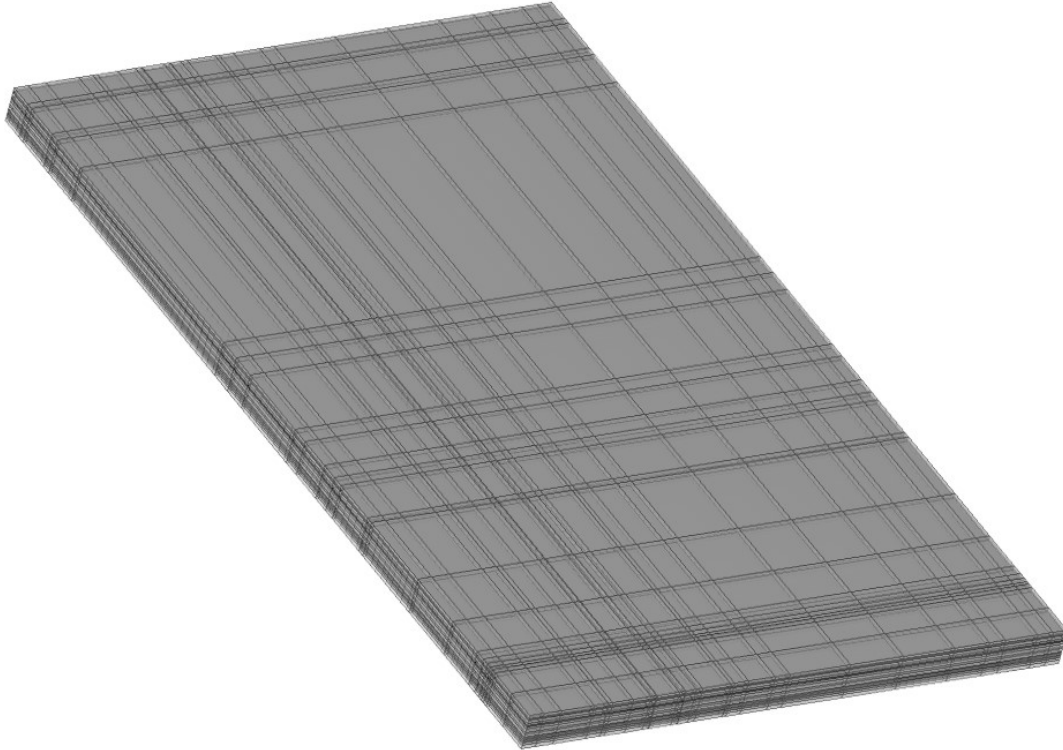
Fig. 2.5 Subdivision of the numerical domain

2.2.1.1 Display Assembly

The display assembly consists of eight different layers of polymer or glass, and a stainless-steel frame. Layers in the display assembly are very thin, ranging in thickness from 0.14 mm to 0.6 mm. In the numerical simulation, these display layers have been lumped together into two composite layers. These composite layers are a good representation of the thermal conductivity through the layers and the thermal inertia but will not fully capture any spreading which happens between the layers. However, the layers are poor conductors and will produce far less heat spreading than other components in the system (heat spreader, PCB, etc.). Also, a small PCB at the base of the display was ignored. There were no major sources associated with this PCB and it is far from the major sources in the system, it was removed to simplify the model. With these simplifications, the display assembly includes the: lumped display layers, LED backlight, copper conductor plate, and chips on glass (COG), all of which are mounted on a steel frame. The LED backlight and the COGs are minor sources in the tablet. A rendering of the full display assembly is shown in Fig. 2.6 and an illustration of the geometry used in the numerical study is shown in Fig. 2.7.
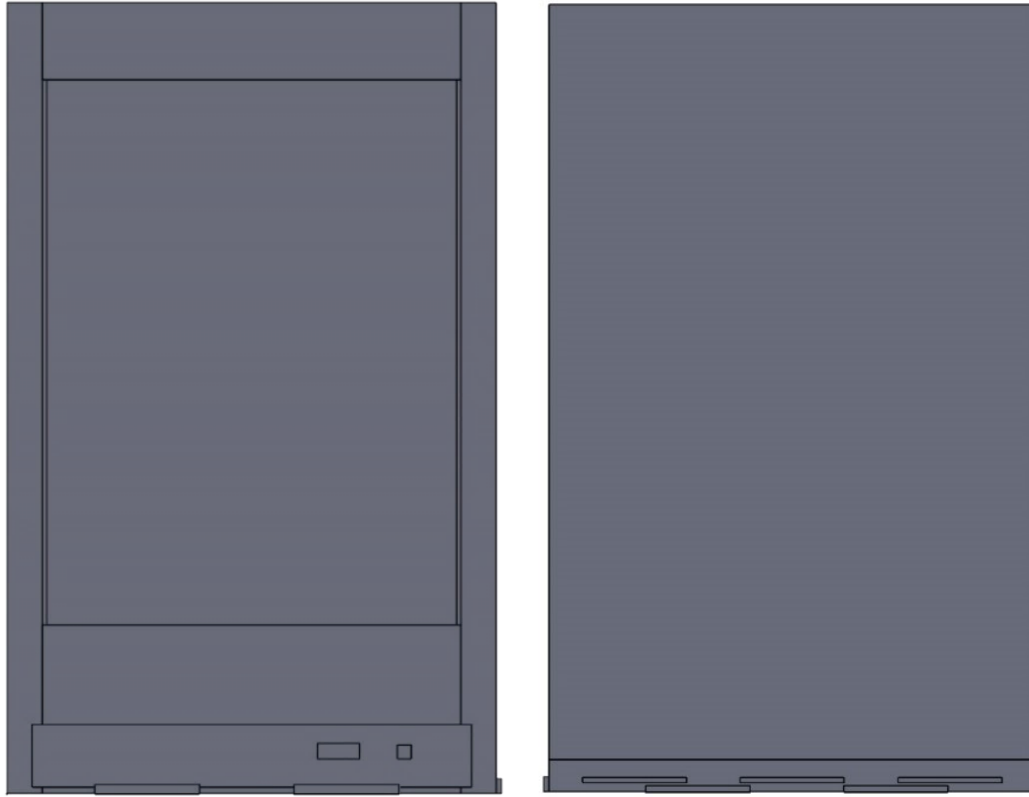
Fig. 2.6 Renderings of the complete display assembly from the front (right) and back (left)

1. plastic cover

2. LED leads

3. COG

4. display panel
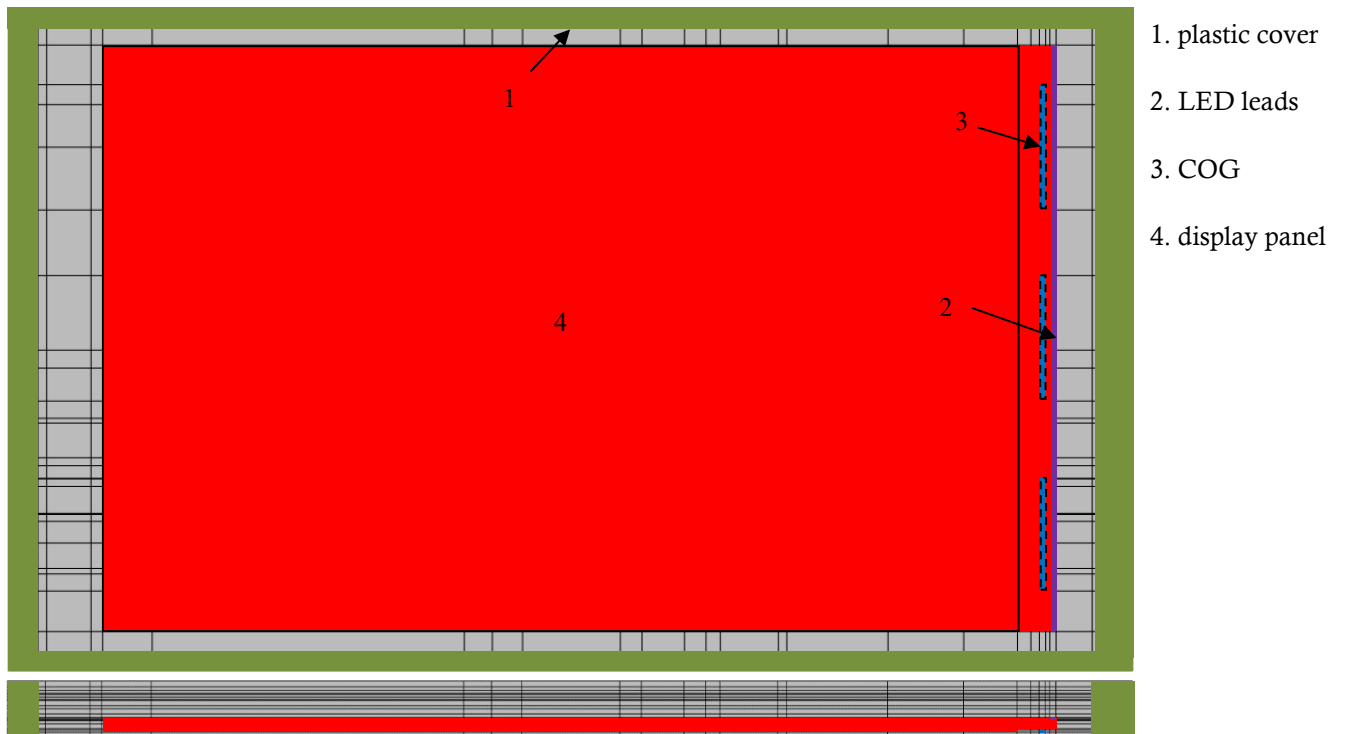
Fig. 2.7 Illustration of the display assembly from the numerical simulation

2.2.1.2 Magnesium Stiffener

The stiffener is a magnesium plate which is installed between the screen assembly and the motherboard. It has a thickness of 0.8 mm and wraps around the battery. The shape of the magnesium stiffener was simplified for the numerical simulation. Figure 2.8 shows the stiffener as it appears in the original geometry and Fig. 2.9 shows the stiffener which was included in the numerical simulation.

2.2.1.3 Battery

The battery takes up a large portion of the tablet's volume and has a complex structure. Lithium ion batteries consist of a thin layer of aluminum foil, copper foil, organic electrolyte, separator, anode material and cathode material which are rolled and packaged. Numerical simulation of these systems is beyond the scope of the current work and this structure was completely omitted. A lumped property was assigned to the battery domain. The properties used were provided by our industrial partners and are shown in Table 2.1.

Table 2.1 Properties used to simulate the battery

Properties	Battery Lumped
ρ	1114 kg/m^3
k	10 W/mK
C_p	2049 J/kgK

Fig. 2.8 Rendering of the complete magnesium stiffener
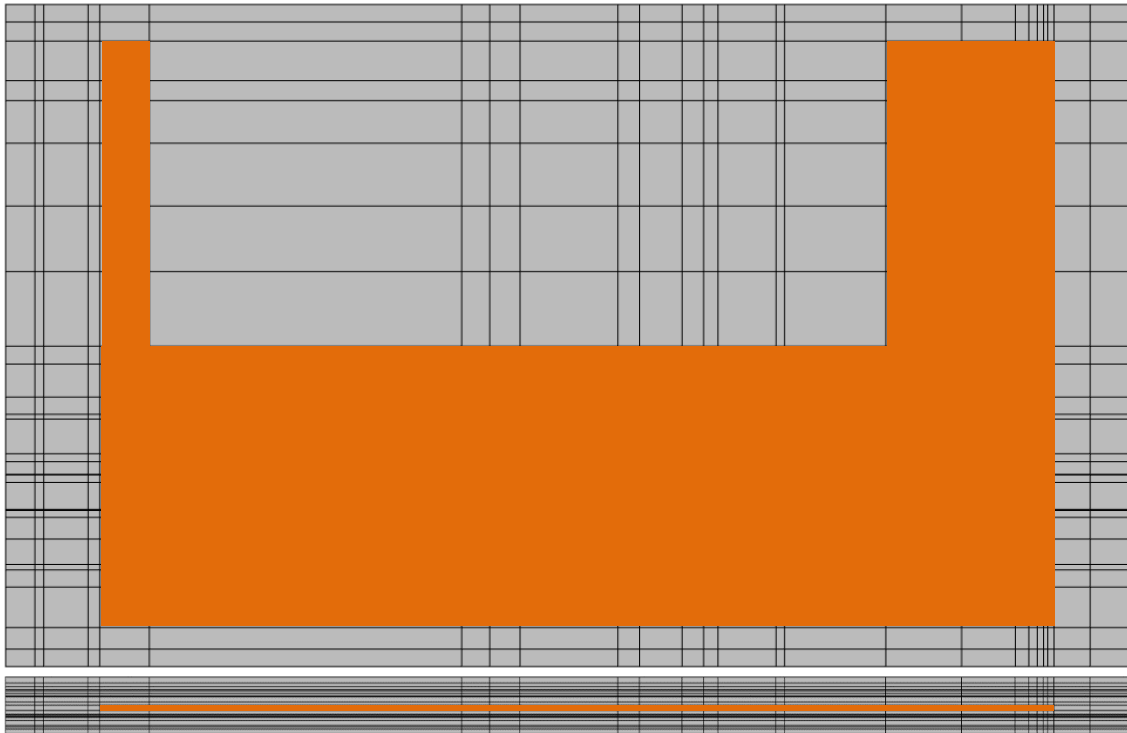
Fig. 2.9 Illustration of the magnesium stiffener from the numerical simulation

2.2.1.4 Motherboard

The motherboard is the printed circuit board (PCB) on which microelectronics components are mounted. All the major sources can be found on the motherboard. Two major modifications were made to the structure of the motherboard. First, the electromagnetic interference shields (EMI shields) were removed. These shields are essentially cages of electrically conductive metallic materials which protect the major components from radio interference. They were removed to give direct access to the heated components, and to reduce the complexity of the model. In a functional tablet, these shields would need to be present, however, they are made from highly conductive materials and could potentially be integrated into the temperature control solution. Secondly, only the components which are significant sources were retained in the numerical model. The other components are small and play only a minor role in the heat transfer. Figures 2.10 and 2.11 show renderings of the motherboard from the original model, Fig. 2.12 shows the motherboard as it appears in the numerical simulation.

Fig. 2.10 Rendering of the complete motherboard assembly
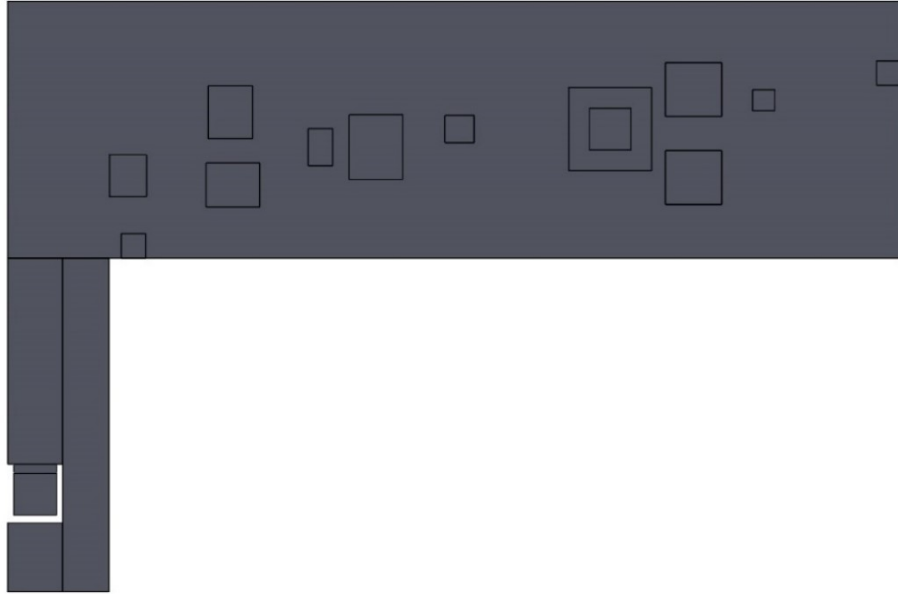
Fig. 2.11 Rendering of the complete motherboard assembly with EMI shields removed

1. SOC die

2. SOC substrate

3. memory

4. PMIC

5. PCB

6. battery

7. camera
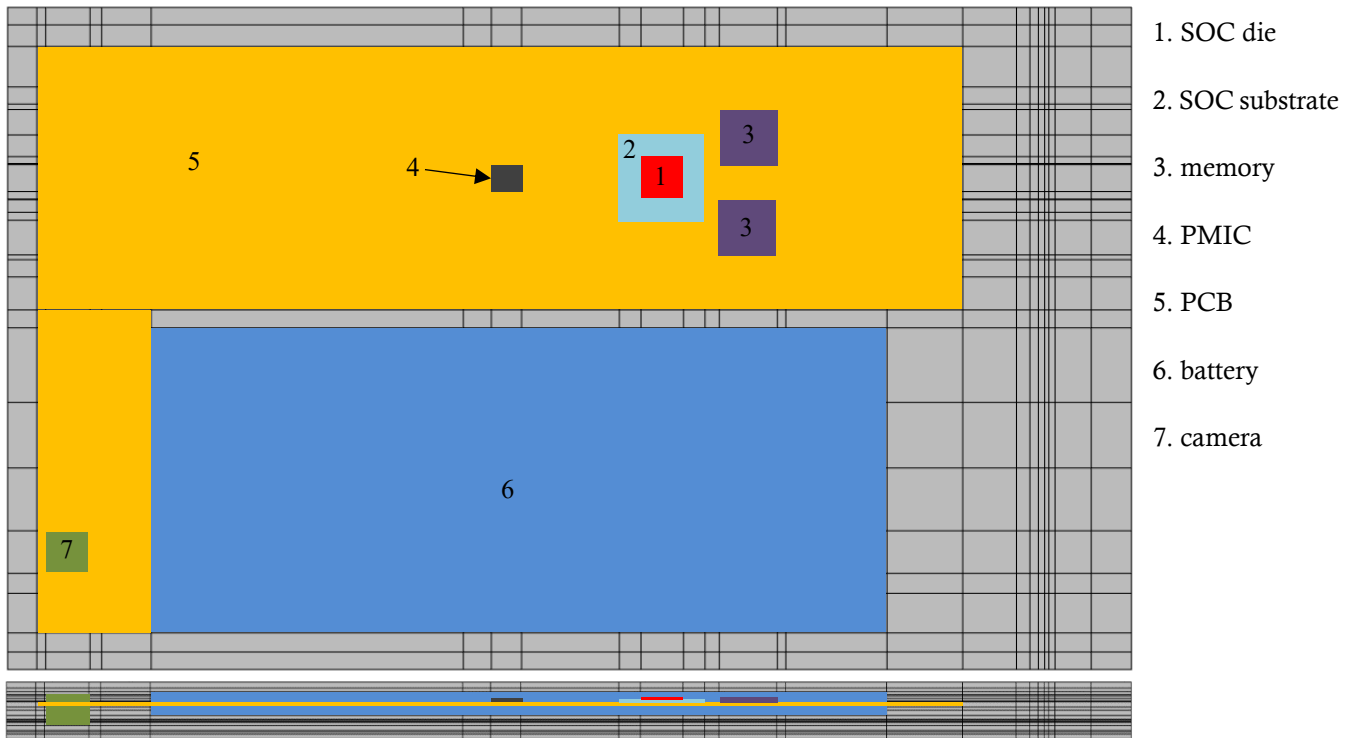
Fig. 2.12 Illustration showing the motherboard and battery in the numerical simulation. Note that the top down view shows the view from the back of the tablet while previous figures have been shown from the front.

2.2.1.5 Sources

Many of the major sources are located on the motherboard. These sources include the system on a chip (SOC), memory and power management integrated circuit (PMIC). In addition to the sources located on the motherboard, the backlight, COG, and camera also dissipate heat. An additional heat dissipation was applied to the entire PCB which represents all other losses associated with components on the motherboard. Table 2.2 gives the power dissipation of each component. This dissipation profile was provided by our industrial partners and is designed to mimic the heat dissipation of a tablet while shooting 4K video.

Table 2.2 Heat dissipated by sources in the numerical simulation

Associated Domain	Heat Generation
SOC	3.687 W
Memory	0.805 W
COG	0.765 W
PMIC	0.742 W
Backlight	0.672 W
Misc. Motherboard	0.479 W
Camera	0.353 W
Total	7.503 W

2.2.1.6 Summary of Material Properties

Table 2.3 summarizes the thermo-physical properties of each of the domains used in the numerical simulation.

Table 2.3 Thermo-physical properties used in the numerical simulation, anisotropic properties are listed in the form [x, y, z] (provided by Intel Corporation)

Material/Domain	ρ (kg/m³)	k (W/m·K)	C_p (J/kg·K)
Nylon	1120	0.27	1600
Touch Glass	2700	1.1	840
Display Layers 1	1624.3	0.58	1090.5
Display Layers 2	1115.6	0.84	1925.8
COG	2330	117.5	700
Aluminum 6061	2710	180	913
Mg Alloy	1810	72	1050
Copper	8930	385	385
Stainless Steel	7900	16.3	500
PCB	1746	[90, 90, 0.5]	706
Memory Overmold	1000	0.8	800
PMIC Overmold	1900	0.8	795
SOC Substrate	2969.59	[40.3, 40.3, 0.72]	358.83
SOC Die	2330	117.5	700
Graphite Tape	2000	[600, 600, 3.5]	711
Battery	1114	10	2049
Camera	1120	0.24	1527

2.2.2 Latent Heat Thermal Energy Storage Module

One of the major goals of this work was to study the impact of transition temperature on the performance of an LHTES module. There is little or no direction on what the optimum transition temperature is for these types of systems. This is due to the general lack of relevant studies but also because of the complex interaction between the different properties of a PCM. Ideally one would select several different materials with identical thermo-physical properties but different

28

transition temperatures. This is difficult if not impossible to do experimentally but is easily achieved numerically.

In this study, three organic phase change materials were selected. Each of these materials is a potentially viable PCM for an LHTES system. They have a wide difference in transition temperature but only a moderate difference in other properties. Using these three PCMs, a composite PCM was created. In the simulations the average properties were used, and the transition temperature was varied between 35°C and 47°C. This range was chosen after a preliminary study, using a similar composite PCM method, found that with a transition temperature of 55.8 °C the PCM did not melt during the simulation, but at 43.3°C it partially melted. It was clear from this preliminary work that a more detailed study focusing on the lower end of the temperature range was needed (Sponagle and Groulx, 2015).

Given that this is already an artificial study using a composite PCM, temperature dependant properties were ignored. In all cases, the arithmetic mean of the liquid properties of the three example PCMs were used to form the value of the composite PCM (see Table 2.4).

Table 2.4 Thermo-physical properties of the composite PCM and the materials used to construct it, properties are from measurements done by Mary Anne White's lab at Dalhousie University, used with permission

PCM	T_m(°C)	ρ_s (kg/m³)	ρ_l (kg/m³)	k_s (W/m·K)	k_l (W/m·K)	$C_{p,s}$ (J/kg·K)	$C_{p,l}$ (J/kg·K)	ΔH_{fusion} (kJ/kg)
nonadecane	31.8	781	777	0.26	0.184	1720	2260	181
dodecanoic acid	43.6	946	871	0.244	0.164	1800	2060	176
1-octadecanol	58	914	805	0.291	0.211	1750	2490	218
Average PCM	**-**	**-**	**818**	**-**	**0.186**	**-**	**2270**	**192**

This LHTES module was placed in the gap between the tablet components and the back cover. Figure 2.13 shows an illustration of the LHTES module as it appears in the numerical simulation. The LHTES module includes a total of 17 g of the composite PCM.
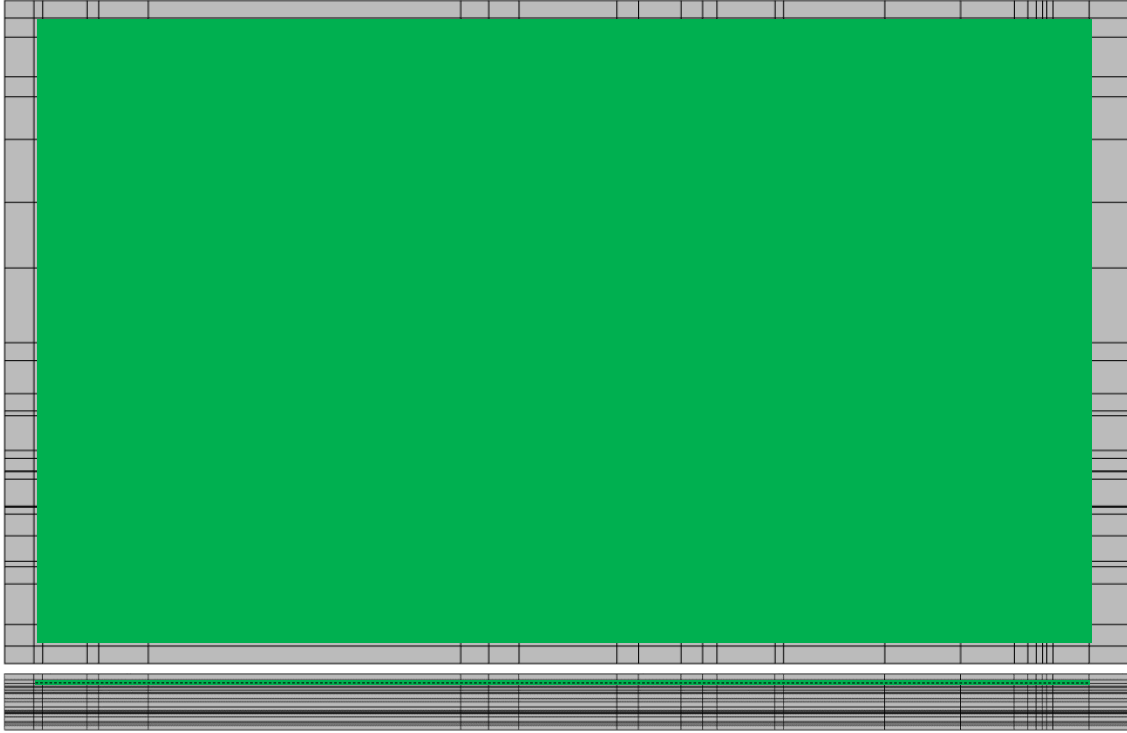
Fig. 2.13 Illustration of the LHTES from the numerical simulation

2.2.3 Numerical Method

A finite element model was constructed using COMSOL Multiphysics 5.3. The PCM domain is very thin (1 mm at the widest point). The simulation is run for a tablet held vertically, so it is possible that a natural convection cell will form in the melted PCM. The modelling of convection in the melted portion of a PCM is very complex and many studies have been devoted solely to its modelling, but some insight into the order of magnitude of the convection heat transfer can be garnered by idealizing the situation as natural convection in a rectangular cavity. Isolating a single correlation is pointless as the region of melted PCM is constantly changing size, however, it is apparent that the Nusselt number (Nu) is a function of the Rayleigh number (Ra) and Prandtl number (Pr). Rayleigh number for a pure single-phase material is given by Eq. (2.1). If Ra is small, then the contribution of natural convection is weak and vice versa. For a steady state single phase problem, if $Ra \leq 10^3$ then heat transfer is primarily by conduction.

$$Ra_L = \frac{g\beta(T_1 - T_2)L^3}{\alpha v} \tag{2.1}$$

For this example, the liquid properties of dodecanoic acid (see Table 2.4) are used along with a liquid viscosity of $\mu_l = 0.004$ Pa·s and a thermal expansion coefficient of $\beta = 0.0008$ K^{-1} (Kheirabadi and Groulx, 2015). It is difficult to approximate the temperature difference which would be seen by the PCM packet but the absolute maximum would be the difference between the processor design temperature and the ambient temperature, $(T_1\text{-}T_2)_{max} \approx 55°C$. Using this extremely conservative temperature difference and the LHTES thickness (1 mm), the Rayleigh number is Ra = 1029, using a smaller but more realistic temperature difference of 10°C, Ra = 187. This analysis has a large uncertainty but demonstrates that convection is only a very minor factor and can likely be ignored. As a result, the governing equation for these simulations is the unsteady three-dimensional conduction equation, Eq. (2.2).

$$\rho C_p \frac{\partial T}{\partial t} = \nabla \cdot (k \nabla T) + Q \tag{2.2}$$

The phase change module in COMSOL Multiphysics was used to simulate the phase change in the numerical simulation. This module uses a modified c_p method to simulate phase change. In this method, the c_p is increased at the transition temperature to account for the latent heat of fusion. For a pure PCM where the phase transition happens at a single temperature, this increase in the specific heat should be an instantaneous increase directly at the transition temperature. However, it is difficult to handle an instantaneous increase using numerical techniques. In the modified c_p method, the change in c_p is spread over a temperature difference according to a smoothed distribution function. Effectively, this results in the PCM changing phase over a range of temperatures centred on the actual transition temperature, the *mushy zone*. The size of this mushy zone is defined by the temperature change over which the phase transition is spread ΔT. The mushy zone in these calculations has ΔT = 3K. The apparent specific heat of the PCM is then calculated using Eq. (2.3).

$$C_{p,\,apparent}(T) = C_p + L \cdot \frac{d\alpha_m(T)}{dT} \tag{2.3}$$

where L is the latent heat of fusion and $\frac{d\alpha_m(T)}{dT}$ is a smoothed function which is zero everywhere accept within the mushy zone where $T_m\text{-}\Delta T/2 < T < T_m\text{+}\Delta T/2$. The function α_m is the melt fraction of the PCM on a mass basis. The exact definition of the function used is not given in the COMSOL

documentation, but based on plots which are presented in the documentation it would appear that α_m is a form of sigmoid function not unlike that used by Kheirabadi and Groulx (2015).

The boundary conditions on the outer surface of the tablet were modelled as natural convection with the tablet held vertically in air with an ambient temperature of 25°C. Built in natural convection boundary condition in COMSOL Multiphysics was used. It uses standard correlations for average convection coefficient on a vertical flat plate (h_{avg} = 3.5 W/m²K).

2.2.4 Mesh

The mesh used in these simulations was a swept rectangular mesh. A mapped mesh was constructed on one side of the domain and then this mapped mesh was swept through the rest of the domain. There are three different parameters which control the mesh: the maximum size of the elements in the mapped mesh, number of elements in each layer of the geometry, and the number of elements in the PCM layer. A rendering of the final mesh is shown in Fig. 2.14.
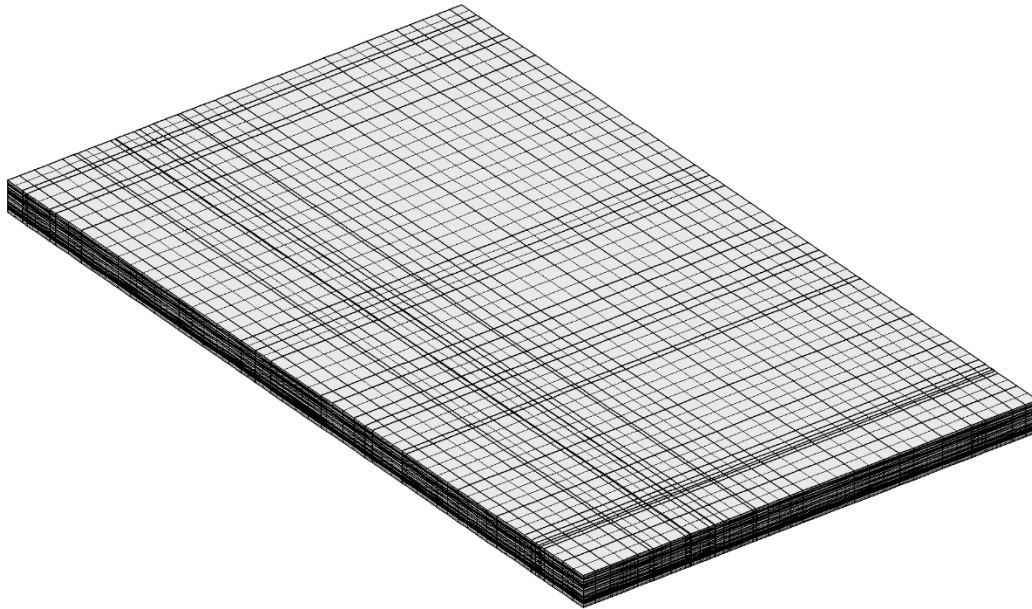
Fig. 2.14 Rendering of the selected mesh

When simulating the tablet without an LHTES module, the numerical simulation is a pure conduction problem. A mesh study was done on the simulation without PCM and it was found that the pure conduction simulation was insensitive to the size of the mapped mesh and the number of elements in each layer. It was found that 2 mesh elements in each of the layers was more than

sufficient to obtain mesh independence for the pure conduction simulation (see Appendix B). The mesh study is more complex with an LHTES module.

The number of elements through the width of the PCM layer and the size of the elements in the mapped mesh were determined using the following study. The mesh parameters and the resulting number of elements in each of the meshes tested are shown in Table 2.5. These simulations were done for a PCM with a transition temperature of 31.8°C. This low transition temperature was chosen to ensure that the rate and extent of melting was high. Seven simulations are presented here. They fall into two groups. Firstly, the number of layers in the PCM was increased from 2 to 32 with a mapped mesh size of 5 mm. Secondly, three different mapped mesh sizes were simulated (10 mm, 5 mm and 4 mm) with 16 elements in the PCM layer.

Table 2.5 Summary of the 9 meshes which were used in the mesh study

maximum size (mm)	# elements in PCM layer	# elements in other layers	Total elements
5	2	2	87320
5	4	2	101480
5	8	2	129800
5	16	2	186440
5	32	2	299720
10	16	2	87690
4	16	2	256197

Figures 2.15 to 2.17 show the transient temperature profiles on the back surface, front surface, and the SOC. In each of these simulations, the sources were turned on at $t = 0$ s and then were shut off after 30 minutes. Each of these plots show the average temperature and maximum temperature over the respective domains (surface average on the front and back, and a volume average for the SOC). Figure 2.18 shows the melt fraction of the PCM.

From a cursory observation of the temperature profiles, two key conclusions can be made. The temperatures of the system are relatively insensitive to mesh size, especially during the heating

phase. However, there is an impact in two places: at the end of the heating phase, and as the PCM begins to solidify.
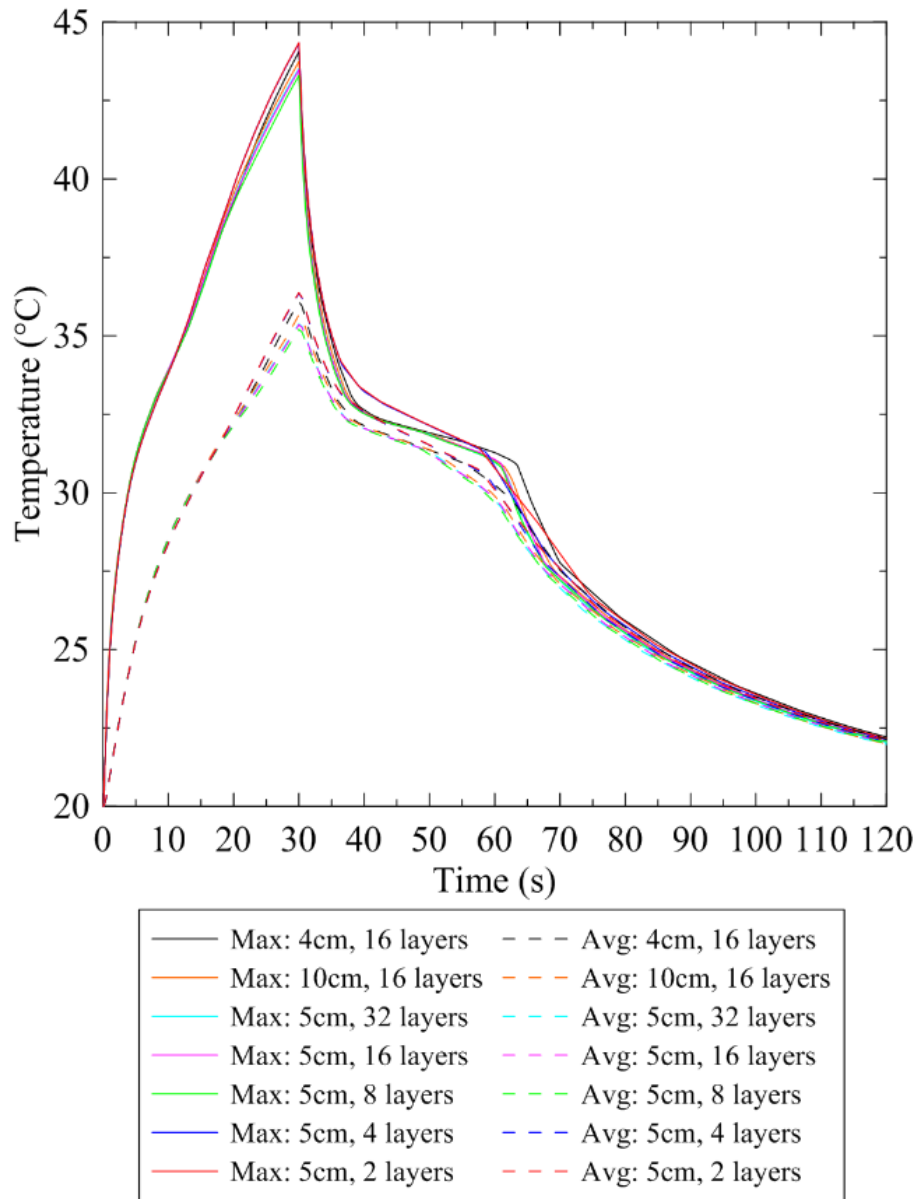
Fig. 2.15 Maximum and average back surface temperature
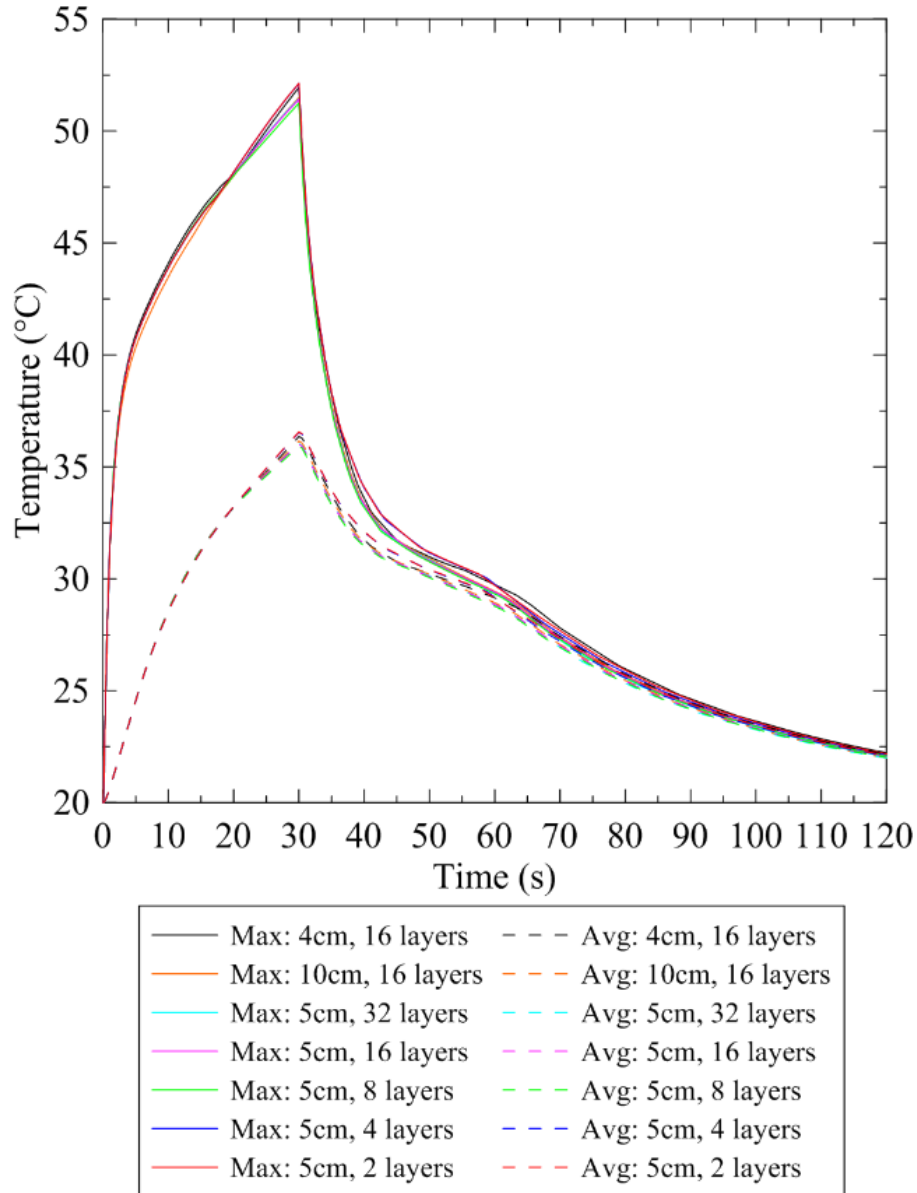
Fig. 2.16 Maximum and average front surface temperature

The impact during the solidification phase is seen in Fig. 2.18, there is a difference in the rate of solidification during the last 15 min of the simulation. The mesh is not fully converged in this region of the simulation, it appears that there is an interaction between the two mesh sizes. The computing resources were not available to simulate a finer mesh, so the results in the solidification region should be taken with this uncertainty in mind. The impact during the heating phase is of paramount interest, the core goal of these simulations is to compare the impact of different PCM transition temperatures. Comparing the heating phase with different transition temperatures is simple and relevant. All simulations start at the same state and experience the same heat flux.

35

However, comparing the cooling phases is more difficult as the state of each simulation when the heat flux is shut off is different. For this reason, the heating phase is of primary interest. Figures 2.19 to 2.22 focus on the heating ($t = 0$ to 30 min) phase of the simulations.
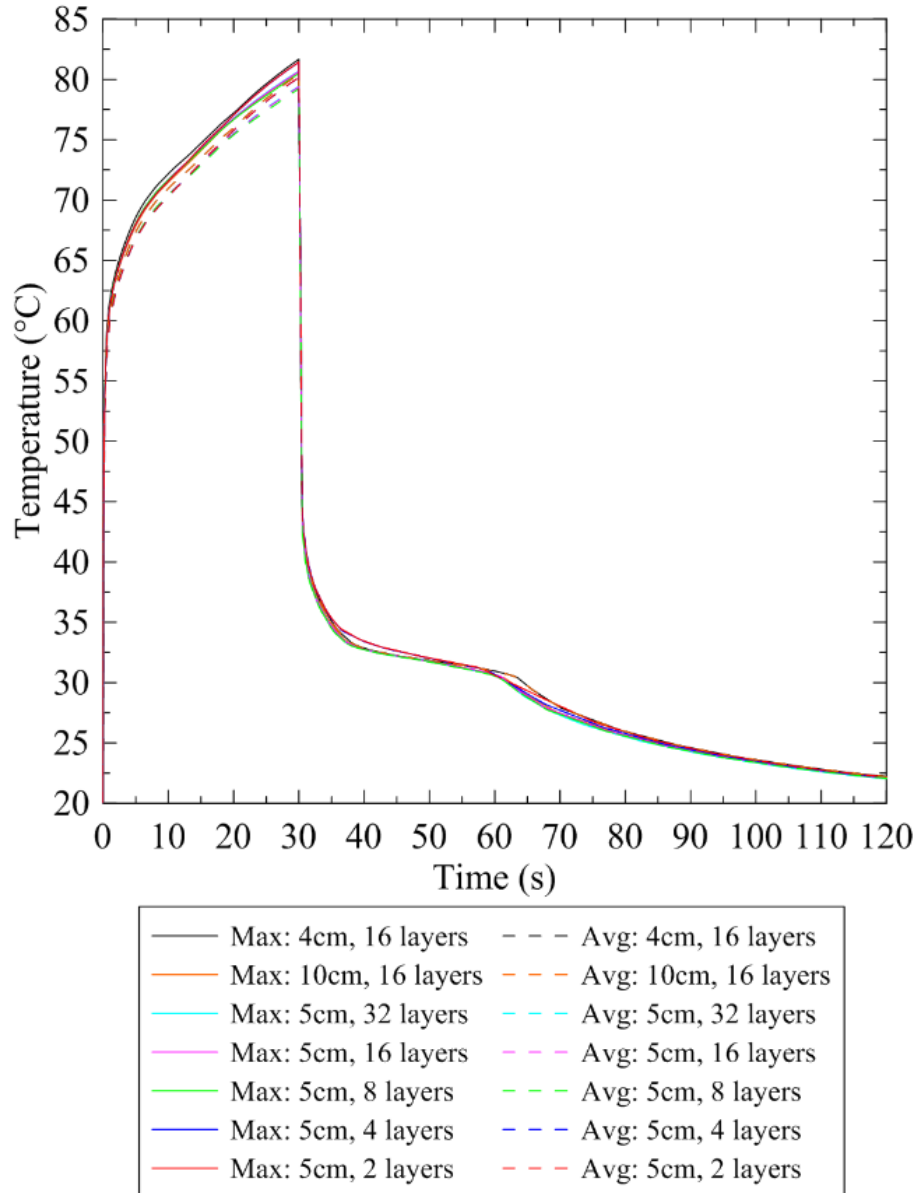
Fig. 2.17 Maximum and average SOC temperature
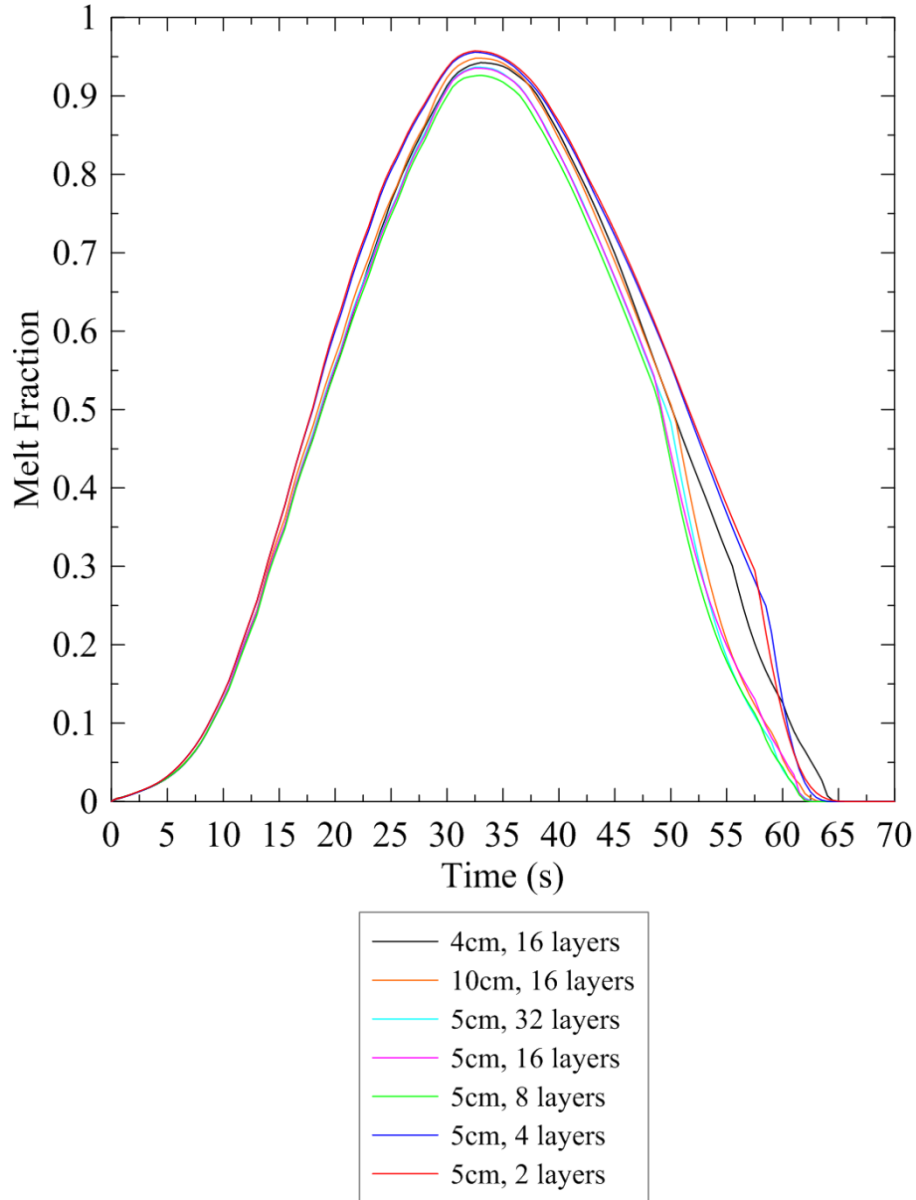
Fig. 2.18 Melt fraction (on a mass basis) of the PCM

Figures 2.19 to 2.21 show the temperature profiles for the back surface, front surface and SOC respectively. The three finest meshes (5cm, 16 layers; 5cm, 32 layers and 4cm, 16 layers) cluster together with little deviation. The course meshes do deviate but by only a small amount (though it is increasing near the end of the heating phase). From these results, it appears that in the heating phase the number of layers in the PCM is more critical than the mapped mesh size. The same trends can be seen in Fig. 2.22 which shows the melt fraction during the heating phase.

It was concluded that a mapped mesh size of 5 mm, 16 layers in the PCM and 2 layers in the rest of the domain was sufficient to provide mesh independent results during the heating phase. Results in the cooling phase will be physical and the temperature data may be used to discern general trends but is not completely independent of the mesh size.
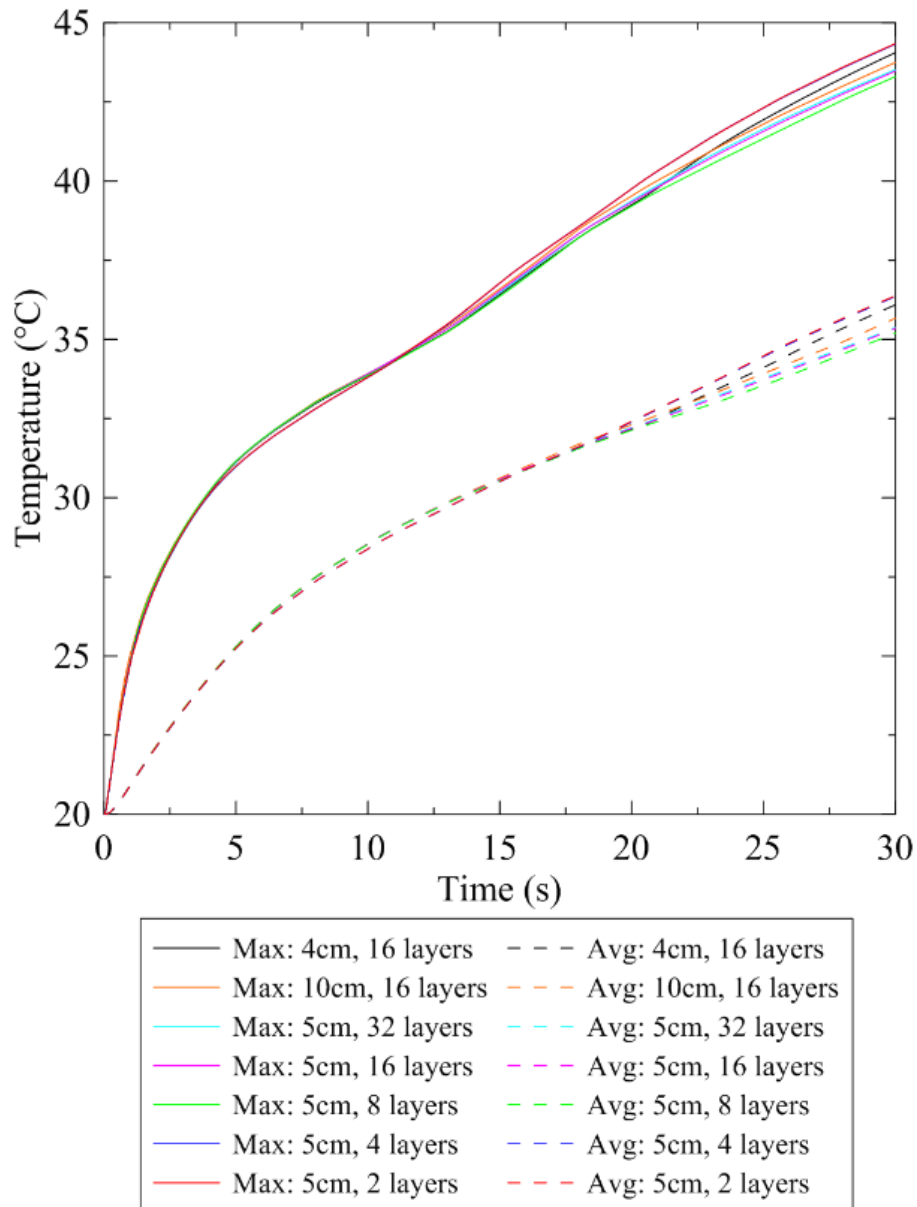
Fig. 2.19 Maximum and average temperature of the back surface of the tablet from the first 30 minutes of the simulation
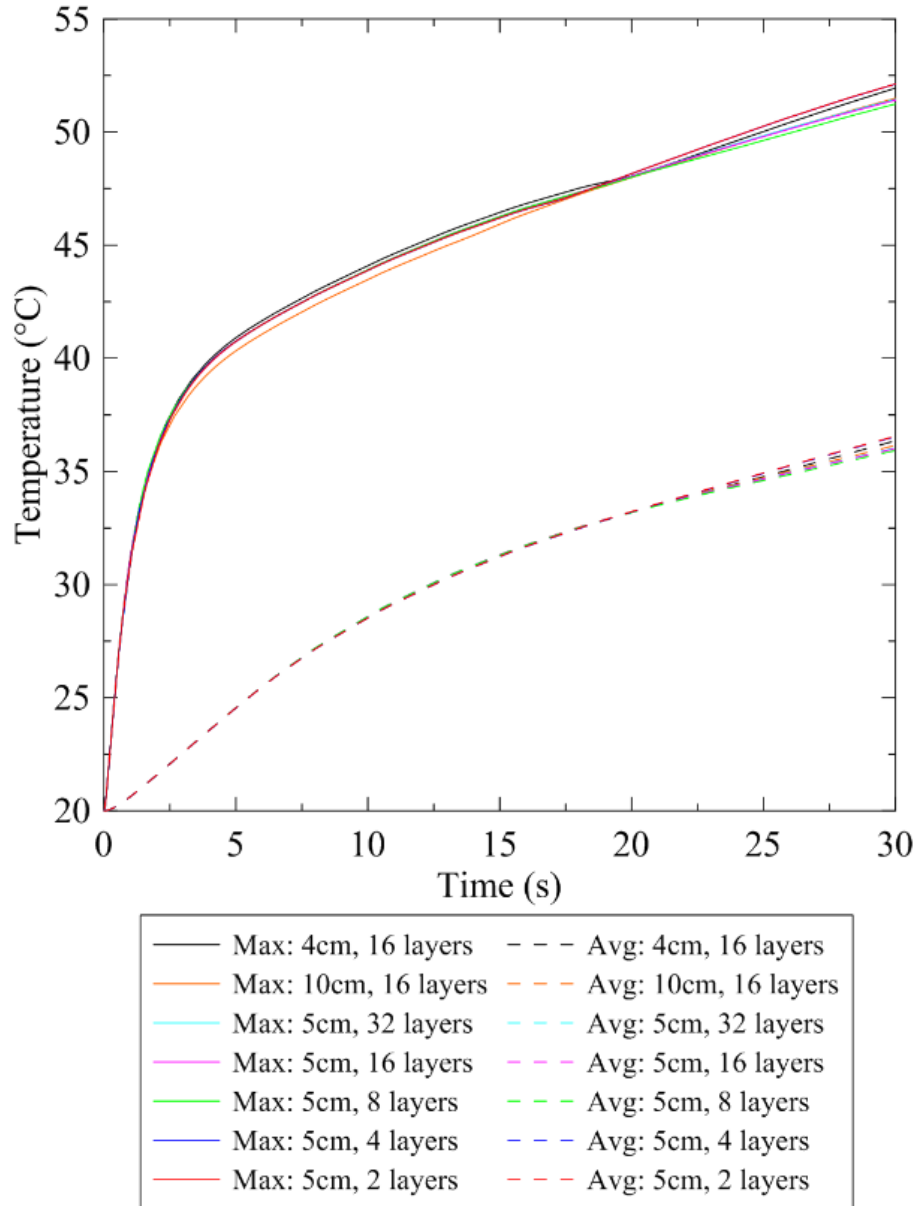
Fig. 2.20 Maximum and average temperature of the front surface of the tablet from the first 30 minutes of the simulation
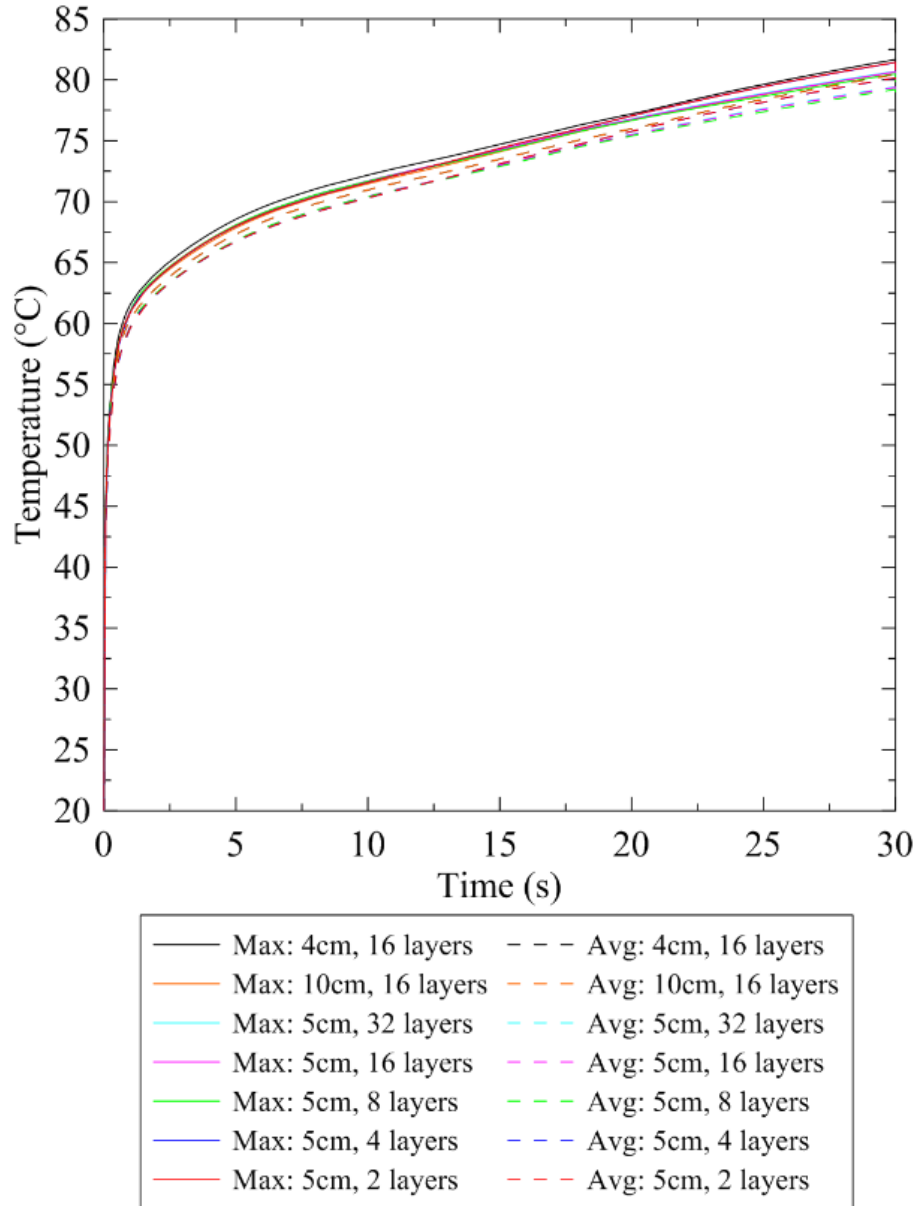
Fig. 2.21 Maximum and average temperature of the SOC from the first 30 minutes of the simulation
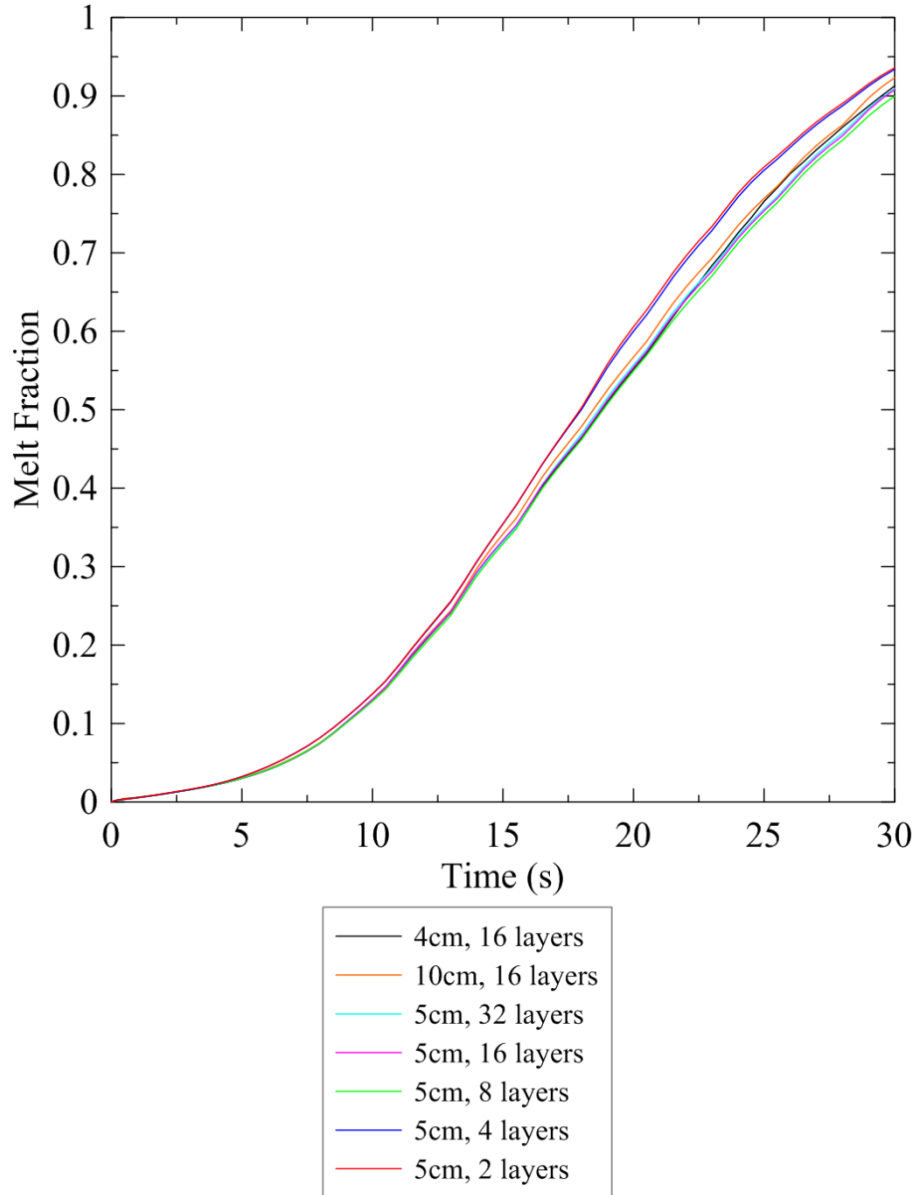
Fig. 2.22 Melt fraction of the PCM for the first 30 minutes of the simulation

2.2.5 Numerical Study

The numerical model and mesh described in the previous sections were used to perform nine simulations. Simulations were performed on a work station with two Intel Xeon E5-2630 v3 (8 cores @ 2.4 GHz) and 128 GB of RAM running COMSOL Multiphysics 5.3. Seven simulations were run with LHTES modules in the tablet. Each study included a heating phase where all the sources (see Table 2.2) were turned on for 45 min and a cooling phase where all of the sources were turned off for 75 min. The transition temperatures (T_m) studied were 35°C, 37°C, 39°C, 41°C,

43°C, 45°C, and 47°C. A simulation with no LHTES module installed was run (the LHTES module was replaced by an air gap). Finally, a simulation was run where the LHTES module was installed but does not undergo phase change, this is analogous to setting the heat of fusion to zero. This "No Melt" scenario is a key comparison case. The PCM's conductivity, and thermal mass will impact the temperature profile and this comparison case allows us to separate this effect from the impact of phase transition.

2.2.6 Results

These simulations had two goals: to make general observations of the heat transfer dynamics associated with an LHTES temperature control module in a tablet computer, and to determine what impact the transition temperature has on the performance of the LHTES module.

Figures 2.23 and 2.24 shows the average temperature and maximum temperature of the SOC respectively. The SOC domain is small and thin and has a uniform temperature distribution, therefore, maximum and average temperatures are similar. Transient temperature profiles show the expected features, a change of slope in the temperature profile as the LHTES module melts and when it solidifies. The peak value of both average and maximum temperatures are significantly reduced by the installation of the LHTES module. The LHTES module with the lowest transition temperature produced the largest reduction. While the improvement over the case with no LHTES module is large (~12°C), the improvement over the case without phase change, "No Melt" is much smaller (~2°C). This indicates that the latent heat of fusion is important but is not the most important factor impacting the peak temperature. The PCM has a low thermal conductivity but it is an order of magnitude larger than the empty air gap (at 300 K, 0.186 W/mK > 0.02624 W/mK). Filling the air gap with a more conductive material reduces the resistance to heat conduction from the internal sources to the tablet surface, reducing the SOC temperature.
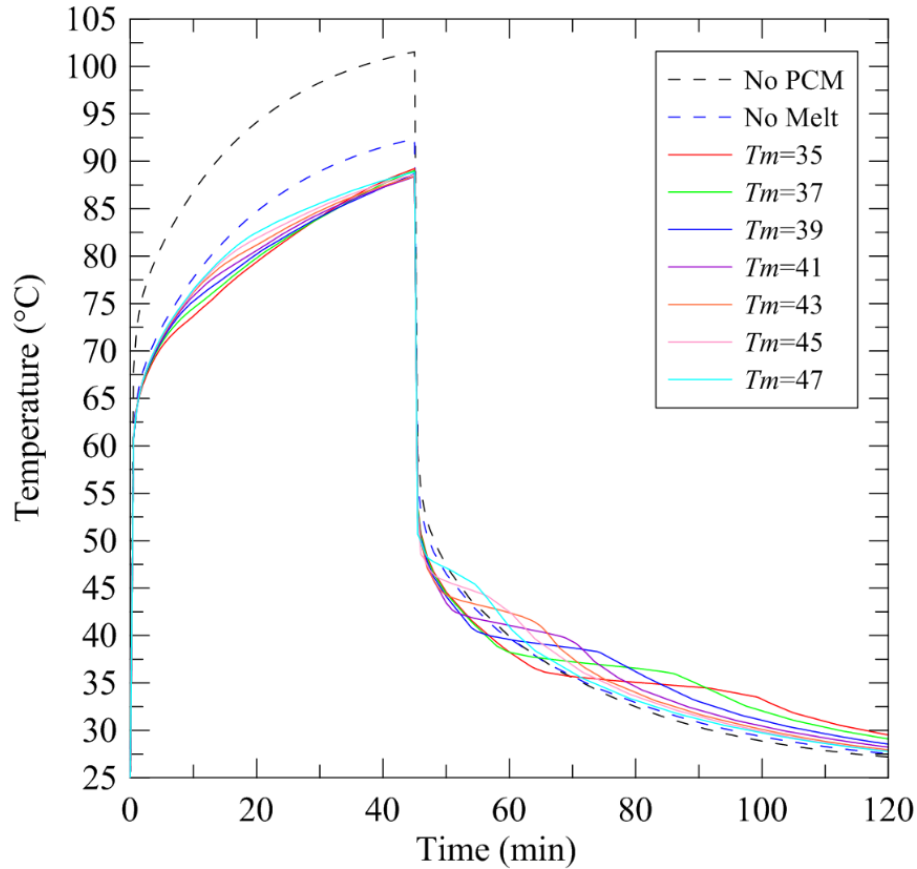
Fig. 2.23 Average SOC temperature produced by the numerical simulation

During the cooling phase, LHTES modules with low transition temperatures stay at an elevated temperature longer. Two factors contribute to this solidification delay. Firstly, the state at the end of the heating phase is different for each of the transition temperatures. Figure 2.25 shows the melt fraction during the simulation. Many higher transition temperature LHTES modules are not completely melted at the end of the heating phase and those which are completely melted will have a different sensible storage (seen in the delay before solidification commences in Fig. 2.25). Secondly, the LHTES module with a lower transition temperature will release its latent heat at a lower temperature and therefore will release it slower. From Fig. 2.25, the contribution of the reduced rate of solidification can be seen (the slope of the temperature profile at $T_m = 39°C$ is steeper than $T_m = 35°C$).
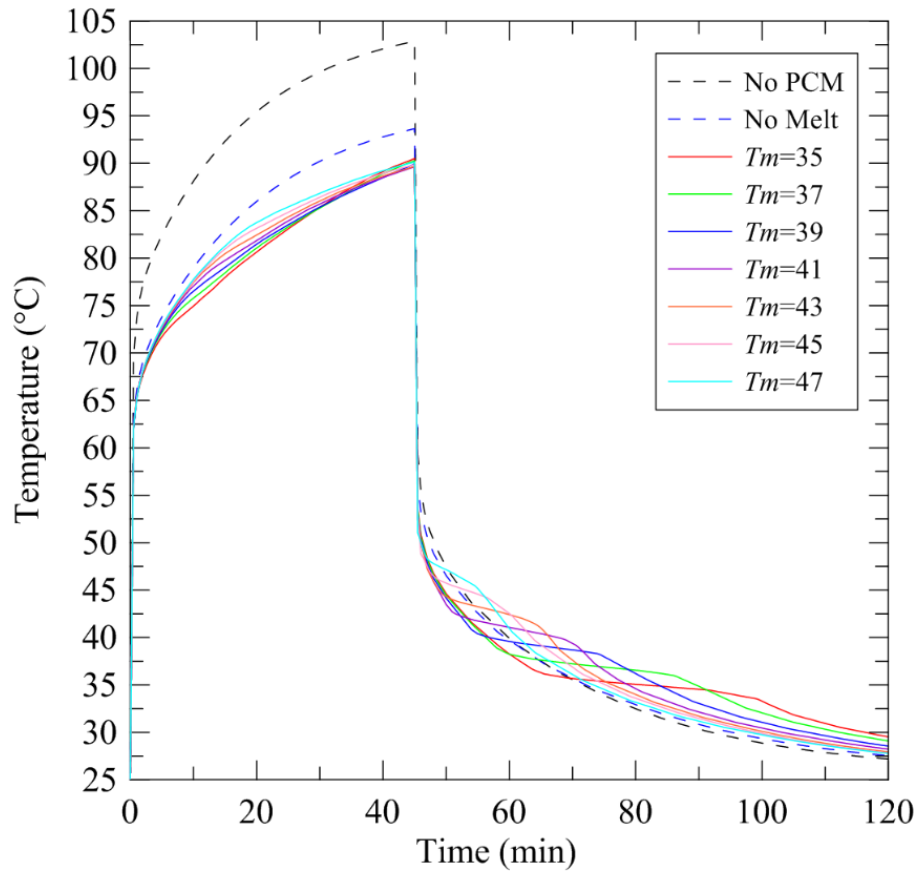
Fig. 2.24 Maximum SOC temperature produced by the numerical simulation
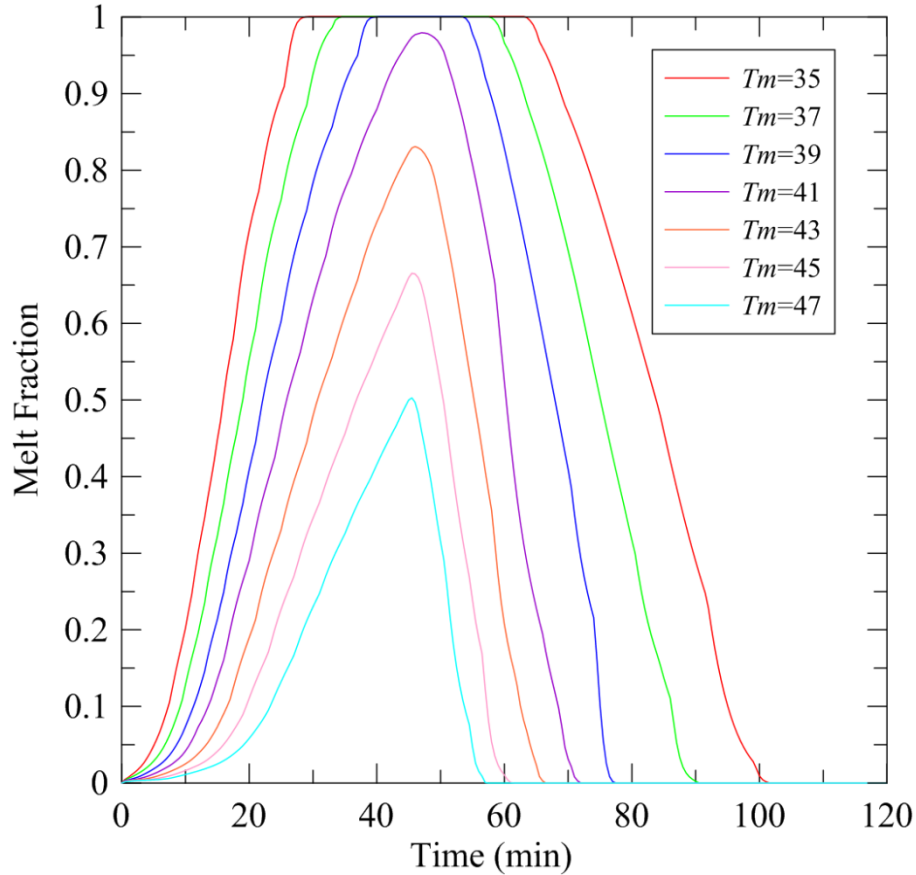
Fig. 2.25 Mass fraction of the PCM which is liquid during the numerical simulation

An interesting observation is that the rate of solidification is noticeably greater than the rate of melting for several of the higher temperature modules. The rate of solidification does decrease as the transition temperature decreases but only to a point marginally greater than the melting rate ($T_m = 35°C$ melted completely in 30 min and solidified over approximately 40 min).

Similar trends can be seen in the front cover temperature profile (see Figs. 2.26 and 2.27). The addition of the LHTES module reduces the peak temperatures of the front cover. The maximum temperature of the front surface (Fig. 2.28) is impacted by the LHTES module but only after it has exceeded the temperature which is comfortable for the user (approximately 40°C). Comparing the difference between the maximum and average temperature in the current tablet model, there is a substantial spreading issue at the front cover. This is inherent to the model, several of the sources (COGs) are close to the front surface and have no spreading material in between (see Fig. 2.28). The author would speculate that this is likely a simplification made by our industrial partners and may have been moderated by the addition of realistic contact resistances. Considering that the

PCM is on the opposite side of the tablet model, it is not surprising the LHTES module did not have a significant impact of the front surface.
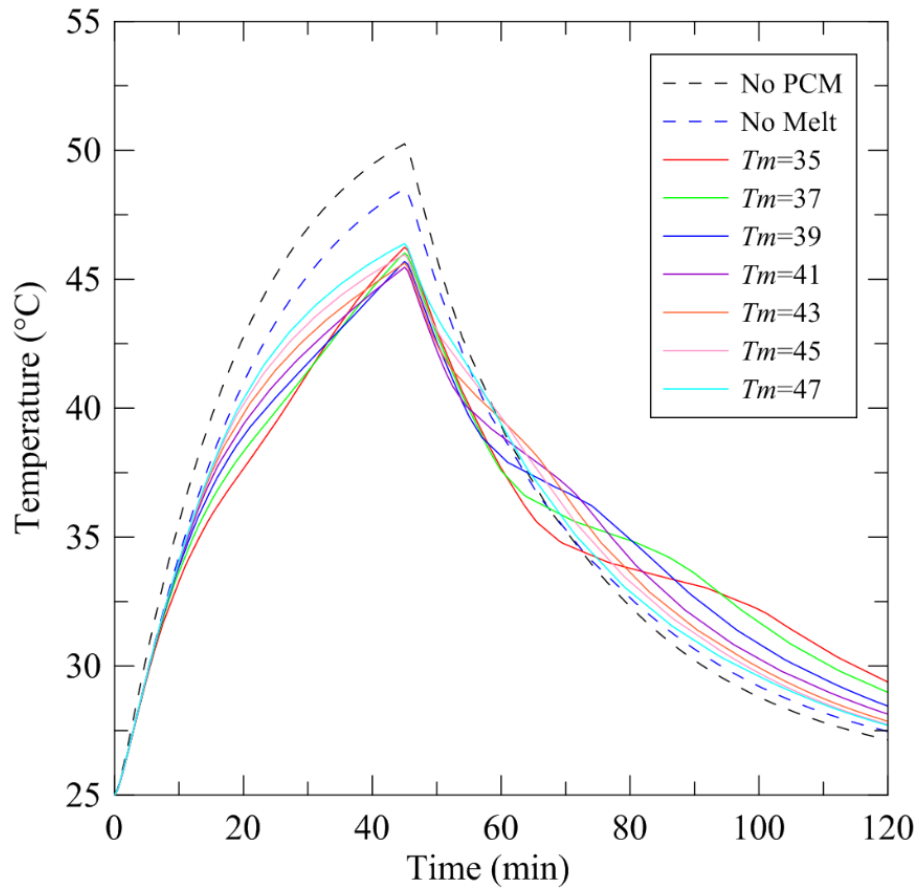
Fig. 2.26 Average front surface temperature produced by the numerical simulation
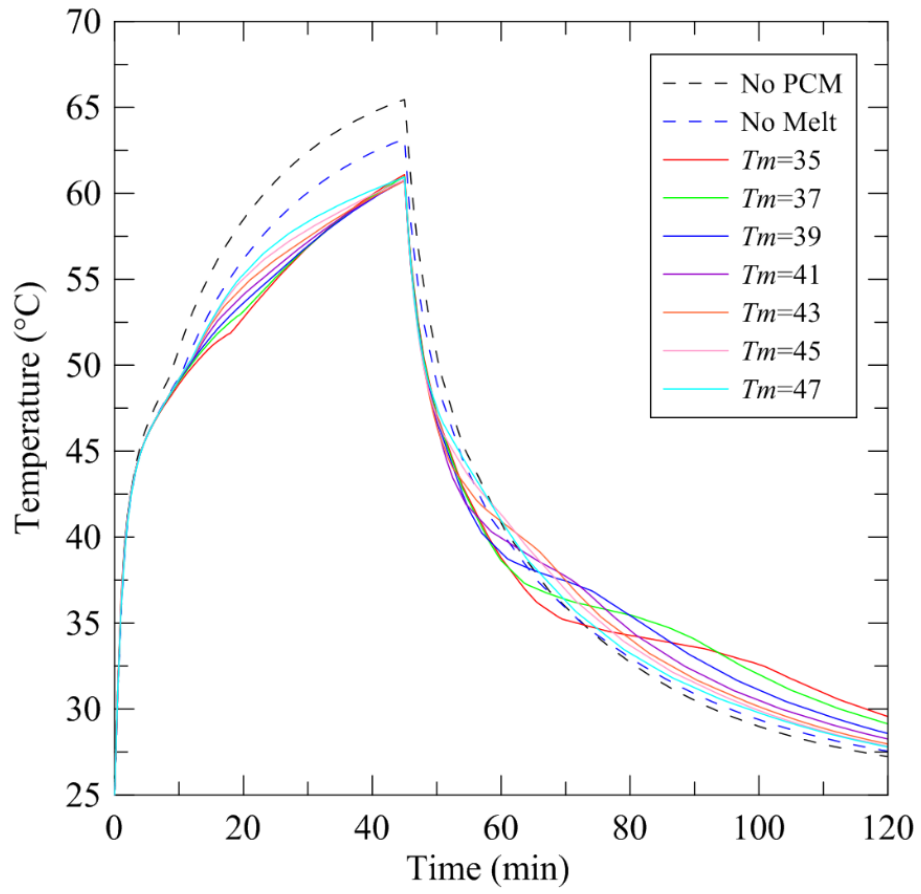
Fig. 2.27 Maximum front surface temperature produced by the numerical simulation
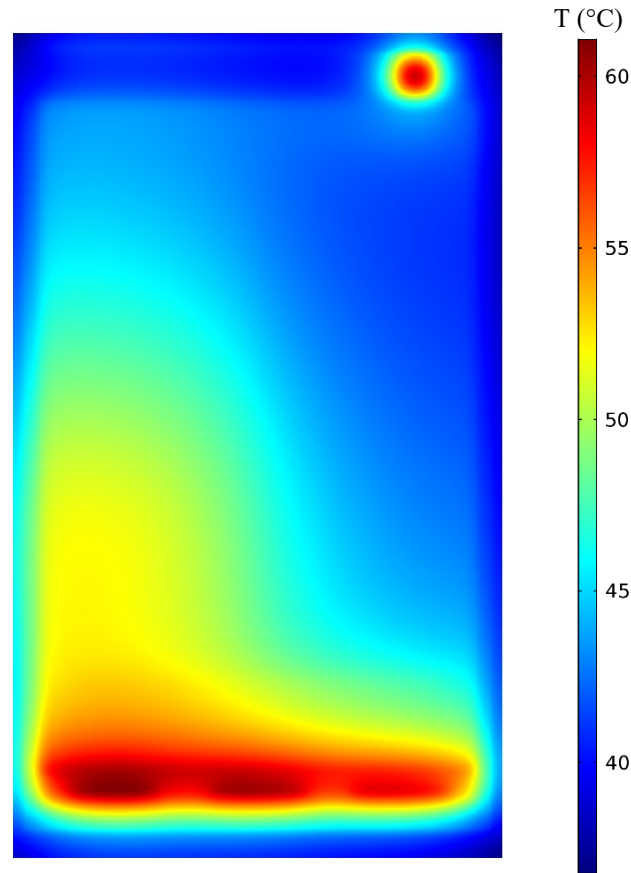
Fig. 2.28 Colour map showing the temperature (°C) distribution on the front surface for $T_m = 35°C$ at 45 minutes

Average temperature profiles for the back surface follow the same trends which were discussed for the SOC and front cover (see Fig. 2.29). The impact of the LHTES module is more visible because of its proximity to the back surface. However, there are several special features in the maximum temperature of the back surface (see Fig. 2.30). The "No Melt" and "No PCM" cases are inverted. Including a solid material between the source and the back cover reduces the resistance between the major sources and the back cover. This reduces the sources temperature but increases the back surface temperature. This same principle means that several of the LHTES modules increase the back surface temperature at some points in the simulation. It is difficult to quantify the relative performance of the LHTES modules from the full transient temperature plots. The core goal of an LHTES temperature control module is to delay the time which is takes for the handheld device to overheat. Overheat has a double meaning in this context, either the devices SOC reaches its design temperature, or the surface temperature of the device reaches a temperature

which is uncomfortable for the user. A real device which is at risk of overheating will then throttle the processor speed to avoid overheating. In this thesis, the maximum SOC temperature is taken as 80°C and the maximum surface temperature as 40°C.
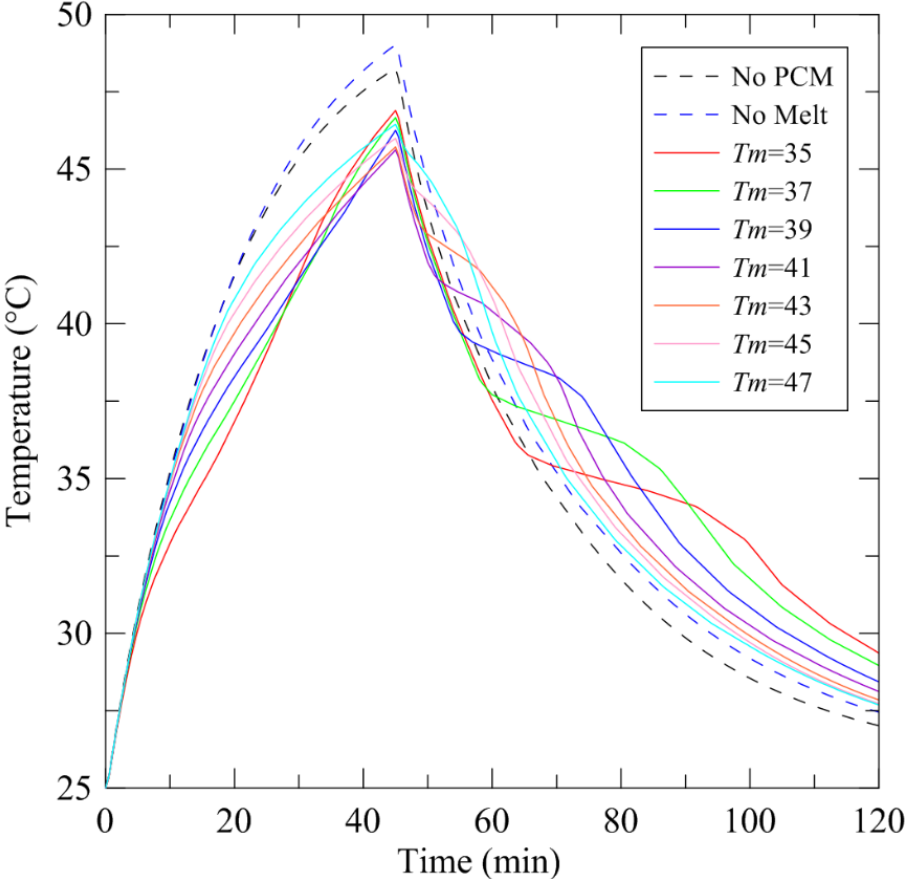
Fig. 2.29 Average back surface temperature produced by the numerical simulation
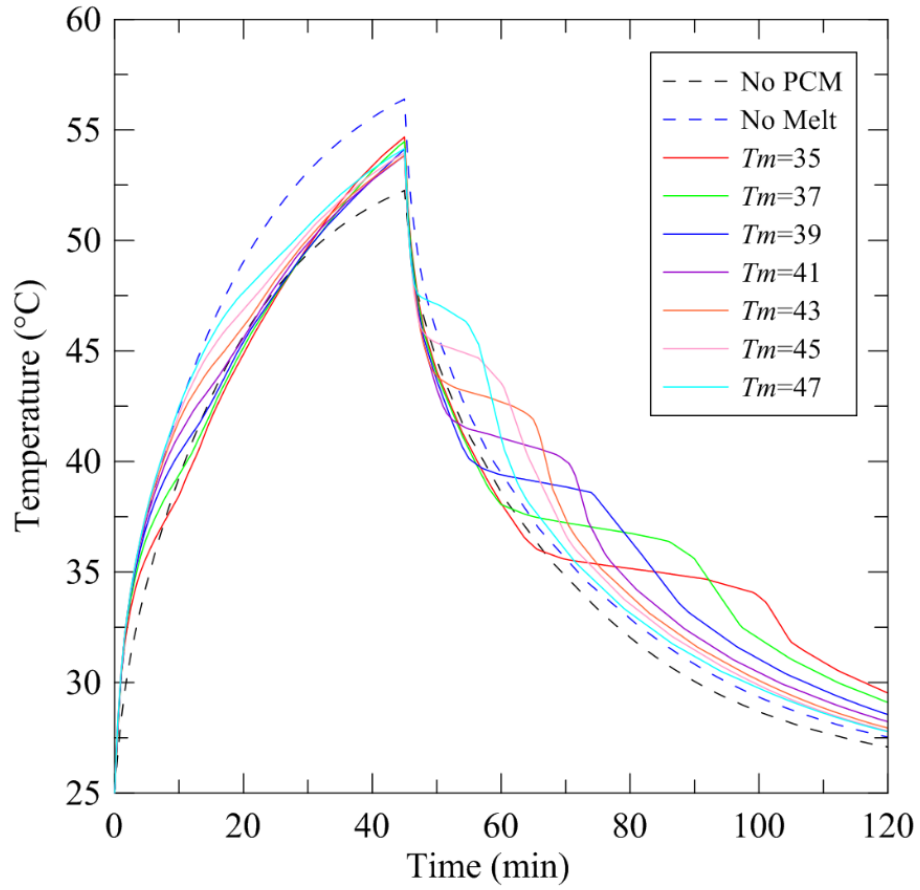
Fig. 2.30 Maximum back surface temperature produced by the numerical simulation
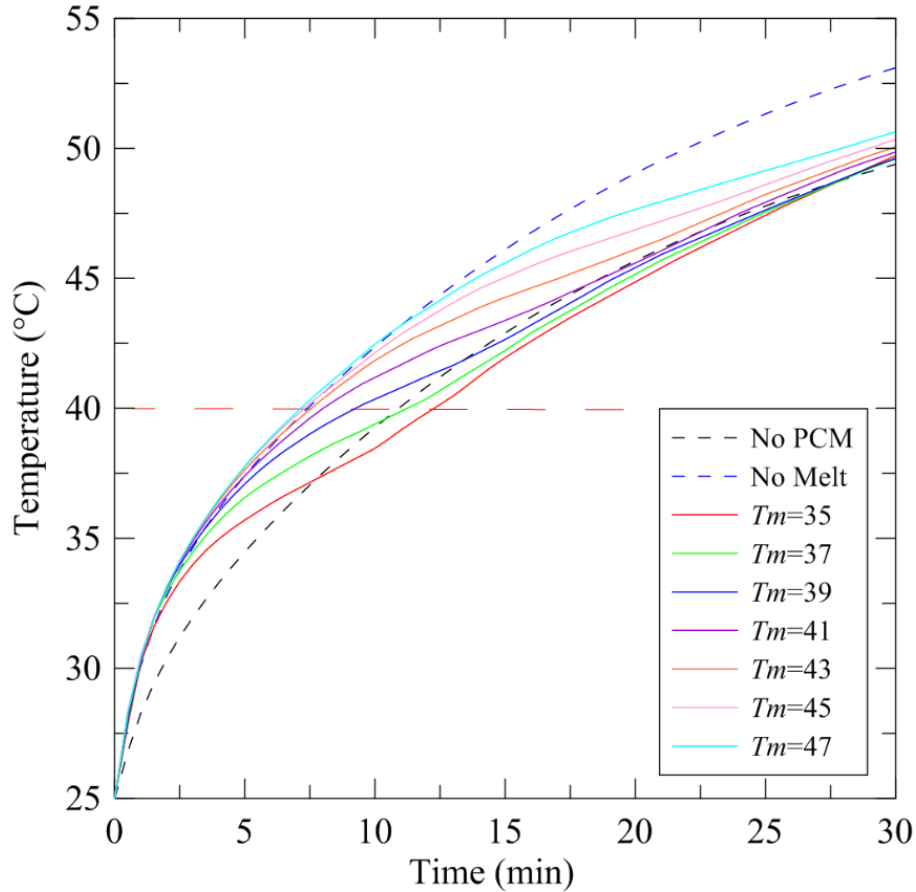
Fig. 2.31 Maximum back surface temperature (*t* = 0 to 30 min) produced by the numerical simulation

Figure 2.31 shows the maximum temperature of the back surface but focuses on the first 30 minutes of the simulation. The only transition temperatures which improve back surface temperature are $T_m = 35°C$ and $T_m = 37°C$. A simple way of further quantifying the difference between the simulations is to look at the "delay time". The delay time will be defined as the extra time the tablet can operate before it reaches 40°C when compared to the case with no LHTES module. Most delay times are negative for the back surface (see Fig. 2.32), however, the LHTES module with the lowest transition temperature is superior to having no LHTES by a small margin (< 2 min). The concept can be applied to the SOC by applying a temperature limit of 80°C (see Fig. 2.33).
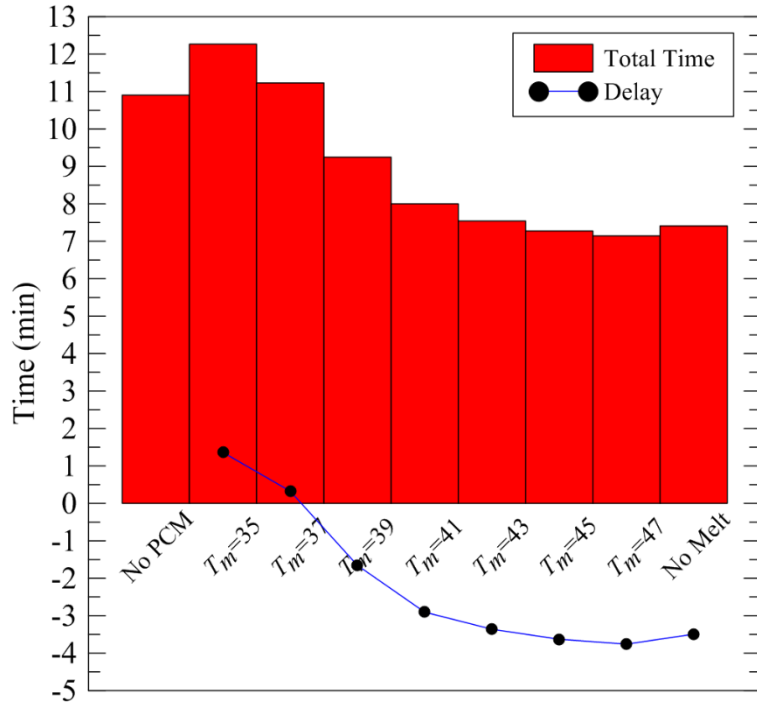
Fig. 2.32 Delay time for the back surface produced by the numerical simulation
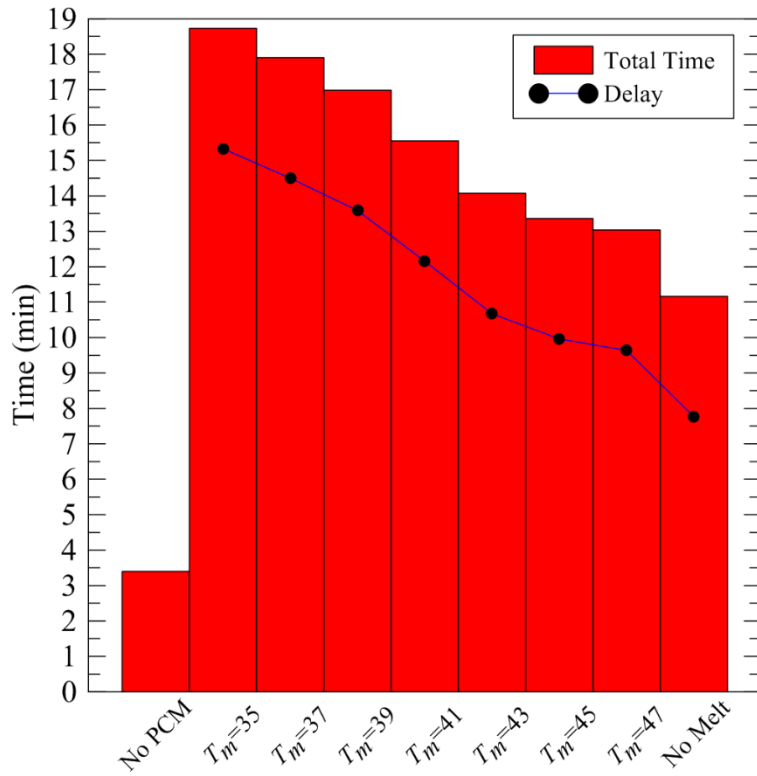
Fig. 2.33 Delay time for the SOC produced by the numerical simulation

52

The delay time for the SOC is more promising than for the back surface. All LHTES modules improve the SOC temperature but the unit with the lowest transition temperature is superior.

2.3 Concluding Remarks and PCM Selection

From the numerical simulations, a few conclusions can be drawn. Firstly, and perhaps most importantly, the optimal transition temperature for a LHTES temperature control module in the simulated tablet computer was 35°C. This conclusion is based on the temperature profiles and delay times during the heating phase. Lower transition temperatures increased the rate and extent of melting and resulted in the highest delay times for the both the SOC and the back surface. It was found that the low transition temperature LHTES delayed the average temperature of the front surface reaching 40°C but due to the hot spots did not delay the maximum temperature.

All findings indicate that the trend toward superior LHTES module performance should continue for even lower transition temperatures. However, lower transition temperatures increase the risk of unintended melting from ambient conditions (high ambient temperatures, direct sun, body temperature, etc.) As a result, the author has concluded that the range of transition temperatures which are of most interest to the application of LHTES temperature control modules is between 35°C and 40°C.

The conclusion that lower melting temperature LHTES modules offer superior temperature control to electronic devices agrees with work by Mahmoud *et al.* (2013) and disagreed with work by Fan *et al.* (2013). Both of these authors did an experimental investigation of different PCMs housed in hybrid heat sinks and based their analysis on the transient temperature history of the heat source alone. PCM was placed between the fins of an aluminum heatsink which was then placed onto a heat source. The dynamics of these systems are fundamentally different from those presented in this chapter.

Fan *et al.* (2013) conducted heating experiments at heat generation rates which are not applicable to handheld electronic devices (60 to 120 W) and used a fan to dissipate heat to the environment. They concluded, for this specific system, that PCMs with higher melting temperatures were providing better protection to the source. In such a high power system coupled with forced convection, the strategy is to bring the heat sink to the largest acceptable temperature that keeps

the source below the critical limit; this provides the largest temperature difference between the heat sink and the air, and therefore the largest rate of heat transfer out of this system. The use of a high transition temperature in a system operating at the maximum allowable limit will present further over-heating.

Mahmoud *et al.* (2013) used a hybrid heat sink system without a fan and heat generation rates which are in a range applicable to hand held devices (3 to 5 W). Mahmoud *et al.* (2013) found that the lower transition temperature PCMs began melting earlier and therefore had a larger impact on the temperature history of the heat source. This is similar to the results produced in this chapter. However, the PCMs used by Mahmoud *et al.* (2013) had different thermos-physical properties in addition to different transition temperatures. Isolating the contribution of other properties from the transition temperature is a challenge.

Moore *et al.* (2015) did a similar study on a larger tablet computer. The tablet computer which they simulated utilized forced convection and was larger than the handheld device which was simulated in this chapter. They concluded that LHTES modules having a lower transition temperature are superior. However, their analysis was based on the temperature profile of the CPU heat spreader. The exact location of this temperature is not given, the shape and size of the PCM module used was also not given. The work presented in this chapter is more complete and better executed than that presented by Moore *et al.* (2015).

Dr. Kahwaji working under Dr. Mary Anne White at Dalhousie University assembled a list of thirteen potential organic PCMs. Table 2.6 gives the transition temperatures of each material. Two of the materials fall within the transition temperature range identified by the numerical simulations: *n*-eicosane and PT37. The PCM *n*-eicosane is a pure paraffin ($C_{20}H_{42}$) and is widely used in PCM research. It has a transition temperature of 35.6°C which is in the range found to be optimal. PT37 is a commercial PCM produced by Entropy Solutions LLC (PureTemp) with a transition temperature of 36.4°C. Table 2.7 gives the thermo-physical properties of each selected materials.

Table 2.6 Transition temperatures of potential PCMs prepared by Dr. Kahwaji and Dr Mary Anne White and used with permission

PCM	T_{onset} (°C) ± 1.5 °C
nonadecane	31.8
decanoic (capric) acid	32.0
PT37	36.4
n-eicosane	37.5
dodecanoic (lauric) acid	43.6
Docosane	43.8
paraffin wax SA327204	48.2
paraffin wax SA327212	51.8
paraffin wax SA411663	57.7
octadecanoic (stearic) acid	68.4
tetradecanoic (myristic) acid	54.7
octadecanol	58.0
hexadecanoic (palmitic) acid	61.7

Table 2.7 Thermo-physical properties of selected PCMs.

Properties	*n*-eicosane	PT37
T_m	35.6 ± 1.5 °C	36.4 ± 1.5 °C
ΔH_{fusion}	239 ± 24 kJ/kg	206 ± 21 kJ.kg
$C_{p,s}$	1.8 ± 0.2 J/gK	1.8 ± 0.2 J/gK
$C_{p,l}$	2.3 ± 0.2 J/gK	2.1 ± 0.2 J/gK
k_s	0.46 ± 0.05 W/mK	0.28 ± 0.03 W/mK
k_l	0.15 ± 0.05 W/mK	-
ρ_s	780 kg/m^3	849 kg/m^3
ρ_l	765 kg/m^3	-

Note: All properties are from Ahmed *et al.* (2016) except the density and thermal conductivity of *n*-eicosane in the liquid state which are from Vélez *et al.* (2015)

An important physical dynamic which was seen in the simulations was the impact of the LHTES module on thermal resistance between the main sources and the back cover. Placing an LHTES module in the air gap between the main sources and the back surface reduced the thermal resistance between them. LHTES module with higher transition temperatures, which did not melt fast enough, had a negative impact on the temperature of the back surface. A poorly designed unit could potentially be worse than no unit at all.

While these conclusions will be useful moving forward, an experimental corroboration of these trends is required. There are several aspects of a real LHTES system which are difficult to include in the numerical simulation. For example, encapsulation and thermal contact resistance are both potentially important and challenging to accurately simulate numerically. A simplified experimental setup was designed which focuses on the charging and discharging of the LHTES modules. This setup and the results are presented in Chapter 3.

CHAPTER 3 EXPERIMENTAL INVESTIGATION OF LHTES MODULES USING A SIMPLIFIED SETUP

3.1 Overview

This chapter presents the experimental setup and results from an investigation of LHTES modules using a simplified setup. The author designed and built the experimental setup while Mr. Maranda, under the supervision of the author, completed experiments as a component of his master's thesis with the University of Lucerne, Switzerland. The primary goal of these studies was to experimentally investigate how thin LHTES modules behave when heated by a discrete heat source and to validate the numerical methods used to model thin PCM systems.

3.2 Experimental Setup

The experimental setup consisted of a Teflon base machined to create a square (152.4 mm (6 in) by 152.4 mm (6 in) by 2 mm deep) cavity on its upper surface. This cavity is the main test chamber where LHTES modules were placed for testing. The cavity was covered with a piece of nylon to simulate the outer surface of a handheld device. A copper heating block was constructed from a cylindrical piece of copper (25.4 mm (1 in) in diameter) which had a cylindrical cavity bored into one side where a cartridge heater was inserted. This copper heating block was then press fit into a hole in the Teflon base so that its top surface was flush with the bottom of the test cavity. The bottom of the Teflon base and the back side of the copper heater block are well insulated with ceramic fibre insulation. Figure 3.1 shows an exploded view of the setup. Photographs of the setup are shown in Figs. 3.2 and 3.3.
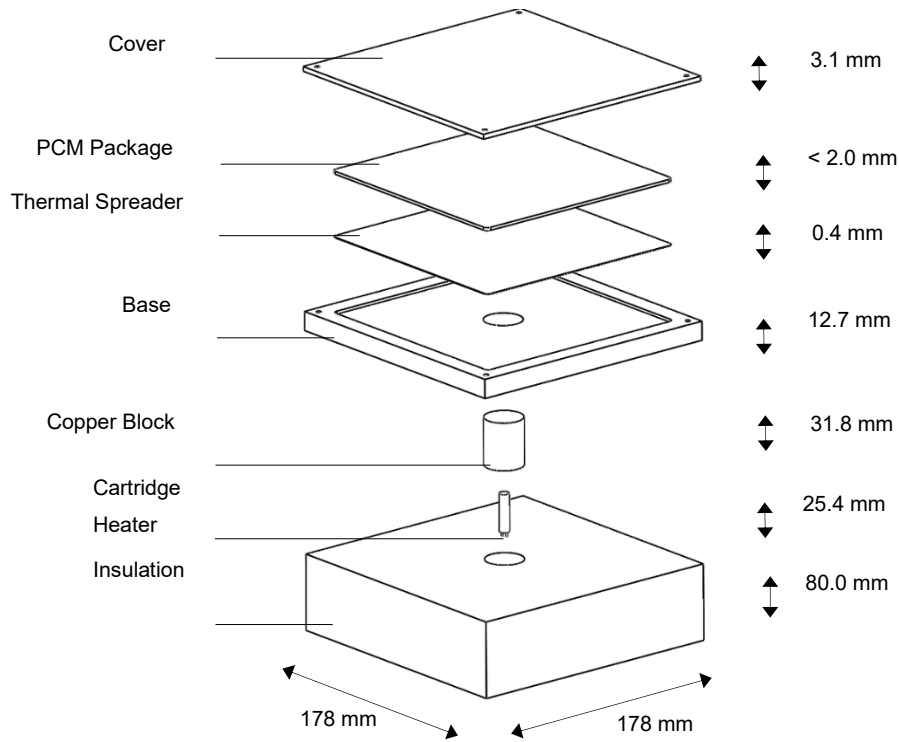
Fig. 3.1 Exploded view of the simplified experimental setup (Maranda, 2017)
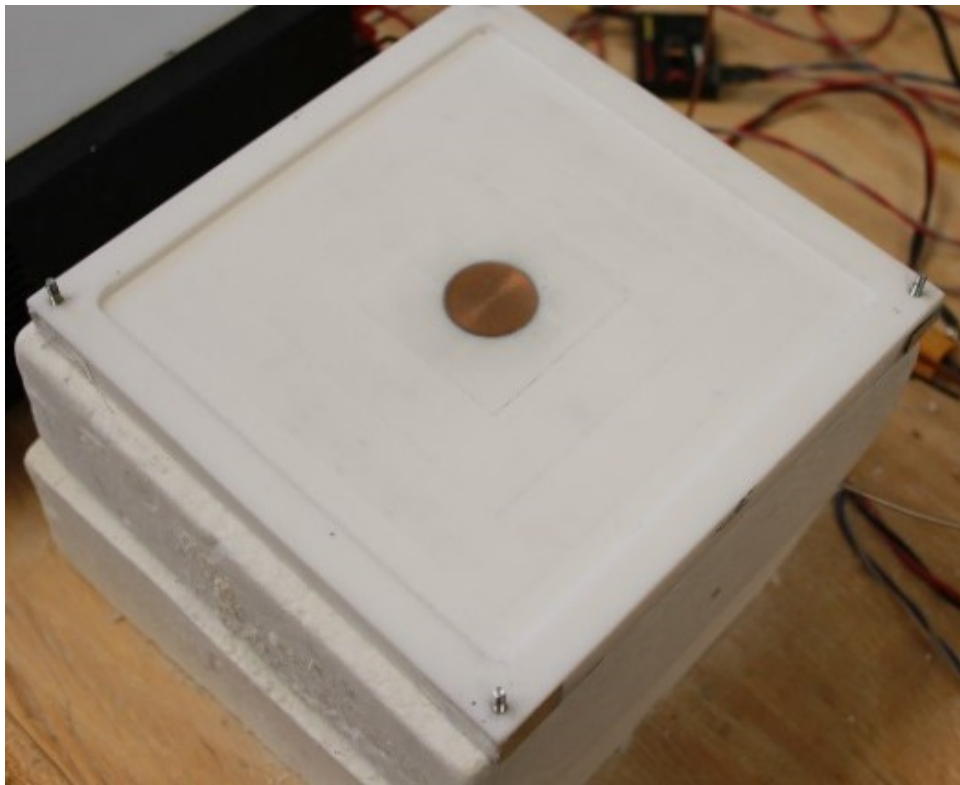
Fig. 3.2 photograph of the experimental setup with nylon cover removed (Maranda, 2017)

58
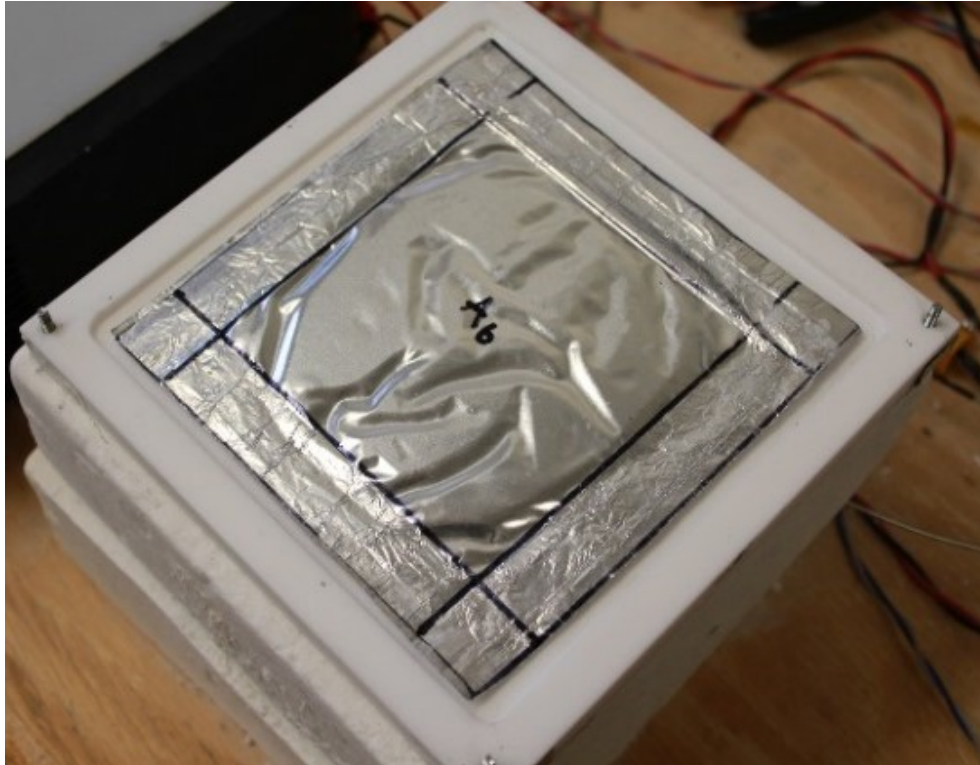
Fig. 3.3 Photograph of the experimental setup with nylon cover removed and an LHTES module placed in the test chamber (Maranda, 2017)

3.3 LHTES Modules

The method for manufacturing LHTES modules, used by Mr. Maranda, was developed by the author and was also used in the experimental work presented in Chapter 5. A more detailed description of the method and setup is presented in Chapter 5.

The LHTES modules consisted of a PCM encapsulated in heat sealable laminated film. This encapsulation material is made from a thin aluminum foil, nylon and polyethylene layers laminated together. Two pieces of film are placed together, heat is applied, and the polymer between the two pieces of film melt, fusing to form a tight seal. Controlling the thickness of the LHTES modules is important, therefore, a special setup was created to facilitate their manufacture. First, two pieces of the laminated film are placed together and sealed at three of the four edges. This creates what it essentially a small bag, which is then inserted into a jig. The jig consists of two aluminum plates separated by a precise distance using shims, the LHTES package is secured between these plates using masking tape. The jig and LHTES package are then placed into a hot water bath with water

temperature above the transition temperature of the PCM being used. PCM is injected into the LHTES package through the top opening using a syringe and blunted needle. When filled with PCM the jig is placed in cold water to allow the PCM to solidify. Once solidified the LHTES package is removed from the jig and the top of the package is heat sealed closed. This process produces LHTES modules with a maximum thickness which is precisely controlled. However, as can be seen from Fig. 3.4, the LHTES modules have an irregular surface topography when they are solidified. This is a result of two different factors. First, the packaging material is quite ridged, it cannot stretch to form the cavity for the PCM, causing the package material to crease as it distorts to accommodate the PCM. Second, the packages are filled with liquid PCM which will then contract as it solidifies exacerbating the wrinkly look of the packages.

The LHTES modules which were produced for these experiments were approximately 120 mm by 120 mm with a 10 mm border where the packages were heat sealed. Therefore, the part of the LHTES which contains PCM is approximately 100 mm by 100 mm and has a maximum thickness of 2 mm.
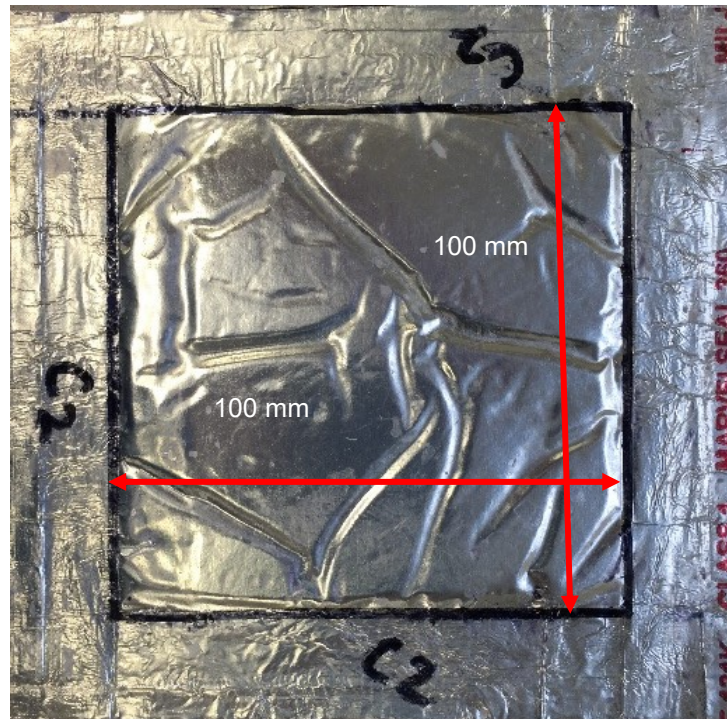
Fig. 3.4 Photograph of an LHTES module tested by Mr. Maranda (Maranda, 2017)

Two LHTES modules were built and tested: one containing *n*-eicosane and the other dodecanoic acid. The PCM *n*-eicosane is a pure paraffin ($C_{20}H_{42}$) and is widely used in PCM research. It has

a transition temperature of 35.6°C which is within the optimal range identified by the numerical simulations (see Chapter 2). Dodecanoic acid is a fatty acid which has been used extensively in large scale thermal storage applications at the LAMTE, with a transition temperature of 43°C. The high transition temperature of dodecanoic acid made for an interesting comparison to n-eicosane. Table 3.1 gives the thermo-physical properties of the PCMs used. The mass and storage capacity of each of the two packages are shown in Table 3.2.

Table 3.1 Thermo-physical properties of *n*-eicosane and dodecanoic acid.

Properties	dodecanoic acid	*n*-eicosane
T_m	43 ± 1.5 °C	35.6 ± 1.5 °C
ΔH_{fusion}	184 ± 9 kJ/kg	239 ± 24 kJ/kg
$C_{p,s}$	2.4 ± 0.2 J/gK	1.8 ± 0.2 J/gK
$C_{p,l}$	1.95 ± 0.03 J/gK	2.3 ± 0.2 J/gK
k_s	0.15 ± 0.004 W/mK	0.46 ± 0.05 W/mK
k_l	0.17 ± 0.004 W/mK	0.15 ± 0.05 W/mK
ρ_s	930 ± 20 kg/m^3	780 kg/m^3
ρ_l	874 kg/m^3	765 kg/m^3

Note: Properties of the dodecanoic acid are from Desgrosseilliers *et al.* (2013). Properties of *n*-eicosane are from Ahmed *et al.* (2016) except the density and thermal conductivity of *n*-eicosane in the liquid state are from Vélez *et al.* (2015)

Table 3.2 Properties of the two LHTES modules

PCM package	PCM	PCM mass (g)	Volume solid (ml)	Volume liquid (ml)	Latent storage capacity (J)	Total storage capacity for $\Delta T = 50$°C (J)
A	*n*-eicosane	10.4	13.3	13.6	2730	3600
B	dodecanoic acid	12.4	13.3	14.2	2486	3569

In addition to the LHTES module described above, some experiments included a heat spreader consisting of a thin aluminum plate placed between the heater and the encapsulated PCM. The plate was 100 mm by 100 mm by 0.4 mm thick and its properties are summarized in Table 3.3.

Table 3.3 Properties of the aluminum spreader

Material	Mass (g)	Volume (ml)	k_s (W/mK)	$C_{p,s}$ (J/gK)	ρ_s (kg/m³)	Total storage capacity for $\Delta T = 50$°C (J)
Aluminum 6061	11.3	4	167	896	2700	506.24

3.4 Instrumentation

A total of 15 T-type thermocouples were used to measure temperatures at locations throughout the experimental setup. Sensors were placed on the top of the cover, on the LHTES module and a 1/16" stainless steel probe was placed into a hole in the base of the heater block to measure its temperature. All temperature sensors have an uncertainty of ±0.5°C. Figures 3.5 to 3.8 show the locations and designations of each of the sensors used in the setup.
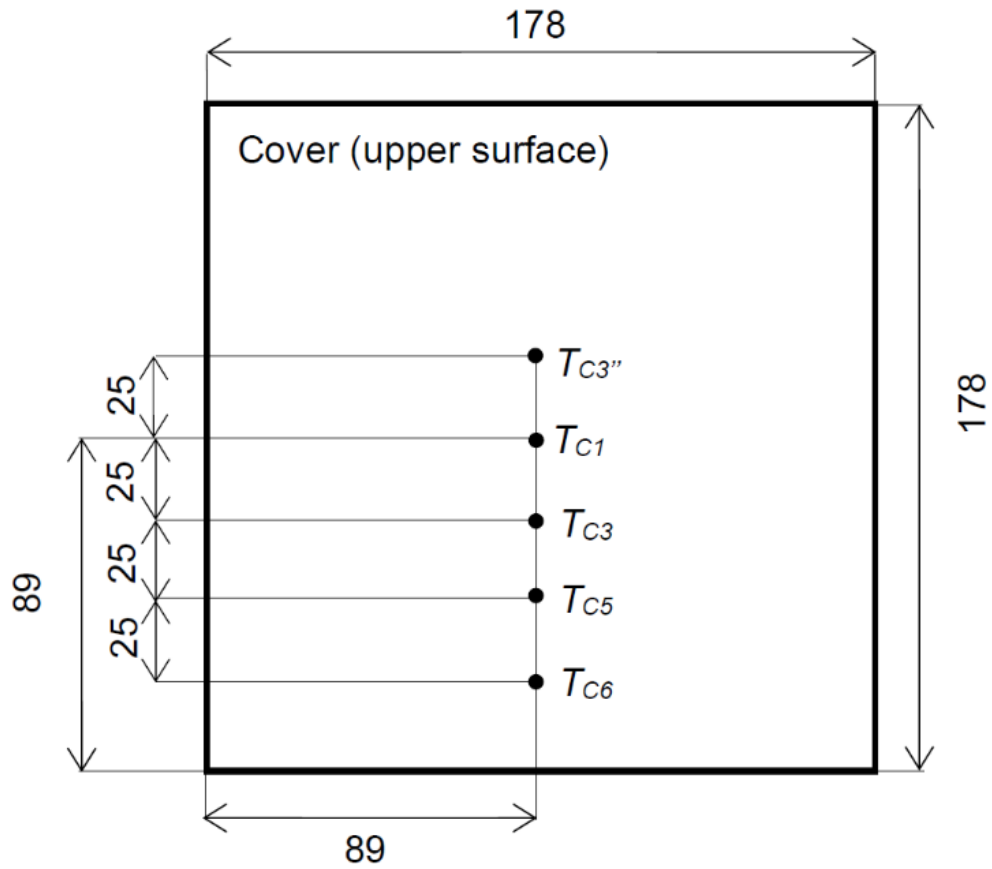
Fig. 3.5 Locations and designations of the thermocouples located on the cover of the setup, dimensions are given in mm (Maranda, 2017)
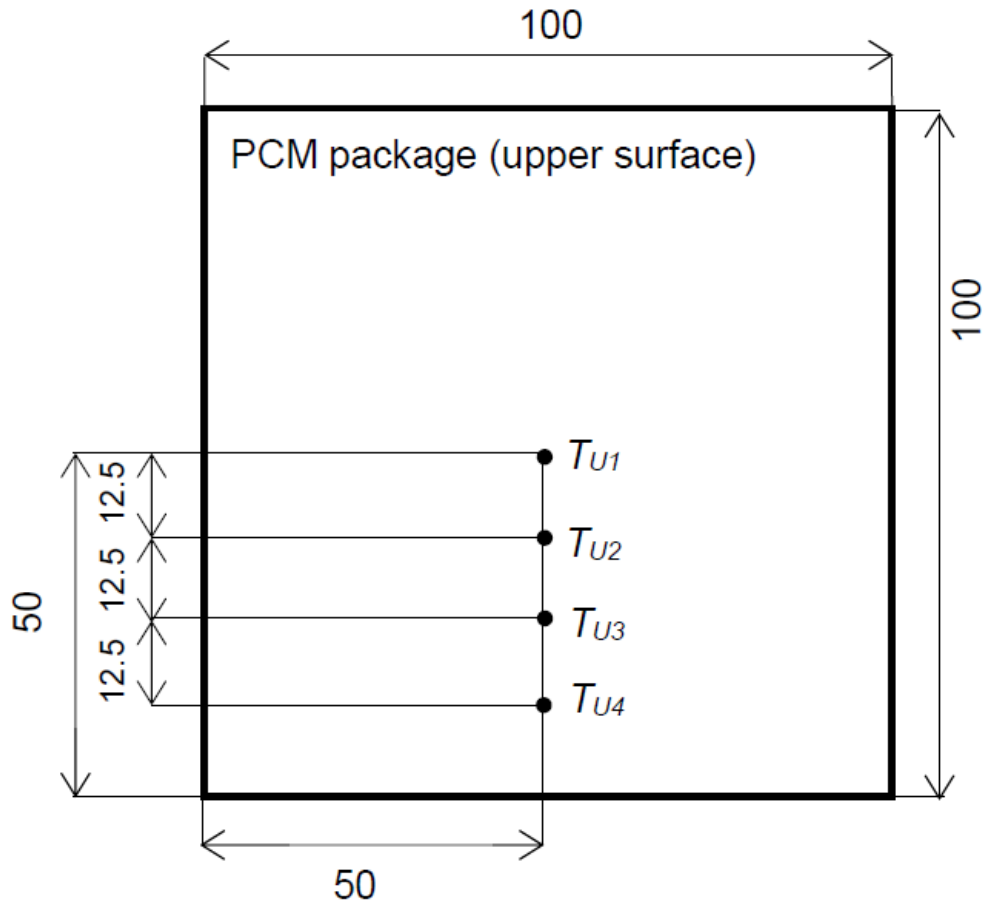
Fig. 3.6 Locations and designations of the thermocouples located on the top of the LHTES module, dimensions are given in mm (Maranda, 2017)
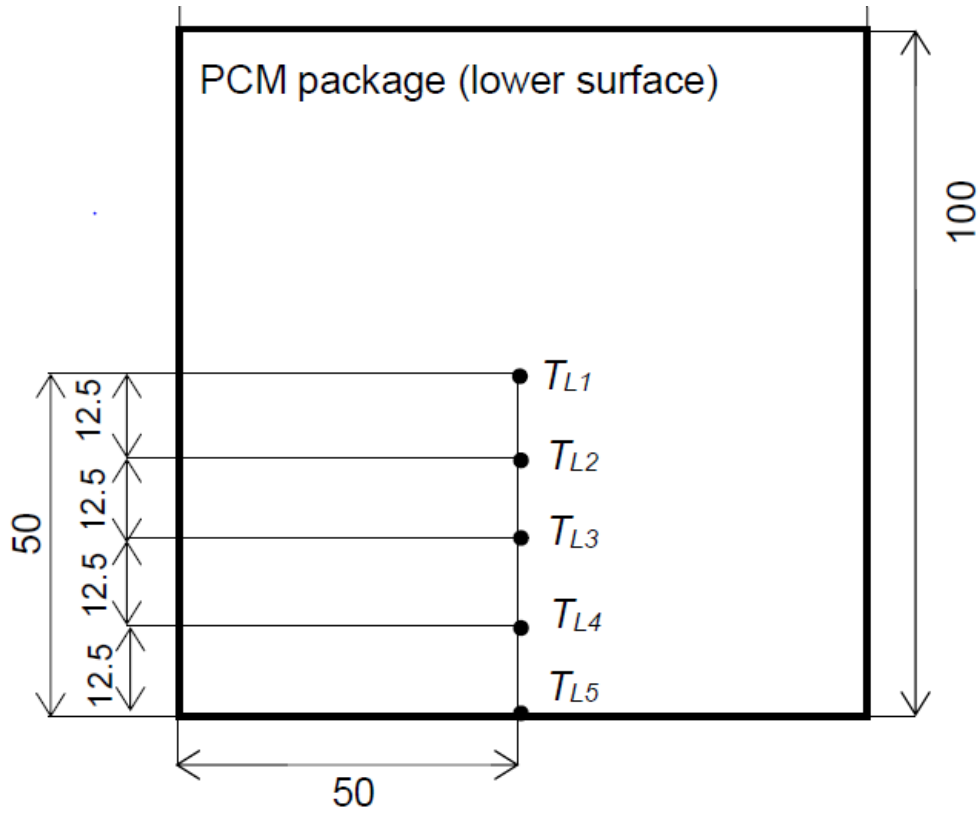
Fig. 3.7 Locations and designations of the thermocouples located on the bottom of the LHTES module, dimensions are given in mm (Maranda, 2017)
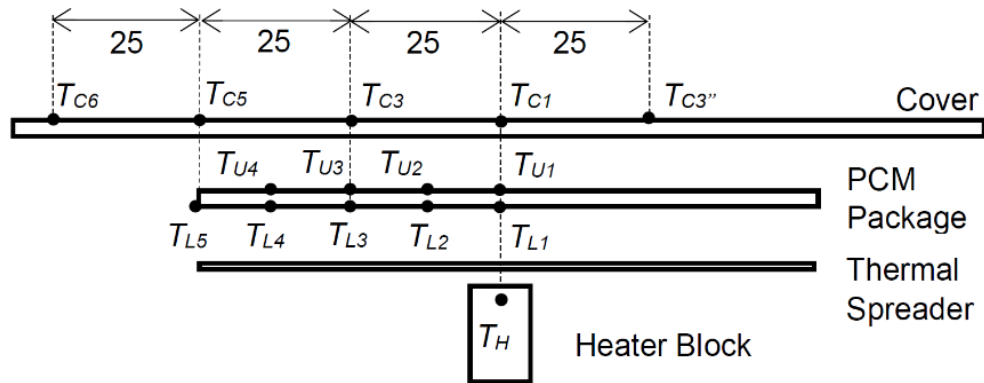
Fig. 3.8 Locations and designations of the thermocouples as seem from a side view of the setup, dimensions are given in mm (Maranda, 2017)

65

3.5 Results

Here is a summary of the most applicable experimental results from the work performed by Mr. Maranda. More detail is provided in his thesis (Maranda, 2017). A total of six experiments were done with a steady heat input of 5 W. The power to the heater was held constant during a heating phase and was then set to 0 W for a cooling phase. These experiments are of the same structure as those done numerically. Table 3.4 summarizes the experiment details. This summary will focus on the comparison of T_{C1} (located on the cover directly above the heater and closely approximating the maximum cover temperature) and the heater temperature T_H for each of three cases: no LHTES module, module A (*n*-eicosane) and module B (dodecanoic acid). In addition, the impact of the heat spreader was also studied.

Table 3.4 Details of each of the steady power experiments

	Package	Thermal spreader	P (W)	t_{on} (min)	t_{off} (min)
# 1	-	-	5	60	120
# 2	A	-	5	60	120
# 3	B	-	5	60	120
# 4	-	Aluminium (0.4 mm)	5	120	120
# 5	A	Aluminium (0.4 mm)	5	120	120
# 6	B	Aluminium (0.4 mm)	5	120	120

Figure 3.9 shows the comparison of experiments with no heat spreader (experiments 1 to 3 from Table 3.4). As expected, the LHTES modules reduced the heater temperature but they also noticeably improve the cover temperature. The inflections in the temperature profiles are subtler in these experiments than they appeared in the numerical simulations (Chapter 2) but they are visible. This could indicate that there is not as much melting as was seen in the numerical simulations. It is difficult to characterize the melt fraction in an experiment but by looking at the outputs from the thermocouples on the LHTES module, an idea of the extent of melting can be ascertained. Figure 3.10 shows the temperatures measured on the LHTES module designated package A (*n*-eicosane). If the temperature measured on matching sensors on the top and bottom of the module are both reading above the transition temperature then it is quite certain that the melting front has moved beyond those sensors, the opposite is true if both are below the transition

temperature. Figure 3.10 shows the melting front has passed the T_{U3}/T_{L3} pair but has not passed the T_{U4}/T_{L4} pair. Indicating there has been significant melting but the LHTES is far from being fully melted.

The observation that both LHTES modules are reducing the heater and cover temperature contrasts with the results of the numerical simulations. It is possible this was due to the impact of contact resistance increasing the amount of spreading which was taking place in the LHTES module.
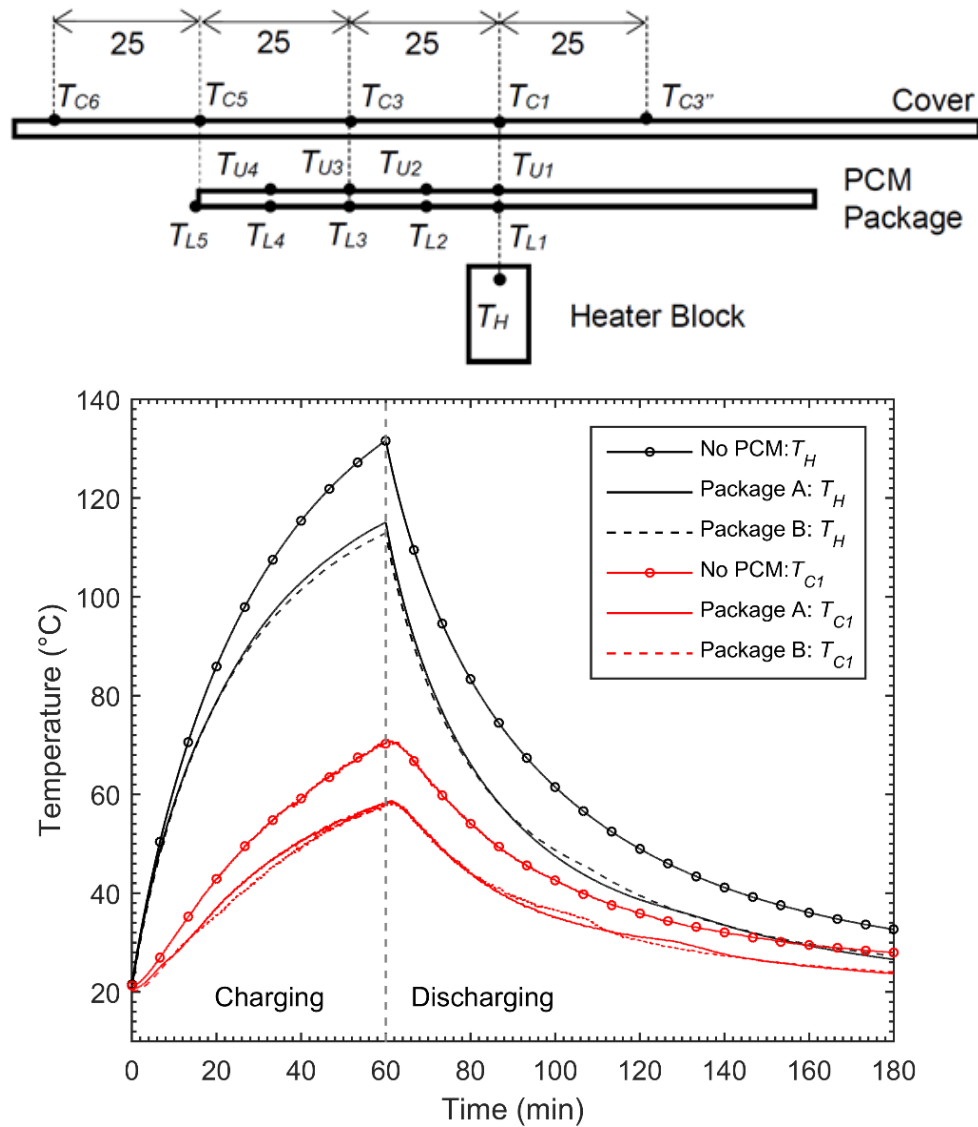
Fig. 3.9 Comparison of the maximum cover temperature (T_{C1}) and heater temperature (T_H) for experiments with no PCM, package A, and package B with out the aluminum heat spreader installed (Maranda, 2017)
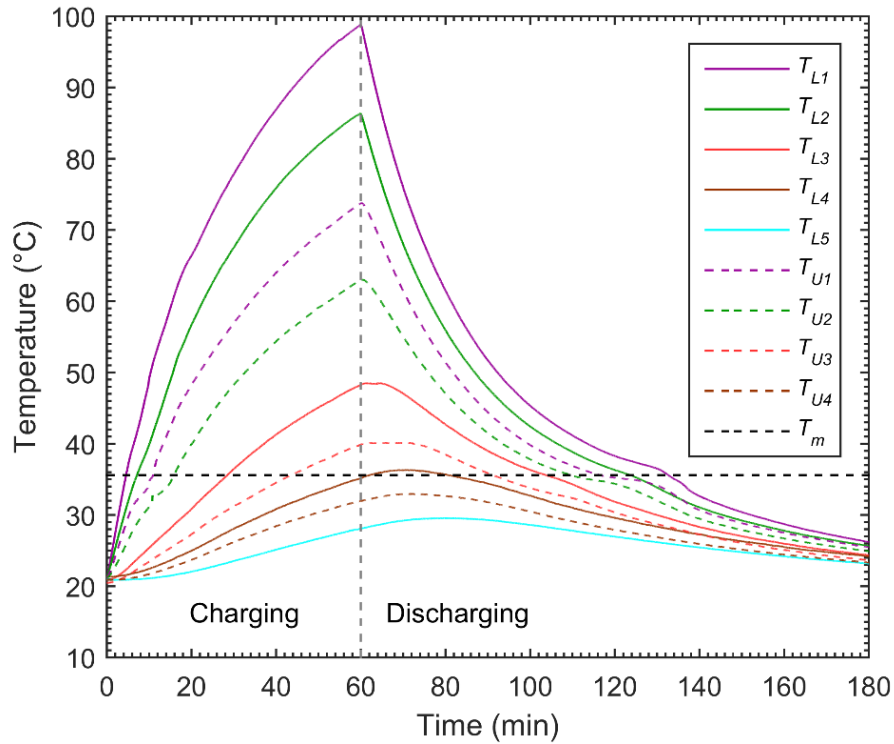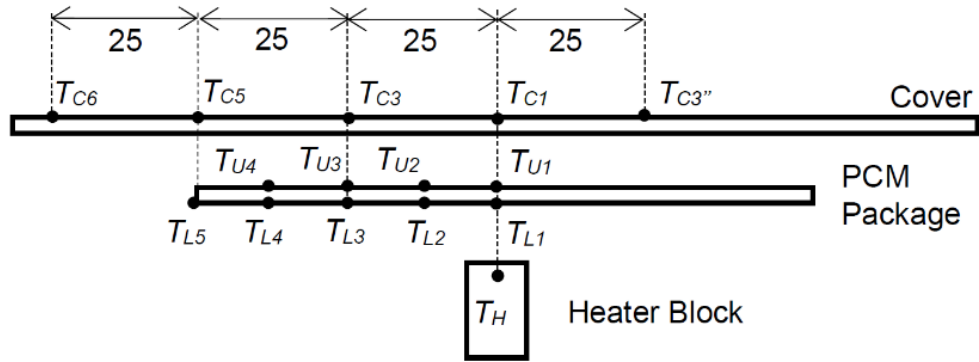
Fig. 3.10 Temperatures measured on the LHTES module which was designated package A (*n*-eicosane) (Maranda, 2017)

The addition of the heat spreader was found to significantly reduce the temperatures of the system. Therefore, the heating phase was increased from 60 to 120 min to ensure there was sufficient melting. Figure 3.11 shows temperatures T_H and T_{C1} for experiments with the aluminum heat spreader installed.

The cover temperature was not impacted greatly by the presence of the LHTES modules. A small temperature decrease is seen after approximately 50 minutes. However, the LHTES modules have a large impact on the heater temperature. This is a result of a combination of two factors: thermal storage in the LHTES module (latent and sensible) and spreading in the LHTES module.

There is a noticeable difference between the two different LHTES modules with *n*-eicosane out performing dodecanoic acid. Due to the differences in the properties of the two PCMs it is difficult to determine what properties contributed most to this (the lower transition temperature, the higher latent heat, the larger solid conductivity, etc.).
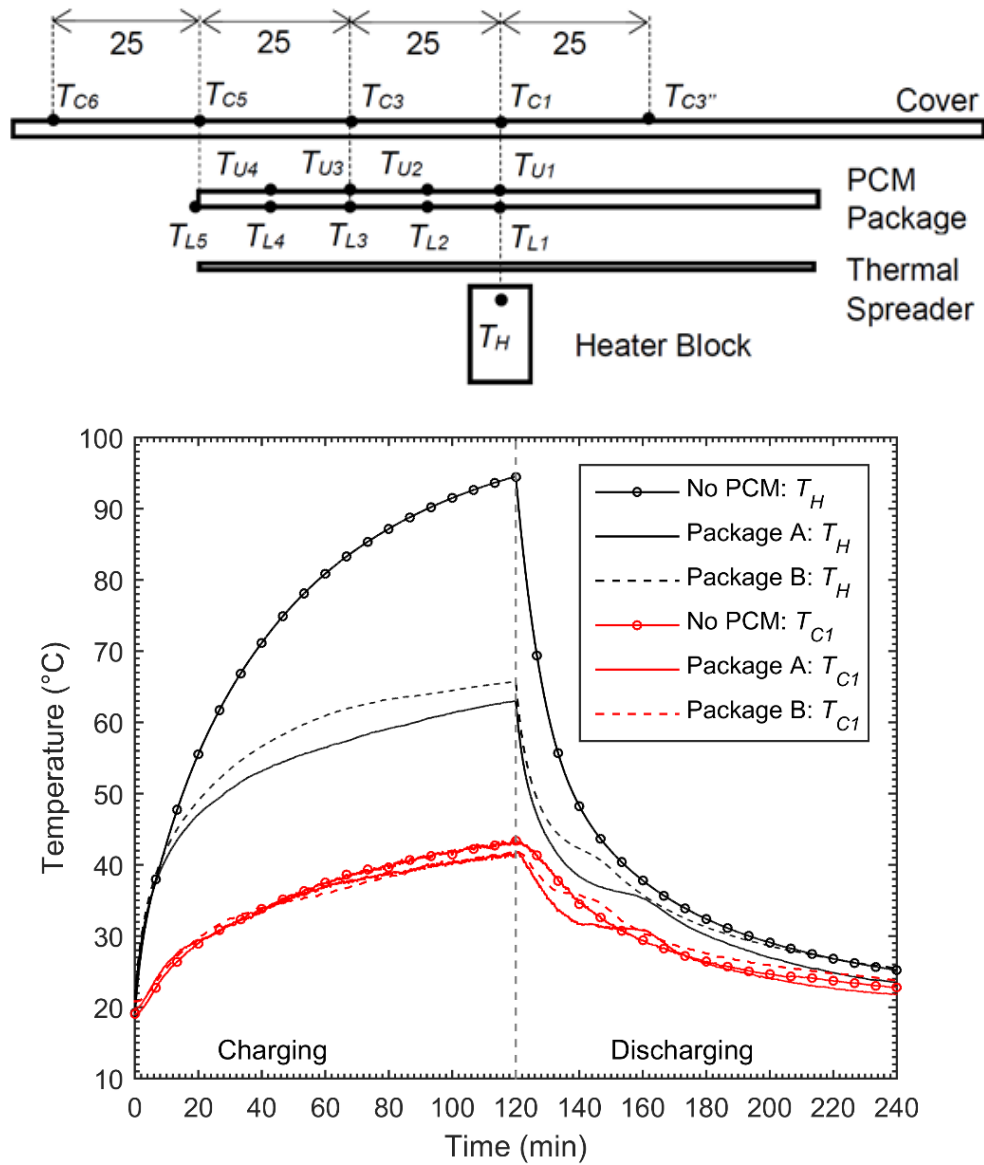
Fig. 3.11 Comparison of the maximum cover temperature (T_{C1}) and heater temperature (T_H) for experiments with no PCM, package A, and package B when the aluminum heat spreader was used (Maranda, 2017)

3.6 Numerical Validation

A secondary objective of this work was to validate the numerical methods used to simulate thin LHTES systems. A three-dimensional finite element simulation of the simplified experimental setup was created in COMSOL Multiphysics 5.0 (see Fig. 3.12).
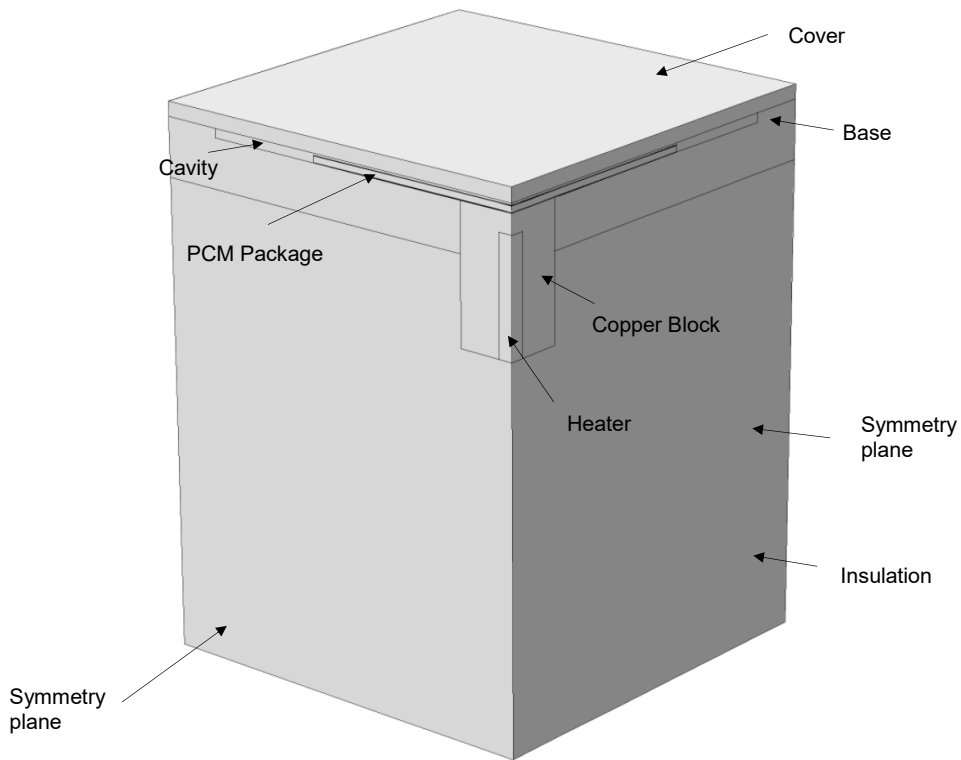
Fig. 3.12 Geometry used in the numerical simulation of the simplified setup (Maranda, 2017)

The modified c_p method, similar to Chapter 2, was used to simulate the phase change. Heat transfer coefficient (h) was assumed to be constant across the external surface and was varied to fit the numerical results to the experimental results. In addition, the contact resistance (R) between the bottom of the PCM package and the experimental setup was also fit. Figure 3.13 shows the heater temperature and the cover with a heat generation rate of 5 W, LHTES module B, $h = 25$ W/m^{2}K, and $R = 0.015$ Km^2/W. The experimental results are shown with solid lines while the numerical simulation is shown as dashed lines.
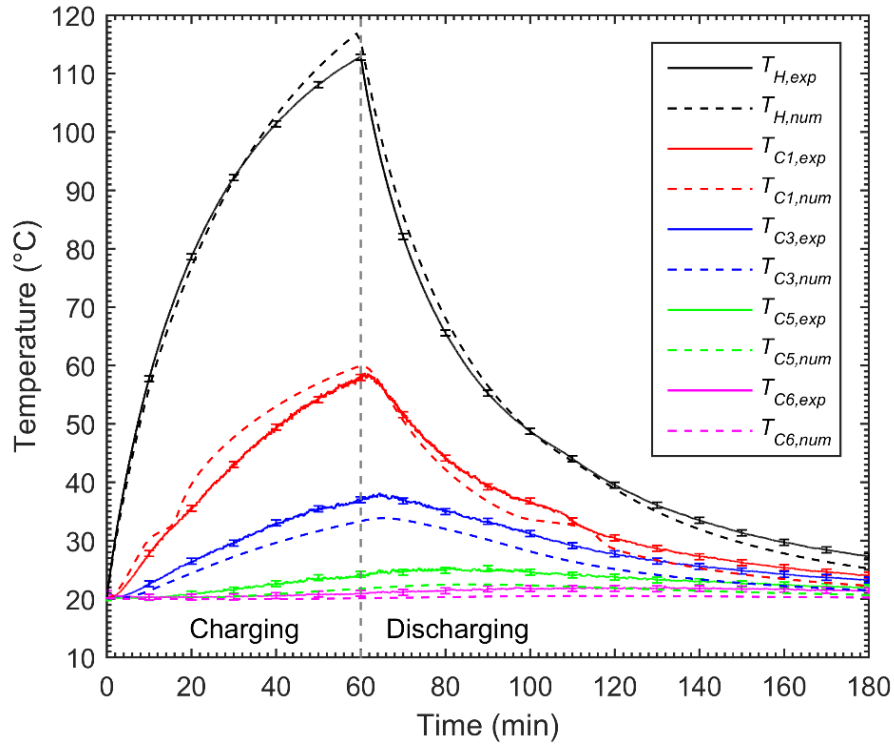
Fig. 3.13 Simulated and measured temperature profiles of the heater (T_H) and the cover surface (T_{C1}-T_{C6}) for the experiment with package B and a constant power input of 5 W for 60 minutes. Measurement uncertainties are indicated with an error bar (Maranda, 2017)

The numerical results compare well with the experimental results. Fitted values of heat transfer coefficient and contact resistance did not follow any correlation that Mr. Maranda could find. It can be concluded that the numerical techniques sufficiently model the internal physics of phase change and heat conduction, offering insight into the dynamics of the system and allowing for comparative studies. However, without an experimental platform to compare to, it would be very difficult to use these simulations to make predictions about a real-world system. A detailed explanation and analysis of these simulations is given in Sponagle *et al.* (2017) and Maranda (2017).

3.7 Conclusions

From the experiments conducted on this simplified setup a few conclusions can be drawn. First, the experimental results do not contradict conclusions from the numerical study but do indicate that transition temperature is not as important a factor as it appeared in the numerical study. While a fair and uncomplicated comparison between different transition temperatures is not possible with real materials (which was the original impetus for the numerical study) the negative impact the

LHTES had on the back cover in the numerical study was not seen in the experiments, perhaps due to contact resistance between the LHTES and the cover.

It was found that n-eicosane appears to be well suited for use in LHTES modules for temperature control of handheld electronic devices.

CHAPTER 4 : PRELIMARY EXPERIMENTAL INVESTIGATION OF TEMPERATURE CONTROL USING LHTES MODULES

4.1 Overview

This section is a summary of work done by Mr. Ahmed as part of his master's thesis which was completed at the LAMTE. The primary objectives of Mr. Ahmed's work were to:

- design and build an experimental setup which was capable of simulating a tablet computer,
- determine an effective method of encapsulating PCM for use in LHTES temperature control modules,
- and, experimentally test the use of these LHTES modules in the simulated tablet computer

Only a portion of the work done by Mr. Ahmed can be presented here, this section will focus on those aspects which informed the work done by the author. Mr. Ahmed's work on developing an experimental platform for simulating tablet computers was adapted and used by the author in the core experimental work presented in Chapter 5. Also, Mr. Ahmed did an extensive study of the impact of orientation on the heat transfer in tablet computers which also directed the author's experimental work.

4.2 Experimental Setup

Creating an experimental platform which accurately simulates the heat transfer in a handheld device is challenging due to the complexity of several major components in these systems: the display assembly and lithium-ion battery.

The display of handheld computing devices is an assembly of parts which generally consists of a steel frame and several layers of plastic and glass. The display assembly is important as it represents nearly half of the heat transfer area of the tablet and has unique conductive and heat spreading properties that are difficult to represent with a simpler structure.

Lithium-ion batteries consist of many layers of thin material, some of which are toxic. Typically, there will be: aluminum foil, copper foil, cathode material, anode material, electrolyte and a separator. These materials are formed into a stack, rolled and packaged. Creating a simulated

battery which accurately replicates the thermal mass and heat conduction properties of a lithium-ion battery is challenging.

Ahmed (2016) employed the simplest approach to solving this problem and used a real tablet display and battery in his experiments. A Dell Venue 8 Pro tablet computer was disassembled, and the display assembly, plastic case, and battery were integrated into the simulated tablet computer (see Fig. 4.1). The PCB from the original tablet was removed and replaced by a piece of copper clad FR4 circuit board which was cut to the same size and shape (see Fig. 4.2).
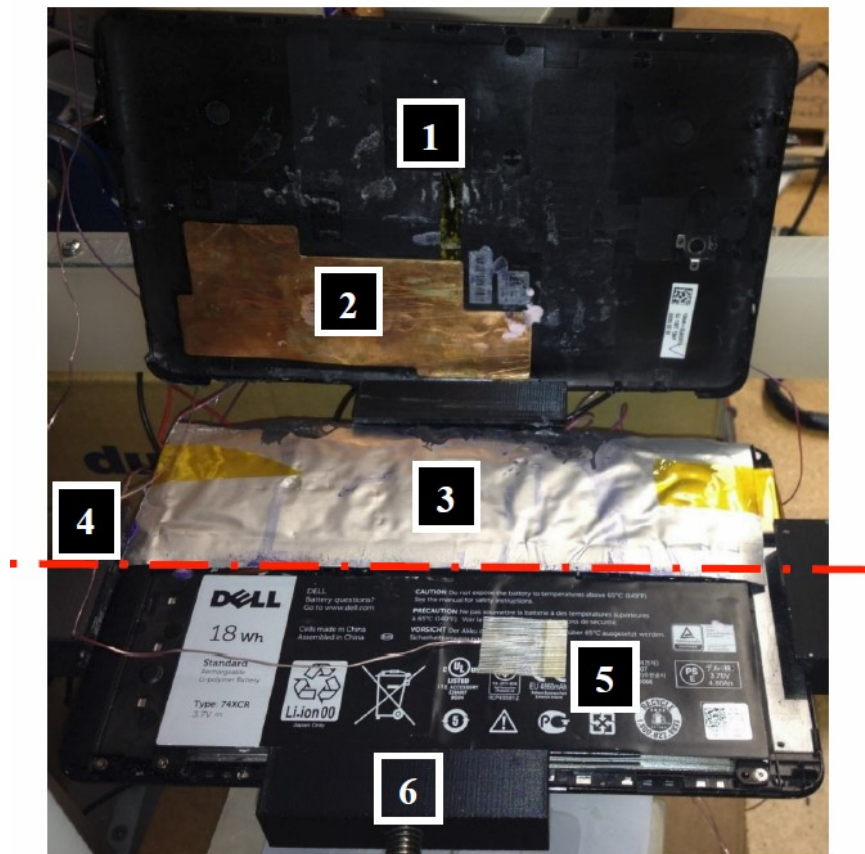
1 – Back Cover
2 – Copper heat spreader
3 – PCM TES Unit (Size 2)
4 – Axis of rotation
5 – Type – T thermocouple
6 – 3D printed clamp

Fig. 4.1 Photograph of the simulated tablet computer used by Mr. Ahmed (Ahmed, 2016)
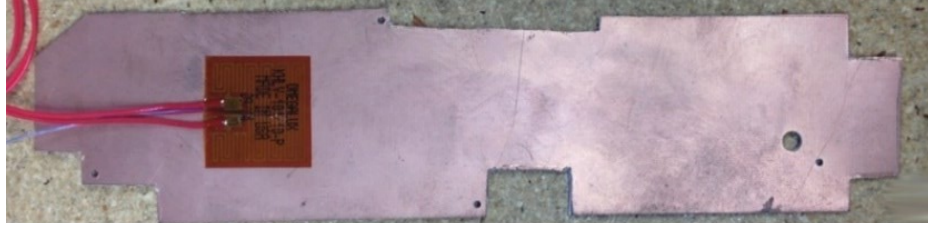
Fig. 4.2 Photograph of the simulated PCB used by Mr. Ahmed (Ahmed, 2016)

The major heat source on the PCB is the SOC, it can be seen in the infrared image shown in Fig. 4.3. This heat source was simulated in the experiment by a 1" square polyimide heater which was secured to the PCB with pre-installed adhesive (purchased from Omega, serial number KHLV-101/10).
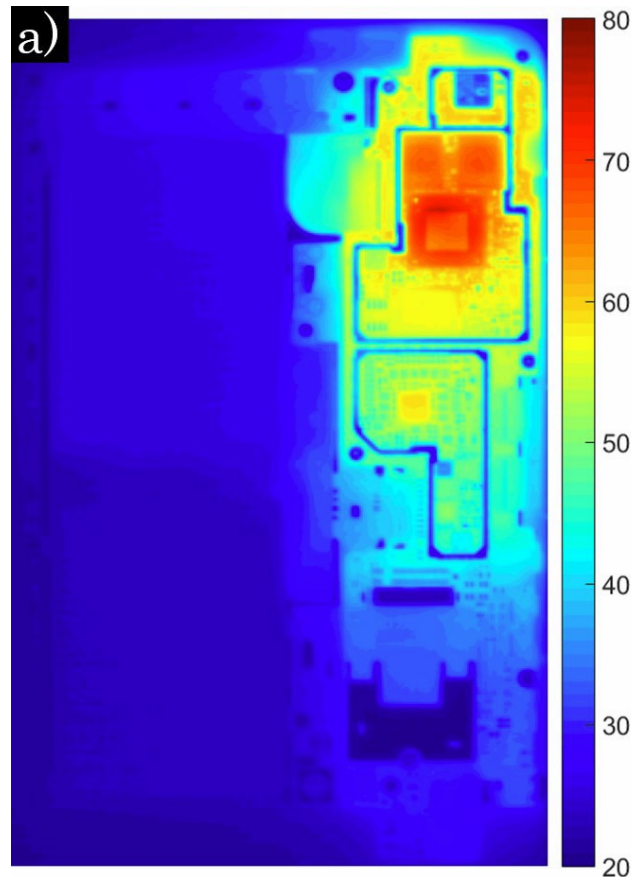
Fig. 4.3 IR image of the Dell Venue 8 Pro tablet computer during operation with the back cover removed (Ahmed, 2016)

75

A rig was built to hold the simulated tablet computer during experiments. This rig allowed the simulated tablet computer to be suspended with only minimal contact with the rig. The simulated tablet could be oriented at any angle and the rig also included a mounting point for an IR camera (see Fig. 4.4)
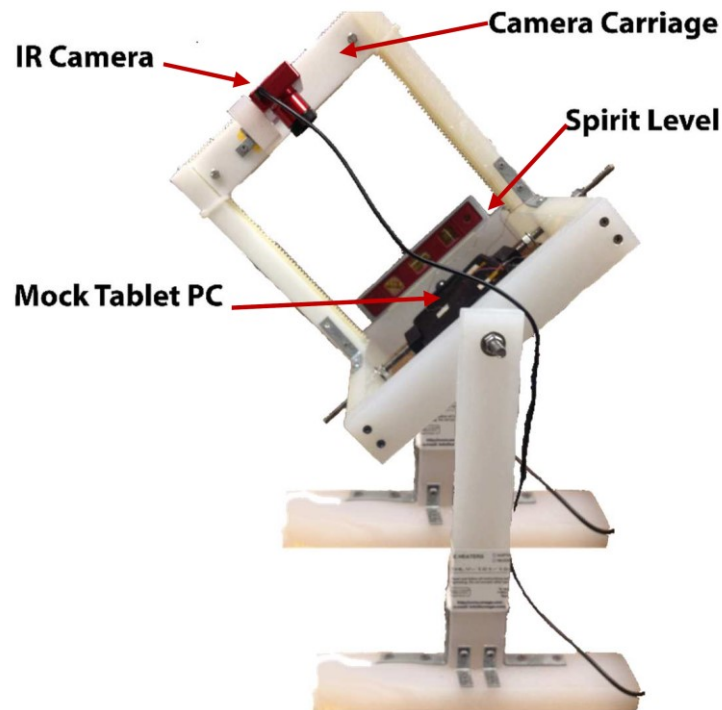
Fig. 4.4 Rig which holds the simulated tablet (Ahmed *et al.*, 2016)

4.3 LHTES Modules

The LHTES modules are similar to those which were used by the author and Mr. Maranda. PCM was encapsulated between sheets of heat sealable laminated film. Mr. Ahmed placed film sheets together and heat sealed three of the four edges. A precise mass of liquid PCM would then be poured into the open end. Air was pressed out of the packet and the open end was heat sealed. After the packet was sealed it was manually formed into the desired shape. This method results in a precise mass of PCM but the maximum thickness of the LHTES module was less controlled than with the method used by the author. In several experiments thermocouples were inserted directly into the LHTES modules. Figure 4.5 shows three of the LHTES modules which were manufactured in this way.

Fig. 4.5 Photographs of three LHTES modules (Ahmed, 2016)

Several LHTES modules were manufactured but only results for two modules will be presented here. Table 4.1 summarizes the details of these modules. The presented modules utilize the two PCMs which were identified in Chapter 2: *n*-eicosane and PT37, Table 4.2 shows the properties of each of these PCMs (Table 4.2 is repeated for convenience and is the same as Table 2.7). Figure 4.6 shows the approximately location of the thermocouples inside of the LHTES modules.

Table 4.1 Properties of the LHTES modules used by Ahmed (2016)

PCM	PCM mass	width	length
***n*-eicosane**	16 g	6.6 cm (2.6 in)	15.2 cm (6 in)
PT37	16 g	6.6 cm (2.6 in)	15.2 cm (6 in)

Table 4.2 Properties of the PCMs used by Ahmed (2016) (repeat of Table 2.7)

Properties	n-eicosane	PT37
T_m	35.6 ± 1.5 °C	36.4 ± 1.5 °C
ΔH_{fusion}	239 ± 24 kJ/kg	206 ± 21 kJ.kg
$C_{p,s}$	1.8 ± 0.2 J/gK	1.8 ± 0.2 J/gK
$C_{p,l}$	2.3 ± 0.2 J/gK	2.1 ± 0.2 J/gK
k_s	0.46 ± 0.05 W/mK	0.28 ± 0.03 W/mK
k_l	0.15 ± 0.05 W/mK	-
ρ_s	780 kg/m^3	849 kg/m^3
ρ_l	765 kg/m^3	-

Note: All properties are from Ahmed *et al.* (2016) except the density and thermal conductivity of n-eicosane in the liquid state which are from Vélez *et al.* (2015)

Fig. 4.6 Approximate location of the thermocouples inside of the LHTES module (Ahmed, 2016)

4.4 Results

Mr. Ahmed performed a number of experiments; however, the following section will present the results of six experiments which focus on the impact of orientation. Each of these experiments included a 60 minute heating phase with a heat generation rate of 6 W and a 30 minute cooling phase where the heater was shut off. Table 4.3 summarizes these experiments. All experiments included a TIM (Parker Chomerics, T670 Thermal grease) placed between the heater and the LHTES module. In these experiments the inclination angle was varied: 0° (horizontal with the display facing upwards), 45°, and 90°.

Table 4.3 Summary of experiments presented

PCM	Inclination angle
n-eicosane	0°
n-eicosane	45°
n-eicosane	90°
PT37	0°
PT37	45°
PT37	90°

Figure 4.7 shows the temperatures which were measured inside the LHTES package. Figure 4.8 shows the temperatures measured at the heater, on the front of the display directly above the heater, and on the back surface above the heater.

There are several interesting observations to be made by looking at Fig. 4.7. First, the LHTES module is not fully melted. The PCM is melted above the heater and the melting front has passed the sensor at *P3* but has not passed either of the other sensors. Second, the orientation of the tablet computer has only a small impact on the temperature profiles. This impact is partially due to changes in the heat transfer coefficient between the surface and the air, which will occur due to the change in orientation.

The same trends were observed on the sensors mounted to the heater and case (Fig. 4.8). The difference seen with orientation change is small in these measurements. Another, important

observation is the performance of the two different LHTES modules are similar. Both *n*-eicosane and PT37 produce similar temperatures on the case and heater.
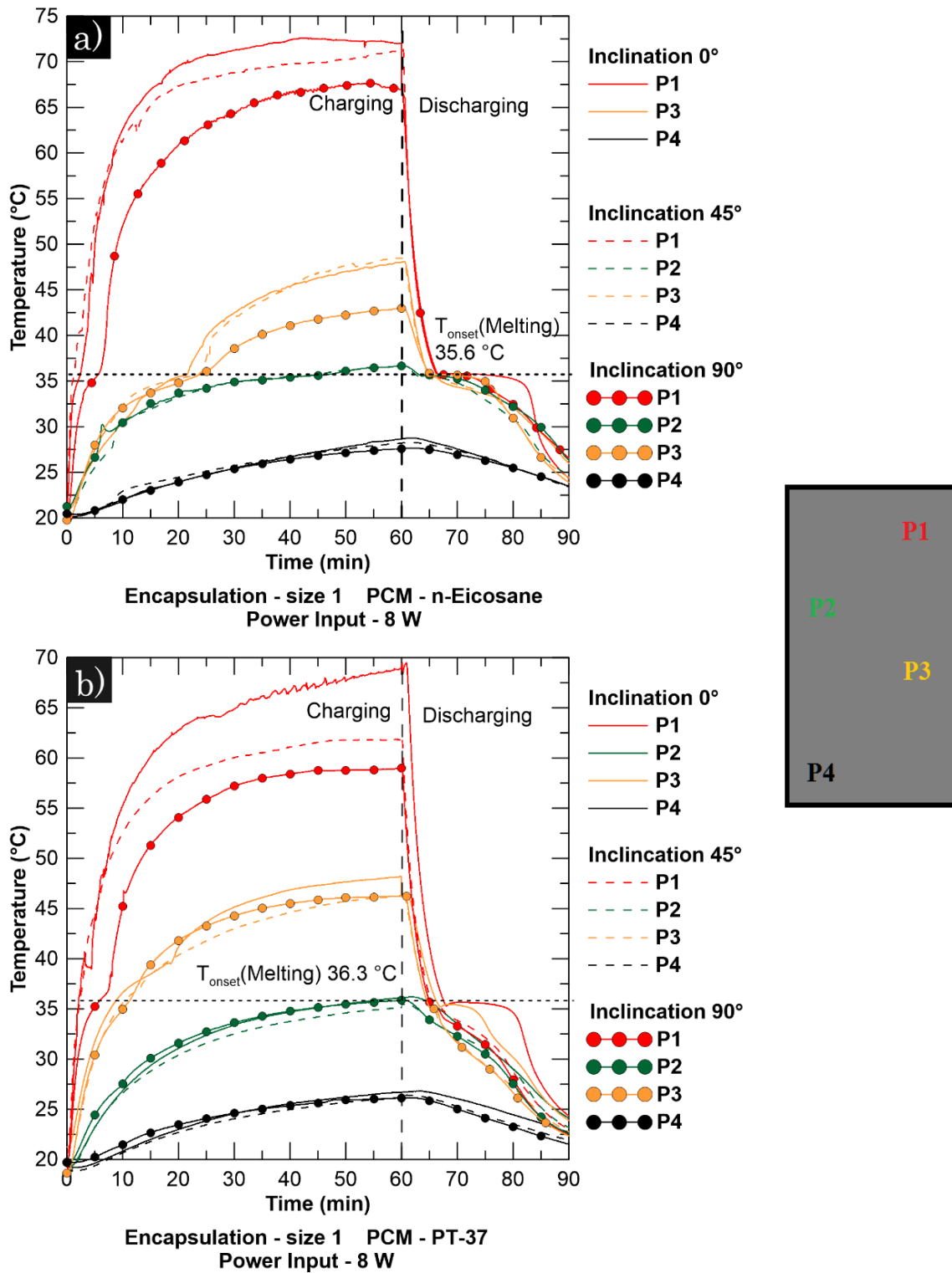
Fig. 4.7 Temperatures measured inside of the LHTES module during the experiments with 6 W of heat generation (Ahmed, 2016)

80
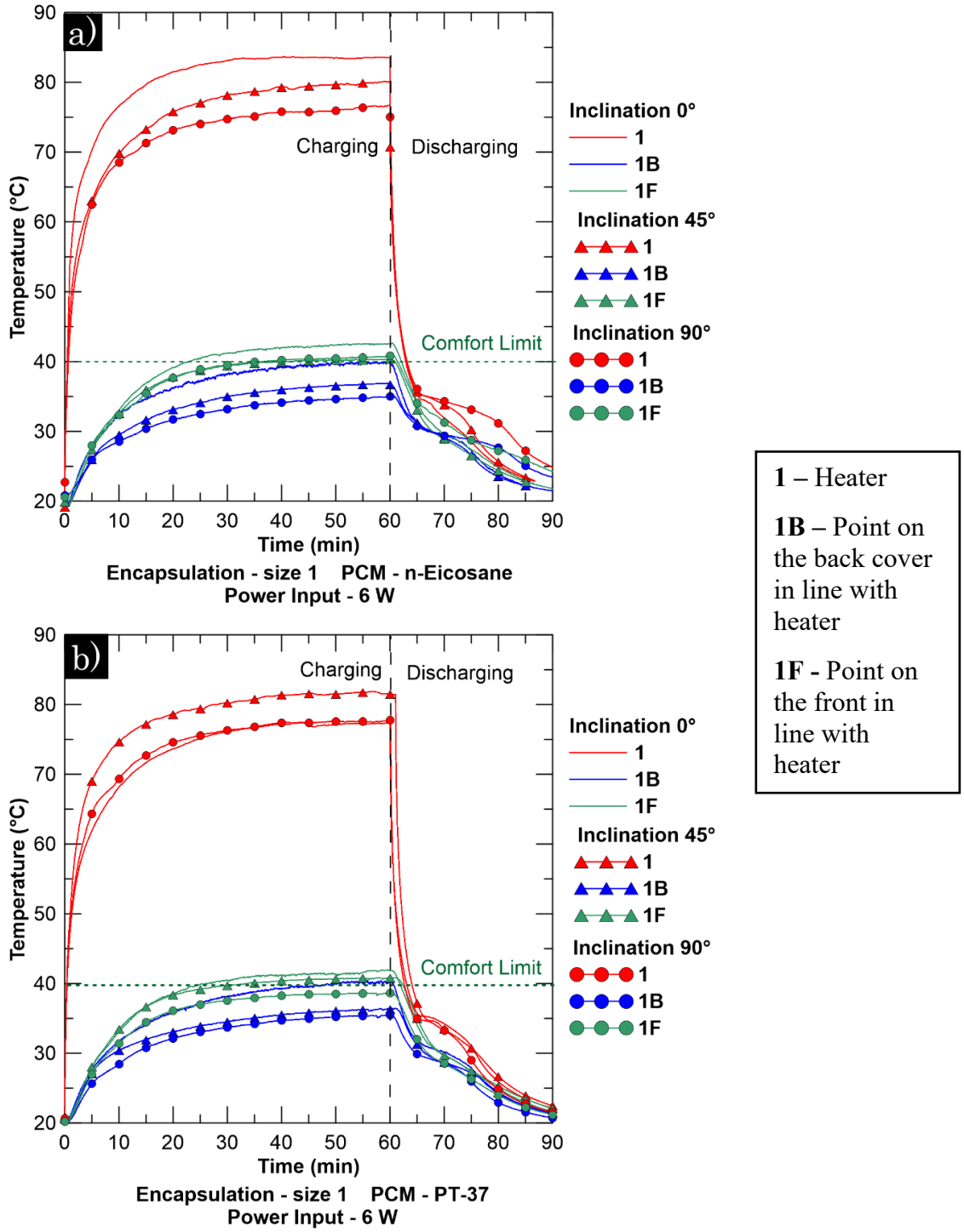
Fig. 4.8 Temperatures measured on the heater (1), one the back cover above the heater (1B), and on the display above the heater; with 6 W of heat generation (Ahmed, 2016)

81

4.5 Conclusions

Mr. Ahmed successfully developed an experimental platform for the testing of LHTES modules. This platform was used to test several LHTES modules consisting of a PCM encapsulated in heat sealable laminated film. These packets were used to run multiple experiments and were found to be robust and did not show signs of deterioration or leaking after use.

Two important conclusions can be drawn from the experimental results presented here. First, the temperatures measured on the mock tablet were not greatly impacted by the orientation angle. Furthermore, in nearly all cases the horizontal orientation was found to be the worst-case scenario. For this reason, the experimental work presented in Chapter 5 does not consider inclination angle, all experiments are conducted with the tablet horizontal.

Second, the performance of *n*-eicosane and PT37 based LHTES temperature modules were similar. Combining these findings with the findings from previous experiments, and numerical simulations, *n*-eicosane was selected as the PCM for the remainder of this work. It was chosen over PT37 because its composition is fully understood and well accepted in literature making it a better choice for publication. However, PT37 would be a viable option from a purely engineering perspective.

While this work is relevant and well executed, it has several limitations. Firstly, Mr. Ahmed's work primarily investigated the impact of varying fundamental aspects of the setup, orientation, heat generation rate, etc. on the behaviour of LHTES modules. This has offered insight into the study of these systems; for instance, the orientation analysis presented previously. However, a comprehensive comparative study of the different aspects of a complete temperature control solution is required to give insight into the key design features and true potential of these systems. In order for a complete analysis, a well controlled set of experiments which compare the impact of: LHTES module, heat spreading and thermal contact enhancement (thermal interface material) is required.

In addition, the methods for manufacturing the LHTES modules used by Mr. Ahmed were simple and resulted in modules which were often overly thick (occasionally to the point that the back cover of the tablet bowed outward) and made it challenging to ensure that all air was removed from the modules.

CHAPTER 5 EXPERIMENTAL STUDY

5.1 Objectives

The objective of this work was to use a mock tablet computer to experimentally determine the degree to which LHTES modules can be used to control the temperature of handheld electronic devices. All aspect of the temperature control solution including, a thin LHTES module (constructed using the new method), an aluminum heat spreader, and thermal interface material (TIM) were included in these studies. A comprehensive comparative study of the impact of these components was conducted.

5.2 Experimental Setup

These experiments were based on the knowledge and understanding which was developed throughout the project. Several aspects of the experiment have been adapted directly from previous work: the mock tablet was based on the same Dell Venue 8 Pro tablet computer which was previously used by Ahmed (2016). Also, the setup for controlling and measuring the power to the heater was designed and built in collaboration with Mr. Maranda.

5.3 Setup Description

The core experimental setup was a mock tablet based on a disassembled Dell Venue 8 Pro tablet computer. Both the display assembly and battery from the original tablet were used in the mock tablet. In the Dell Venue 8 Pro the screen assembly was the main structural component. All other components are secured to the display frame via small screws with the display assembly providing the stiffness and support. The back cover consisted of a thin piece of nylon. This cover was never intended to be removed and reattached many times and was not ideal for inclusion in the experimental setup. Also, it had become worn and started cracking during its use by Ahmed (2016). A new cover was created using a 1/16" thick sheet of nylon, and ABS frame components. This cover was easier to attach and remove, could easily be replaced, and generally allowed for more control of the experimental space. It was a good approximation of the original with the exception of the edges where the frame was thicker. However, the edges are far from the heat source and should not strongly impact the thermal behaviour.

The original PCB was replaced using the same method used by Ahmed (2016). A simulated PCB was cut from copper clad FR4. The heat source used in these experiments was a 2.54 mm (1") square polyimide film heater (see Table 5.1).

Table 5.1 Specifications of the polyimide film heater

manufacturer	Omega Engineering Inc.
part number	KHLV-101/10-P
Watt density (W/m^2)	10
maximum voltage (V)	28
maximum heat generation (W)	10
width (mm (inch))	2.54 (1)
length (mm (inch))	2.54 (1)
thickness (mm (inch))	0.0254 (0.010)

This heater came with an adhesive on one side, it was adhered to a 2.54 mm (1") square, 0.4 mm thick piece of aluminum and was then coupled to the PCB using thermal paste (Tgrease 880). This heater assembly was secured to the PCB by a piece of polyimide tape. Attaching the heater to the aluminum sheet had dual purposes. First, a real SOC is thicker than the polyimide heater and would be raised above the PCB, this was better mimicked by the thicker heater assembly. Second, the aluminum sheet helped to even out the heater assembly temperature making it easier to measure the systems maximum temperature. Third, the assembly was rigid and could be removed and reattached/relocated with ease, it was generally easier to work with. The use of the polyimide tape placed a polymer layer in between the heater and the temperature control solution. The tape was also used to mount a thermocouple to the heater. Figure 5.1 shows the setup, Fig 5.2 shows the setup with the cover removed. Figure 5.3 shows an exploded view of the experimental setup with the components labelled. Appendix C contains dimensioned drawings of the mock tablet.
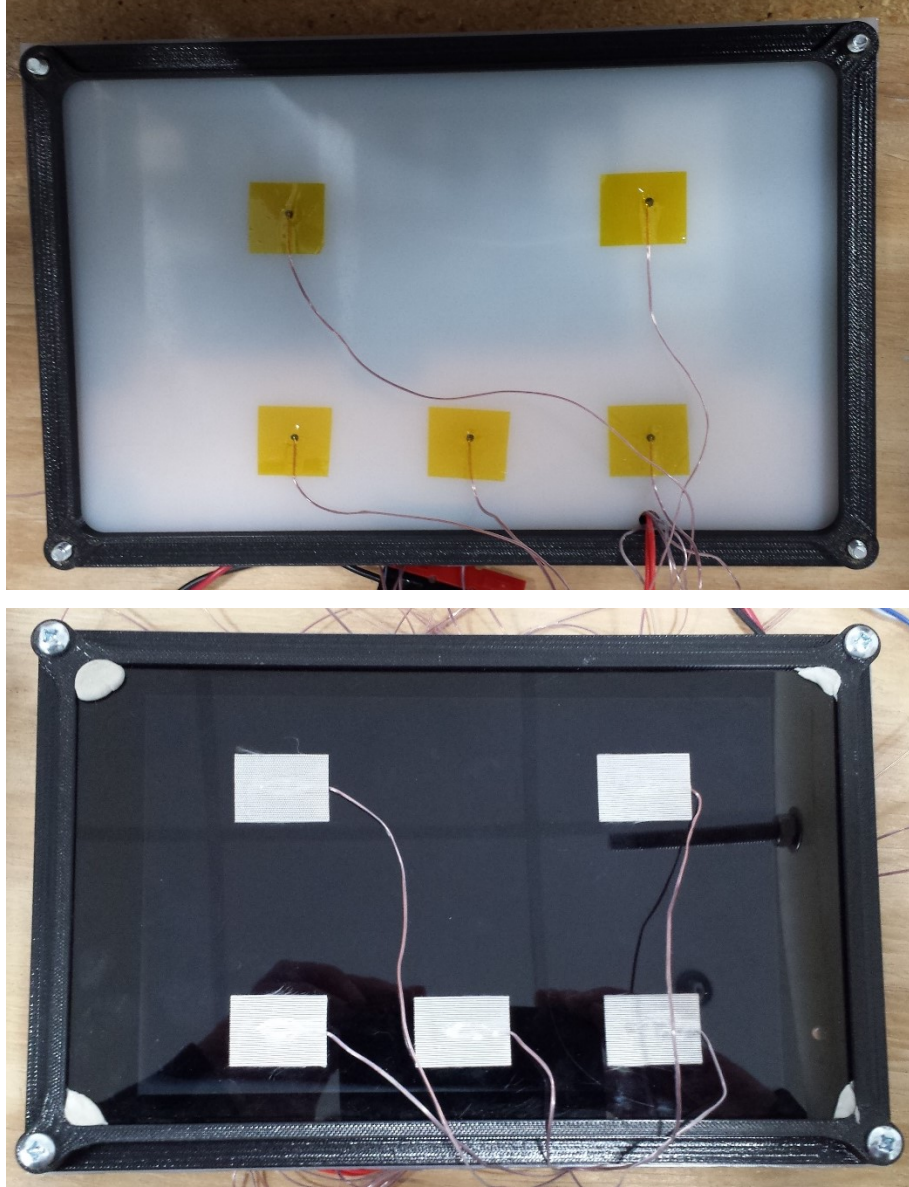
Fig. 5.1 Photograph of the mock tablet
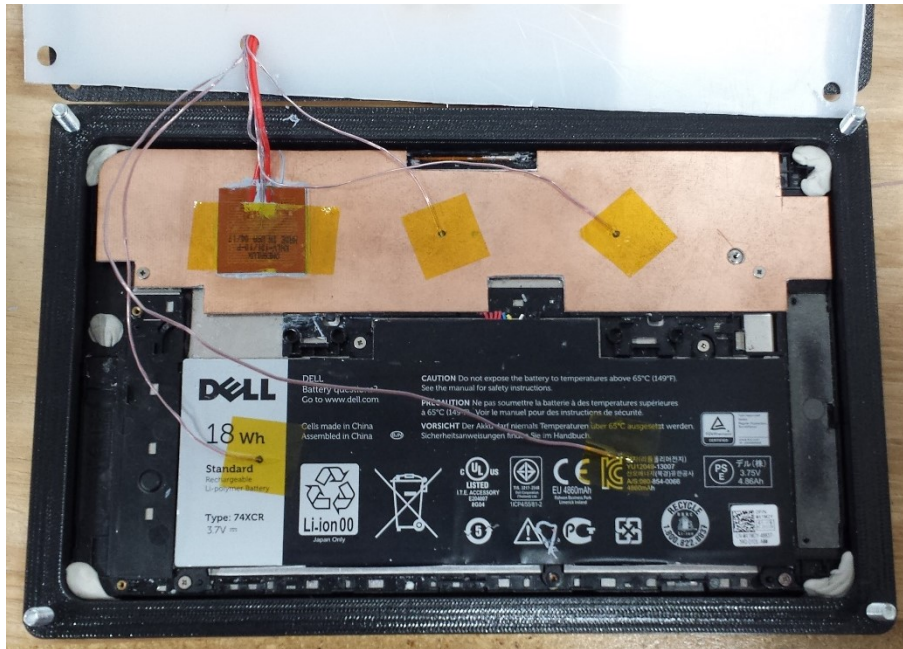
Fig. 5.2 Photograph of the mock tablet with the back cover removed
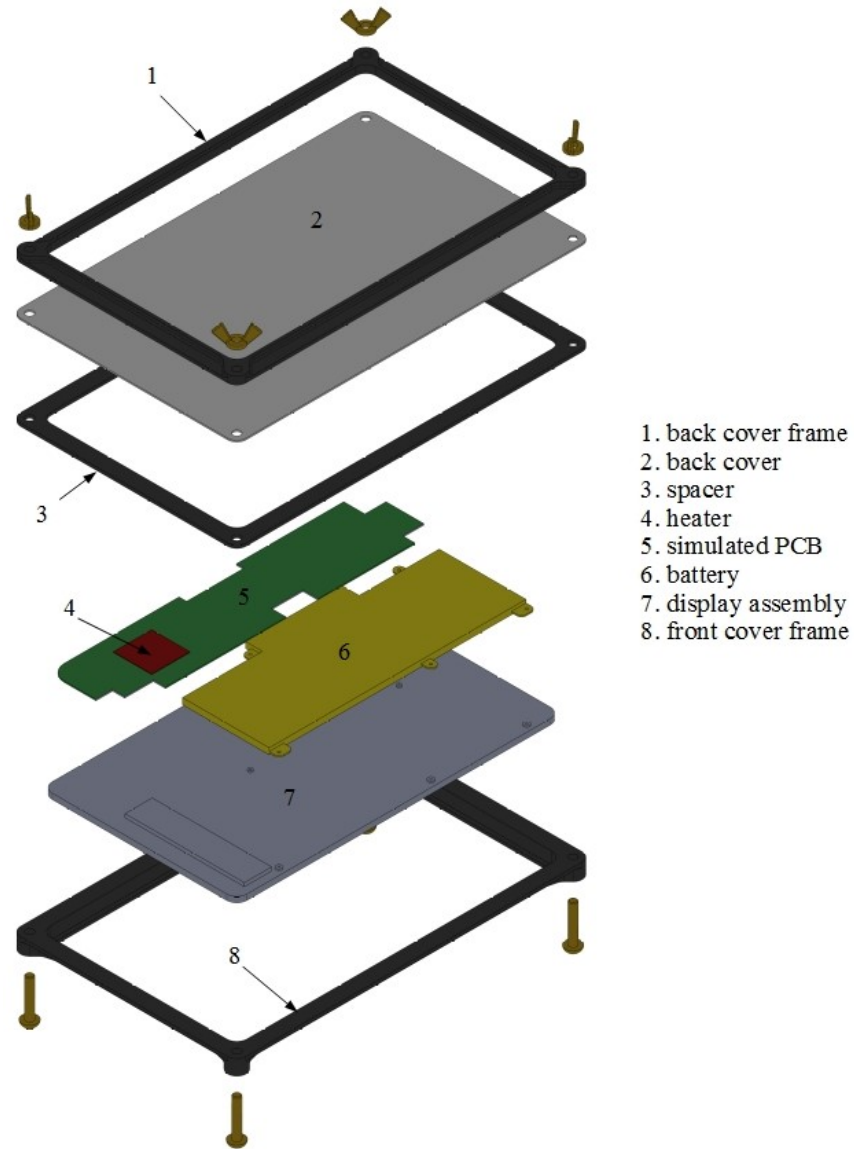
Fig. 5.3 Rendering showing an exploded view of the mock tablet

During use, the tablet was suspended in a test rig built by Ahmed (2016). The mock tablet was secured with four clamps, which allowed it to be suspended with minimal contact at varying angles. Figure 5.4 shows the mock tablet secured in the rig.
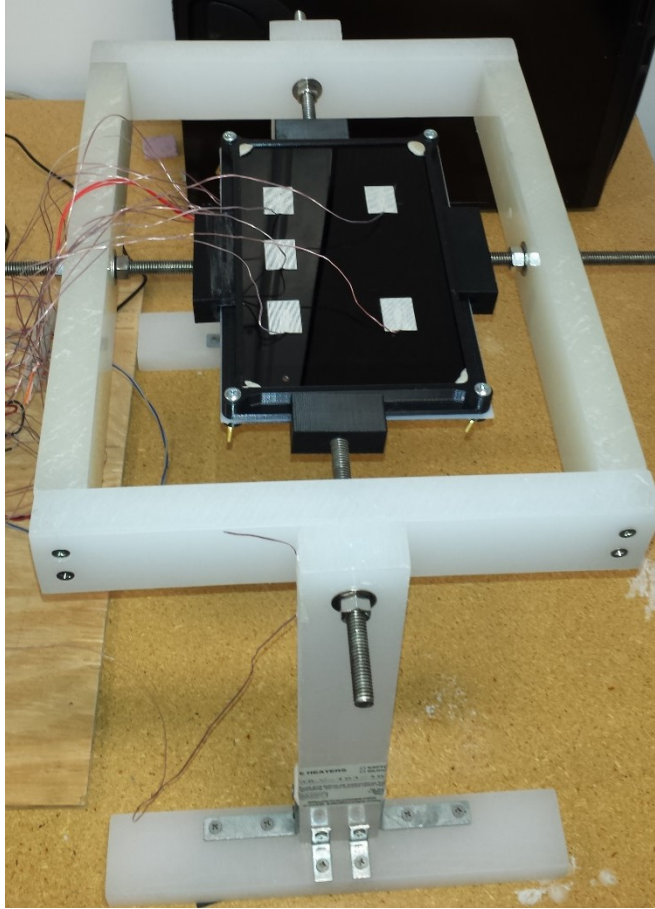
Fig. 5.4 Photograph of the mock tablet in the test rig

5.4 Heater Control and Power Measurement

The electrical power for the polyimide heater was supplied by a direct current (DC) power supply (Statco Energy 3PN501B) which could supply up to 30 V. This power supply could be controlled via an analogue voltage signal. This analogue signal was produced by a National Instruments Compact DAQ system with an NI-9263 voltage output module. The Compact DAQ was controlled via a program written using LabView 2014. Using this system, the voltage to the heater could be controlled from a PC work station.
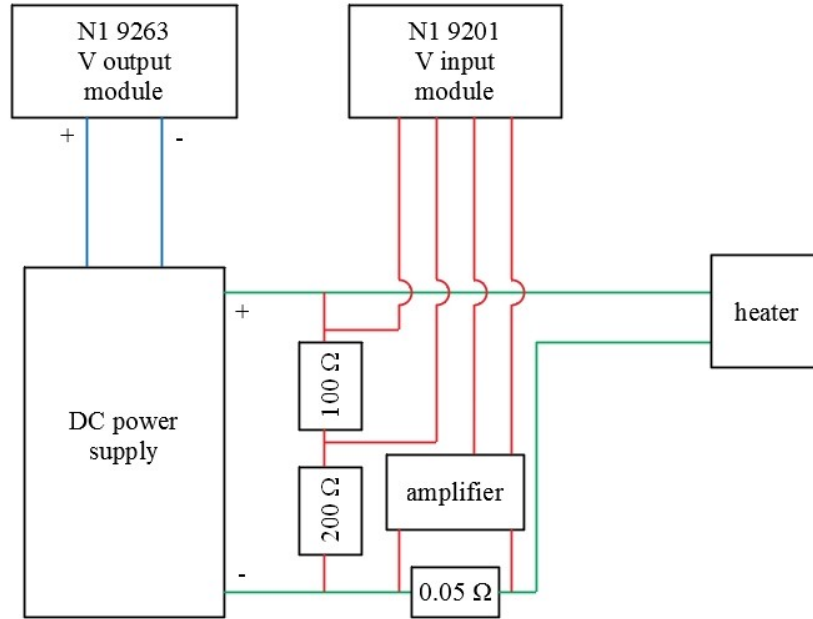
Fig. 5.5 Illustration of the circuit used to supply and measure the power supplied to the heater

The voltage across the heater (V_{in}) was measured using an analog input NI-9201 module. This module was limited to measuring voltages in the range of 0-10 V, therefore, a voltage divider was used to reduce the voltage read by the module (see Fig. 5.5).

The current through the heater (I_{in}) was determined by measuring the voltage drop (V_{Shunt}) over a shunt resistor (HSA25R05J, 0.05 Ω) which was placed in series with the heater (see Eq. (5.1)).

$$I_{in} = \frac{V_{Shunt}}{R_{Shunt}} \tag{5.1}$$

However, the voltage drop across the shunt resistor was small, therefore, an amplifier (type INA122P) with an internal resistor (1 kΩ) was used. The voltage across the amplifier (V_{Gain}) was measured with an analog input model NI-9201. The voltage drop (V_{Shunt}) across the shunt resistor could be calculated using Eq. (5.2) and the measured V_{Gain}.

$$V_{Shunt} = \frac{V_{Gain}}{5 + \frac{200 \text{ k}\Omega}{R_3}} \tag{5.2}$$

The heat dissipation rate was then calculated from with Eq. (5.3).

$$P = V_{in} \cdot I_{in} \tag{5.3}$$

The uncertainty in the power measurements was found to be ±7.3%. A detailed uncertainty analysis is presented in Appendix D.

5.5 LHTES module

The LHTES module consisted of *n*-eicosane encapsulated in heat sealable laminated film. The PCM containing pocket was 10 cm by 18.5 cm. LHTES manufacturing began by placing two sheets of laminated film together and heat sealing three of the four sides. At this point the LHTES packaging was essentially a bag. The packaging was then placed in a manufacturing jig. This jig consists of two flat aluminum plates which are secured together by nuts and bolts and separated by shims (see Fig. 5.6).
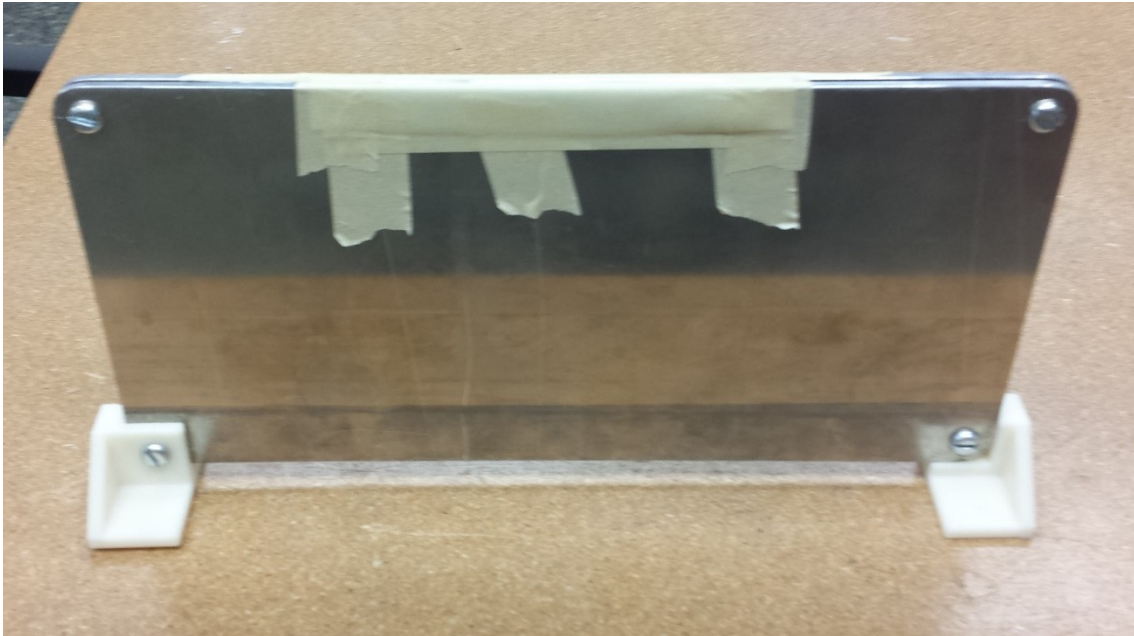
Fig. 5.6 Photograph of the jig used in the manufacture of the LHTES modules

The LHTES packaging was placed between the aluminum plates with the open side facing upwards. A hot water bath was heated to a temperature well above the PCM transition temperature, in this case about 50°C, and the jig and LHTES package were placed in the bath and left to sit for about 15 minutes (see Fig 5.7).

Fig. 5.7 Photograph of the jig with a LHTES package placed in the hot water bath

The water level was only high enough to cover about half of the jig, the aluminum plates conduct heat to the LHTES package. The *n*-eicosane was melted in a beaker on a hot plate. Once the jig was up to the correct temperature a syringe with a blunted needle was used to fill the package with PCM. The hot water and jig kept the PCM melted and allowed it to flow easily into the LHTES package and prevented the PCM in the needle from solidifying and blocking the flow. Once the package was completely filled the jig was removed from the hot water and placed into a cold water bath until the PCM solidified, at which point the LHTES was removed from the jig and the open side heat sealed closed. Table 5.2 gives the properties of the LHTES module which was used in the experiments and Fig. 5.8 shows a photograph of the module. For comparison, a Samsung Tab S3 with a 9.7" screen has a total weight of 429 g and an iPad pro with a 10.5" screen has a weight of 469 g. Including this thermal storage module would represent a weight increase of approximately 5%.

Table 5.2 Summary of the LHTES module's properties

PCM	Total mass	PCM mass	width	length	Maximum thickness
***n*-eicosane**	23.15 g	16.22 g	10 cm	18.5 cm	2 mm
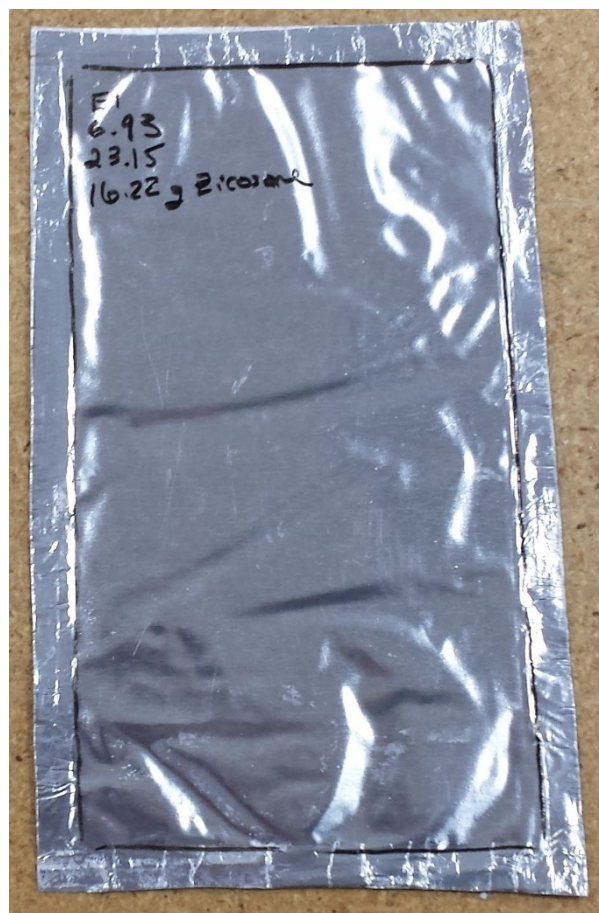
Fig. 5.8 Photograph of the LHTES module

5.6 Instrumentation

A total of 16 T-type thermocouples were used to instrument the setup, all temperature sensors has an uncertainty of ±0.5 °C. Five of the thermocouples were surface thermocouples with preinstalled adhesive pads (SA1-T, Omega Engineering Inc.). These surface sensors were placed on the display. Surface sensors adhere securely and have been flattened, this made them ideal for taking surface temperature measurements but also means they were quite fragile. In addition, the adhesive pads were thick, too thick for use inside of the mock tablet. Inside the tablet and on the back cover, traditional thermocouples, (5TC-TT-T-30-36, Omega Engineering Inc.) with a diameter of 0.25 mm, were used. They were more robust than the surface sensors and did not come with adhesive pads. These thermocouples were secured in place with a dab of cyanoacrylate glue and a small piece of polyimide tape. This method was thin, secure, and could be remove/relocated by pealing off the tape and dabbing the glue with some acetone. An array of five probes were placed inside the tablet computer, on the display and on the back cover in the same

positions. Their locations were measured with a ruler and are accurate to at least ± 1 mm. The locations and designations of each thermocouple are shown in Fig. 5.9-5.11. Dimensioned drawings of the experimental setup can be found in Appendix C.
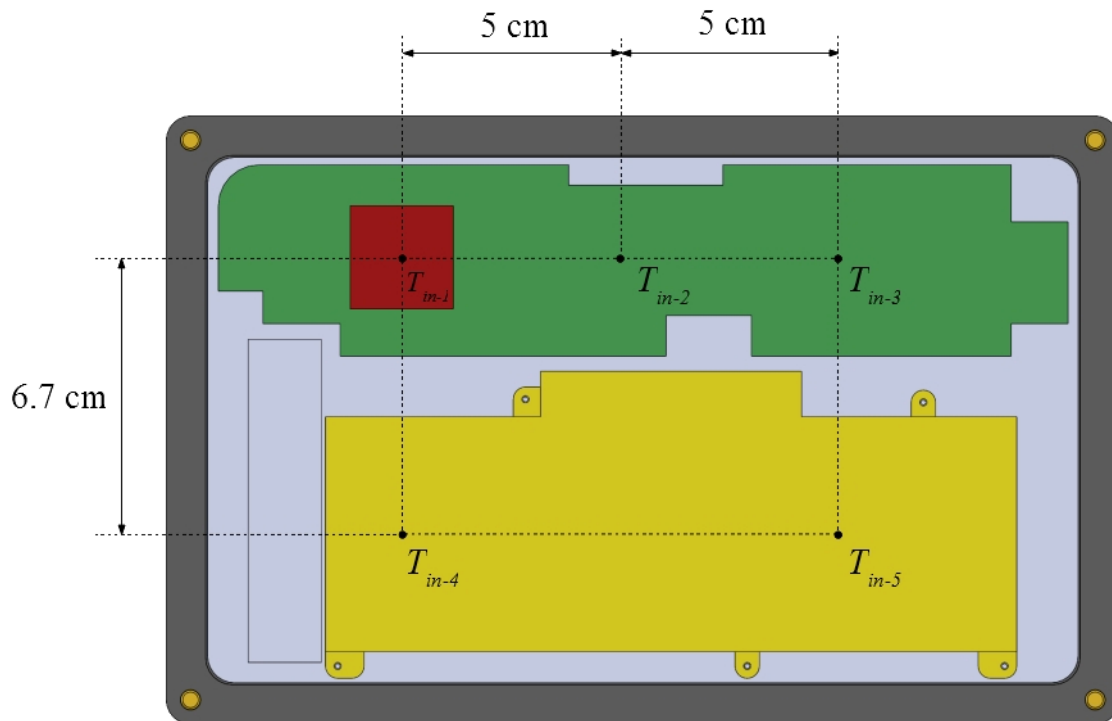
Fig. 5.9 Illustration of the inside of the mock tablet showing the locations of the thermocouples
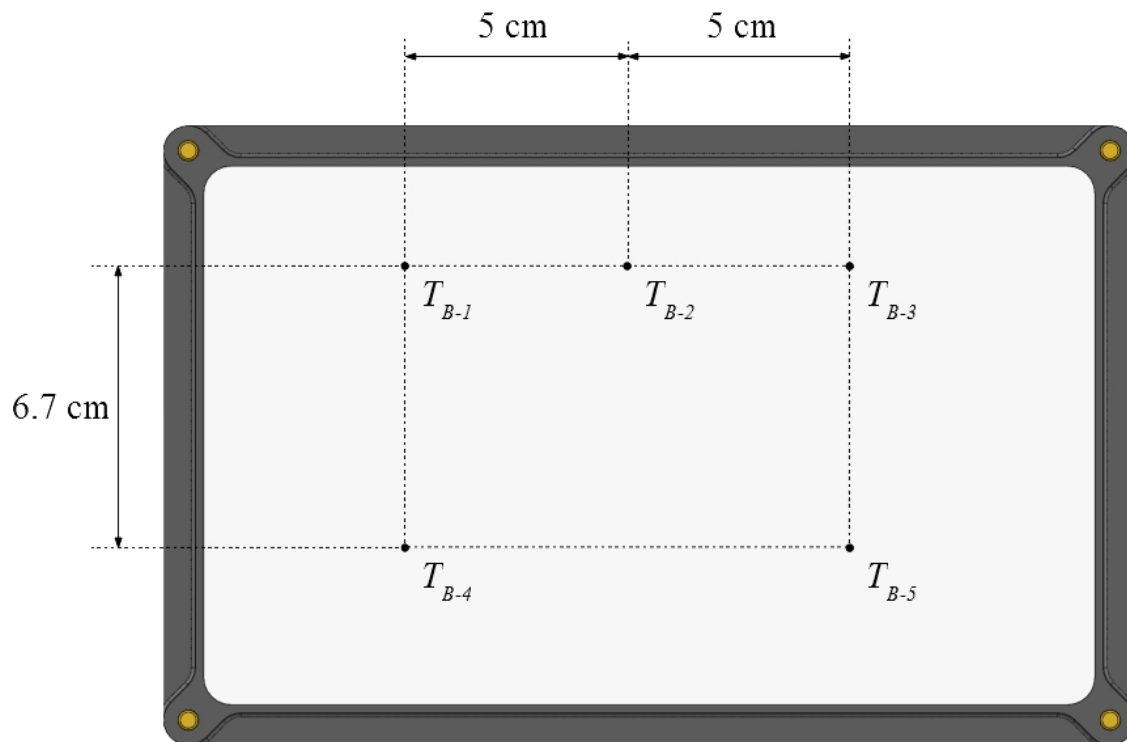
Fig. 5.10 Illustration of the back surface of the mock tablet showing the locations of the thermocouples
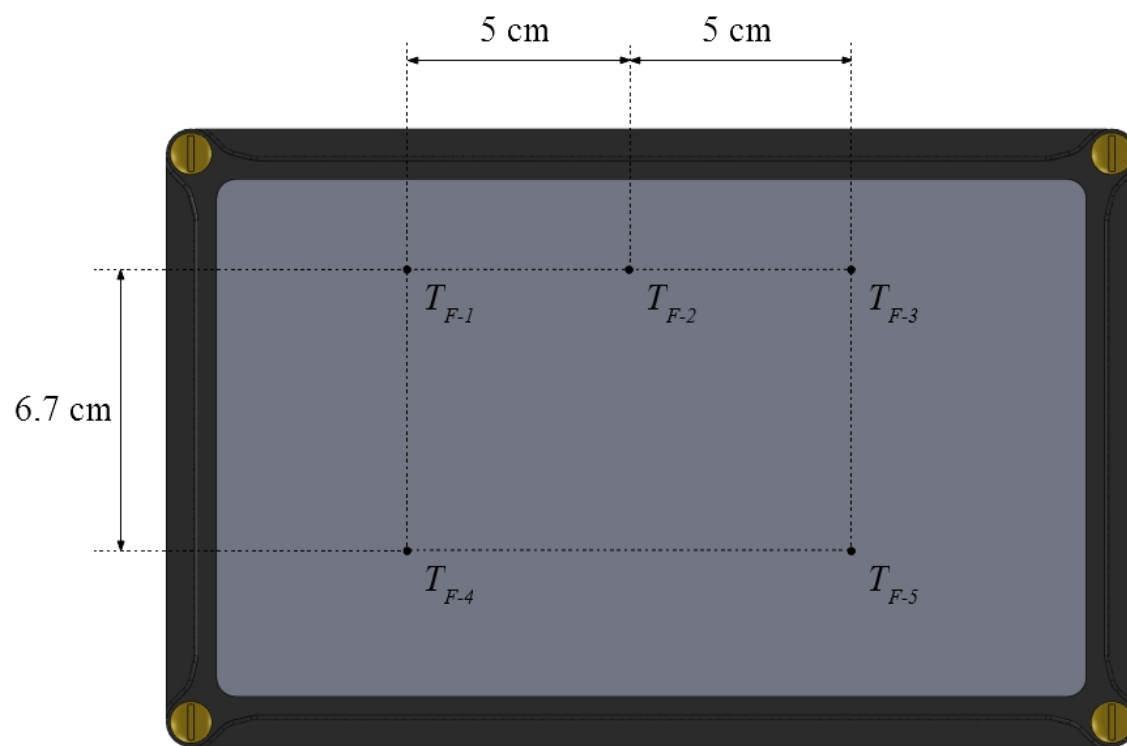
Fig. 5.11 Illustration of the front surface of the mock tablet showing the locations of the thermocouples

94

In addition, a single thermocouple was attached to the rig holding the mock tablet. It was secured with masking tape, so that it protruded up into the air above the rig. This sensor was used to measure the transient temperature history of ambient air. It can be seen in Fig. 5.4.

All of the measurements were recorded using a Compact DAQ data acquisition system and a 16-channel thermocouple module (NI 9213). Data were collected at 1 Hz using a program written in LabVIEW 2014.

5.7 Experimental Methodology

5.7.1 Repeatability Analysis

The experimental results presented in this thesis represent individual experiments. Ideally, multiple experiments would be run and then averaged together. However, these experiments were exposed to the ambient temperature in the laboratory which fluctuated by a couple of degrees. Normalizing these experiments is not possible as they are impacted by both the ambient temperature and the PCM transition temperature. That said, the experimental setup proved to be repeatable except for the impact of ambient temperature. Figures 5.12 to 5.14 show results for two preliminary tests run with no LHTES module, a heat spreader, and a heat generation rate of 5 W. These two experiments illustrate both the repeatability of the experimental setup and the small issue of ambient temperature variability. The temperatures measured on the inside of the tablet (see Fig. 5.12) show a small and nearly constant difference between the two runs. The source of this difference is clearly seen in the temperatures measured on the back surface (Fig. 5.13). The initial temperature of the tablet was different in the two experiments and the influence of that temperature difference can be seen throughout the experiment.
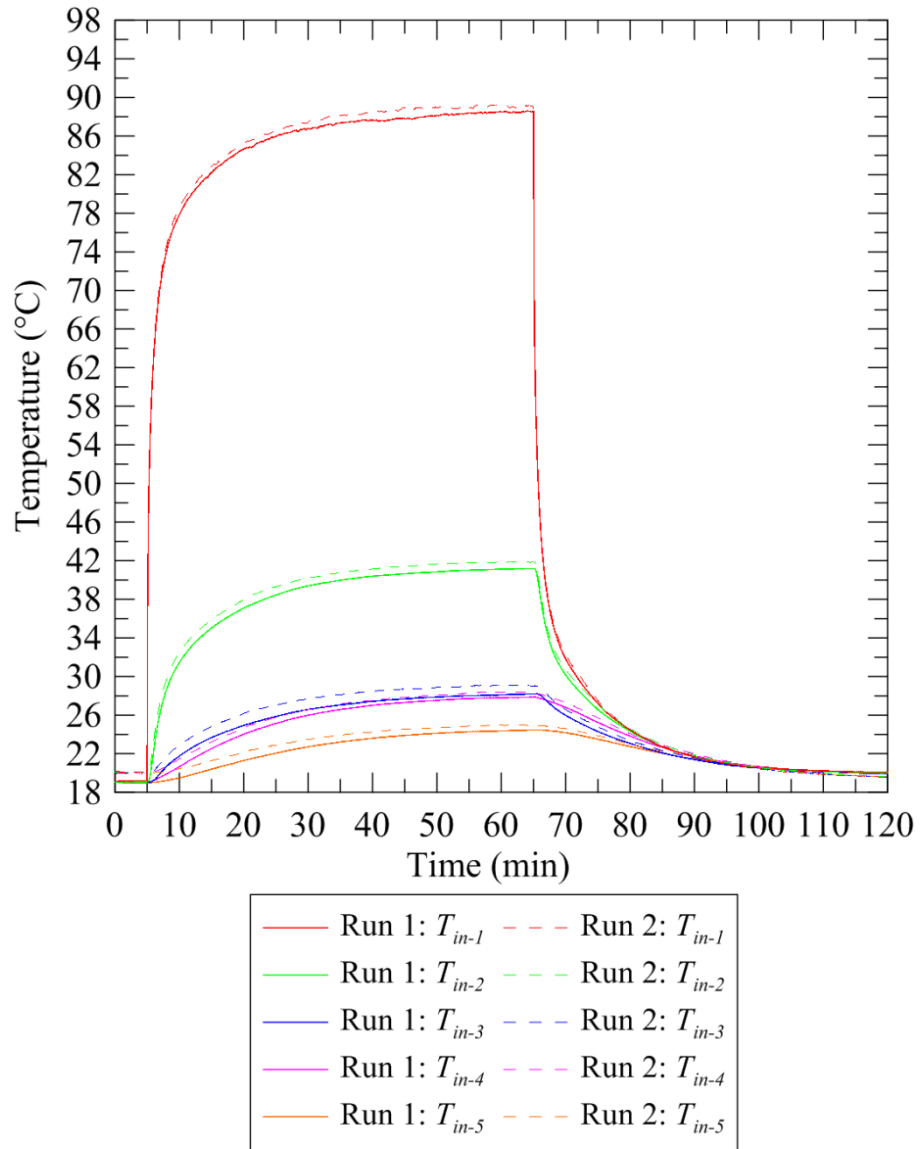
Fig. 5.12 Temperature measurements, from two runs of the experiment, on the inside of the mock tablet with the heat spreader installed and a heat generation rate of 5W.
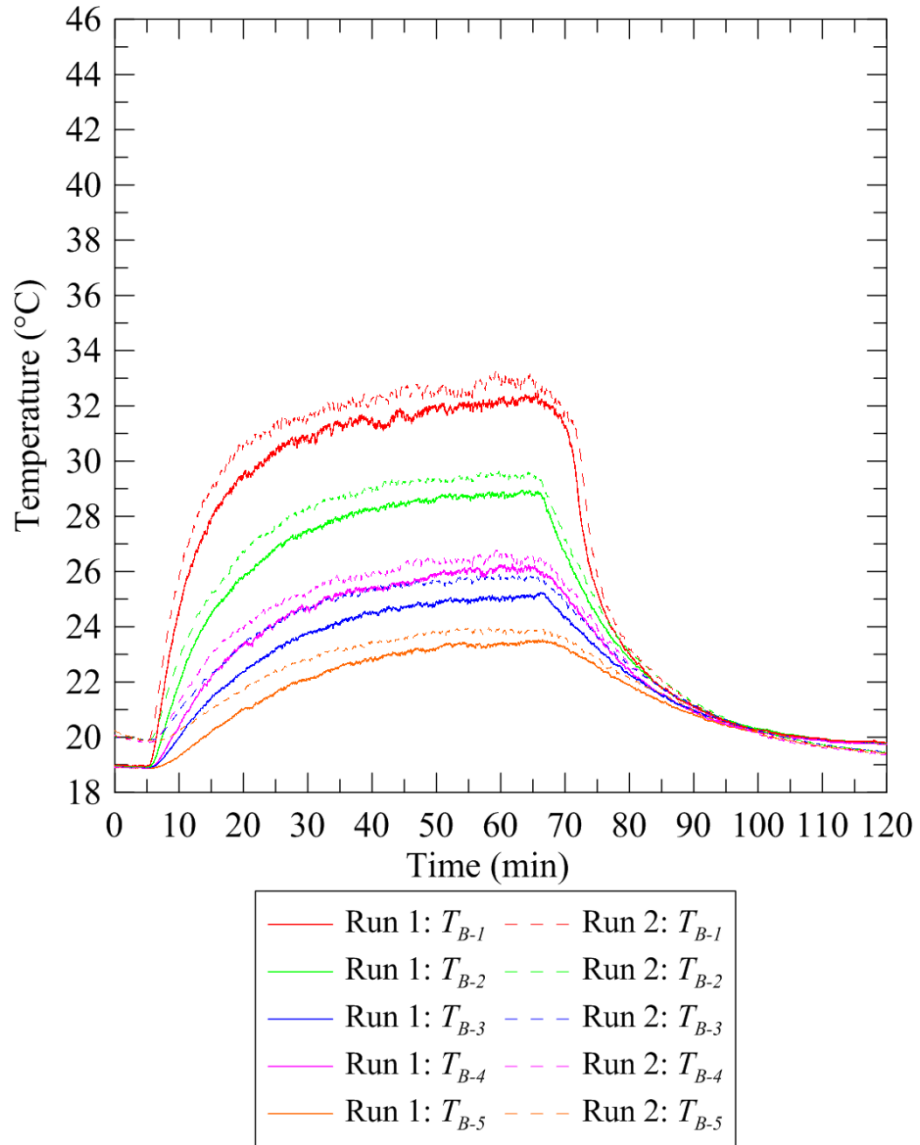
Fig. 5.13 Temperature measurements, from two runs of the experiment, on the back surface of the mock tablet with the heat spreader installed and a heat generation rate of 5W
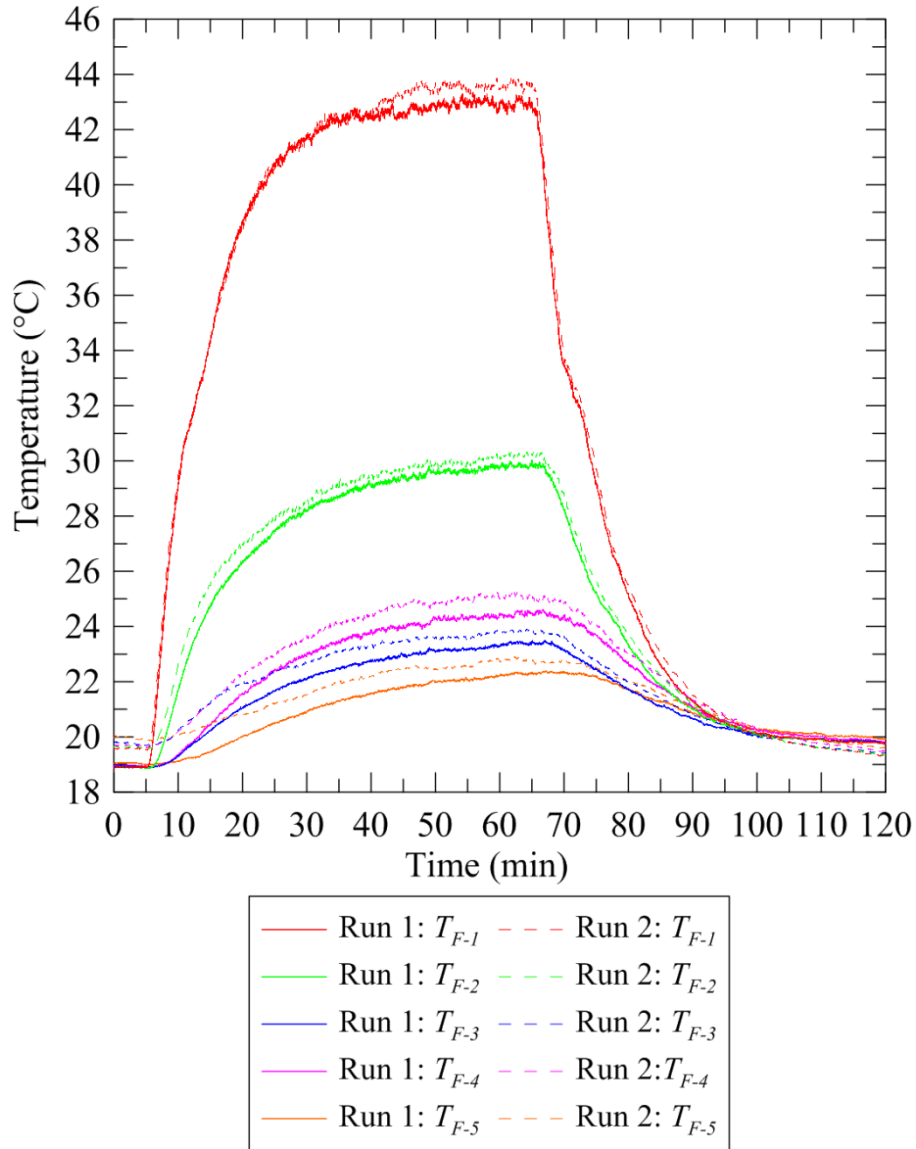
Fig. 5.14 Temperature measurements, from two runs of the experiment, on the front surface of the mock tablet with the heat spreader installed and a heat generation rate of 5W

5.7.2 Experimental Protocol

The steady heat generation experiments, presented in this chapter, consisted of a 60-minute heating phase, and a cooling phase where the heater was inactive. Three main cases were studied and compared. All cases are summarized in Table 5.3.

Table 5.3 Summary of the different cases which were studied

Experimental Case	Description
No temperature control solution	The space between the heater and the back cover is left empty. Mock tablet was oriented with the display facing upwards.
Aluminum heat spreader	The aluminum heat spreader is placed next to the heat source. Mock tablet was oriented with the display facing upwards.
Aluminum heat spreader and LHTES module	The aluminum heat spreader is placed next to the heat source and the LHTES module is placed between the heat spreader and the back cover. Mock tablet was oriented with the display facing upwards.

The three cases above were run for heat generation rate of 4.5 and 7 W. Experiments were initially run with the heat spreader and LHTES module placed into the mock tablet and secured in place using polyimide tape. When the spreader and the LHTES module were installed the spreader was placed between the LHTES module and the heater. Ultimately, it was determined that there was too little thermal coupling between the heater and the temperature control solution and a thermal interface material (TIM) was placed between the heater and the thermal spreader. The TIM used was a silicone based thermal grease, purchased from Laird Technologies Inc., called Tgrease 880. Tests with and without grease are presented.

Heating times were 60 minutes for all experiments except those cases which exceeded a cut-off temperature of 95°C at the heater. In those cases, the power was manually shutoff early to avoid damage to the experimental setup.

Combining the three cases, two heat generation rates, and TIM a total of 10 experimental studies are presented. Table 5.4 summarizes each of the individual studies.

Table 5.4 Summary of experimental studies presented

Experimental Case	Heat Generation Rate (W)	Thermal Grease	
No temperature control solution	4.5	no	#1
	7	no	#2
Aluminum heat spreader	4.5	no	#3
		yes	#4
	7	no	#5
		yes	#6
Aluminum heat spreader and LHTES module	4.5	no	#7
		yes	#8
	7	no	#9
		yes	#10

5.8 Results and Discussion

5.8.1 Heat Generation Rate of 4.5 W

5.8.1.1 No Temperature Control Solution

In this study, no temperature control solution was included in the mock tablet and the heat generation was set to 4.5 W. This is the heat generation which was produced by the SOC and memory (sources which are typically located near one another) in the heat dissipation profile supplied to the author by Intel Corporation for the numerical study presented in Chapter 2. During this experiment, the heater exceeded the high temperature limit for an SOC (80°C) in 2.6 minutes, and the cut-off temperature at approximately 12.5 minutes. Figure 5.15 shows the temperatures which were measured inside the mock tablet. The heater temperature increased rapidly. There was limited spreading along the PCB, and virtually no temperature increase in the battery.

Fig. 5.15 Temperature measurements on the inside of the mock tablet with no temperature control solution installed and a heat generation rate of 4.5 W (dotted line represents the SOC temperature limit)

Figure 5.16 shows the temperatures measured on the back surface. Even though the heating phase was halted at just over 12.5 minutes, the back surface still exceeded the comfort threshold of 40°C. This was partially due to a lack of spreading. The temperature profile on the back cover was non-uniform.

Fig. 5.16 Temperature measurements on the back surface of the mock tablet with no temperature control solution installed and a heat generation rate of 4.5 W (dotted line represents the surface temperature limit)

Figure 5.17 shows the temperatures measured on the front surface (display). The temperatures on the front surface were much lower than those on the back surface. The heater was closer to the back surface, and there was much more thermal mass between the heater and the front surface.

Fig. 5.17 Temperature measurements on the front surface of the mock tablet with no temperature control solution installed and a heat generation rate of 4.5 W (dotted line represents the surface temperature limit)

With 4.5 W of heat generation and no temperature control solution, the tablet could only operate for 2.6 minutes before it overheated. This temperature limit was reached at the heater first. The thermal resistance between the heater and other components was high. There was limited heat spreading potential in the mock tablet without the aid of a temperature control solution.

5.8.1.2 Aluminum Heat Spreader

In this study, the aluminum heat spreader was placed against the heater, no TIM was used, and the heat generation was set to 4.5 W. The 60-minute heating phase was completed. Temperatures inside the tablet increased slower than with no temperature control solution (see Fig. 5.18). The heater exceeded 80°C after approximately 5.3 minutes. The temperatures inside were still non-uniform, there was little temperature increase in the battery or far end of the PCB.

The back surface temperatures were strongly impacted by the presence of the heat spreader (See Fig. 5.19). The maximum back surface temperature did not exceed the comfort threshold and the temperatures were much more uniform than in the study with no temperature control solution. The maximum temperature difference measured across the back surface (between T_{B-1} and T_{B-5}) was approximately 8.7 °C.

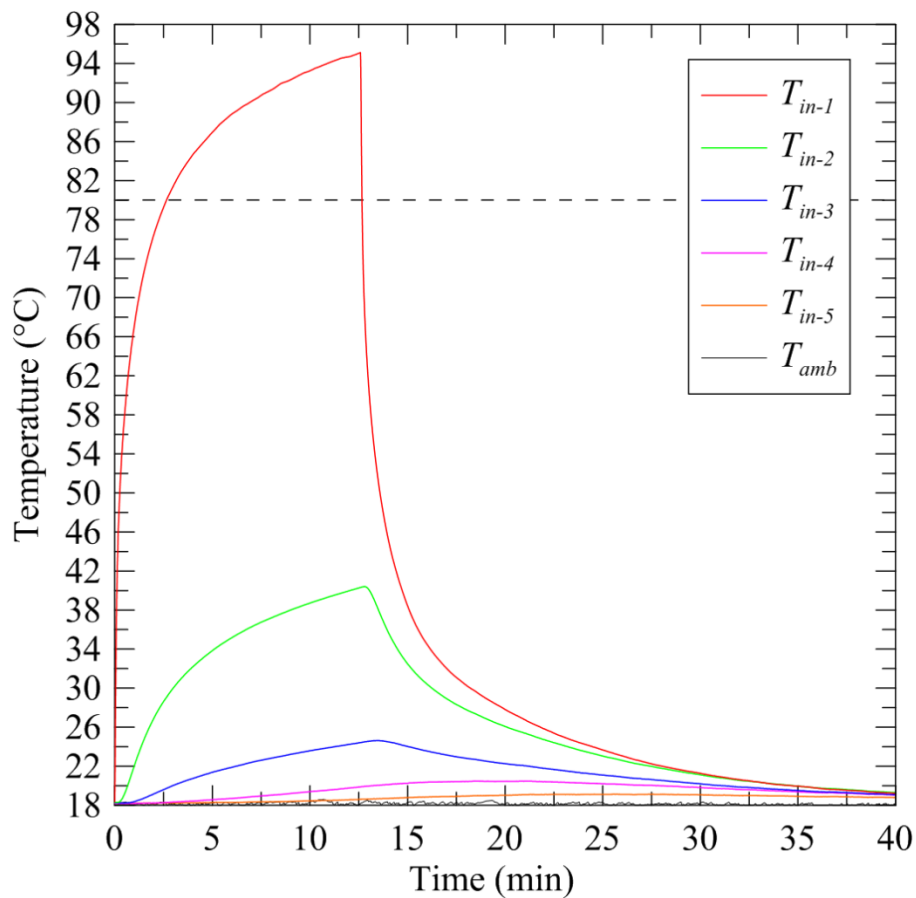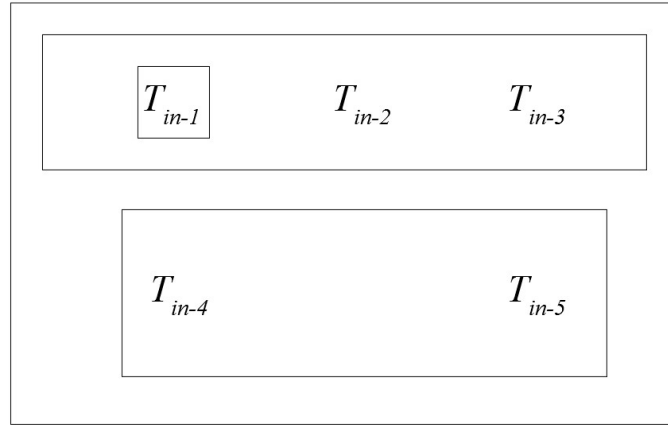**Fig. 5.18 Temperature measurements on the inside of the mock tablet with the heat spreader installed and a heat generation rate of 4.5 W (dotted line represents the SOC temperature limit)**
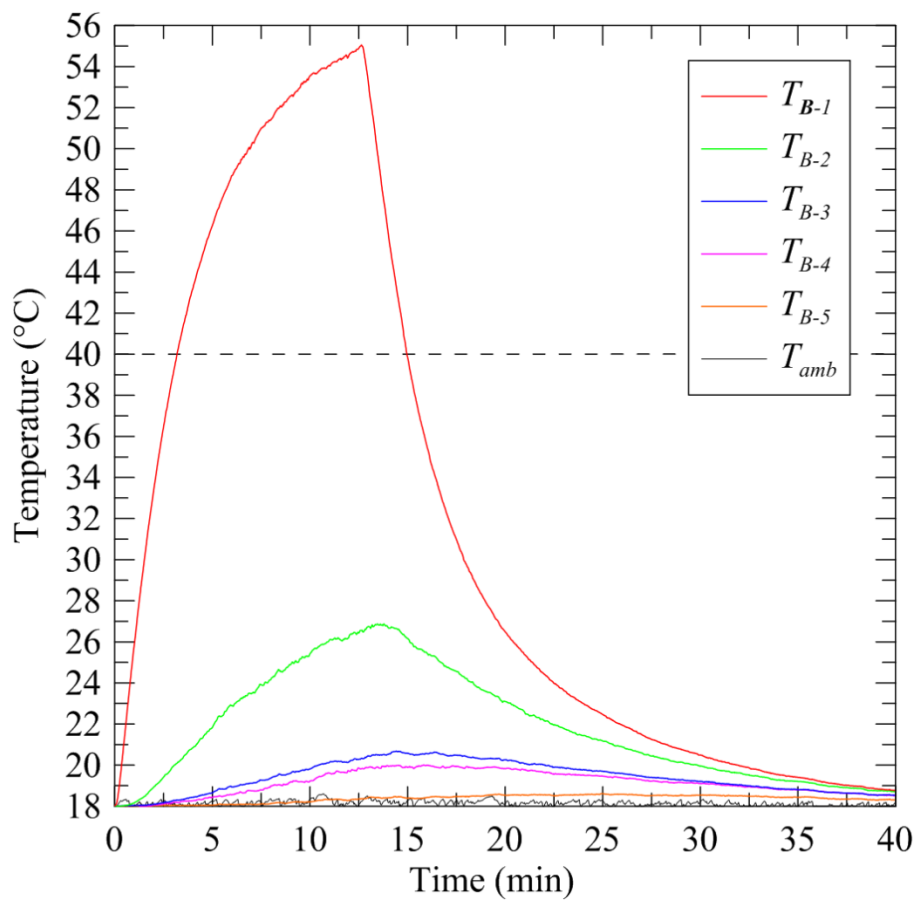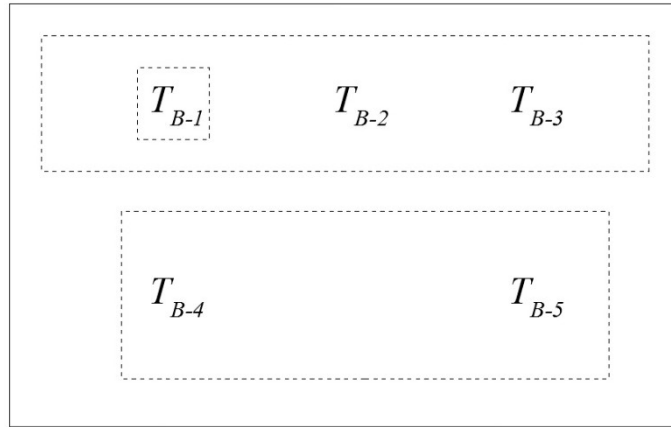
Fig. 5.19 Temperature measurements on the back surface of the mock tablet with the heat spreader installed and a heat generation rate of 4.5 W (dotted line represents the surface temperature limit)

The front surface temperatures were higher than the back surface temperatures (see Fig. 5.20). The temperature distribution on the front cover was not as uniform as the back surface and passed the comfort threshold at approximately 23.7 minutes. In an actual tablet, the processor would have

had to throttle after 5.3 minutes to keep the SOC cool and the front cover temperature likely would not have been a problem.

There was an odd inflection in the front cover temperature profile. This inflection existed during the heating and cooling phase and appeared to come from latent heat storage. The author cleaned all residual PCM from the accessible areas of the display assembly. There was potentially a small amount of PCM imbedded in the display assembly, likely due to leaks which occurred during testing by Ahmed (2016). The inflections are small and will not pose a significant problem for the testing, they only seem to appear in measurements at T_{F-1}. If anything, it makes the findings more conservative as there was a small amount of latent heat storage present in the empty comparison cases.

It was challenging to make a direct comparison to the experiment with no temperature control solution due to the difference in the length of the heating phase. However, comparing the temperatures for the first 12.5 minutes, the impact of the heat spreader can be seen. The increase in temperatures measured at position 4 were higher (between 3 and 4°C) for both the back surface and inside. This indicates that heat was being more easily conducted across the width of the mock tablet.

The back surface temperature was approximately 26°C cooler at 12.5 minutes. inserting the heat spreader reduced the maximum back surface temperature by spreading the heat conducted to the surface over a larger area. The reduction in the heater temperature at 12.5 minutes was also large (~10°C). Interestingly, the inclusion of the heat spreader had little impact on the front surface temperature at 12.5 minutes.

If the decrease in the heater temperature represented a decrease in its average temperature, due to the spreader decreasing the resistance to convection on the back cover, then the author would expect to see a reduction in the temperatures measured on the front cover. The author would speculate that the temperature decrease in the heater was due largely to an increase in uniformity through the heater itself, not a reduction in its average temperature.

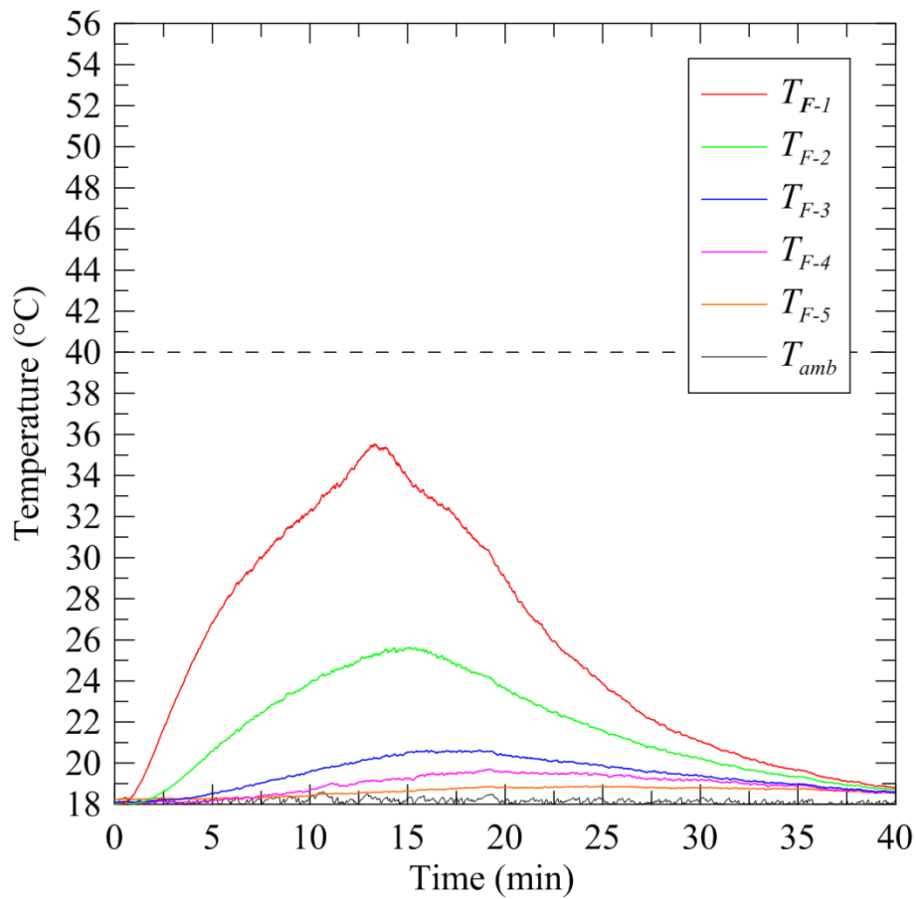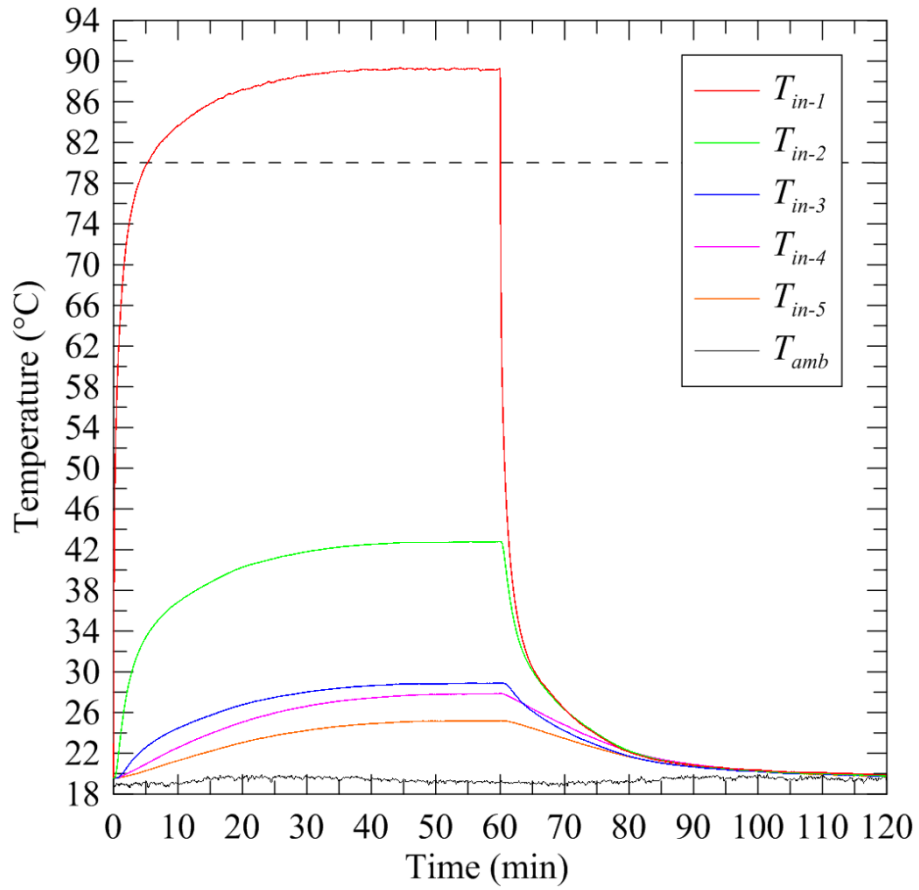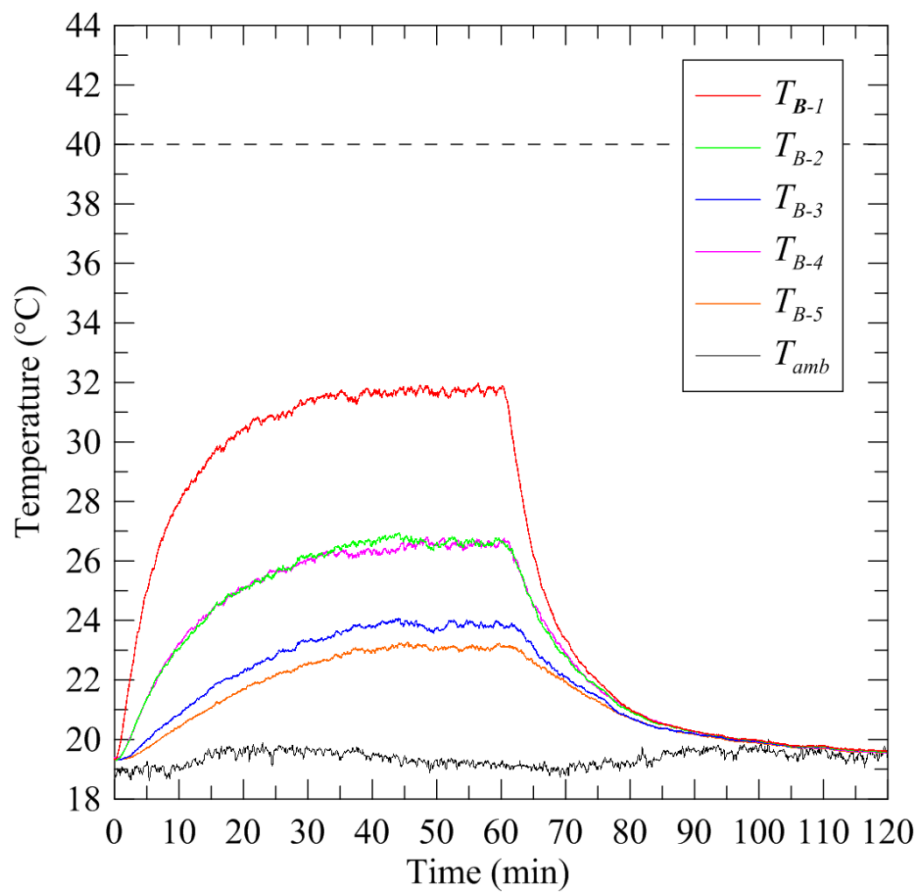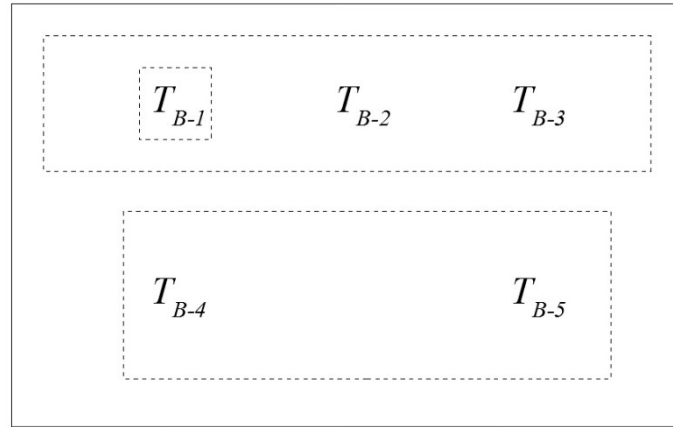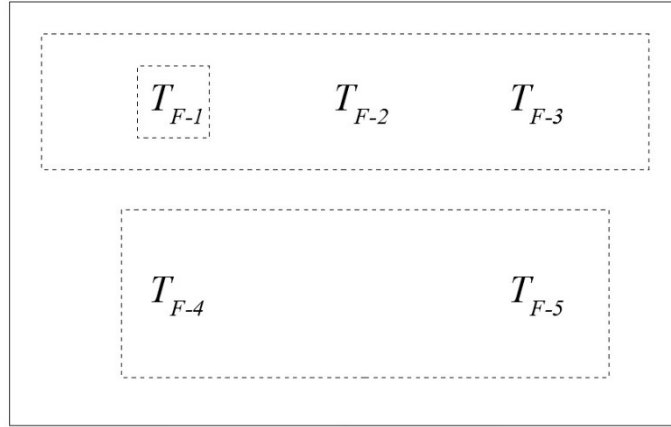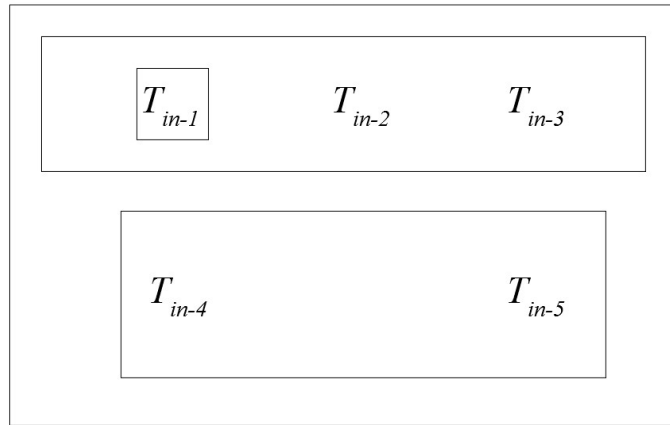**Fig. 5.20 Temperature measurements on the front surface of the mock tablet with the heat spreader installed and a heat generation rate of 4.5 W (dotted line represents the surface temperature limit)**

5.8.1.3 Aluminum Heat Spreader and TIM

In this study, thermal grease was placed on the heater and the aluminum heat spreader was placed against the heater. The heat generation rate was set to 4.5 W. The 60 minute heating phase was

completed. Temperatures inside the tablet were lower when compared to the experiment without grease (see Fig. 5.21). The heater did not exceed 80°C. The temperatures inside the mock tablet were more uniform, but this was mostly due to the heater temperature being lower while the temperature along the PCB and battery were similar to the study without grease.
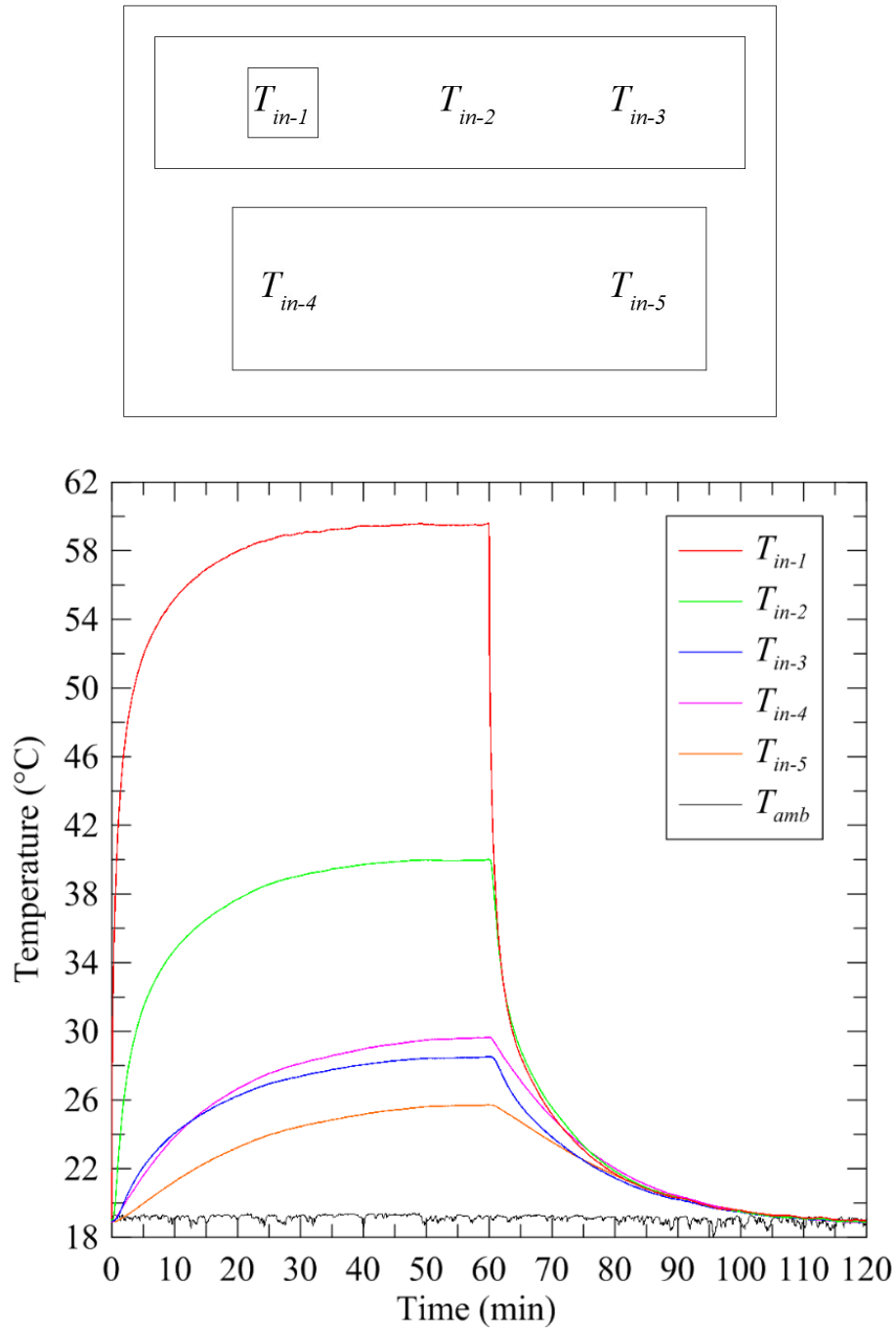
Fig. 5.21 Temperature measurements inside the mock tablet with the heat spreader installed with TIM and a heat generation rate of 4.5 W

Temperatures measured on the back surface were higher than the case without grease (see Fig. 5.17). Placing the grease between the heater and heat spreader reduced the resistance to heat transfer between the heater and the back surface. Reducing this resistance decreased the temperature of the heater and increased the back surface temperature. However, while the temperatures were higher with grease (2.4°C at 60 min), they still did not exceed the comfort threshold.

The temperatures measured on the front surface showed a modest decrease (see Fig. 5.23) when compared to the case without grease. More heat was dissipated through the back surface diverting it away from the front surface, resulting in this decrease. Temperatures on the front surface did not exceed the comfort threshold. The system did not reach steady state during the 60 minute heating phase but it was clear this temperature control solution would allow the mock tablet to operate at 4.5 W for an extended period of time, much longer than 60 minutes.

Fig. 5.22 Temperature measurements on the back surface of the mock tablet with the heat spreader installed with TIM and a heat generation rate of 4.5 W
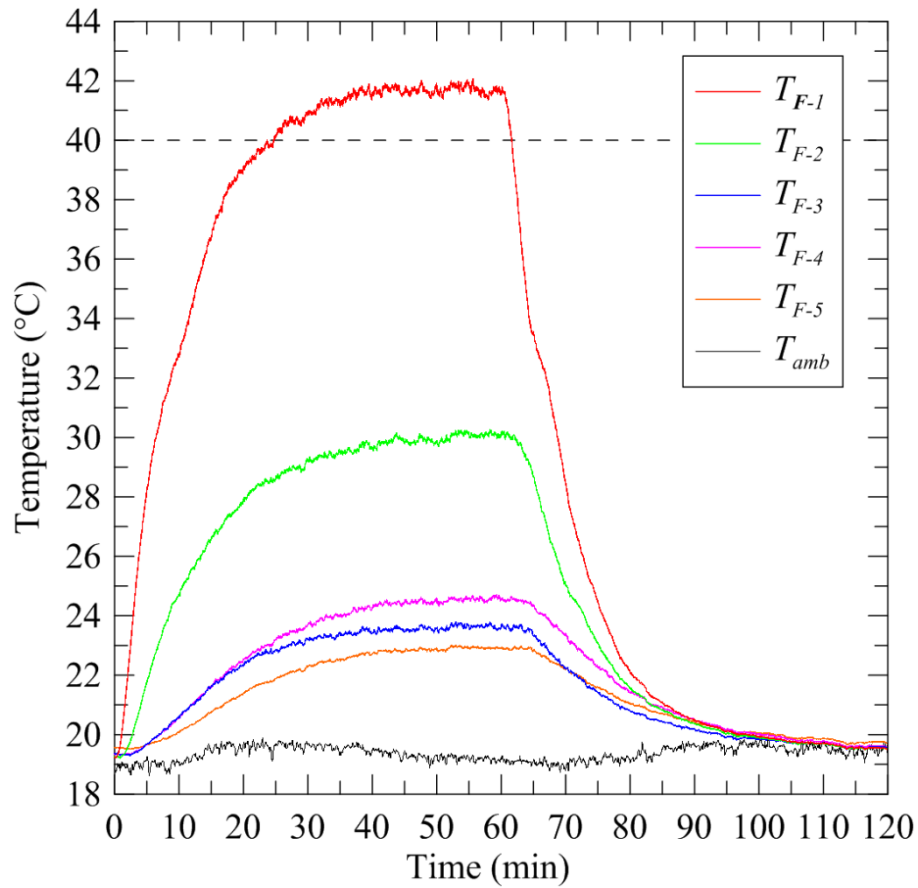
Fig. 5.23 Temperature measurements on the front surface of the mock tablet with the heat spreader installed with TIM and a heat generation rate of 4.5 W

5.8.1.4 LHTES Module and Aluminium Heat Spreader

In this study, the aluminum heat spreader was placed against the heater and the LHTES module was placed between the heat spreader and the back cover. The heat generation rate was set to 4.5 W. The 60-minute heating phase was completed. The heater exceeded 80°C after approximately

15.3 minutes (see Fig. 5.24). This was slower than the case with only the heat spreader. However, there was no sign of an inflection in the temperature profiles, indicating there was little, if any, melting in the LHTES module. Figure 5.25 shows the temperatures measured on the back surface. There was little change in the magnitude of the back cover with the addition of the LHTES module and the uniformity was similar. The lack of any inflection in the temperature profiles measured on the back surface indicated that latent heat energy storage did not having much impact on the back surface temperature. Temperatures measured on the front surface were only moderately impacted by the presence of the LHTES module (see Fig. 5.26). It exceeded the comfort threshold at approximately 28.6 minutes compared to 23.7 minutes for the experiments without the LHTES module.

Fig. 5.24 Temperature measurements inside the mock tablet with LHTES module, heat spreader and a heat generation rate of 4.5 W (dotted line represents the SOC temperature limit)
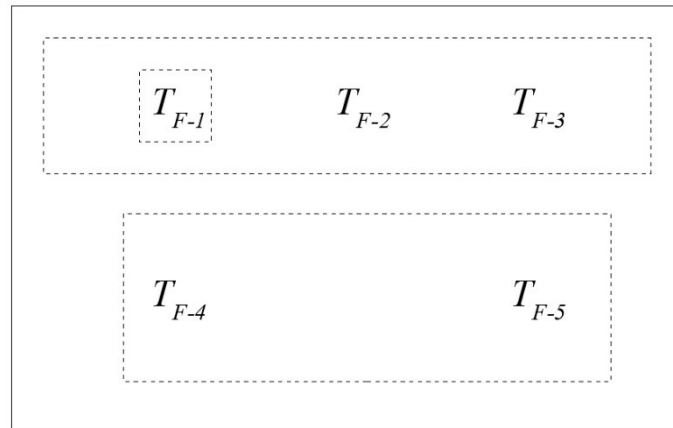
Fig. 5.25 Temperature measurements on the back surface of the mock tablet with LHTES module, heat spreader and a heat generation rate of 4.5 W (dotted line represents the surface temperature limit)
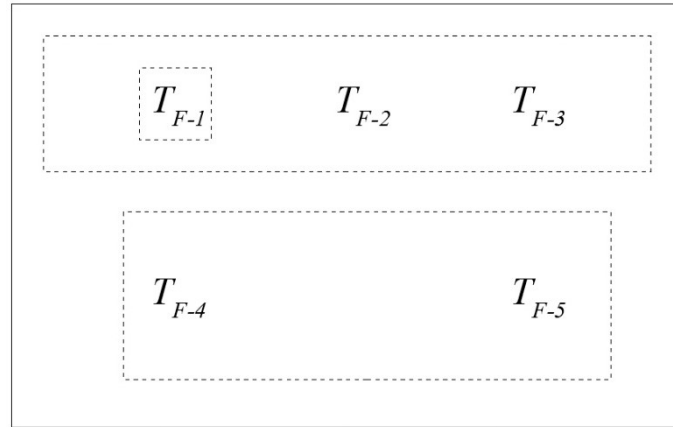
Fig. 5.26 Temperature measurements on the front surface of the mock tablet with LHTES module, heat spreader and a heat generation rate of 4.5 W (dotted line represents the surface temperature limit)

There was a lack of clear evidence indicating any significant phase change in the LHTES module. The LHTES module improved the performance of the system, the author speculates that the reduction in temperatures was associated with the thermal mass of the LHTES module. There was likely localized melting just above the heater as was seen in the experiments presented in Chapter

3. However, with a heat generation rate of 4.5 W, the LHTES module did not have a large impact on the temperature control of the mock tablet computer. Coupling the temperature control solution more closely to the heat source may resolve some of these issues. The heaters temperature was far above the melting temperature of the PCM. Placing TIM between the heater and the temperature control solution should increase the temperature of the LHTES module and amount of melting.

5.8.1.5 LHTES module, Aluminum Heat Spreader, and TIM

In this study, the aluminum heat spreader was placed against the heater and the LHTES module was placed between the heat spreader and the back cover. TIM was placed between the heater and the heat spreader. The heat generation rate was set to 4.5 W. The 60-minute heating phase was completed. As with previous experiments, the impact of the TIM was large. Neither the heater temperature nor the tablet surface reached their critical temperature limit (see Figs. 5.27 to 5.29). There was clear evidence of phase change in this experiment. Inflections were visible in the temperature profile inside the mock tablet (T_{in-1} and T_{in-2}), on the back surface (T_{B-1}) and the front surface (T_{F-1}). It was not possible to estimate the melting fraction in these experiments. However, there was significant evidence that the LHTES module was storing heat and positively effecting the temperature control of the mock tablet computer. The maximum temperatures of each experiment are compared in the next section.

All of the previous experiments with 4.5 W of heat dissipation have shown a similar trend taking about 60 minutes to cool back to ambient temperature after the 60 minute heating phase. This remained true when there was melting in the LHTES. There was speculation in literature that the presence of the LHTES module could prolong the time required to cool the device off. This was not seen in this experiment, it cooled back to ambient in approximately 60 minutes.
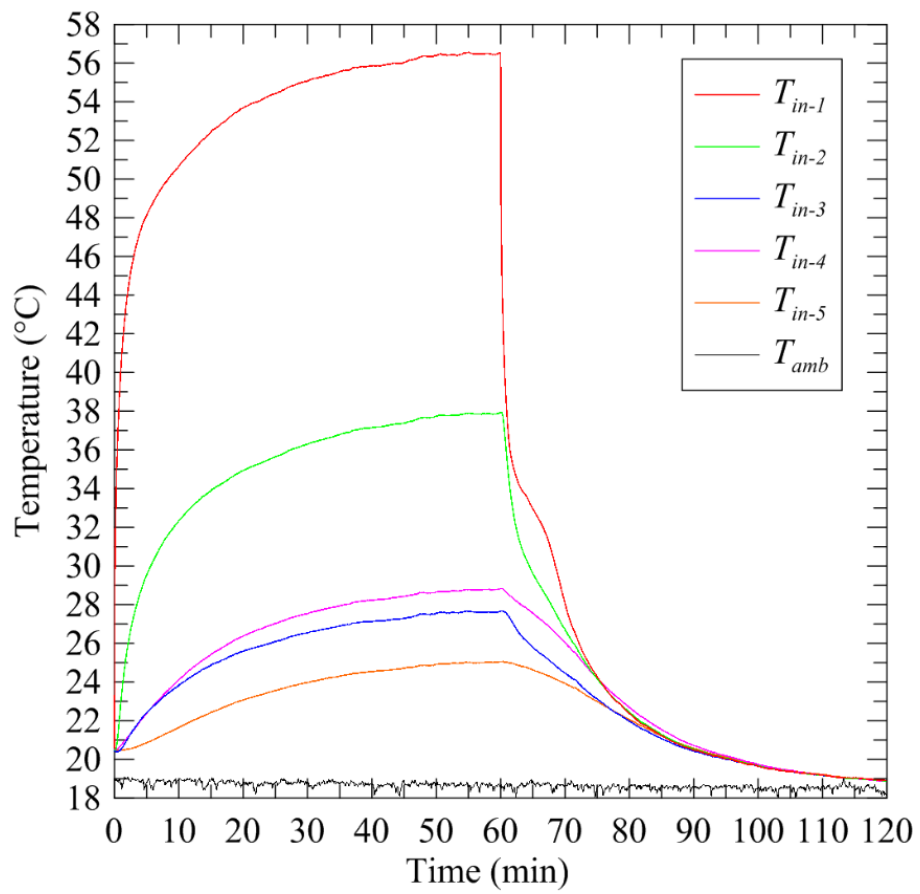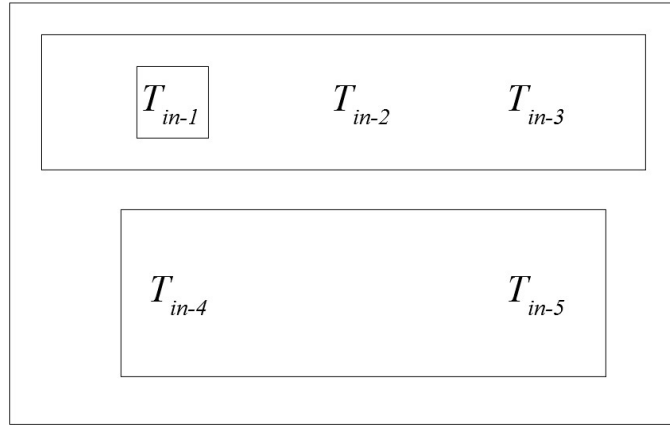
Fig. 5.27 Temperature measurements inside the mock tablet with LHTES, heat spreader, TIM, and a heat generation rate of 4.5 W
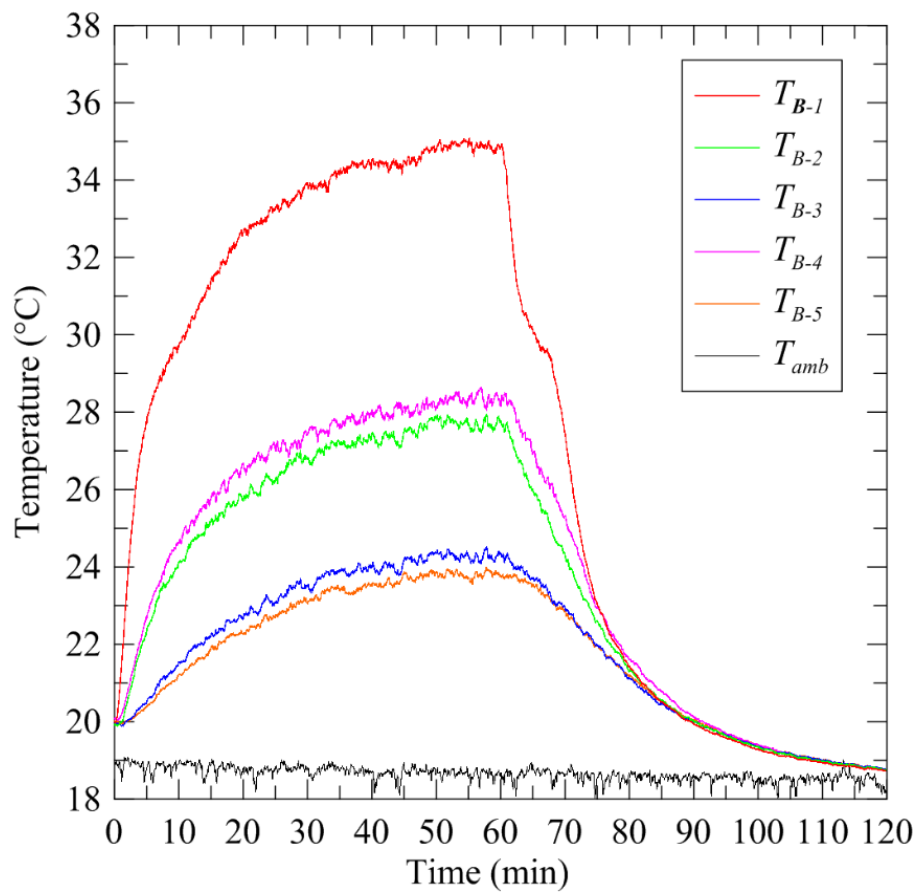
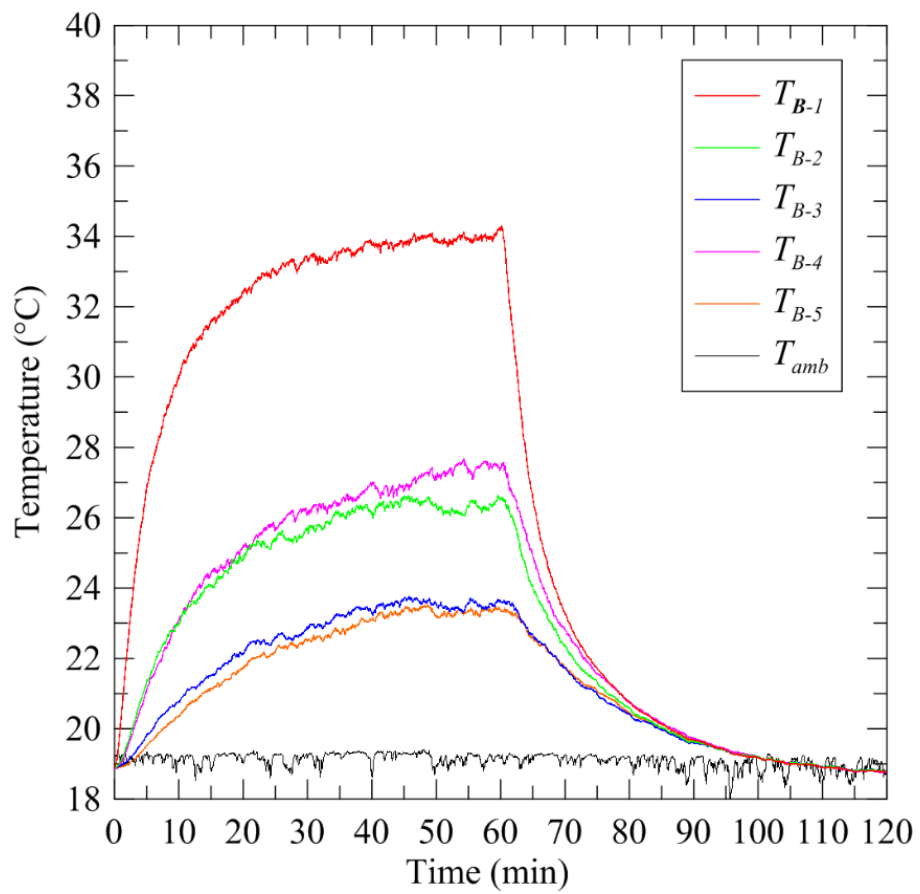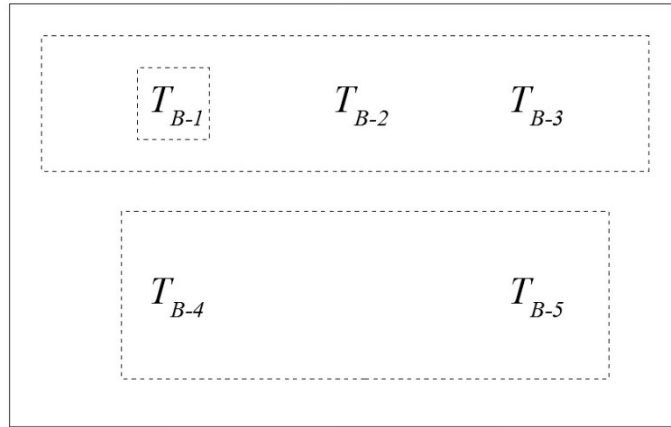**Fig. 5.28 Temperature measurements on the back surface of the mock tablet with LHTES, heat spreader, TIM, and a heat generation rate of 4.5 W**
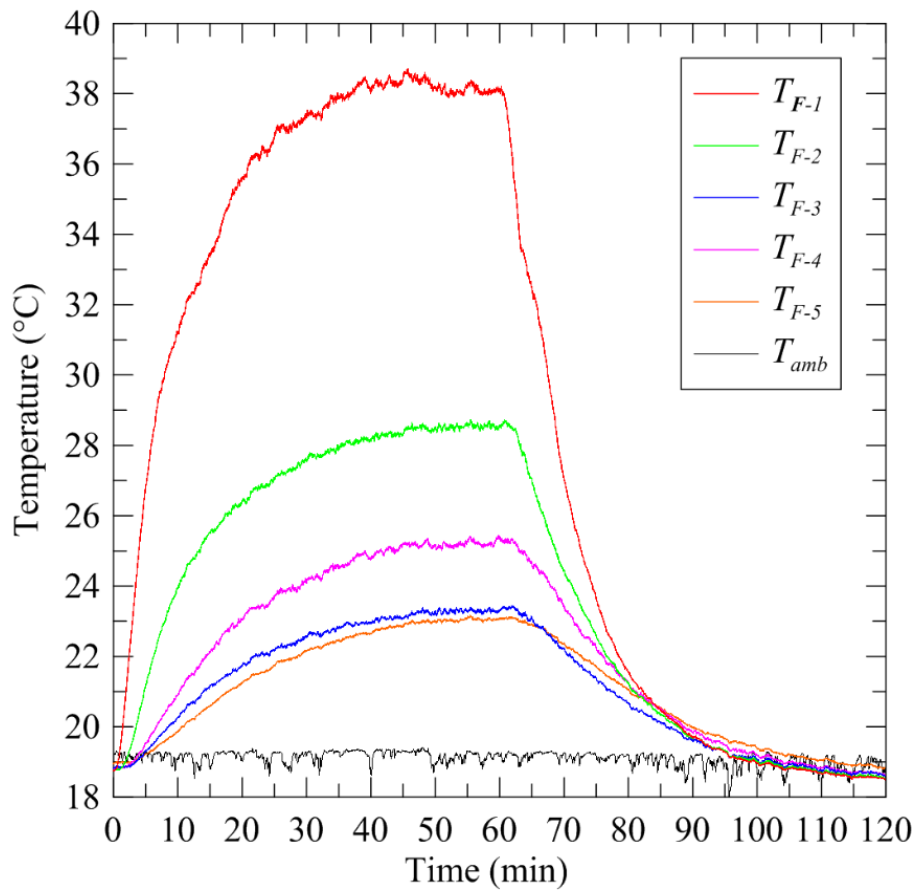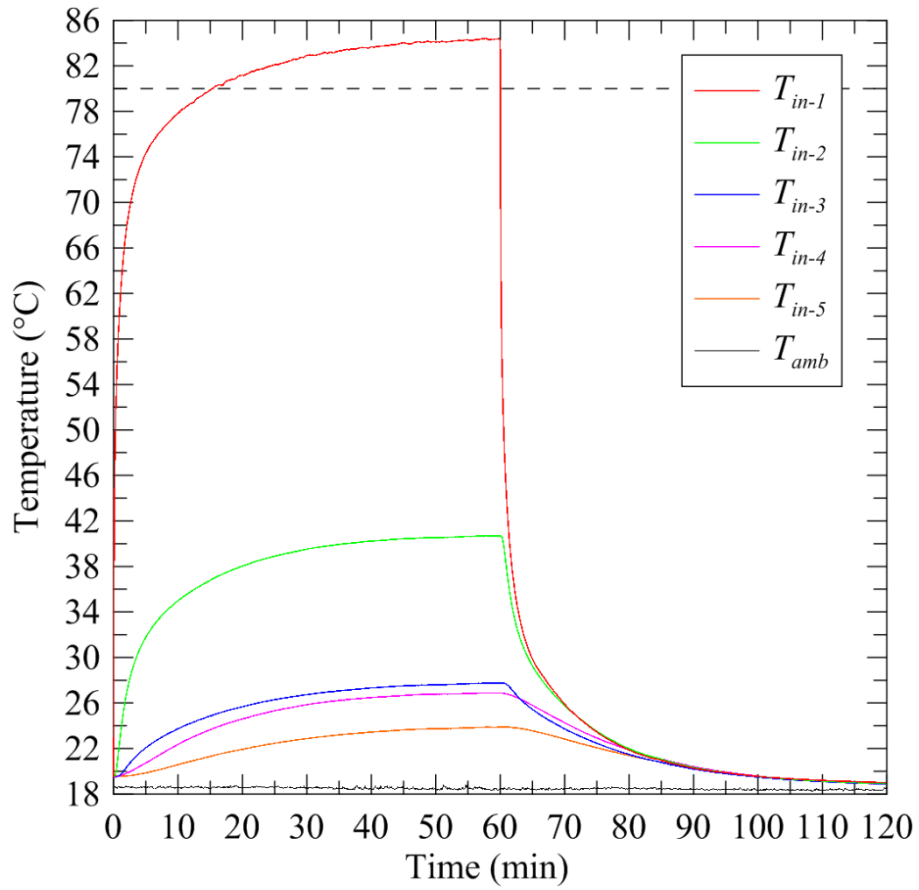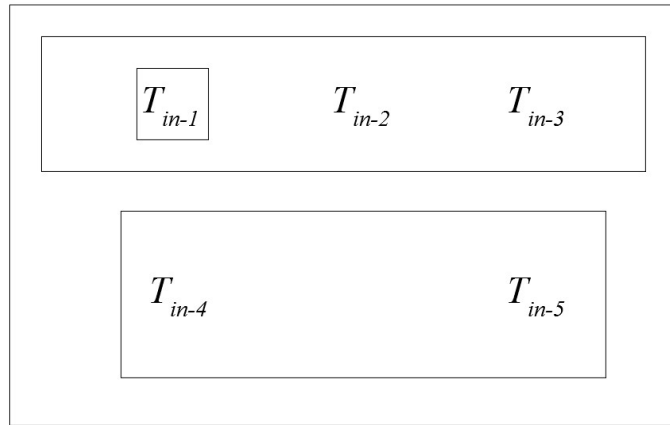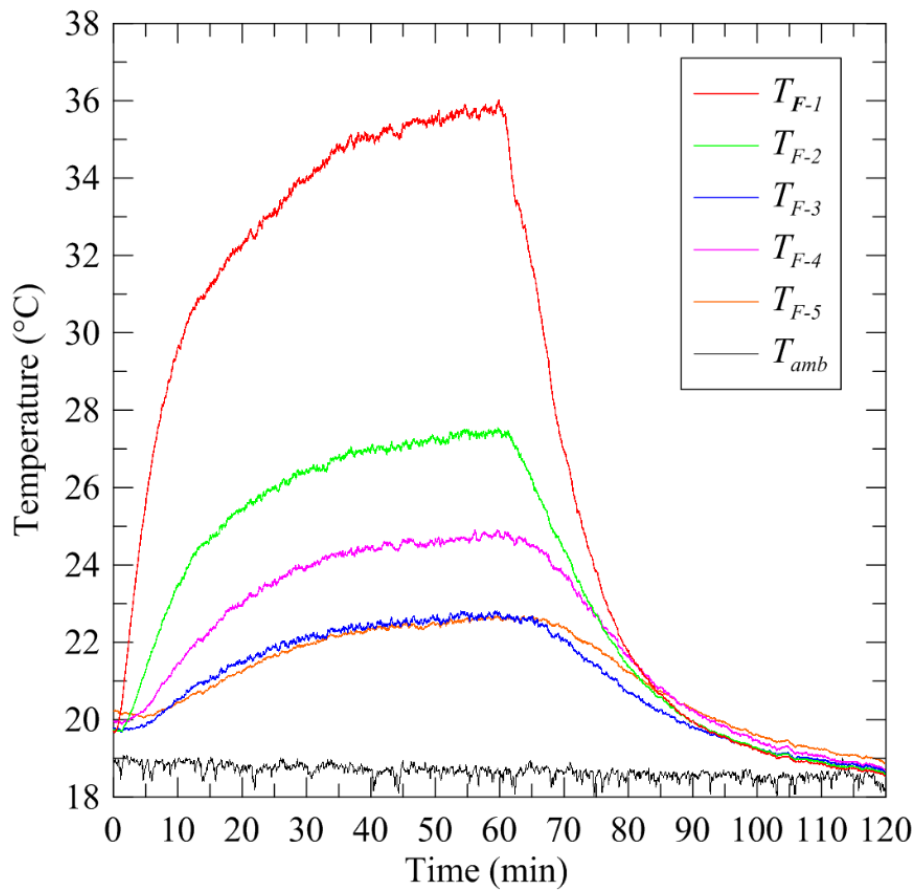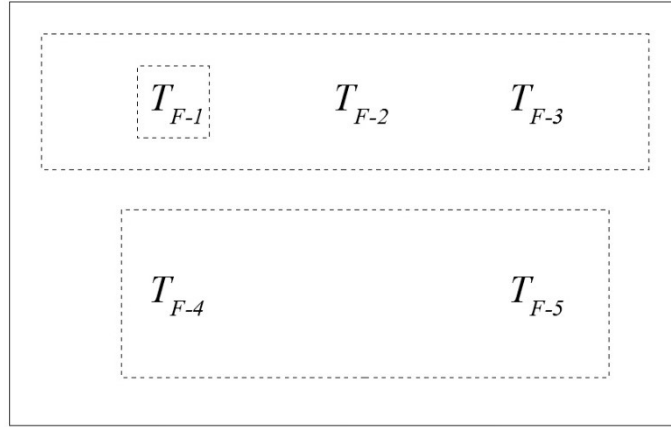
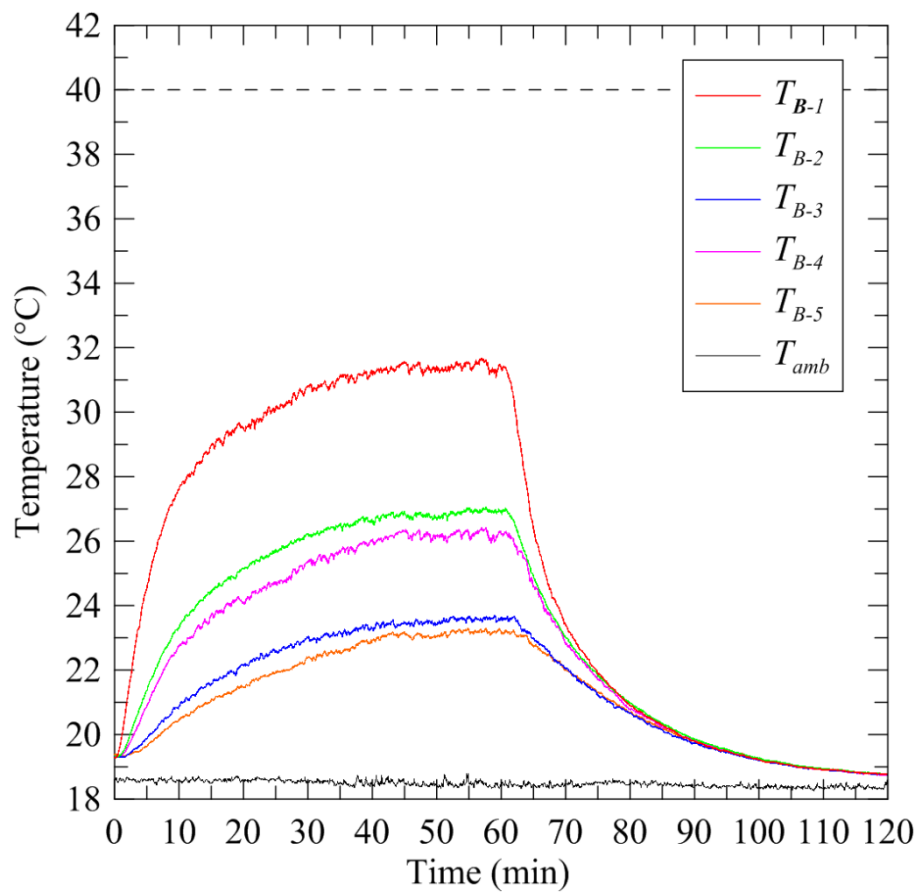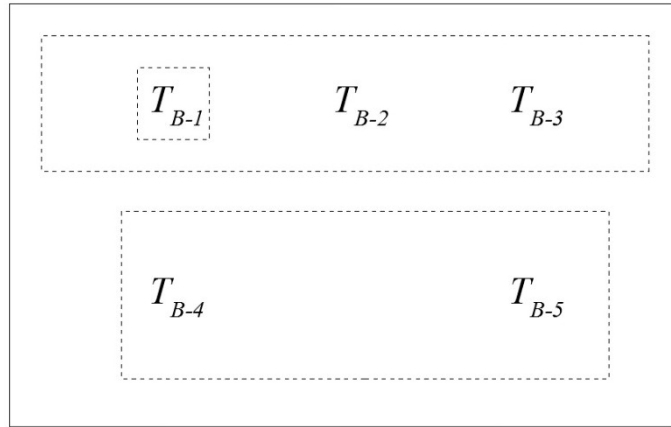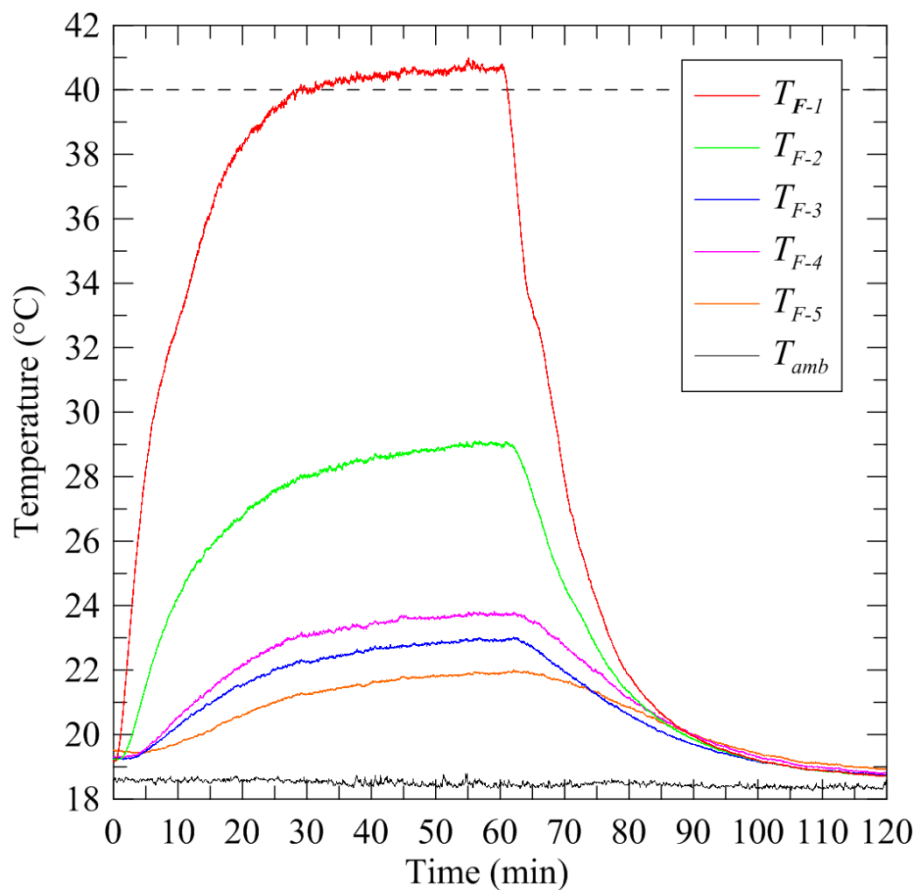**Fig. 5.29 Temperature measurements on the front surface of the mock tablet with LHTES, heat spreader, TIM, and a heat generation rate of 4.5 W**

5.8.1.6 Summary for a heat generation rate of 4.5 W

Figure 5.30 shows the heater temperature for each experiment in this section. The temperature control solution with the LHTES module, heat spreader, and TIM resulted in the lowest heater temperatures. However, while this was the best solution from the perspective of the heater, the

120

solution with a heat spreader and TIM was also able to keep the heater temperature below the SOC temperature limit (80°C). An experiment with a higher heat generation rate could give more information about the magnitude of difference between these temperature control systems.
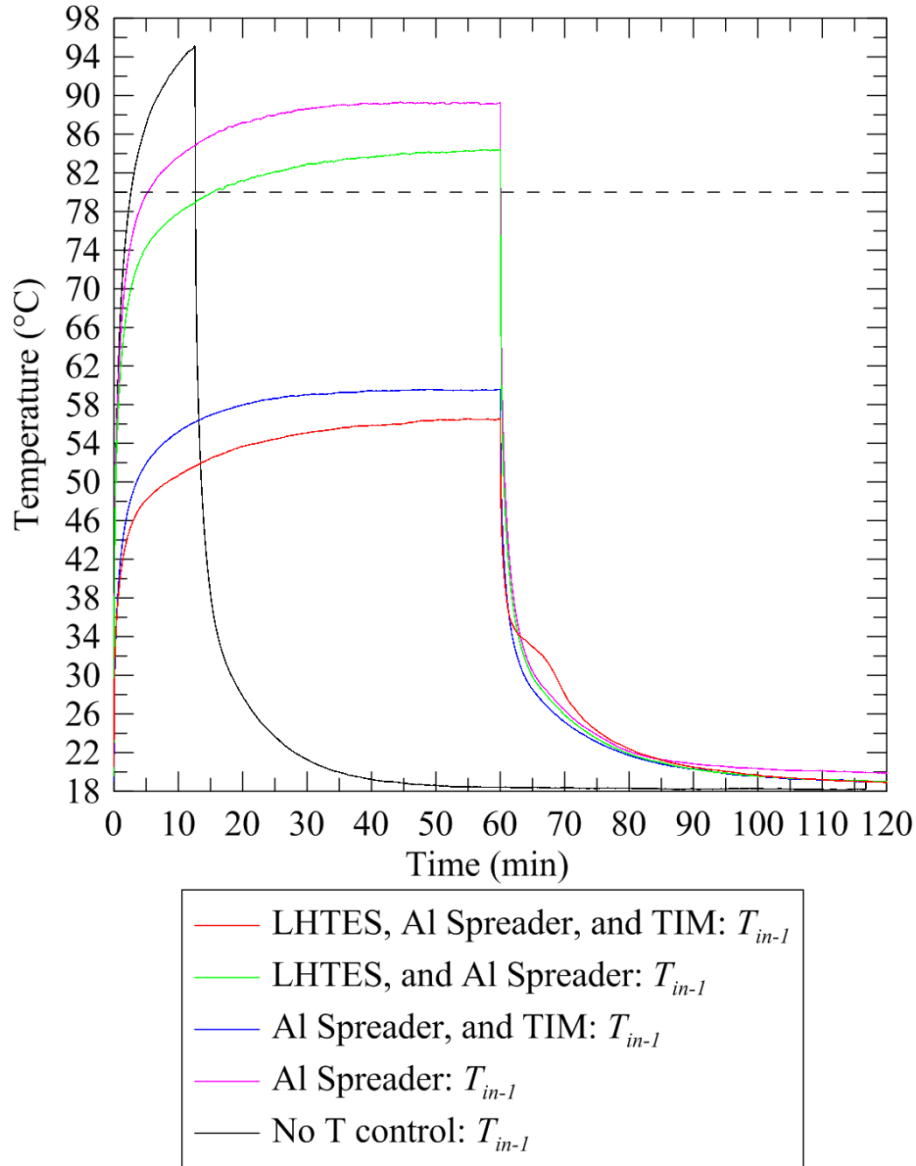
Fig. 5.30 Comparison of the temperature profiles of the heater for all experiments with a heat generation rate of 4.5 W (dotted line represents the SOC temperature limit)

The maximum back surface temperature will be found just above the heat source (T_{B-1}). Figure 5.31 compares the maximum back surface temperature for all experiments with a heat generation rate of 4.5 W. Differences between the various temperature control solutions were much less pronounced on the back surface than they were on the heater temperatures. All temperature control

solutions protected the back surface from overheating. However, the temperature control solution with the LHTES module, heat spreader, and TIM was the worst solution except for in a small window between 10 and 20 minutes. These trends are reminiscent of those seen in the numerical simulations. The temperature control solution at the back of the mock tablet reduced the thermal resistance between the heater and the back surface. This reduced the heater temperature but if sufficient heat was not absorbed by the LHTES module it could increase the back surface temperature.
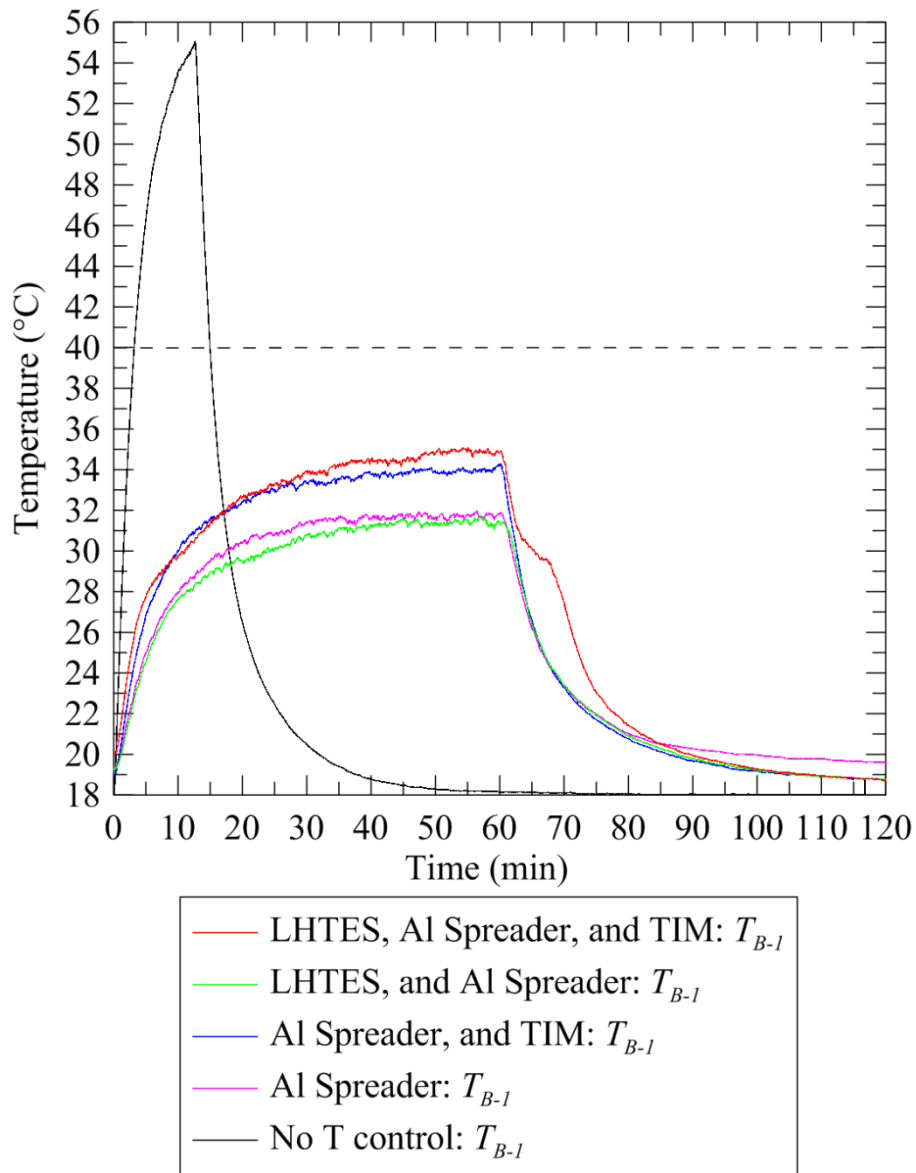
Fig. 5.31 Comparison of the temperature profiles of the back surface (T_{B-1}) for all experiments with a heat generation rate of 4.5 W (dotted line represents the surface temperature limit)

The maximum temperatures of the front surface are compared in Fig. 5.32. Clearly the LHTES module, heat spreader and TIM was the most effective temperature control solution for the front surface of the mock tablet.
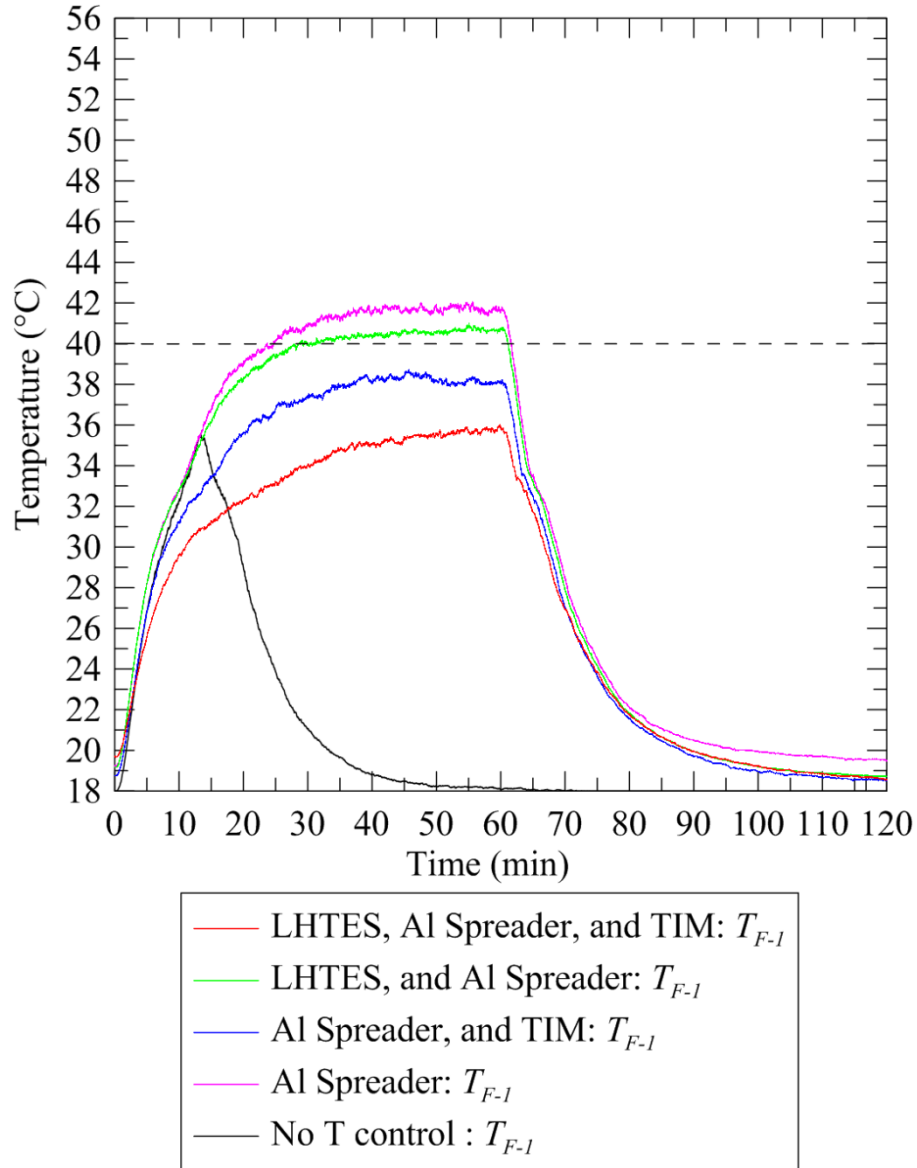
Fig. 5.32 Comparison of the temperature profiles of the front surface (T_{F-1}) for all experiments with a heat generation rate of 4.5 W (dotted line represents the surface temperature limit)

Table 5.5 summarizes the time required for the heater, back surface, and front surface to reach their respective temperature limits. Entries in the table showing dashes indicate the feature did not reach its limiting temperature during a 60-minute experiment. Asterisks indicate that the feature did not reach its limiting temperature but that the experiment in questions was stopped early. In

123

this format, larger times show superior performance. The two temperature control solutions which utilize TIM are by far the best solutions as seen be neither of them reaching their temperature limits within the 60-minute heating phase of the experiment.

Table 5.5 Summary of the time required for the mock tablet to reach the respective temperature limits with a heat generation rate of 4.5 W

	operational time before reaching temperature limit (min)			
	heater source (T_{lim}=80°C)	back surface (T_{lim}=40°C)	front surface (T_{lim}=40°C)	minimum
no T control	2.6	3.2	*	2.6
heat spreader	5.3	-	23.7	5.3
Spreader, and TIM	-	-	-	-
LHTES, and spreader	15.3	-	28.6	15.3
LHTES, spreader, and TIM	-	-	-	-

" - " indicates region did not overheat during the experiment

" * " indicates region did not overheat, however, the heating phase was stopped before 60 minutes

The use of a TIM had a large impact on the results, closely coupling the temperature control solution to the heater was critical. The contact resistance between the heater and the temperature control solution was large and without TIM, the heater overheated before the LHTES module reached its transition temperature.

Thermal spreading inside the tablet was relatively poor and much of the thermal mass of the mock tablet had little temperature increase. For example, the maximum temperature increase which was measured in the battery was approximately 10.7°C (T_{in-4} with heat spreader and TIM). The mean temperature increase in the battery was an order of magnitude smaller than the heater temperature increase. Much of the sensible storage capacity of the mock tablet was poorly used and this was not improved by any of the temperature control solutions.

Ultimately, the temperature control solution which included the LHTES module, heat spreader, and TIM was the most effective temperature control solution, preventing both the back and front surface from reaching 40°C and maintaining the lowest temperature at the heater. As was

previously stated, the temperatures were low for many of these tests. For this reason, the heat generation rate was increased to 7 W for the next set of experiments presented in the next section.

5.8.2 Heat Generation Rate of 7 W

5.8.2.1 No Temperature Control Solution

Figures 5.33 to 5.35 show the temperatures measured with no temperature control solution installed and a heat generation rate of 7 W. As with the lower heat generation rate, the system quickly overheated. The heater reached the cut-off temperature after approximately 1.1 minutes. This follows the same trends as the 4.5 W experiments, the back surface temperatures were higher than the front surface temperatures. It was not surprising that the mock tablet overheated so quickly. Mr. Ahmed estimated that the maximum heat generation rate for the original Dell tablet was 5 W (Ahmed, 2016). A heat generation rate of 7 W is well outside what it was designed to handle.
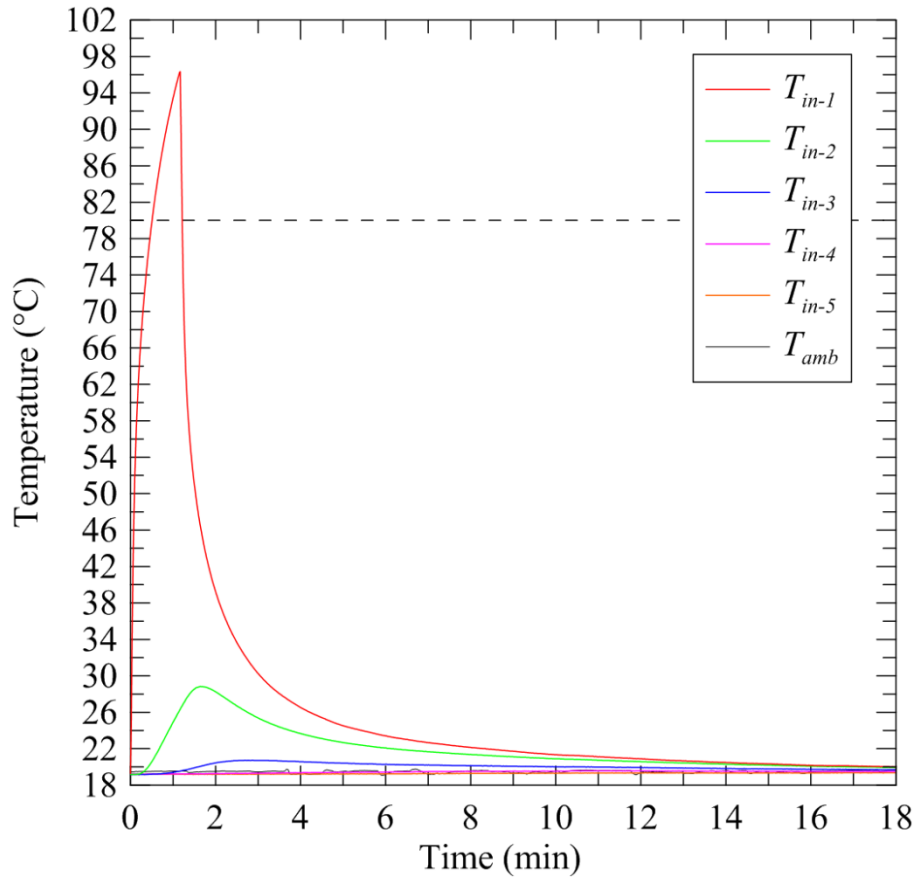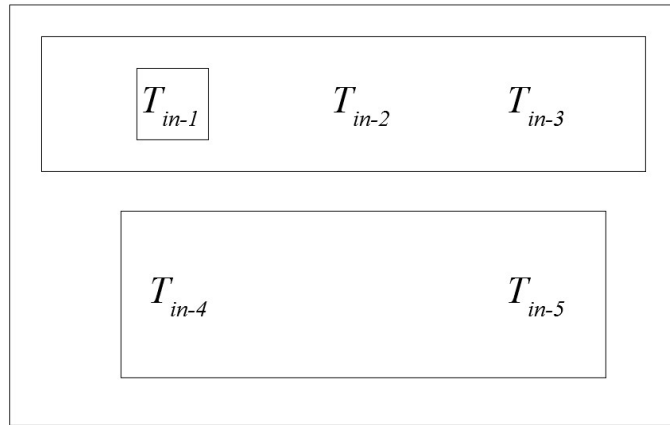
Fig. 5.33 Temperature measurements on the inside of the mock tablet with no temperature control solution installed and a heat generation rate of 7 W (dotted line represents the SOC temperature limit)
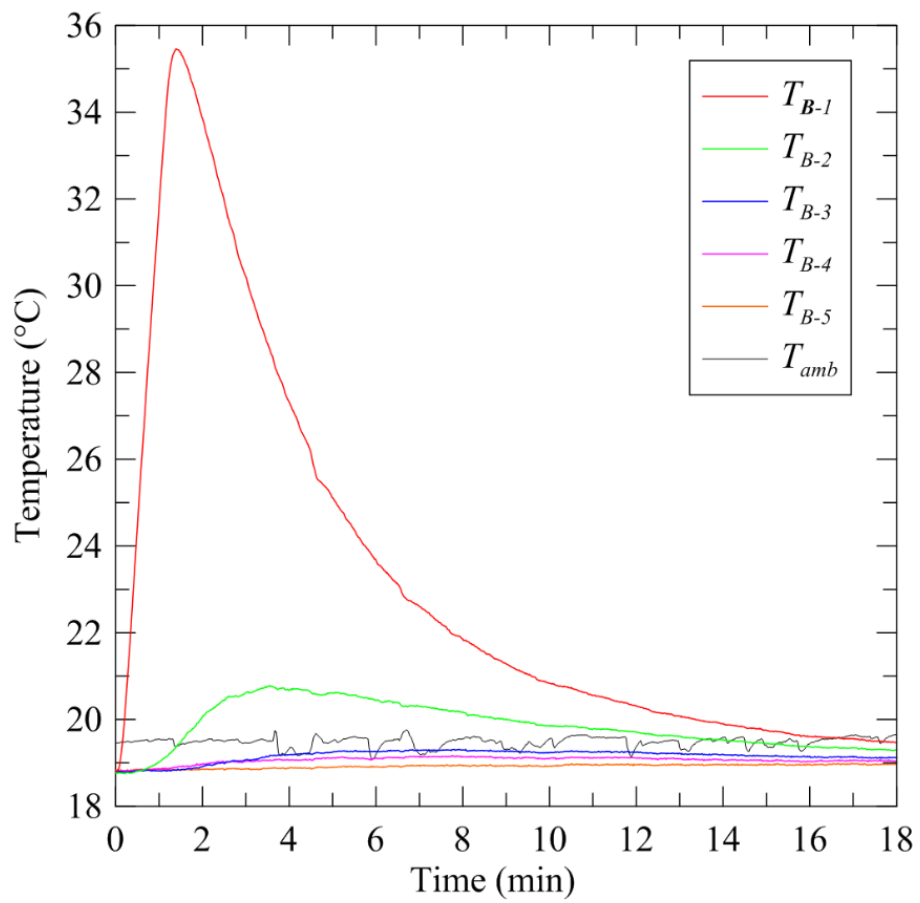
Fig. 5.34 Temperature measurements on the back surface of the mock tablet with no temperature control solution installed and a heat generation rate of 7 W
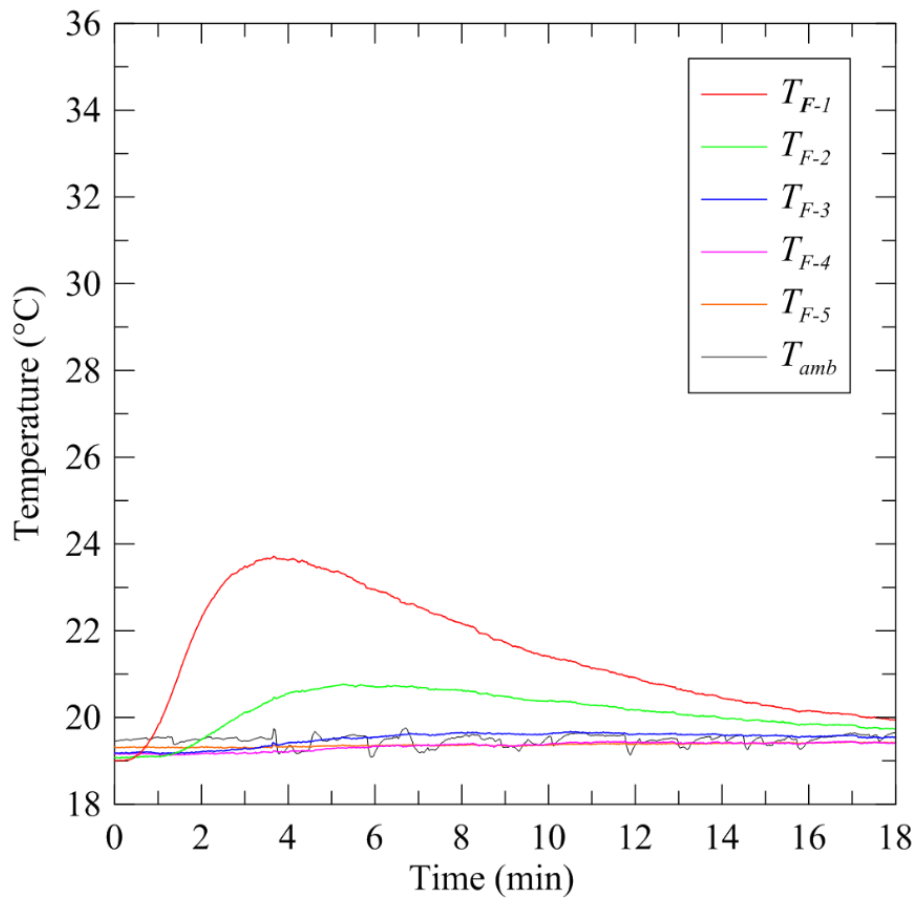
Fig. 5.35 Temperature measurements on the front surface of the mock tablet with no temperature control solution installed and a heat generation rate of 7 W

5.8.2.2 Aluminum Heat Spreader

Figures 5.36 to 5.38 show the temperatures measured with a heat spreader installed and a heat generation rate of 7 W. With the increased heat generation rate, the heater reached the cut off temperature after approximately 2.1 minutes. Installing a heat spreader slightly decreased the rate

of increase and lowered the peak back surface temperature. The heater was poorly coupled to the spreader, TIM should improve the temperature control significantly.
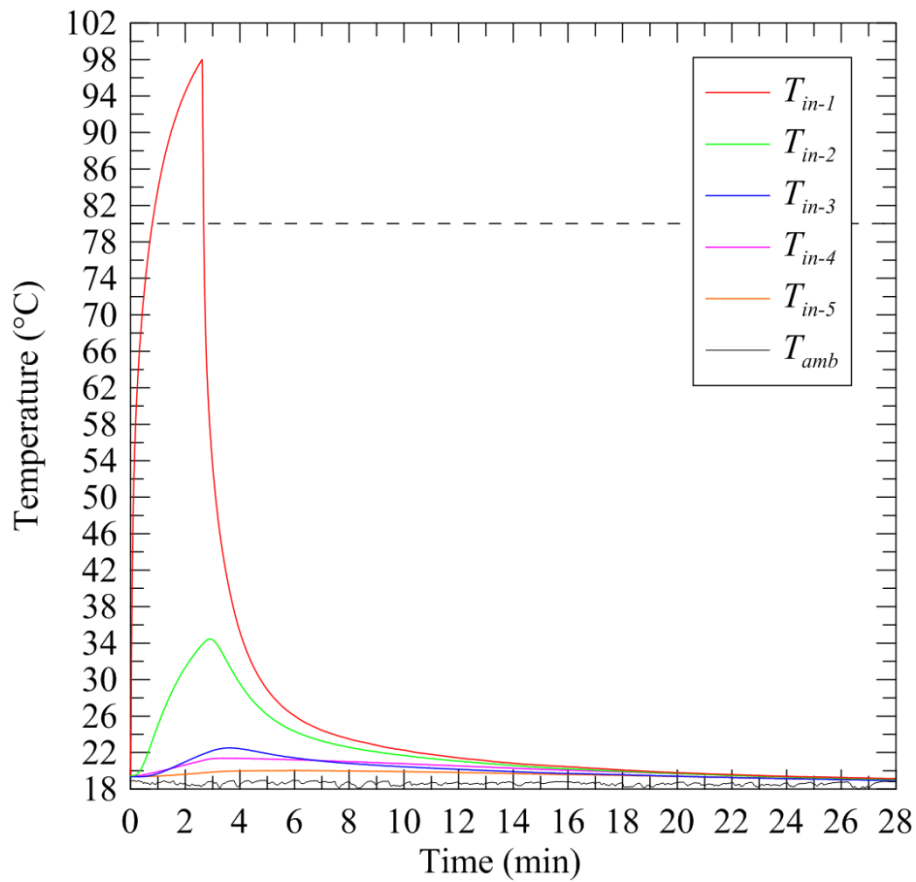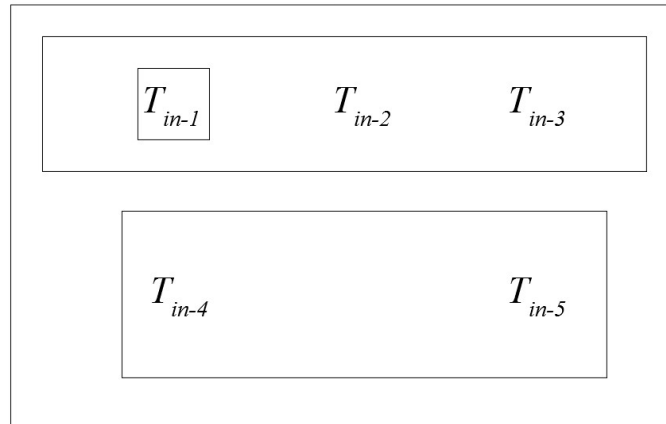
Fig. 5.36 Temperature measurements on the inside of the mock tablet with heat spreader and a heat generation rate of 7 W (dotted line represents the SOC temperature limit)
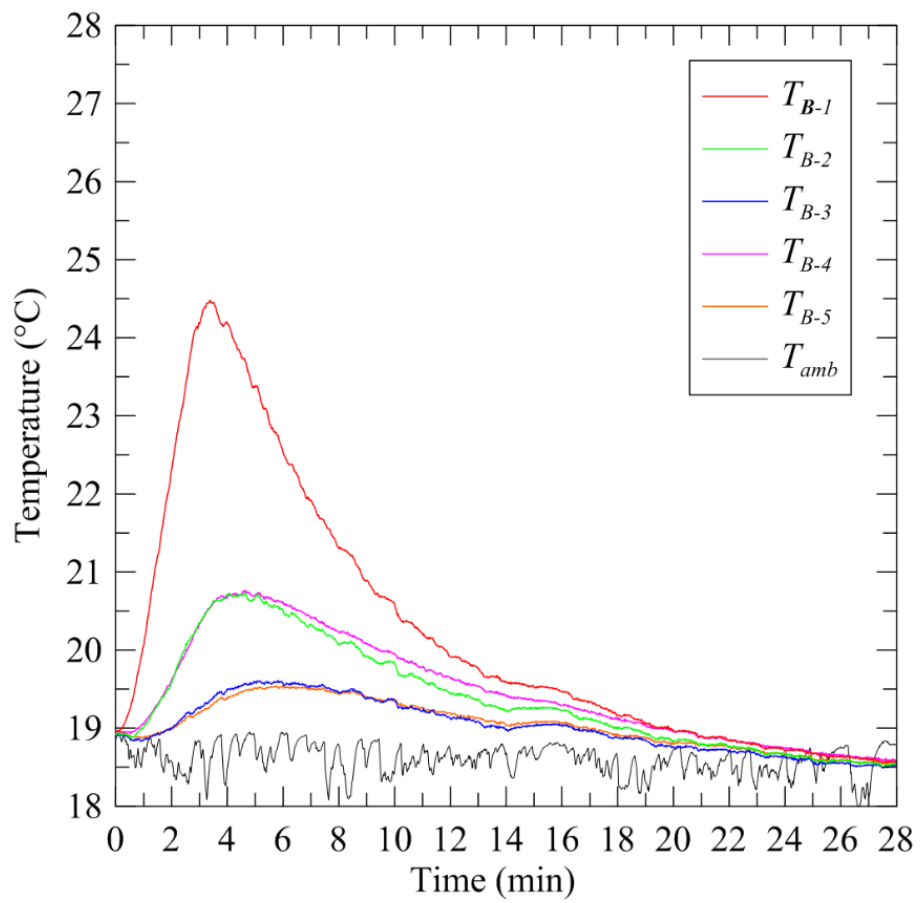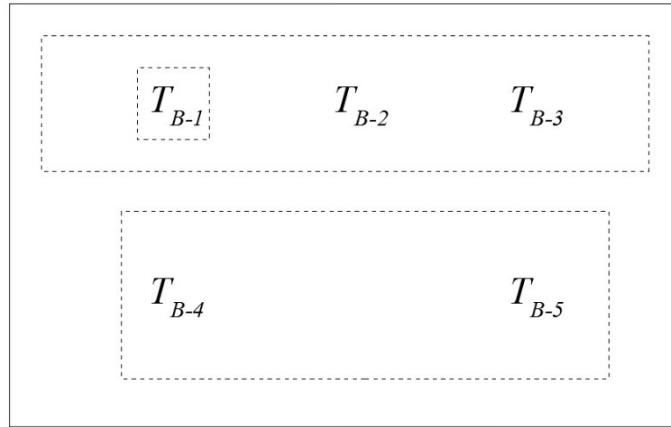
Fig. 5.37 Temperature measurements on the back surface of the mock tablet with heat spreader and a heat generation rate of 7 W
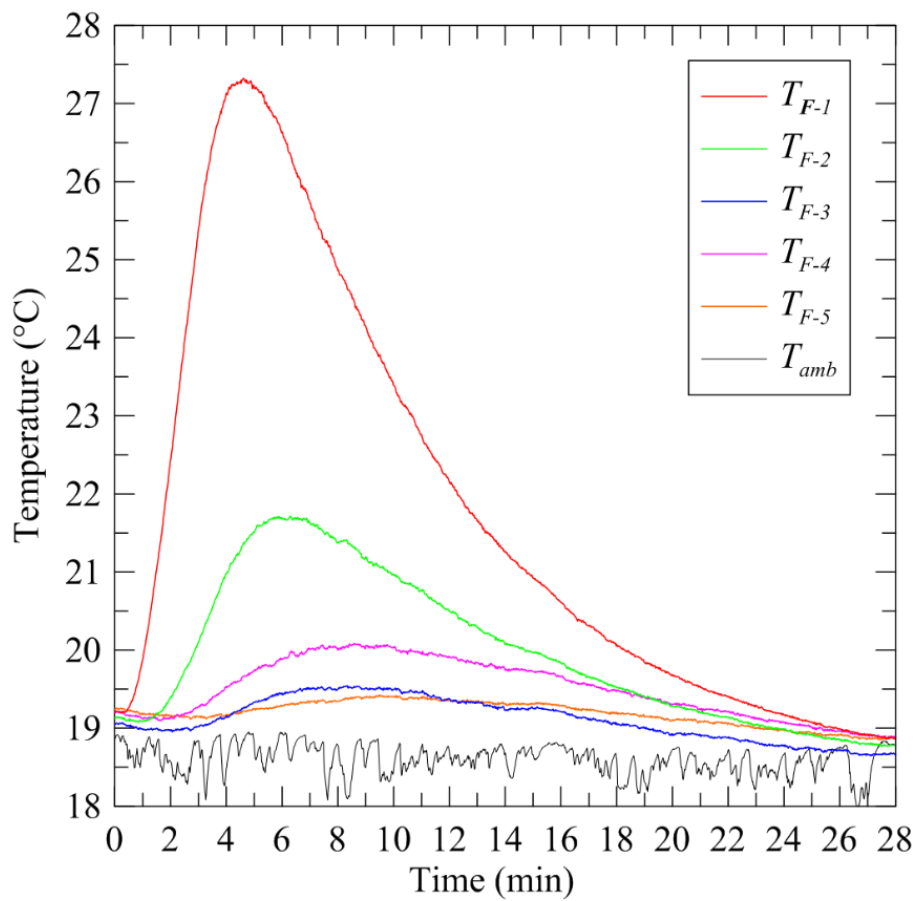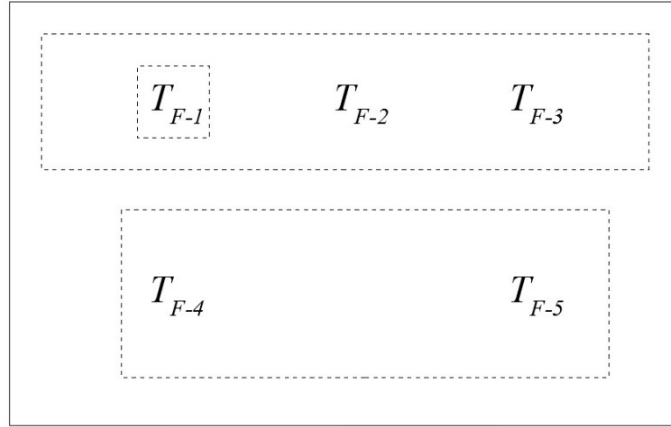
Fig. 5.38 Temperature measurements on the front surface of the mock tablet with heat spreader and a heat generation rate of 7 W

5.8.2.3 Aluminum Heat Spreader and TIM

Figures 5.39 to 5.41 show the temperatures measured with a heat spreader, TIM and a heat generation rate of 7 W. The 60-minute heating phase was completed. The heater temperature did not reach the SOC maximum temperature but only by a small margin, reaching a maximum

measured temperature of 79.7 °C. Temperatures of the front and back surface exceeded the comfort threshold after approximately 14.7 minutes and 25.8 minutes respectively. Trends were similar to those seen in experiments with 4.5 W but with a corresponding increase in temperature. The front surface temperature was larger than the back surface and by a degree which was similar to the experiments with a lower heat generation rate. In the experiments with a heat generation rate of 4.5 W, the difference between the maximum back surface and maximum front surface temperatures was 4.0 °C at 60 minutes. For this experiment, with a heat generation rate of 7 W, the difference between the maximum back surface and maximum front surface temperatures was 5.4 °C at 60 minutes.

The inclusion of the heat spreader and TIM decreased the resistance to conduction between the heater and back cover. This decreased the heater temperature significantly when compared to the heat spreader and no TIM.
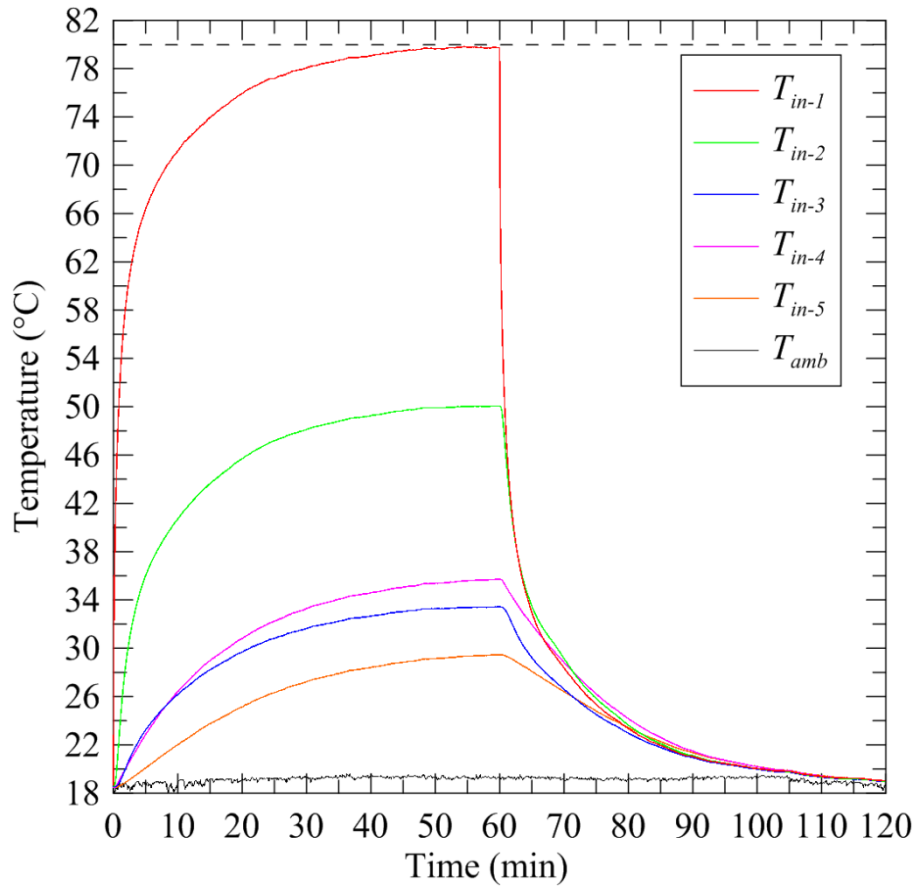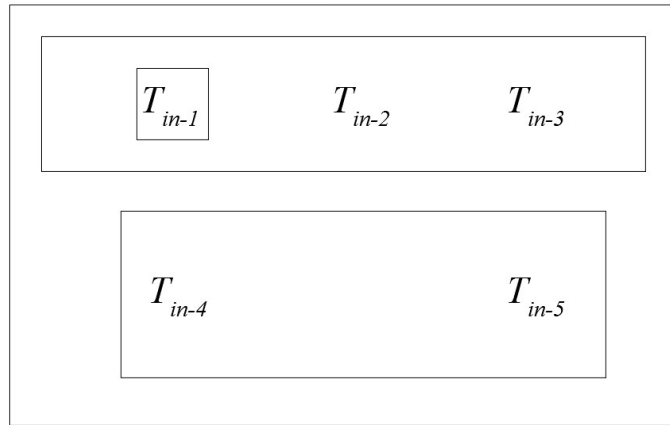
Fig. 5.39 Temperature measurements on the inside of the mock tablet with heat spreader, TIM, and a heat generation rate of 7 W (dotted line represents the SOC temperature limit)
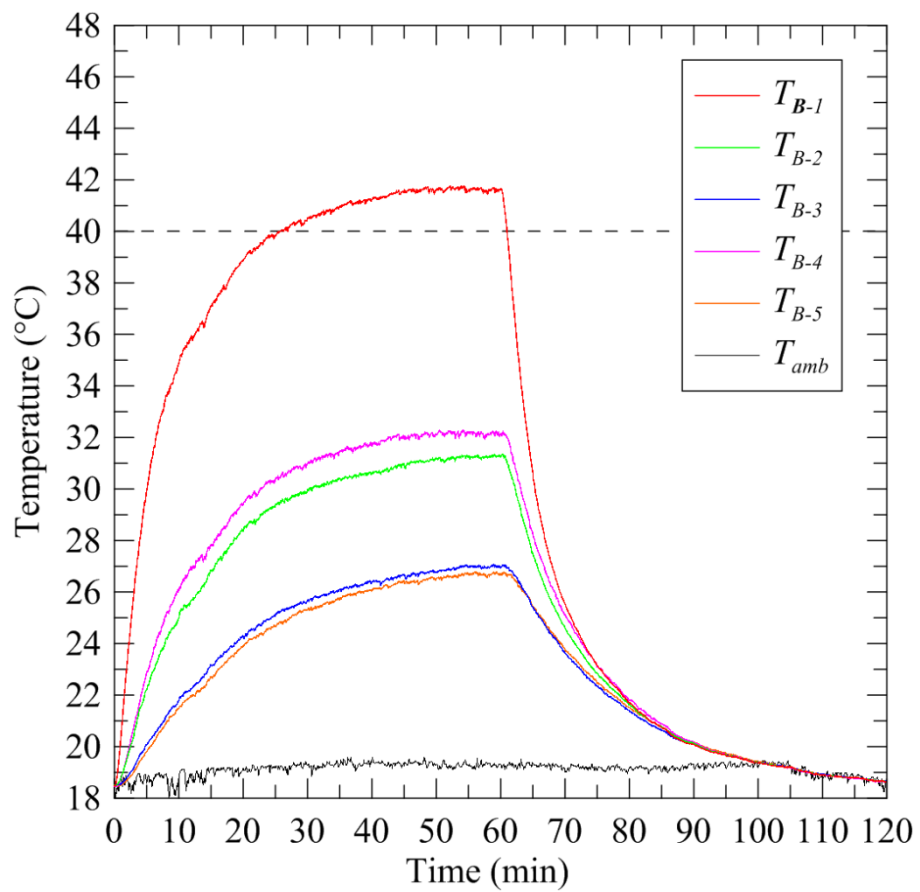
Fig. 5.40 Temperature measurements on the back surface of the mock tablet with heat spreader, TIM, and a heat generation rate of 7 W (dotted line represents the surface temperature limit)
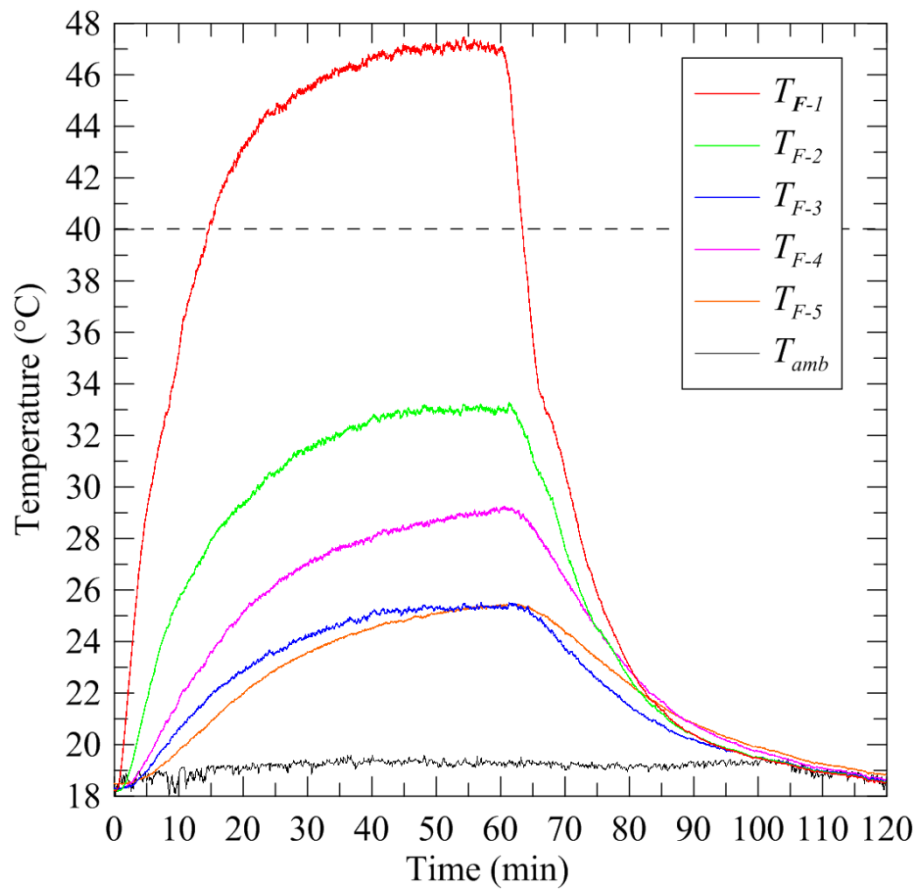
Fig. 5.41 Temperature measurements on the front surface of the mock tablet with heat spreader, TIM, and a heat generation rate of 7 W (dotted line represents the surface temperature limit)

5.8.2.4 LHTES module and Aluminum Heat Spreader

Figures 5.42 to 5.44 show the temperatures measured with the LHTES module, heat spreader and a heat generation rate of 7 W. The heater reached the cut off temperature after approximately 2.2 minutes. The heaters temperature increased rapidly and quickly exceeded the maximum SOC temperature. There was no evidence of any phase change in the measured temperatures. As with the previous experiments without TIM, the heater was poorly coupled to the temperature control solution. At 7 W of heat generation it overheated before there was time for the LHTES to melt significantly. Thermal interface material is clearly critical for effective implementation of a temperature control solution at higher heat generation rates.
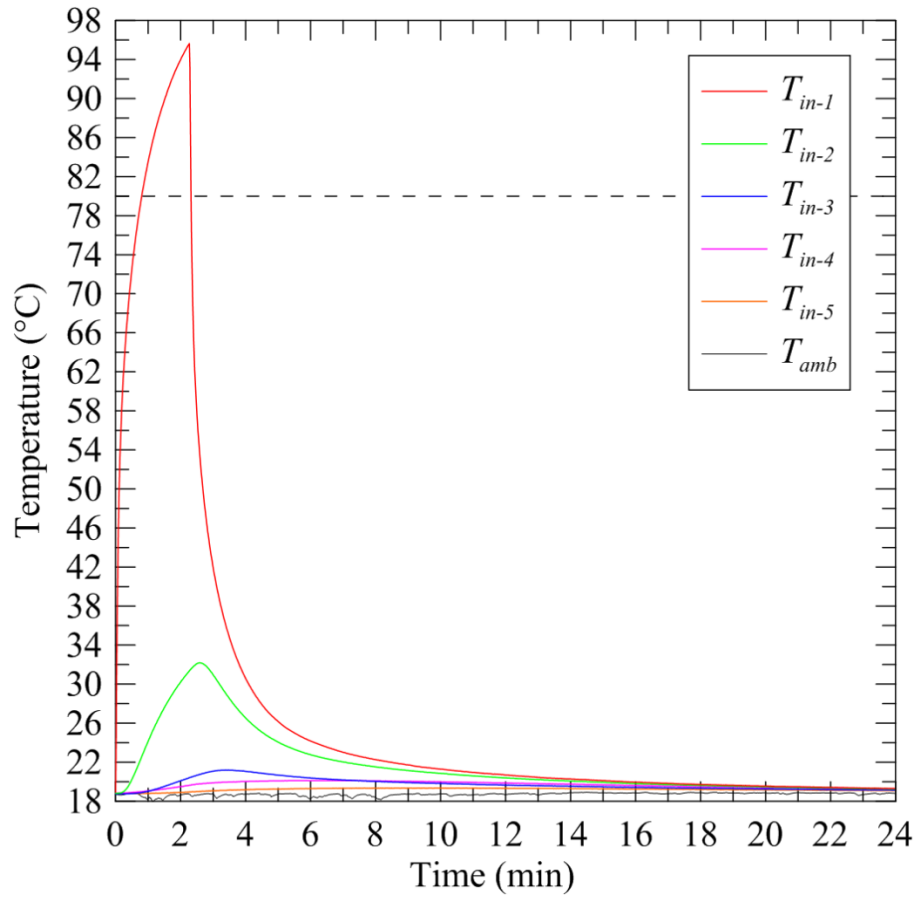
Fig. 5.42 Temperature measurements on the inside of the mock tablet with LHTES module, heat spreader, and a heat generation rate of 7 W
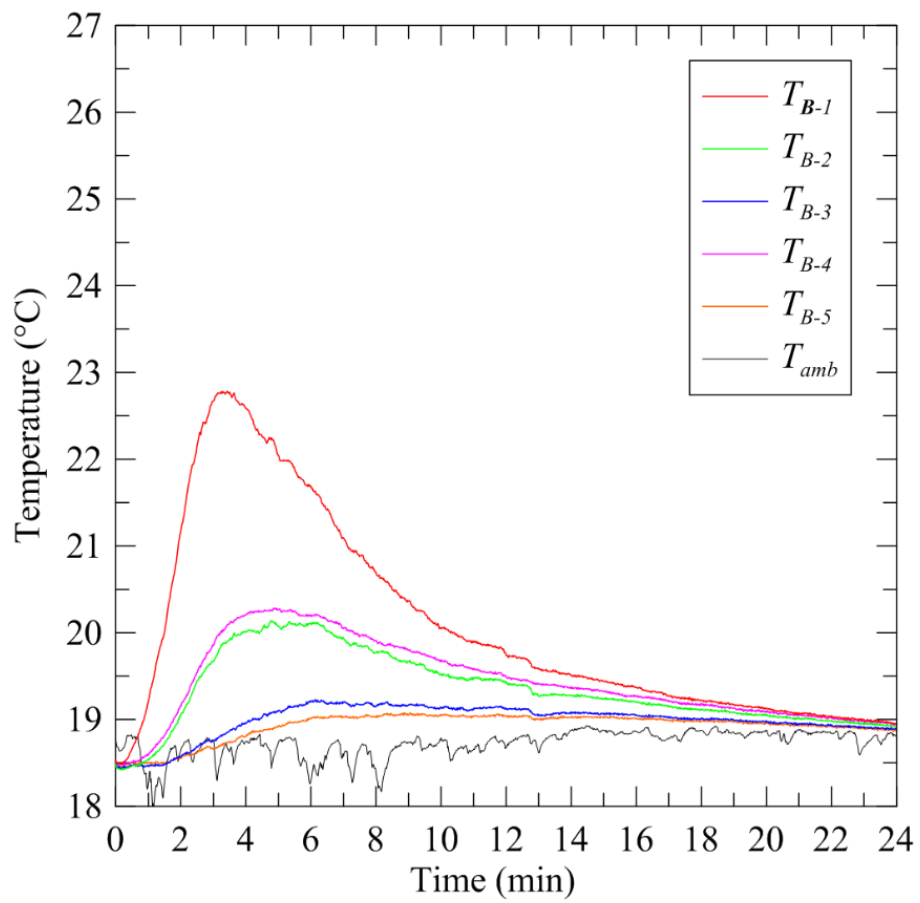
Fig. 5.43 Temperature measurements on the back surface of the mock tablet with LHTES module, heat spreader, and a heat generation rate of 7 W
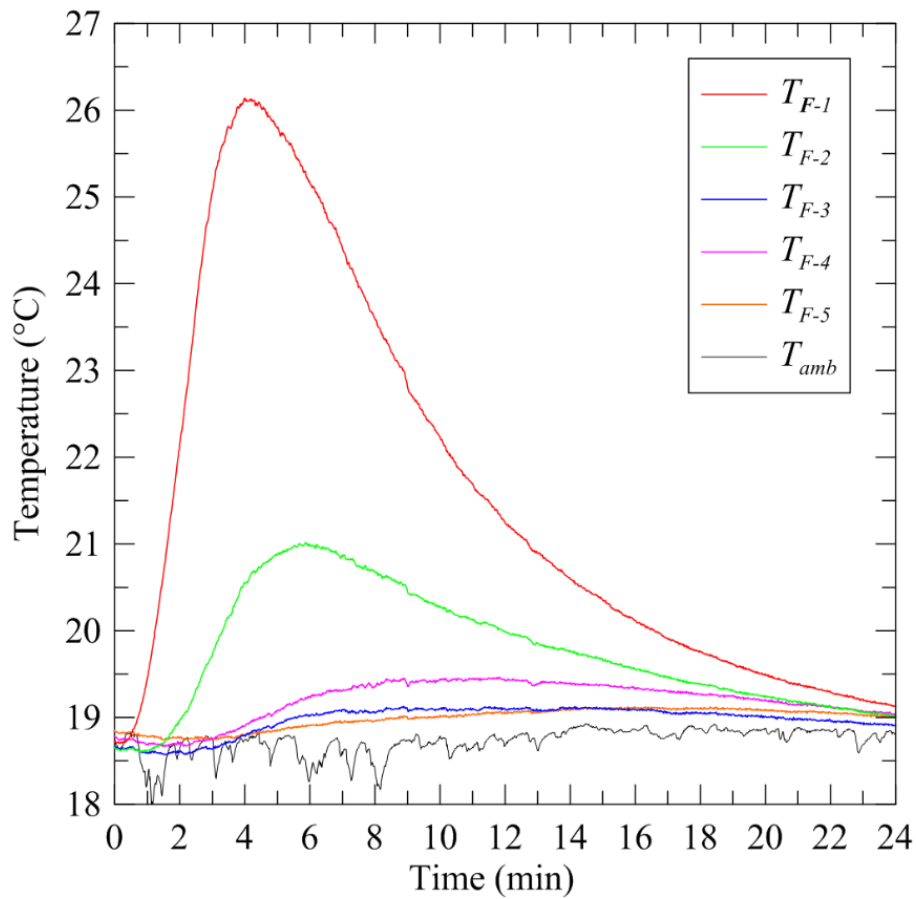
Fig. 5.44 Temperature measurements on the front surface of the mock tablet with LHTES module, heat spreader, and a heat generation rate of 7 W

5.8.2.5 LHTES module, Aluminum Heat Spreader, and TIM

Figures 5.45 to 5.47 show the temperatures measured with the LHTES, heat spreader, TIM and a heat generation rate of 7 W. The 60 minute heating phase was completed. There was clear evidence of phase change. There are inflections in many of the temperature profiles. The heater temperature

does not exceed the SOC maximum temperature. The back surface temperature exceeded the comfort limit after approximately 28.2 minute while the front exceeded the comfort temperature after approximately 19.2 minutes.
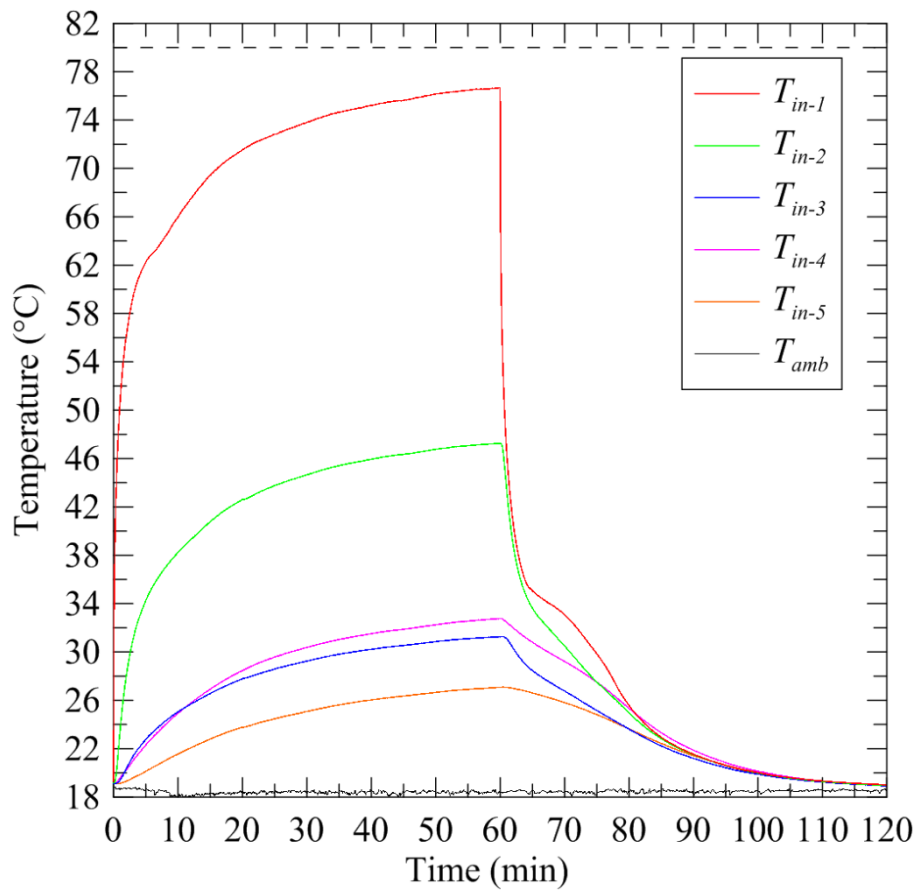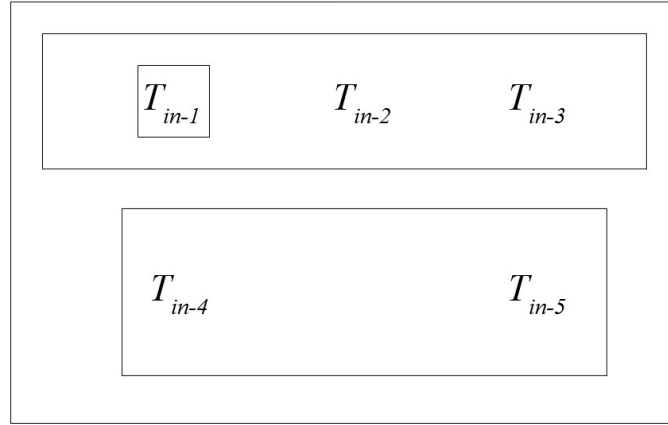
Fig. 5.45 Temperature measurements on the inside of the mock tablet with LHTES module, heat spreader, TIM, and a heat generation rate of 7 W
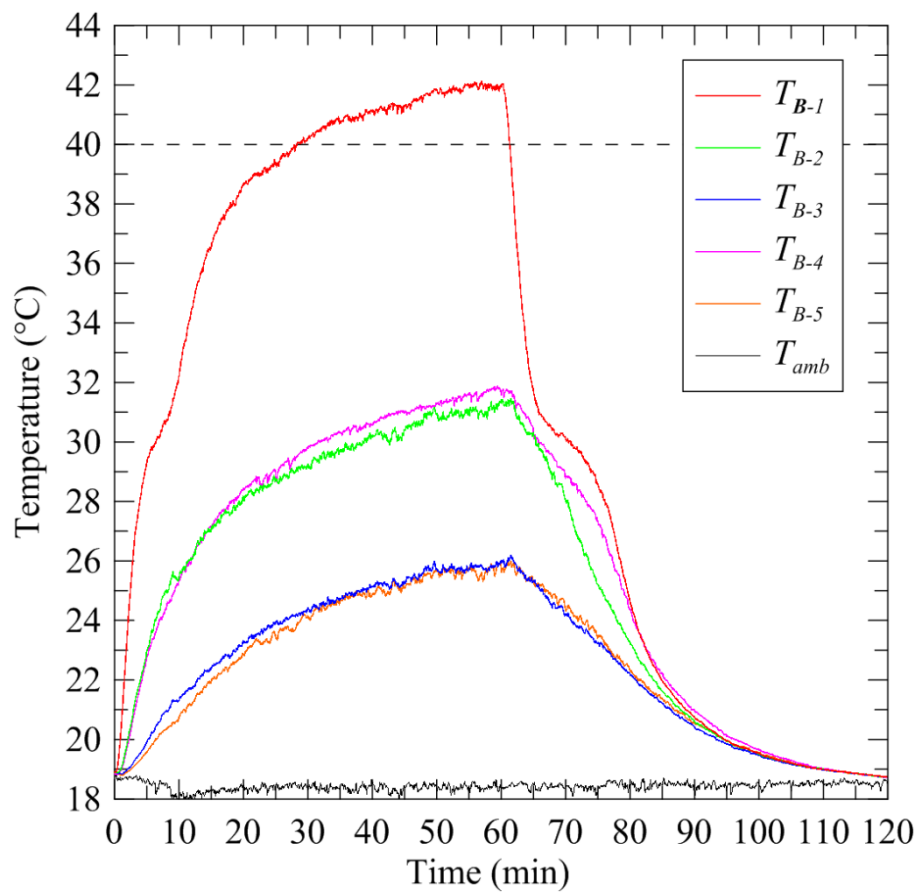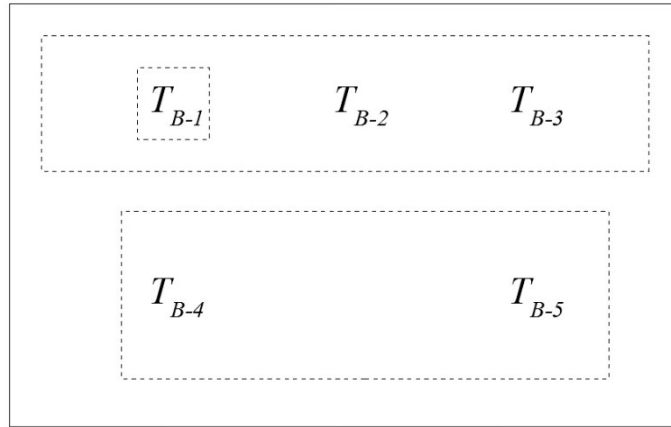
Fig. 5.46 Temperature measurements on the back surface of the mock tablet with LHTES module, heat spreader, TIM, and a heat generation rate of 7 W
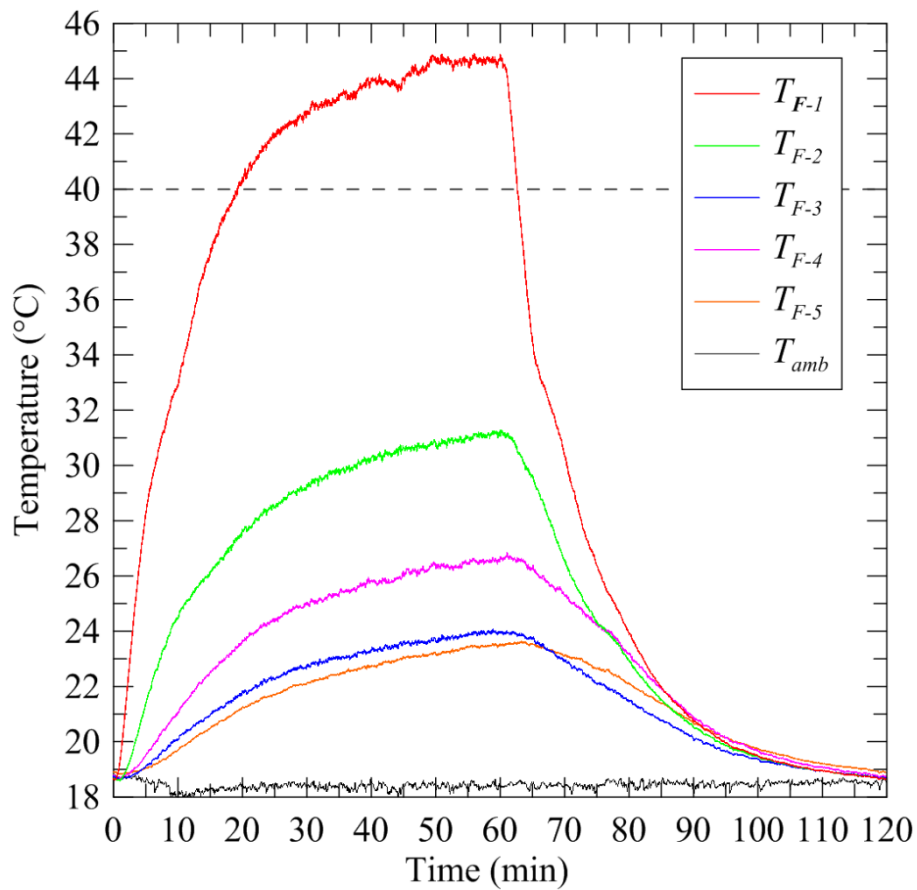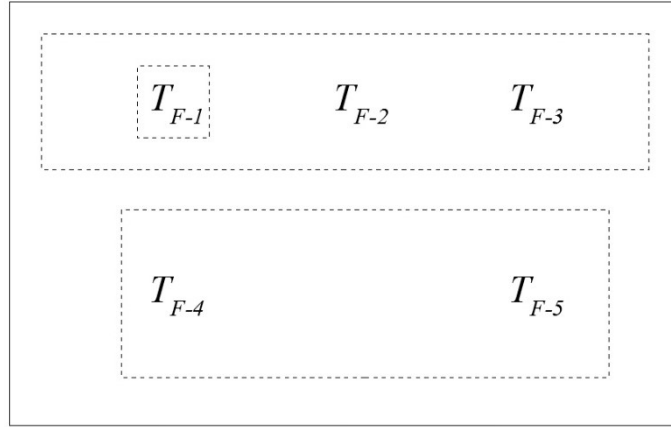
Fig. 5.47 Temperature measurements on the front surface of the mock tablet with LHTES module, heat spreader, TIM, and a heat generation rate of 7 W

5.8.2.6 Summary for a heat generation rate of 7 W

Figure 5.48 shows the heater temperature for each experiment run with 7 W of heat generation. All temperature control solutions without TIM have poor performances. Of the two solutions with TIM, the temperature control solution with an LHTES module was superior. It reduced the heater

142

and front surface temperature while slightly increasing the time for the back surface to exceed 40°C (approximately 2.4 minutes) (see Figs. 5.49 and 5.50). However, the limiting factor was the front cover temperature. Without the LHTES module the front surface exceeded 40°C after 14.7 minutes while with the addition of the LHTES module it took 19.2 minutes for the front cover to reach its temperature limit. Therefore, the addition of the LHTES module reduced the heater temperature, and extended the safe operating time from 14.7 minutes to 19.2 minutes, a 30% improvement.
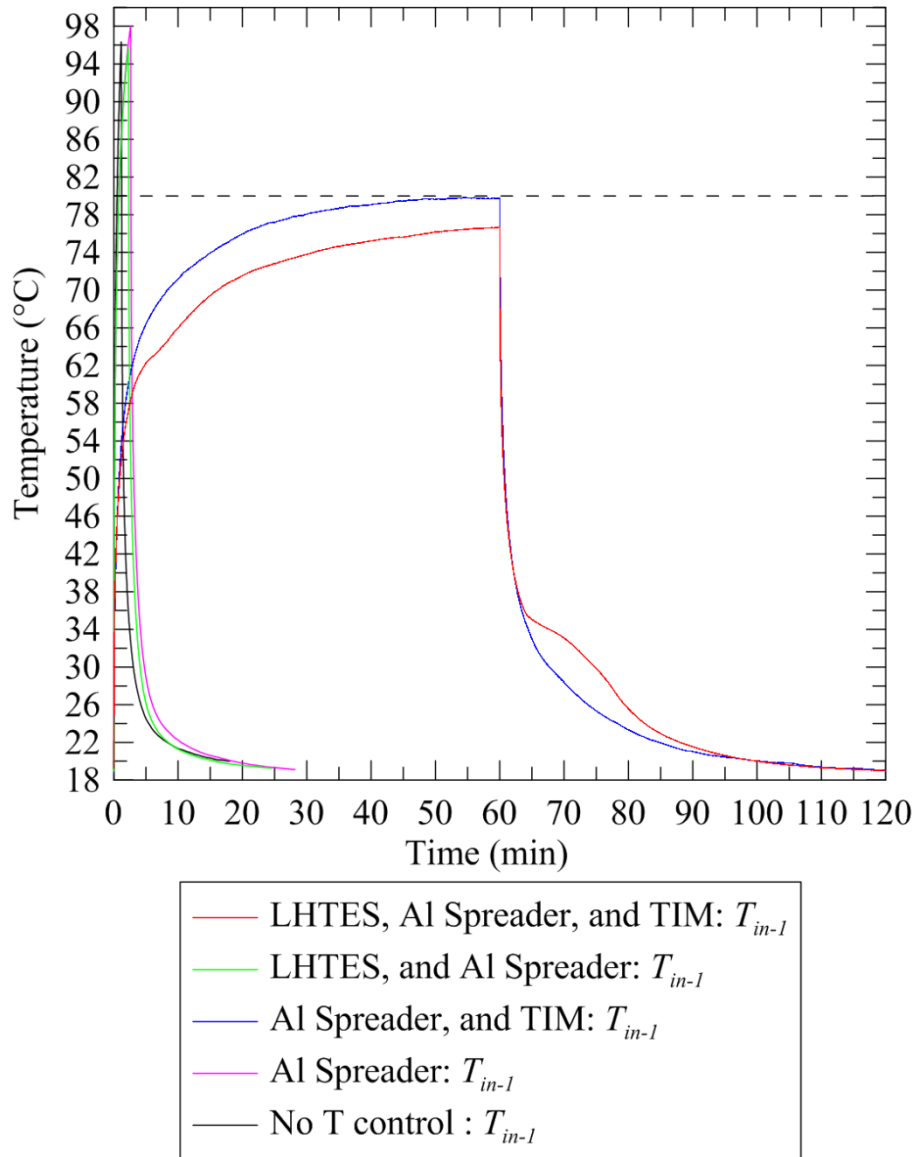
Fig. 5.48 Comparison of the temperature profiles of the heater for all experiments with a heat generation rate of 7 W
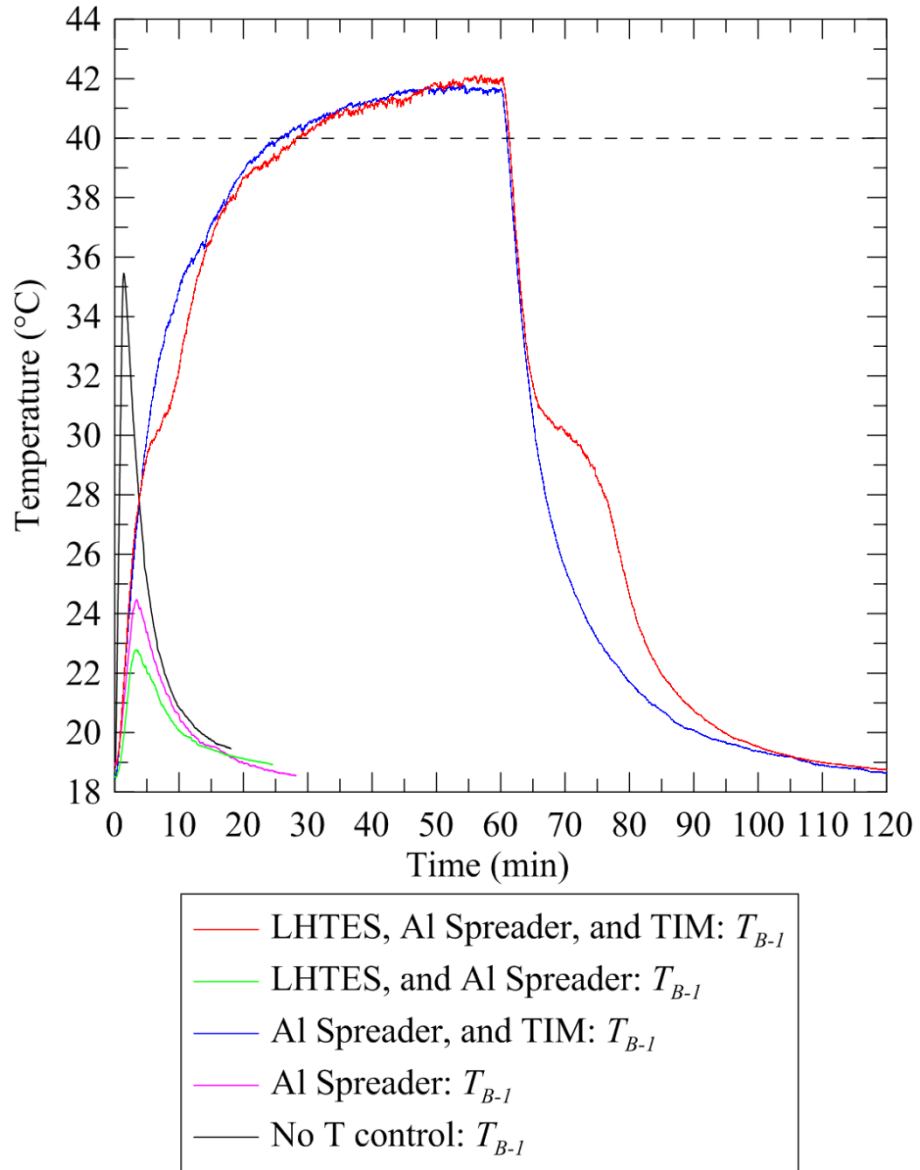
Fig. 5.49 Comparison of the temperature profiles the back surface (T_{B-1}) for all experiments with a heat generation rate of 7 W
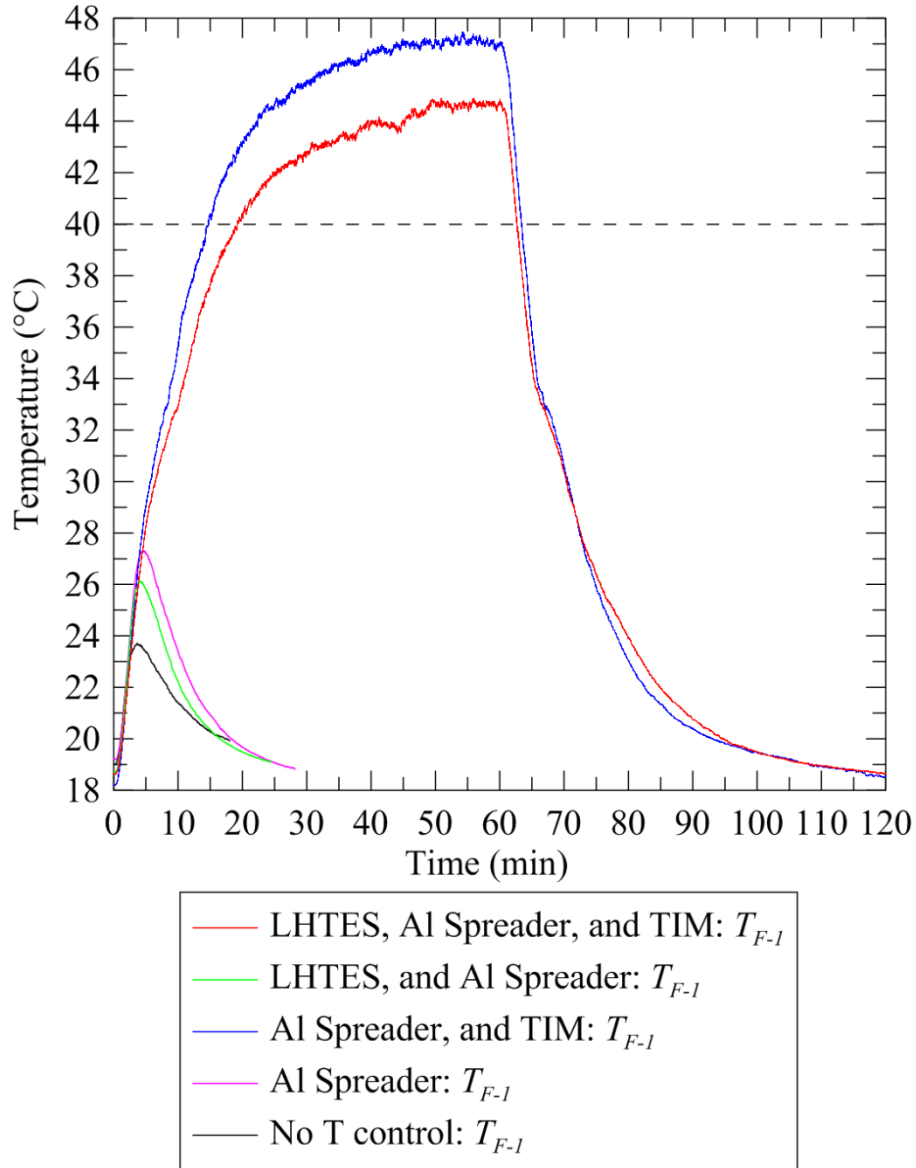
Fig. 5.50 Comparison of the temperature profiles the front surface (T_{F-1}) for all experiments with a heat generation rate of 7 W

Table 5.6 shows the time required for the mock tablet to reach the limiting temperatures for the experiments with a heat generation rate of 7 W. Clearly the only solutions of interest are the two which utilize a TIM. They take significantly longer to reach a temperature limit than the other cases.

145

Table 5.6 Summary of the time required for the mock tablet to reach the respective temperature limits with a heat generation rate of 7 W

	operational time before reaching temperature limit (min)			
	heater source (T_{lim}=80°C)	back surface (T_{lim}=40°C)	front surface (T_{lim}=40°C)	minimum
no T control	0.5	*	*	0.5
heat spreader	0.8	*	*	0.8
Spreader, and TIM	-	25.8	14.7	14.7
LHTES, and spreader	0.8	*	*	0.8
LHTES, spreader, and TIM	-	28.2	19.2	19.2

" - " indicates region did not overheat during the experiment

" * " indicates region did not overheat, however, the heating phase was stopped before 60 minutes

5.9 Analysis

Ultimately, the only temperature control solutions which are truly of interest, for either of the heat generation rates, are those which included TIM. Good thermal coupling between the heater and the temperature control solution is critical. Therefore, the comparison which will give the most insight into the value and viability of the LHTES modules is the comparison between the use of the heat spreader with TIM and the LHTES, spreader, and TIM. Figures 5.51 to 5.53 shows the comparison between these two temperature control solutions for both heat generation rates. The inclusion of the LHTES module into the temperature control solution increased the time which the device operated before overheating. The LHTES module reduced the heater and front cover temperature. Neither experiment shows the LHTES module having a significant impact on the back surface temperature.

There are two core objectives of a temperature control solution in handheld electronics. First, to extend the operating time before the handheld device will reach a temperature limit and be required to throttle the processor speed. Second, to reduce the mean operating temperature of the major sources in the system. The LHTES module improved both of these aspects in the mock tablet computer. The cooling phase of the experiment was also impacted by the LHTES module. The

inflection in the temperature profile due to latent heat storage reduces the cooling rate, keeping the tablet near the transition temperature as the PCM solidifies. However, after the PCM solidifies the temperature quickly approaches the temperature profile of the experiments without latent heat storage. Also, all of the experiments show the tablet cooling back to ambient in just under 60 minutes.
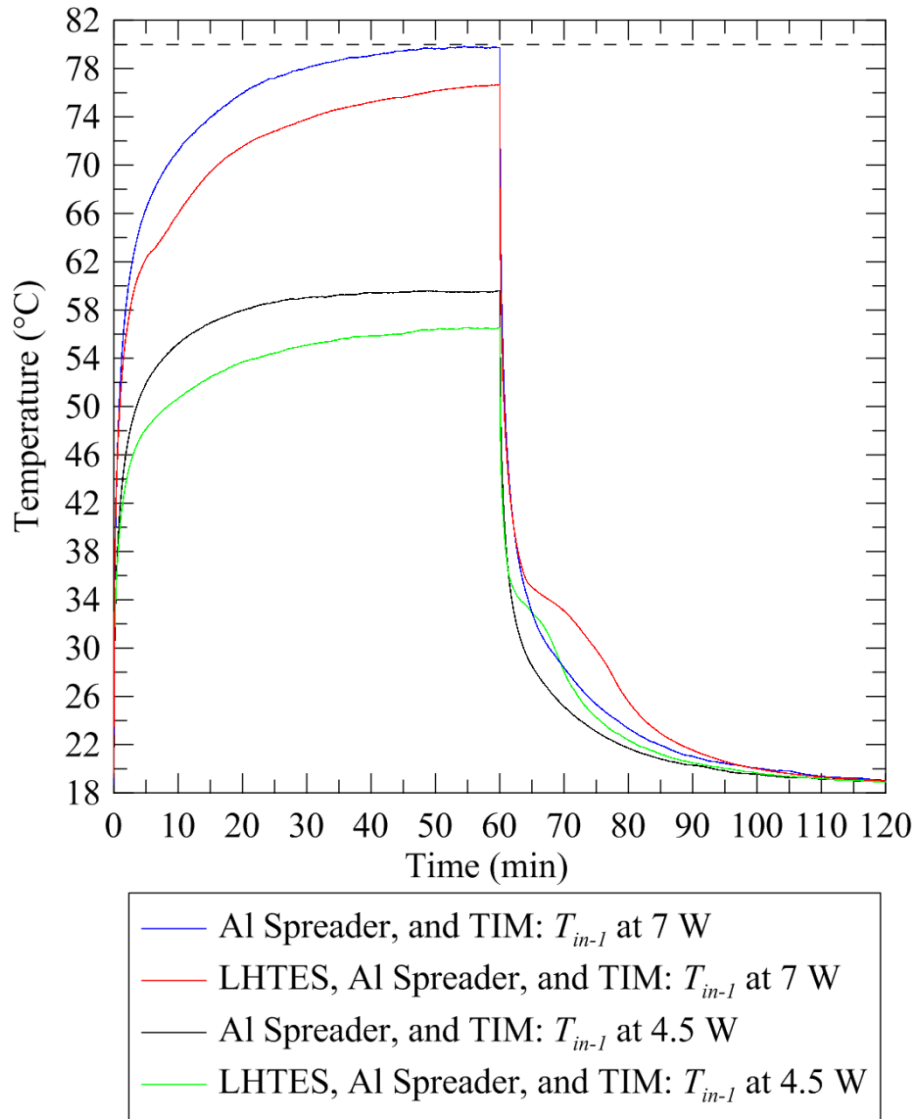
Fig. 5.51 Maximum temperatures measured inside the mock tablet for the best two temperature control solutions at 7 and 4.5 W

147
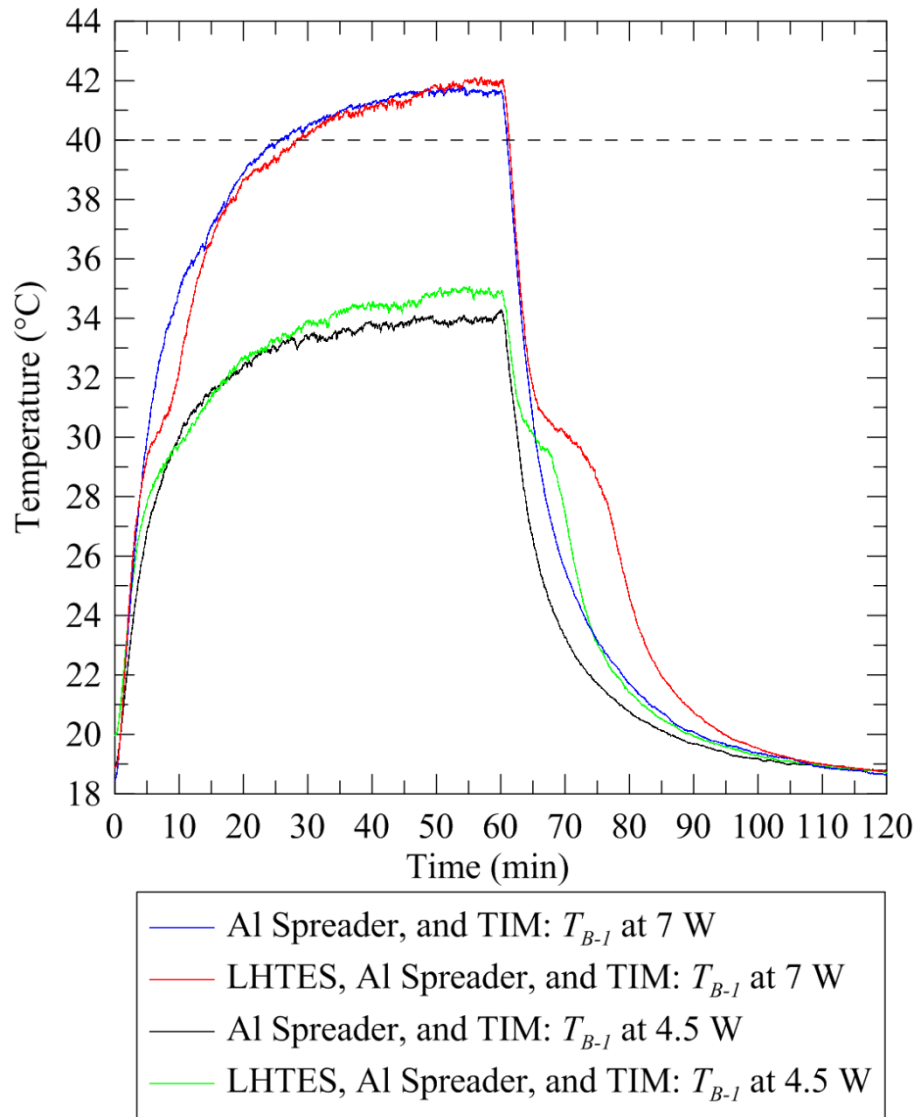
Fig. 5.52 Maximum temperatures measured on the back surface of the mock tablet for the best two temperature control solutions at 7 and 4.5 W
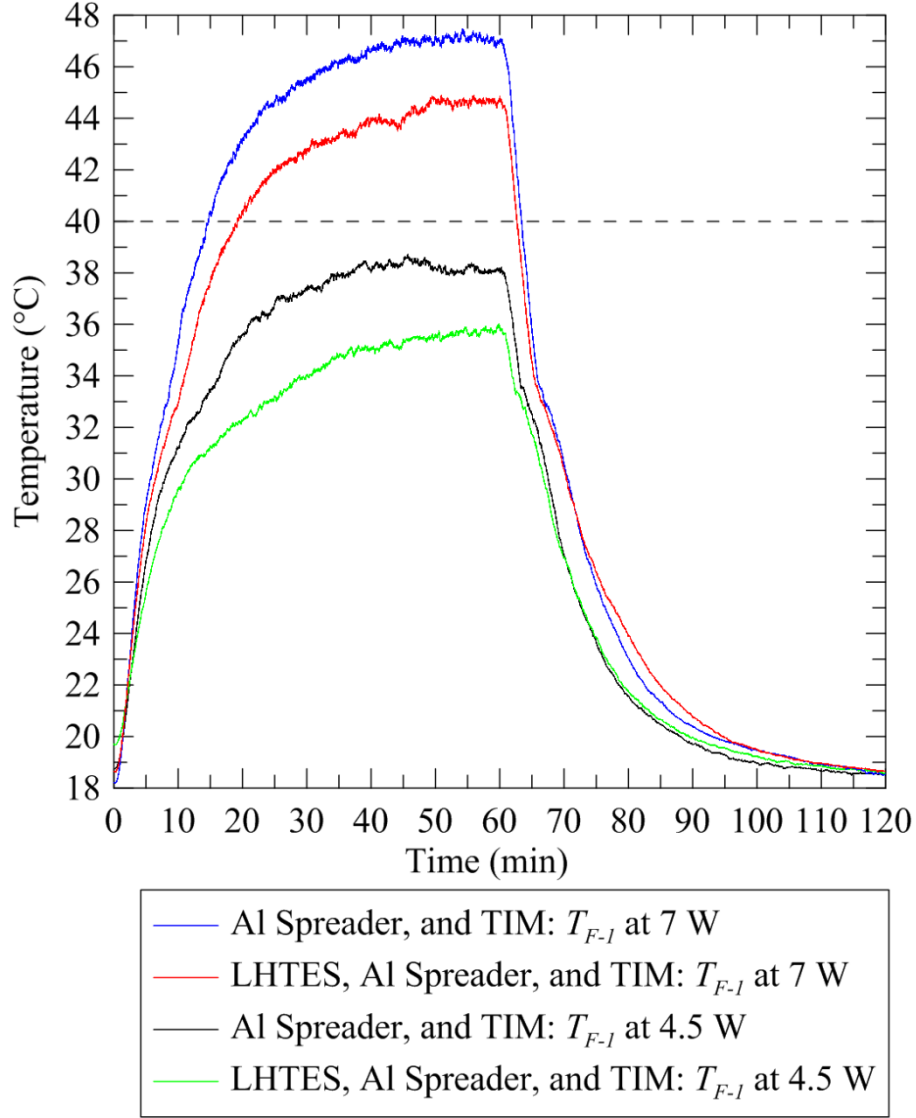
Fig. 5.53 Maximum temperatures measured on the front surface of the mock tablet for the best two temperature control solutions at 7 and 4.5 W

In order to better quantify the difference between the temperature response of the system, an exponential curve was fit to the heating and cooling phase. Equations (5.4) and (5.5) show the functions which were used for the heating and cooling phases respectively.

$$\left(\frac{T(t)-T_i}{T_{lim}-T_i}\right) = \theta = C\left(1 - e^{\left(-\frac{t}{\tau}\right)}\right) \tag{5.4}$$

$$\left(\frac{T(t)-T_f}{T_{lim}-T_f}\right) = \theta = C\left(e^{\left(-\frac{t-t_{heating}}{\tau}\right)}\right) \tag{5.5}$$

149

where T_i is initial temperature, T_f is final temperature, T_{lim} is the relevant temperature limit (e.g. 40°C for the front surface), $t_{heating}$ is the length of the heating phase (60 min), and θ is nondimensionalized temperature. The experimental setup was at ambient temperature at the beginning and end of the experiment so the initial and final temperatures (T_i and T_f) are nearly equal.

Parameter C dictates the maximum dimensionless temperature of the model. The time constant τ controls the shape of the exponential curve, larger values of τ indicate that the temperature increased more slowly. Figures 5.54 and 5.55 demonstrate the impact of C and τ on the exponential function.
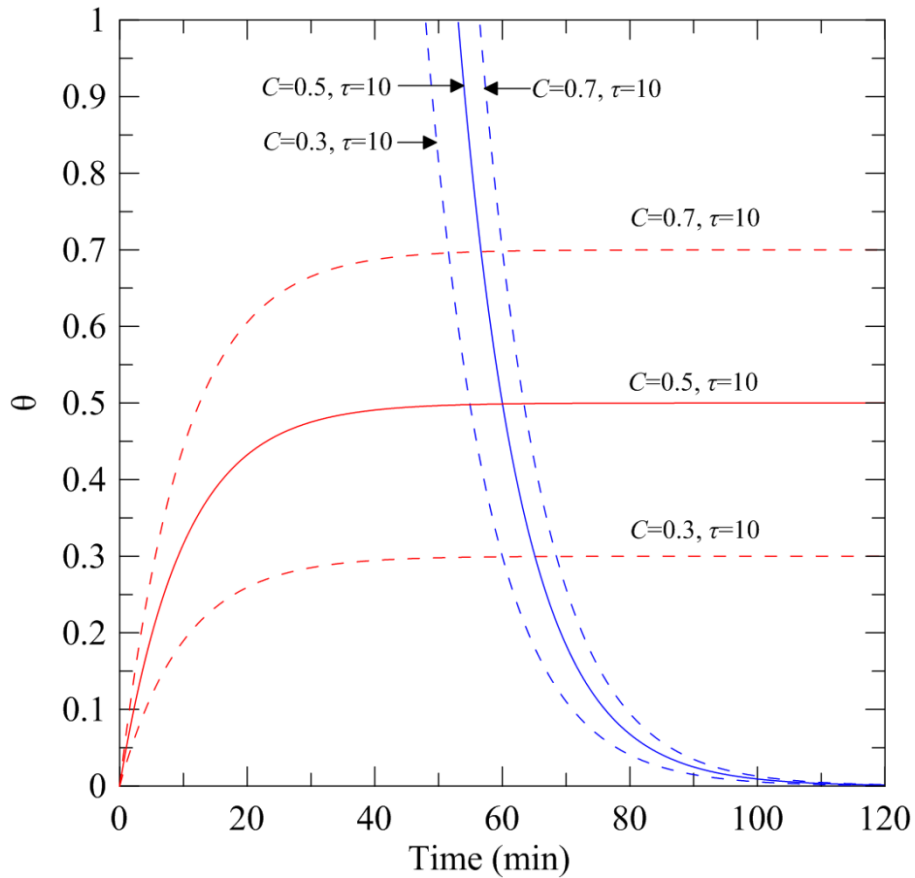
Fig. 5.54 Impact of C on the shape of the exponential function
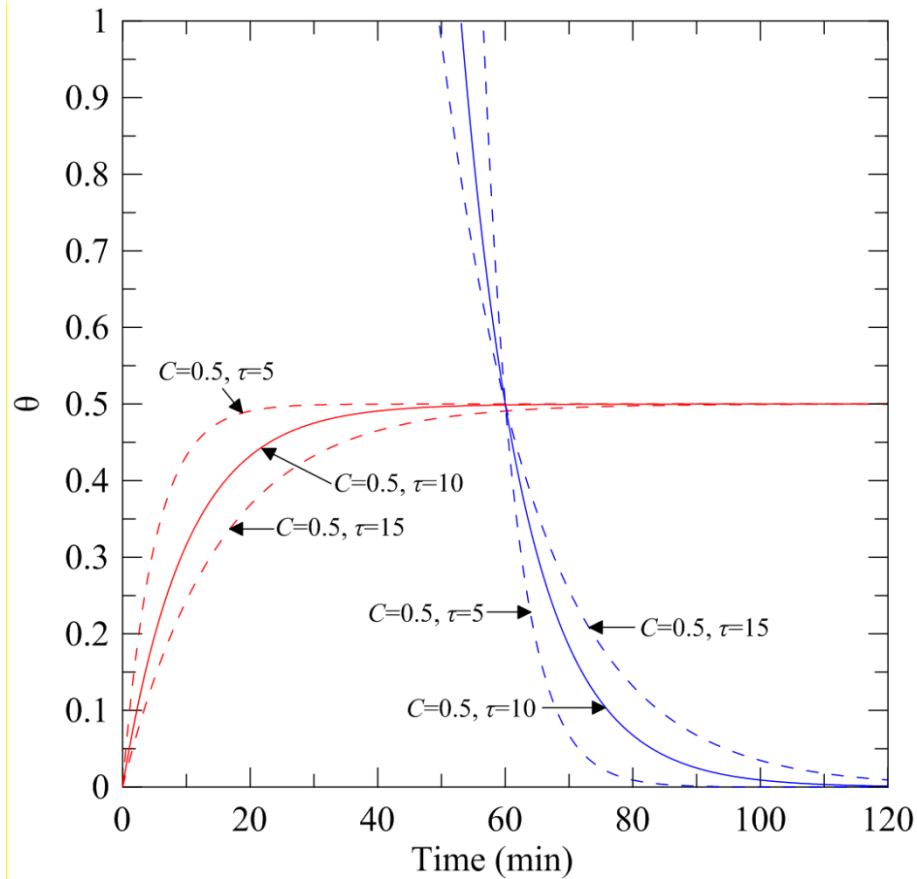
Fig. 5.55 Impact of τ on the shape of the exponential function

This simple exponential function fits the temperature profiles of the front and back surfaces well. However, heat generation in the SOC and transfer from the SOC was strongly three dimensional and does not conform to a simple exponential function. A more complex exponential function could be used; however, the goal of this analysis was to quantify the difference between the models by comparing the different functions. Functions with many parameters are difficult to compare. This analysis will focus on the temperature profiles measured on the front and back surface.

As an example, Figs. 5.56 and 5.57 shows the temperature profiles measured with LHTES module, spreader and a heat generation rate of 7W plotted with the corresponding exponential functions.
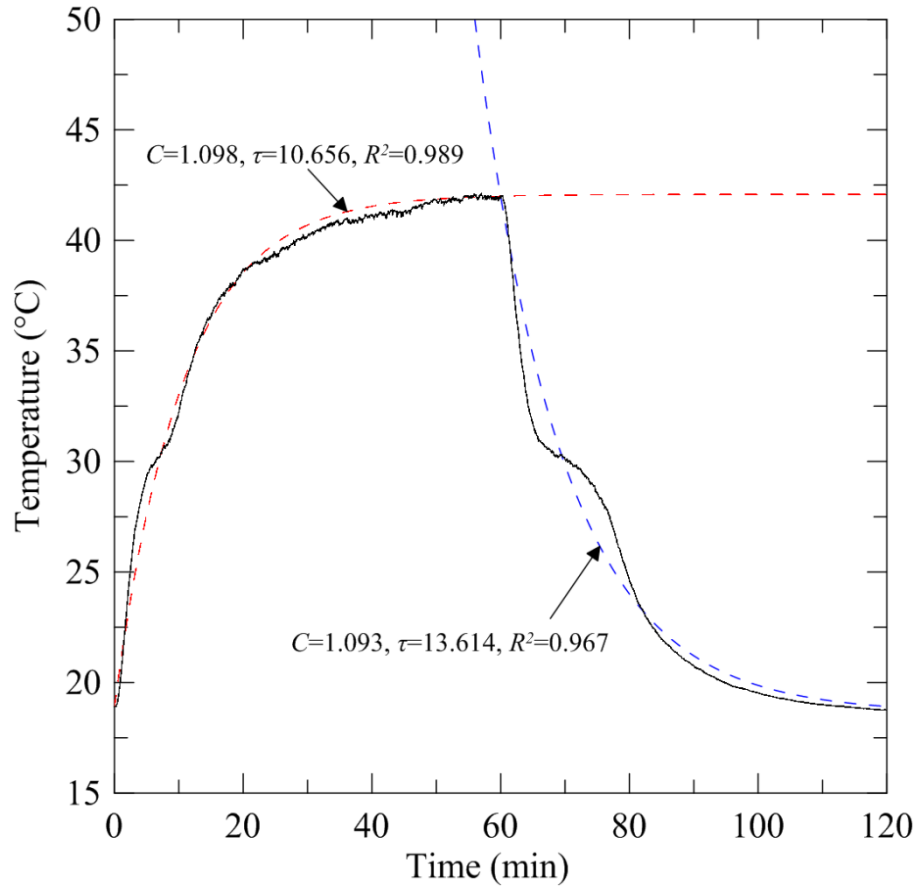
Fig. 5.56 Exponential functions and back surface temperatures measured with an LHTES module, spreader and heat generation rate of 7W
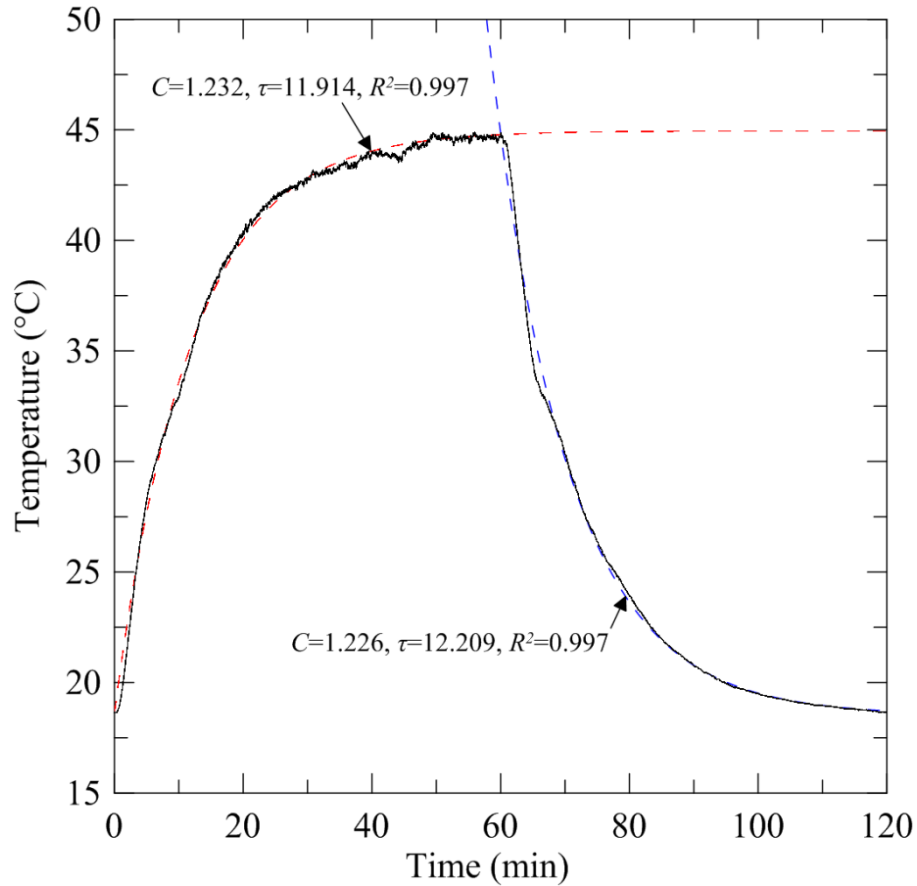
Fig. 5.57 Exponential functions and front surface temperature with an LHTES module, spreader and heat generation rate of 7W

Tables 5.7 and 5.8 summarize the constants C and τ as well as the R^2 for the exponential functions which were fitted to the heating and cooling phase respectively. An increase in the value of C indicates an increase in the maximum temperature of the system. The value of C for the heating and cooling phase are similar but not identical because values of T_i and T_f are slightly different for several of the experiments. Comparing the values of C and τ allows for a quantitative analysis of the impact of the storage. The percent difference change in C and τ as a result of the addition of the LHTES is shown in Table 5.9.

Table 5.7 Parameters and R^2 for the exponential function fit to the heating phase of the experimental data

		4.5 W		7 W	
		Spreader	LHTES and Spreader	Spreader	LHTES and Spreader
Back Surface	C	0.724	0.744	1.076	1.098
	τ	8.115	9.432	8.505	10.656
	R^2	0.984	0.967	0.991	0.989
Front Surface	C	0.913	0.803	1.328	1.232
	τ	9.856	12.469	10.709	11.914
	R^2	0.993	0.993	0.997	0.997

Table 5.8 Parameters and R^2 for the exponential function fit to the cooling phase of the experimental data

		4.5 W		7 W	
		Spreader	LHTES and Spreader	Spreader	LHTES and Spreader
Back Surface	C	0.726	0.759	1.076	1.093
	τ	8.832	12.766	9.017	13.614
	R^2	0.985	0.984	0.986	0.967
Front Surface	C	0.914	0.808	1.325	1.226
	τ	11.908	13.177	11.327	12.209
	R^2	0.993	0.991	0.996	0.997

Table 5.9 Percent difference in the exponential parameters after the addition of the LHTES

		Heating Phase		Cooling Phase	
		4.5 W	7 W	4.5 W	7 W
Back Surface	$\left(\dfrac{C_{Spreader} - C_{LHTES}}{C_{Spreader}}\right) \times 100\%$	2.8%	2.1%	4.4%	1.5%
	$\left(\dfrac{\tau_{Spreader} - \tau_{LHTES}}{\tau_{Spreader}}\right) \times 100\%$	16.2%	25.3%	44.5%	51.0%
Front Surface	$\left(\dfrac{C_{Spreader} - C_{LHTES}}{C_{Spreader}}\right) \times 100\%$	-12.1%	-7.3%	-11.6%	-7.5%
	$\left(\dfrac{\tau_{Spreader} - \tau_{LHTES}}{\tau_{Spreader}}\right) \times 100\%$	26.5%	11.3%	10.7%	7.8%

Including the LHTES module into the experimental setup resulted in a small increase in C for the back cover and a large decrease for the front cover. This was expected from inspection of Figs. 5.52 and 5.53. In all cases the inclusion of an LHTES module increased the value of τ. A larger value of τ indicates a shallower curve with a slower rate of increase/decrease. Therefore, including the LHTES module both decreased the rate of heating and cooling.

There is an interaction between the value of C and τ. The time constant τ relates to the rate of temperature increase/decrease. In cases of the back cover where the value C and τ both increase, it is difficult to draw definitive conclusions from this analysis. Inspecting Fig. 5.52 and focusing on the temperature profiles of the 4.5 W experiments, the temperature profile without the storage is steeper and reaches its maximum sooner than the curve with storage, however, because the maximum of the curve with storage is larger, which of these curves is "better" is not clear.

The conclusions from the analysis of the front cover is clear. Parameter C is decreased and τ is increased. With storage, the system is spending less time at an elevated temperature and that elevated temperature is also lower.

The universal increase in the value of τ during the cooling phase is a result of the solidification of the PCM. This decreased cooling rate is a necessary negative trade off of the LHTES module. Heat which is absorbed during the heating phase must be dissipated during the cooling phase. Increase in the rate of cooling is not excessive with the current module but is an important aspect of LHTES design.

5.10 Conclusions

A few conclusions can be drawn from these experiments and analysis. First, the performance of the LHTES module is intimately coupled to the heat spreading and contact resistance of the system. If the system is not well designed to channel heat into the storage module its storage capacity will be poorly utilized. This is seen in the huge impact which the TIM had on the temperatures of the simulated tablet computer.

The full LHTES temperature control solution (TIM, spreader and LHTES module) was superior to all other temperature control solutions which were tested and was vastly superior to no temperature control solution. However, the most meaningful comparison is between experiments with the TIM and spreader; with and without the LHTES module. In this case the time to overheat

was extended by 30% (at 7 W) and the maximum temperature and rate of temperature increase of the SOC and front surface were reduced. The inclusion of the LHTES module had only a small impact of the temperature response of the back surface.

Comparable work in the literature is limited. The only authors who have done similar studies using thin LHTES modules are Ahmed (2016) and Tomizawa (2016). Work using hybrid heat sinks do not have a similar heat transfer path between the source and the surroundings, use a different heat transfer process to the surroundings (namely forced convection compared to natural convection in the case of this work on tablet PCs), and are used to dissipate much more power than the few Watts found in tablet PCs. Therefore, they will have completely different temperature profiles making any direct comparison fundamentally flawed.

The limitations of the work done by Ahmed (2016) were discussed extensively in chapter 4, however, this work is still relevant. Ahmed's work showed similar trends. However, the temperature control modules used by Mr. Ahmed were less successful at controlling the heater temperature. Using an LHTES module with a similar amount of PCM (16 g of *n*-eicosane compared to 16.22 g of *n*-eicosane), Ahmed (2016) showed that the heater exceeded 80°C after approximately 25 min with a heat generation rate of 6 W (see Fig. 4.8). While the current experiments showed that the heater temperature did not exceed 80°C during a 60 minute heating phase at 7 W. However, even with a similar amount of *n*-eicosane, a fair and meaningful comparision between these two studies is difficult due to the difference in the shape of the packets. Mr. Ahmed used an LHTES module which was 6.6 cm by 15.2 cm while the the author used an LHTES packet which was 10 cm by 18 cm. Clearly, the packets used by Mr. Ahmed were much thicker than those used by the author. In general the work presented here is a more complete and controlled comparative study of LHTES modules than that which was presented by Mr. Ahmed.

Tomizawa (2016) used a simulated handheld device which did not include a display or battery and presented heating experiments for a heat generation rate of 1.3 W. Experiments did not utilize a TIM to facilitate conduction from the source to the LHTES module. The total latent heat storage capacity of the LHTES modules, which were used in the simulated handheld device, were not explicitly given. However, based on the data which was presented by Tomizawa (2016), the author estimated that the total latent heat storage capacity was less than 0.2 kJ (small compared to the modules with 3.9 kJ of latent heat storage capacity used by the author). Tomizawa (2016)

presents temperature rise (defined as the difference between the measured temperature and the ambient temperature) not absolute temperature. The ambient temperature for each of the experiments was not given making a direct comparison impossible. The temperature rise plots did not show an observable inflection point but showed that the addition of the LHTES modules delayed the time it took for the heater and cover temperature to reach steady state. However Tomizawa (2016) did not present data showing how long it took for the system to reach a temperature limit, they based their analysis on the rate of temperature increase and the maximum temperature rise at steady state. There were no indication, from the presented data, that the small changes in the temeprature profiles was due to latent heat energy storage and was most likely due to sensible storage and heat spreading. Ultimately, the work which was presented in this chapter, used a more accurate experimental setup, a more realistic heat generation rate, and a much larger storage capacity.

CHAPTER 6 : CONCLUSIONS AND FUTURE WORK

6.1 Concluding Remarks

The goal of this project was to investigate the integration of solid-liquid LHTES modules into the temperature control system of modern and future handheld electronics. To further this goal, numerical and experimental platforms for modeling these systems were developed. These platforms were used to conduct investigations into many aspects these systems. This section will attempt to use the findings presented in the previous five chapters to answer the three core research questions which were posed in Chapter 1.

6.1.1 What are the Key Design Requirements for an LHTES Temperature Control Module for use in a Tablet Computer?

One key consideration when designing an effective LHTES module is balancing the need to decrease the resistance between the heater and the temperature control solution and the need to control the devices surface temperature. It is critical to create a low resistance conduction path between the major sources and the LHTES module. If the temperature control solution is not sufficiently coupled with the main heat source the PCM may not reach transition temperature and will be essentially useless in controlling the sources temperature. However, if the LHTES module is housed at the back of the device, improving the conduction path to the LHTES module will also increase the conduction path to the device case. If the LHTES module does not store sufficient energy it is possible the temperature control solution could have a negative impact on the devices cover temperature. This was clearly observed in chapters 2 and 5.

Another key aspect is integrating heat spreading into the temperature control solution. Due to the aspect ratio of modern handheld electronics effective heat spreading is critical for controlling the devices surface temperature and increasing the area over which heat is transferred from the surface to the ambient air. This is true with or without an LHTES module. However, heat spreading is also critical to increase the volume of LHTES module which is engaged in the heat transfer. Without heat spreading the heat source tends to melt through the PCM which is directly above the source and then conduct straight through to the surface. Heat must be directed down the width and length of the device to properly utilize the storage capacity which is available.

The design of the temperature control solution is limited by the ability to effectively transfer heat from the sources to the thermal storage. Impact from thermal spreading and thermal interface materials are as significant as the size of the thermal storage.

6.1.2 What is the Magnitude of Temperature Control Improvements which can be Gained by Utilizing an LHTES Module?

The use of a well designed LHTES module can have a significant impact on the time which a handheld device can operate before it is required to throttle the processor. The experiments presented in Chapter 5 utilize a mock tablet computer which closely mimics the most important aspects of a real device. Using this setup, it was found that without the LHTES module the front surface (display) temperature reached the comfort limit after 14.7 minutes. After the addition of the LHTES module the front surface reached the comfort limit after 19.2 minutes. The LHTES module increased the safe operating time by about 30%.

However, these findings are not transferable to all situations. It was also shown that for lower wattage situations where the heat spreader and TIM are sufficient, the impact of the LHTES module was limited. Also, LHTES modules are fundamentally limited by available PCMs. At higher heat generation rates the thermal storage in the LHTES modules used in this work will become insufficient. Further gains could potentially be made if the LHTES module could be made thicker. However, improving heat spreading to transport heat to all corners of the LHTES module is the most promising improvement which could be made.

6.1.3 What PCMs are Most Suited for use in an LHTES Temperature Control Module?

All the work in this thesis, numerical and experimental, has corroborated the findings that PCMs with lower transition temperatures provide better temperature control when integrated into an LHTES module. PCMs with transition temperatures near 35°C were shown to be effective.

The work in this thesis focused on the use of organic PCMs. They were found to be effective, stable and easy to use. The paraffin *n*-eicosane which was selected by the research team is non-toxic, an electrical insulator, and represents a very viable material for these systems.

6.2 Limitations

There are several limitations inherent to the work which was presented in this thesis. First, all of these studies have focused on relatively simple experiments/simulations where the heat source was turned on for a prescribed period of time and then was shut off allowing the system to cool back to ambient. This is not how real handheld electronic devices function. The studies are likely to be the worst case scenario and give meaningful insight into how effective LHTES modules can be. However, the exact magnitude of improvement (30% increased operating time) will not be predictive of what will happen in a real system. This topic is discussed further in future work.

Second, the experiments presented in Chapter 5 were intended only to measure the performance of these systems. The setup was instrumented to record the critical temperatures of the tablet itself. However, without measuring the temperature of the PCM directly (sensors embedded inside the encapsulation would be ideal) in multiple locations, it is impossible to estimate the melt fraction. The experiments proved that LHTES modules can improve temperature control in tablet computers but are lacking some of the information which would be helpful in designing and improving the system.

6.3 Future Work

While this project has successfully achieved its objectives, there are many aspects which warrant additional research.

First, a major unresolved aspect of modeling and simulating these systems is, determining what a realistic heat generation profile looks like. This work focussed on constant heat generation experiments. They are a well-established means of investigating these systems and are likely the worst-case scenario. However, actual devices do not operate in this way. The heat generated by components in a tablet are variable and may change rapidly. None of the researchers who worked on this project could find published data on this topic. If researchers are going to move forward with developing temperature control solutions for these systems, they will need better information about how they operate. Even reliable transient data on the energy used by the device (draw on the battery) would be valuable. It should be possible to instrument a "live" device and then measure its electrical usage during operation. Researchers at the LAMTE do not have the technical

background in electronics to deal with this but could collaborate with an electrical engineering researcher.

Second, this work has established the techniques which can be used to analyze these systems and the fundamental design constraints on LHTES modules. However, there is a lot of room for innovative design work on the shape, size, composition, and encapsulation of these systems. Integrating the encapsulation with the heat spreader, using multiple different PCMs in different locations of the device, and thermal conductivity enhancement are just a few aspects of LHTES module design which should be investigated. There are many advanced heat spreading techniques which would pair well with LHTES modules. For example, heat pipes could be used to transport heat from the main sources to parts of the LHTES modules which are geometrically remote.

Finally, LHTES based temperature control solutions could be integrated into an active handheld device. Simulated devices can only take the design of these systems so far. As stated above improved information on heat dissipation profiles and better instrumentation will help in the design process. However, placing an LHTES based temperature control solution into an active device will provide insight into several aspects that can not be simulated any other way. An active device will experience realistic heat dissipation and throttle the processor in response to high temperature conditions. A user can interact with the device in realistic ways and provide first hand feedback on user comfort. Instrumenting, and implementing this type of experiment would be quite challenging but is a necessary step in the development of these systems.

REFERENCES

Ahmed, T. (2016). *Development of a Novel Thermal Management Technology of Tablet Computers using Phase Change Materials.* MASc, Dalhousie University, Halifax, NS, Canada. 175 p.

Ahmed, T., Bhouri, M., Kahwaji, S., Groulx, D., & White, M. A. (2016). *Experimental Investigation of Thermal Management of Tablet Computers using Phase Change Materials (PCMs).* Paper presented at the ASME 2016 Summer Heat Transfer Conference,Washington, DC, USA. 10 p.

Alawadhi, E., & Amon, C. (2003). PCM Thermal Control Unit for Portable Electronic Devices: Experimental and Numerical Studies. *IEEE Transactions on Components and Packaging Technologies, 26*(1), 116-125.

Asadi, M., Xie, G., & Sunden, B. (2014). A review of heat transfer and pressure drop characteristics of single and two-phase microchannels. *International Journal of Heat and Mass Transfer, 79*, 34-53. doi: 10.1016/j.ijheatmasstransfer.2014.07.090

Baby, R., & Balaji, C. (2012). Experimental investigations on phase change material based finned heat sinks for electronic equipment cooling. *International Journal of Heat and Mass Transfer, 55*(5-6), 1642-1649. doi: 10.1016/j.ijheatmasstransfer.2011.11.020

Baby, R., & Balaji, C. (2013). Thermal optimization of PCM based pin fin heat sinks: An experimental study. *Applied Thermal Engineering, 54*(1), 65-77. doi: 10.1016/j.applthermaleng.2012.10.056

Baby, R., & Balaji, C. (2014). Thermal performance of a PCM heat sink under different heat loads: An experimental study. *International Journal of Thermal Sciences, 79*, 240-249. doi: 10.1016/j.ijthermalsci.2013.12.018

Bar-Cohen, A., Arik, M., & Ohadi, M. (2006). Direct Liquid Cooling of High Flux Micro and Nano Electronics Components. *Proceedings of the IEEE, 94*(8), 1549-1570.

C. Kheirabadi, A., & Groulx, D. (2016). Cooling of server electronics: A design review of existing technology. *Applied Thermal Engineering, 105*, 622-638. doi: 10.1016/j.applthermaleng.2016.03.056

Desgrosseilliers, L. (2016). *Design and Evaluation of a Modular, Supercooling Phase Change Heat Storage Device for Indoor Heating.* PhD, Dalhousie University, Halifax, Canada. 292 p.

Desgrosseilliers, L., Whitman, C. A., Groulx, D., & White, M. A. (2013). Dodecanoic acid as a promising phase-change material for thermal energy storage. *Applied Thermal Engineering, 53*, 37-41. doi: 10.1016/j.applthermaleng.2012.12.031

Fan, L.-W., Xiao, Y.-Q., Zeng, Y., Fang, X., Wang, X., Xu, X., . . . Cen, K.-F. (2013). Effects of melting temperature and the presence of internal fins on the performance of a phase change material (PCM)-based heat sink. *International Journal of Thermal Sciences, 70*, 114-126. doi: 10.1016/j.ijthermalsci.2013.03.015

Fok, S. C., Shen, W., & Tan, F. L. (2010). Cooling of portable hand-held electronic devices using phase change materials in finned heat sinks. *International Journal of Thermal Sciences, 49*(1), 109-117. doi: 10.1016/j.ijthermalsci.2009.06.011

Greenspan, J. D., Roy, E. A., Caldwell, P. A., & Farooq, N. S. (2003). Thermosensory intensity and affect throughout the perceptible range. *Somatosensory & motor research, 20*(1), 19-26.

Grimes, R., Walsh, E., & Walsh, P. (2010). Active cooling of a mobile phone handset. *Applied Thermal Engineering, 30*(16), 2363-2369. doi: http://dx.doi.org/10.1016/j.applthermaleng.2010.06.002

Hodes, M., Weinstein, R. D., Pence, S. J., Piccini, J. M., Manzione, L., & Chen, C. (2002). Transient Thermal Management of a Handset Using Phase Change Material (PCM). *Journal of Electronic Packaging, 124*(4), 419. doi: 10.1115/1.1523061

Incropera, DeWitt, Bergman, & Lavine. (2007). *Iroduction to Heat Transfer* (5th ed.). John Wiley and Sons Inc. 901 p.

Jaworski, M. (2012). Thermal performance of heat spreader for electronics cooling with incorporated phase change material. *Applied Thermal Engineering, 35*, 8. doi: 10.1016/j.applthermaleng.2011.10.036

Kadam, S. T., & Kumar, R. (2014). Twenty first century cooling solution: Microchannel heat sinks. *International Journal of Thermal Sciences, 85*, 73-92. doi: 10.1016/j.ijthermalsci.2014.06.013

Kahwaji, S., Johnson, M. B., Kheirabadi, A. C., Groulx, D., & White, M. A. (2017). Fatty acids and related phase change materials for reliable thermal energy storage at moderate temperatures. *Solar Energy Materials and Solar Cells, 167*, 109-120. doi: 10.1016/j.solmat.2017.03.038

Kandasamy, R., Wang, X.-Q., & Mujumdar, A. S. (2008). Transient cooling of electronics using phase change material (PCM)-based heat sinks. *Applied Thermal Engineering, 28*(8-9), 1047-1057. doi: 10.1016/j.applthermaleng.2007.06.010

Kheirabadi, A. C., & Groulx, D. (2014). *Design of an Automated Thermal Cycler for Long-term Phase Change Material Phase Transition Stability Studies.* Paper presented at the COMSOL Conference 2014, Boston, MA (USA). 7 p.

Kheirabadi, A. C., & Groulx, D. (2015). *The Effect of the Mushy-Zone Constant on Simulated Phase Change Heat Transfer*. Paper presented at the CHT-15 ICHMT International

Symposium on Advances in Computational Heat Transfer,Rutgers University, Piscataway (USA). 22 p.

Kim, J. (2007). Spray cooling heat transfer: The state of the art. *International Journal of Heat and Fluid Flow, 28*(4), 753-767. doi: 10.1016/j.ijheatfluidflow.2006.09.003

Kozak, Y., Abramzon, B., & Ziskind, G. (2013). Experimental and numerical investigation of a hybrid PCM–air heat sink. *Applied Thermal Engineering, 59*(1-2), 142-152. doi: 10.1016/j.applthermaleng.2013.05.021

Lu, J., Fan, L.-w., Zeng, Y., Xiao, Y.-q., Xu, X., & Yu, Z.-t. (2014). Effect of the inclination angle on the transient performance of a phase change material-based heat sink under pulsed heat loads. *Journal of Zhejiang University SCIENCE A, 15*(10), 789-797. doi: 10.1631/jzus.A1400103

Mahmoud, S., Tang, A., Toh, C., Al-Dadah, R., & Soo, S. L. (2013). Experimental investigation of inserts configurations and PCM type on the thermal performance of PCM based heat sinks. *Applied Energy, 112*, 1349-1356. doi: 10.1016/j.apenergy.2013.04.059

Maranda, S. (2017). *Experimental and Numerical Investigation of Thin PCM Packages for Thermal Managment of Portable Electronic Device.* Master of Science in Engineering Lucerne University of Applied Science and Arts, Lucerne, Switzerland. 94 p.

Maydanik, Y. F., Chernysheva, M. A., & Pastukhov, V. G. (2014). Review: Loop heat pipes with flat evaporators. *Applied Thermal Engineering, 67*(1-2), 294-307. doi: 10.1016/j.applthermaleng.2014.03.041

Moore, D., Raghupathy, A., & Maltz, W. (2015). *Application of Phase Change Materials in Handheld Computing Devices.* Paper presented at the 31st Semi-Therm Symposium.

Patapoutian, A., Peier, A. M., Story, G. M., & Viswanath, V. (2003). ThermoTRP channels and beyond: mechanisms of temperature sensation. *Nature Reviews Neuroscience, 4*(7), 529-539.

Saha, S. K., Srinivasan, K., & Dutta, P. (2008). Studies on Optimum Distribution of Fins in Heat Sinks Filled With Phase Change Materials. *Journal of Heat Transfer, 130*(3), 034505. doi: 10.1115/1.2804948

Sanusi, O., Fleischer, A. S., & Weinstein, R. D. (2010). An Investigation ointo the solidification of Nano-Enhanced Phase Change Materials For Transient Thermal Managment of Electronics. *IEEE*, 6 p.

Siedel, B., Sartre, V., & Lefèvre, F. (2015). Literature review: Steady-state modelling of loop heat pipes. *Applied Thermal Engineering, 75*, 709-723. doi: 10.1016/j.applthermaleng.2014.10.030

Singh, R., Mochizuki, M., Shahed, M. A., Saito, Y., Jalilvand, A., Matsuda, M., . . . Goto, K. (2013). *Low Profile Cooling Solutions for Advanced Packaging Based on Ultra-Thin Heat Pipe and Piezo Fan*. Paper presented at the 3rd IEEE CPMT Symposium Japan. 4 p.

Sponagle, B., & Groulx, D. (2015). *Thermal Modeling of Tablets: Temperature Management using Phase Change Materials*. Paper presented at the 1st Thermal and Fluid Engineering Summer Conference, TFESC,New York City (USA). 14 p.

Sponagle, B., Maranda, S., & Groulx, D. (2017). *Investigation of the Thermal Behaviour of Thin Phase Change Material Packages as a Solution to Temperature Control in Electronics*. Paper presented at the Proceedings of the ASME 2017 Summer Heat Transfer Conference,Bellevue, Washington, USA. 10 p.

Tomizawa, Y., Sasaki, K., Kuroda, A., Takeda, R., & Kaito, Y. (2016). Experimental and numerical study on phase change material (PCM) for thermal management of mobile devices. *Applied Thermal Engineering, 98*, 320-329. doi: 10.1016/j.applthermaleng.2015.12.056

Vélez, C., Khayet, M., & Ortiz de Zárate, J. M. (2015). Temperature-dependent thermal properties of solid/liquid phase change even-numbered n-alkanes: n-Hexadecane, n-octadecane and n-eicosane. *Applied Energy, 143*, 383-394. doi: 10.1016/j.apenergy.2015.01.054

Weinstein, R. D., Kopec, T. C., Fleischer, A. S., D'Addio, E., & Bessel, C. A. (2008). The Experimental Exploration of Embedding Phase Change Materials With Graphite Nanofibers for the Thermal Management of Electronics. *Journal of Heat Transfer, 130*(4), 042405. doi: 10.1115/1.2818764

Yeh, L. T. (1995). Review of Heat Transfer Technologies in Electronic Equipment. *Journal of Electronic Packaging, 117*, 333-339.

Zheng, N., & Wirtz, R. A. (2004). A Hybrid Thermal Energy Storage Device, Part 1: Design Methodology. *Journal of Electronic Packaging, 126*(1), 1. doi: 10.1115/1.1646419

APPENDIX A: DRAFT DRAWINGS OF THE TABLET GEOMETRY
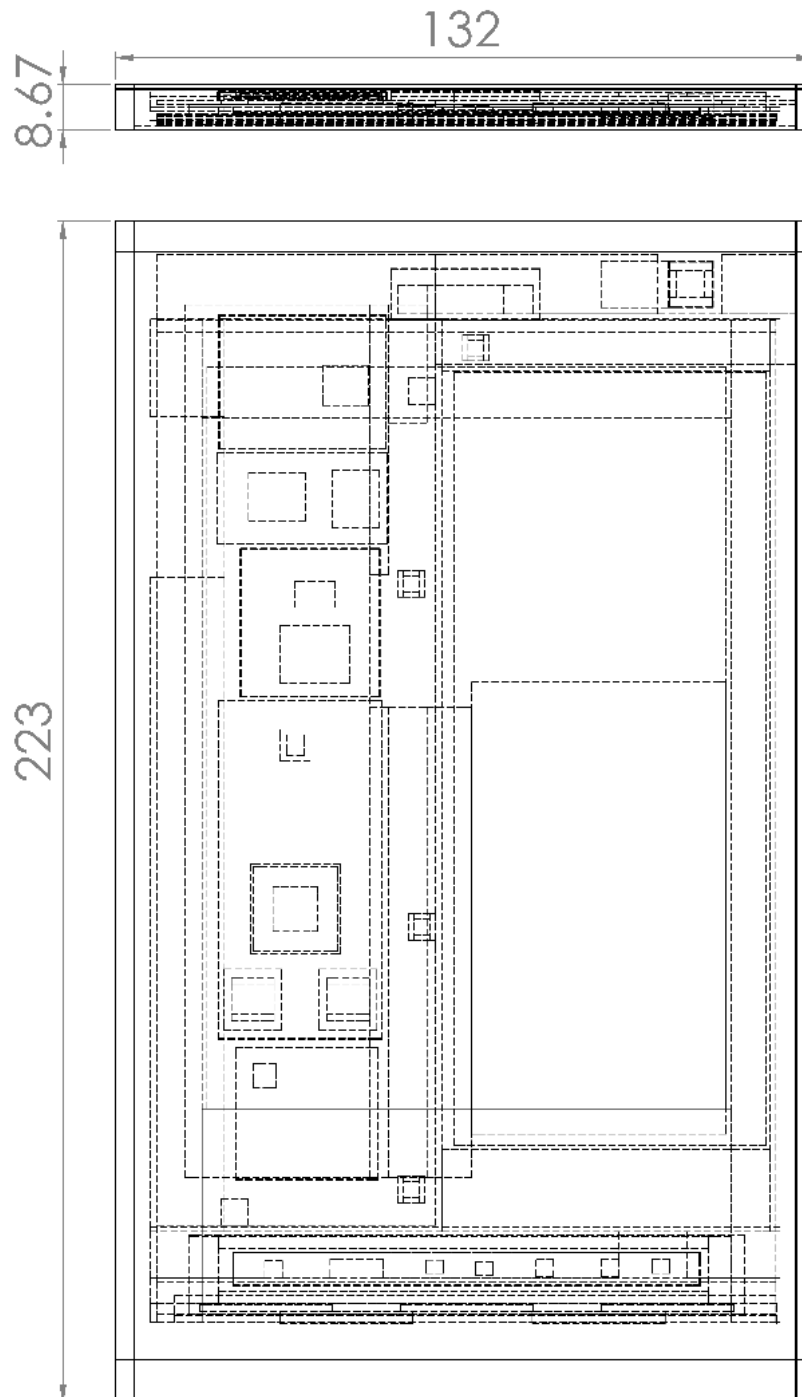
Fig. A.1 Dimensioned drawing of the tablet geometry, dimensions given in mm

DETAIL A
SCALE 4 : 1

2.31

116.90

189.20

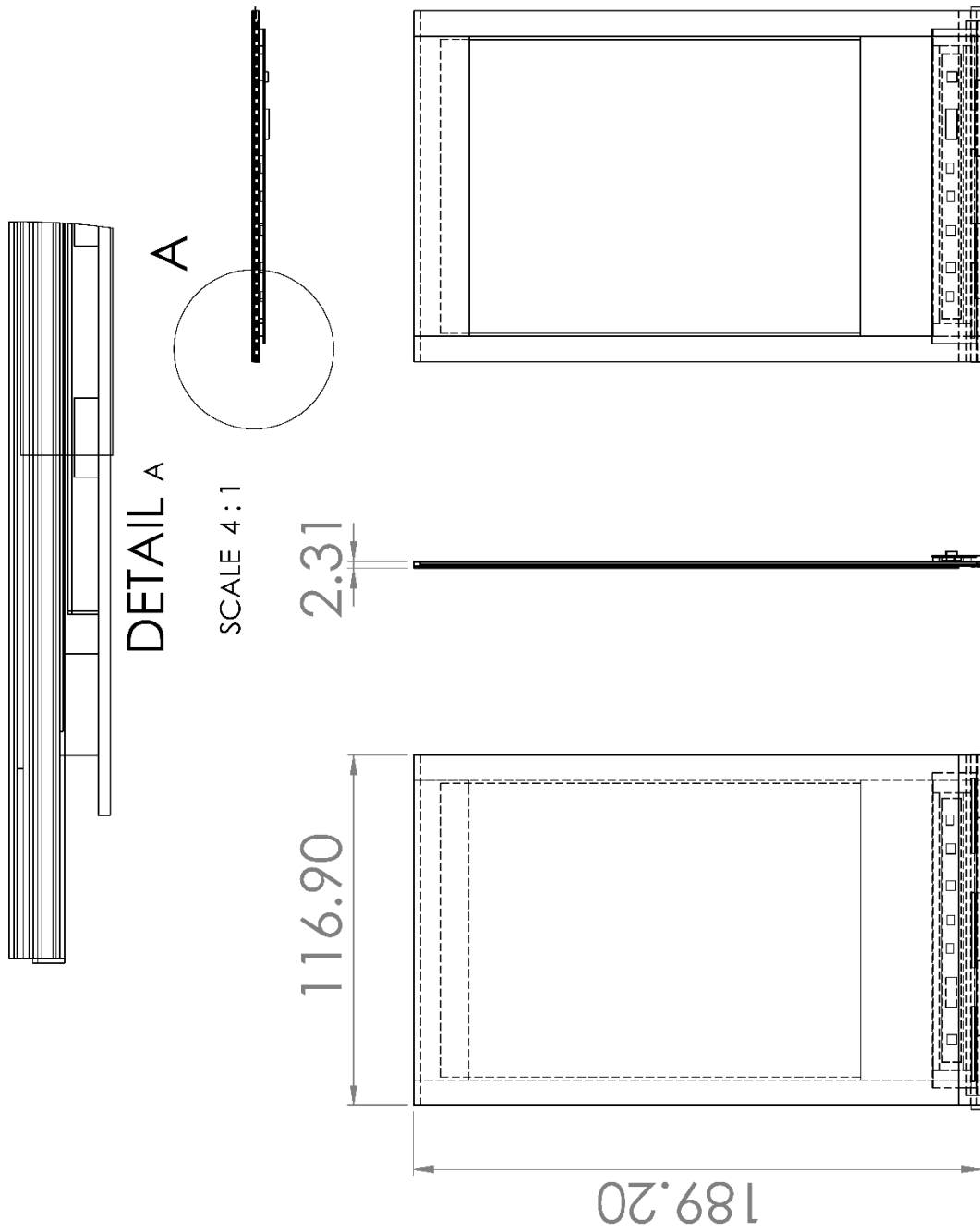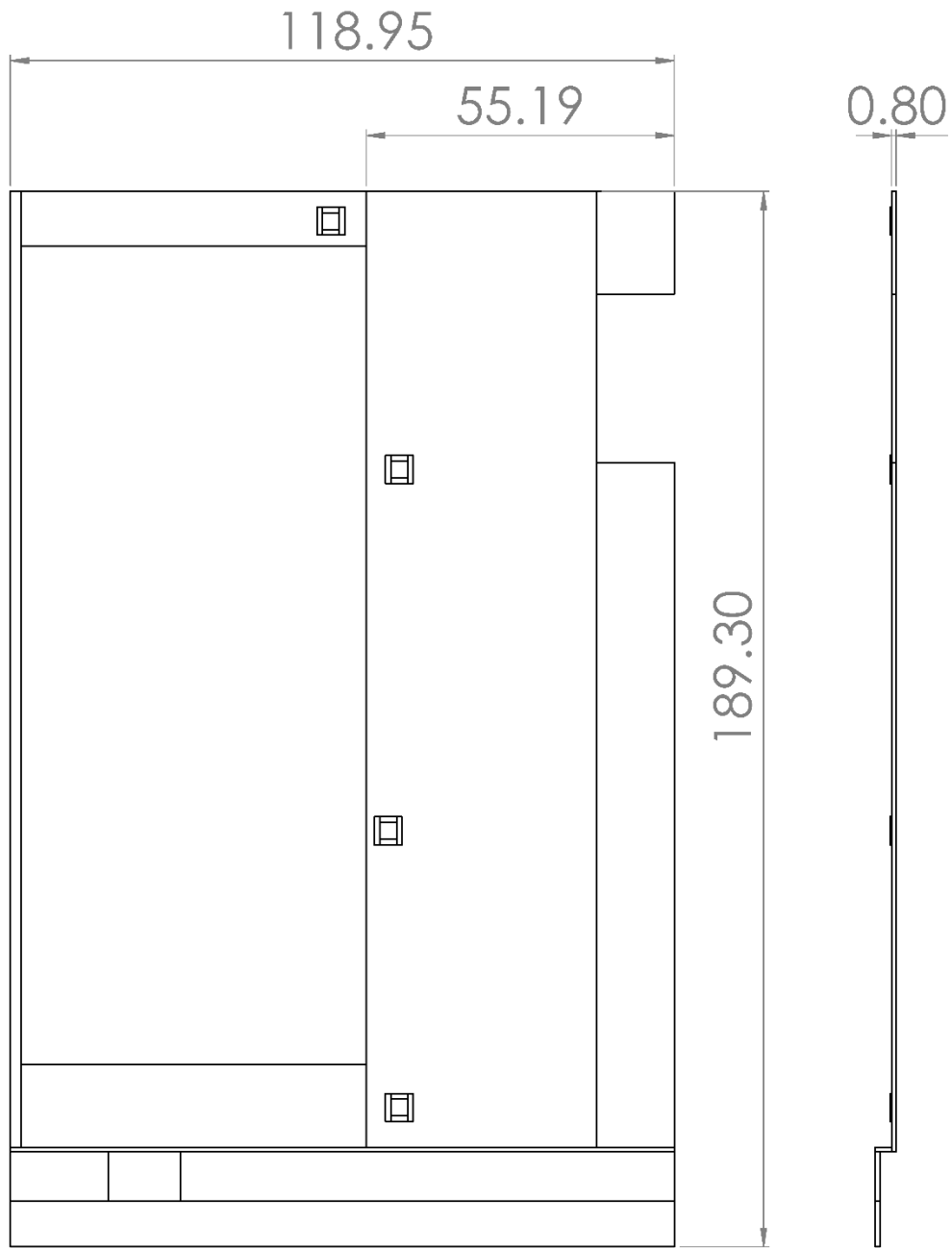**Fig. A.2 Dimensioned drawing of the display assembly, dimensions given in mm**

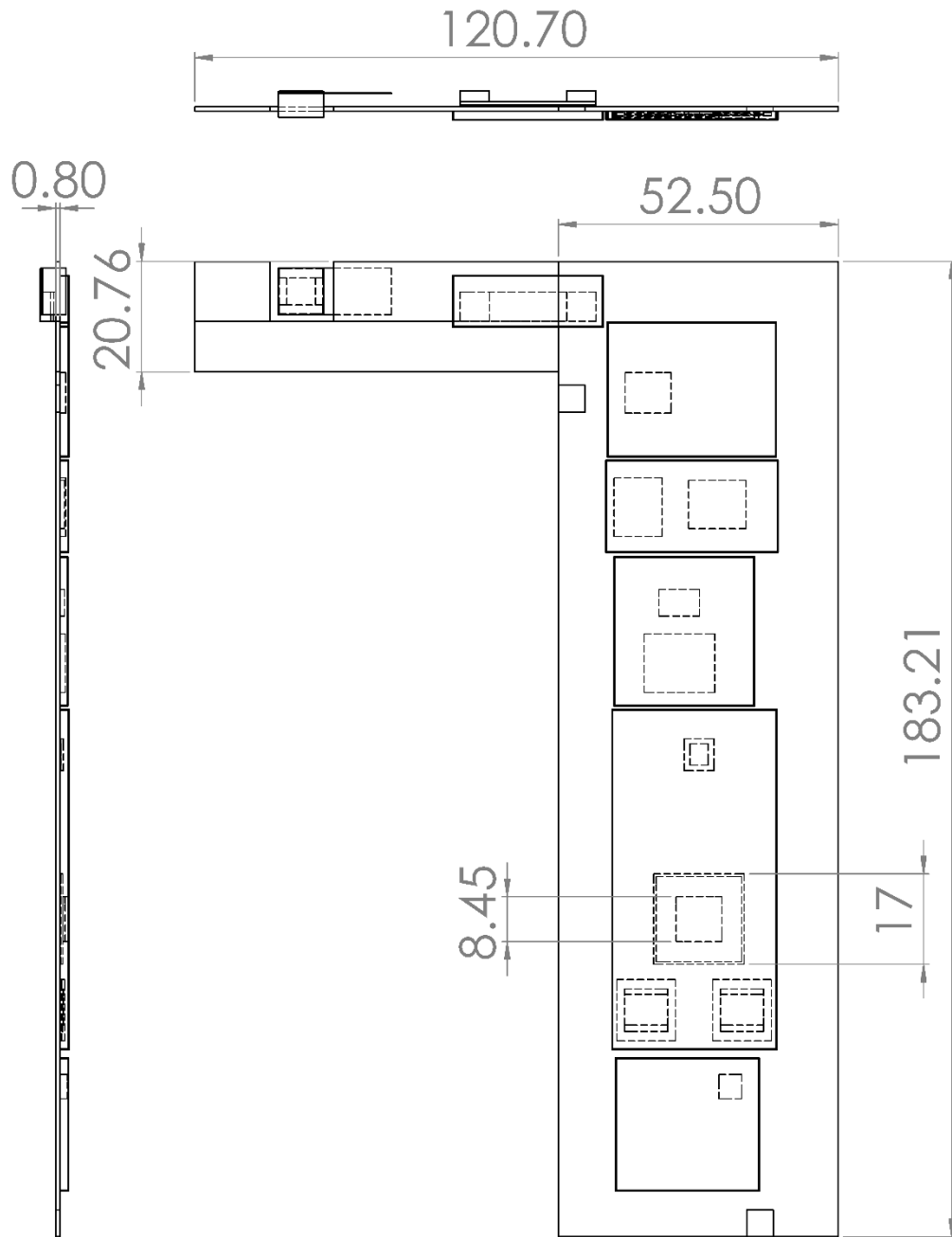**Fig. A.3 Dimensioned drawing of the magnesium spreader, dimensions given in mm**

Fig. A.4 Dimensioned drawing of the PCB, dimensions given in mm
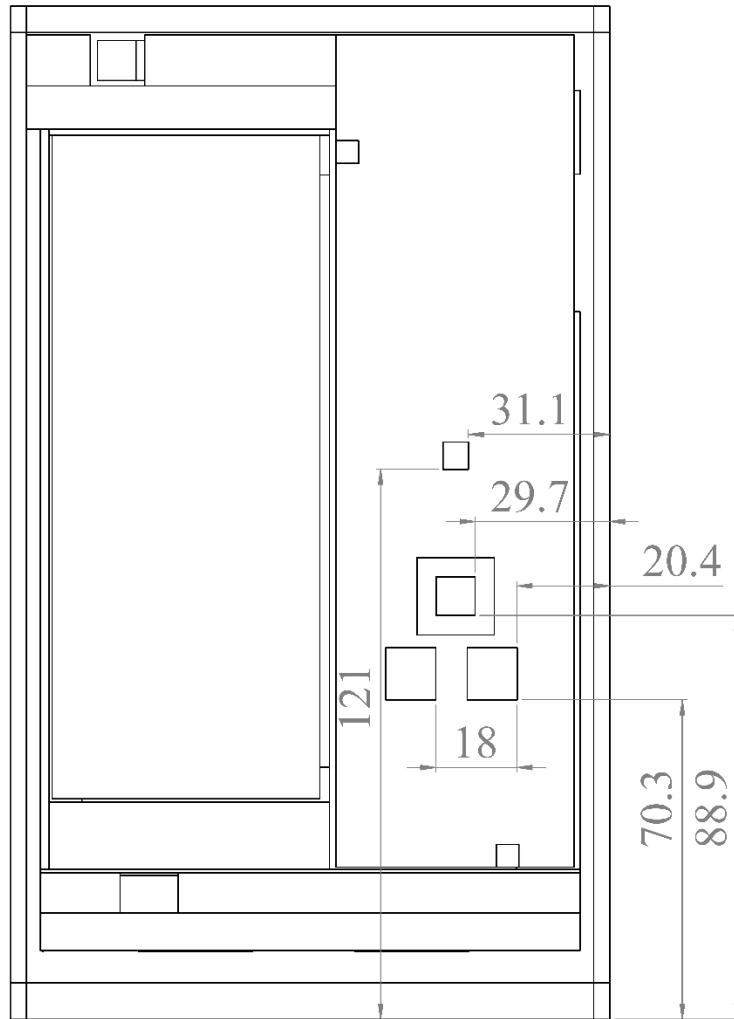
Fig. A.5 Dimensioned drawing of the tablet showing the location of the main sources on the PCB, dimensions given in mm

APPENDIX B: MESH STUDY OF THE SIMULATED TABLET WITHOUT PCM

Figures B.1, B.2 and B.3 show the maximum and average temperature of the SOC, back surface and front surface respectively. As was explained in the mesh study presented in Chapter 2 the geometry consists of many thin layers through the thickness of the tablet. Results are presented for simulations without PCM where there was 1, 2 and 4 elements through the thickness of each of these layers. Clearly the simulation is independent of an increase in the number of elements in these layers. There is no visible change in the shape of the temperature profiles. This is expected as the simulation will be solely conduction and should be insensitive to mesh size. For parts of the geometry where there is only conduction and no phase change it was chosen to use 2 elements in each of these layers for all subsequent simulations.
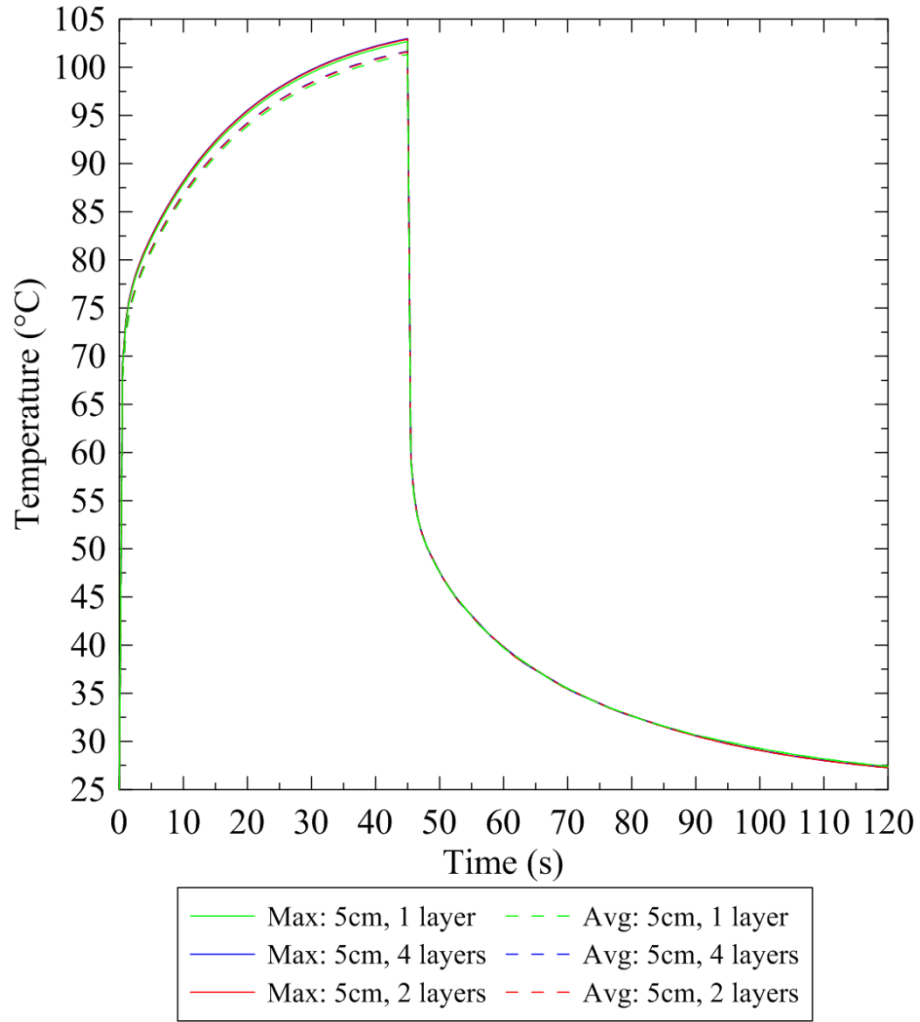
Fig. B.1 Mesh study comparing the Maximum and average temperatures of the SOC for a simulation without PCM
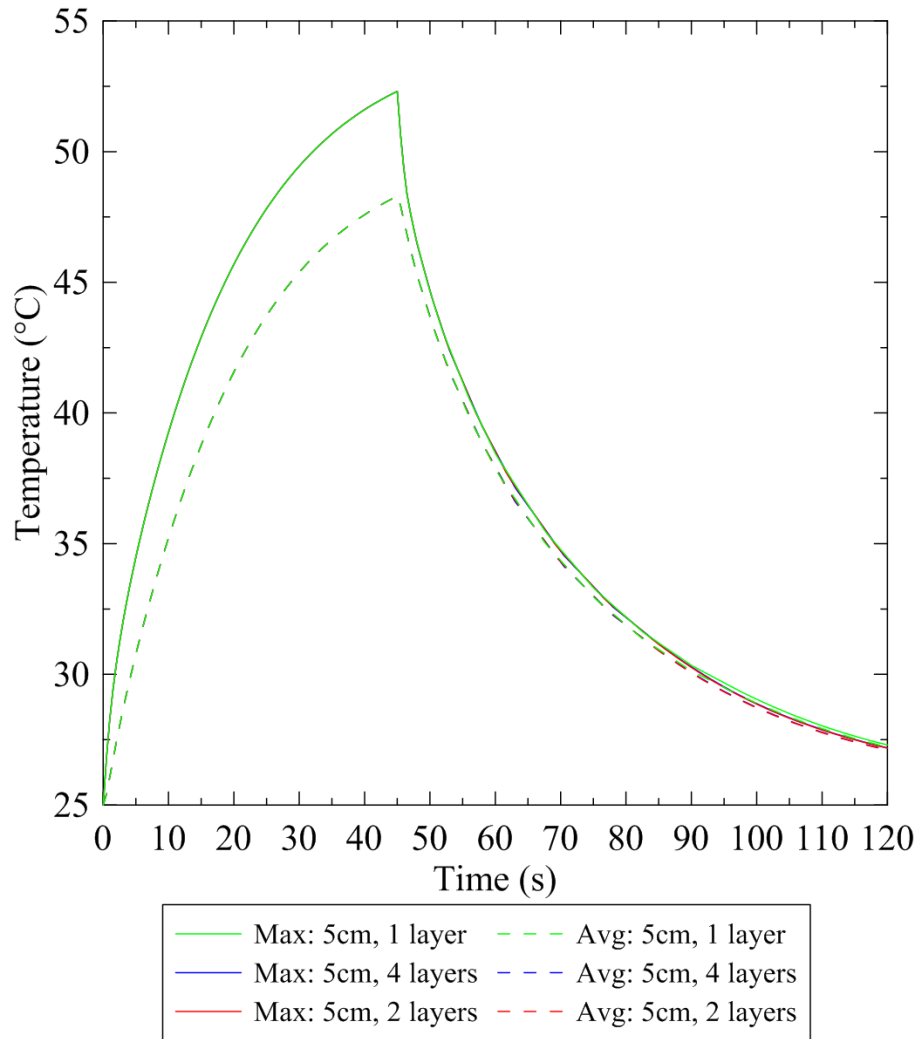
Fig. B.2 Mesh study comparing the Maximum and average temperatures of the back surface for a simulation without PCM
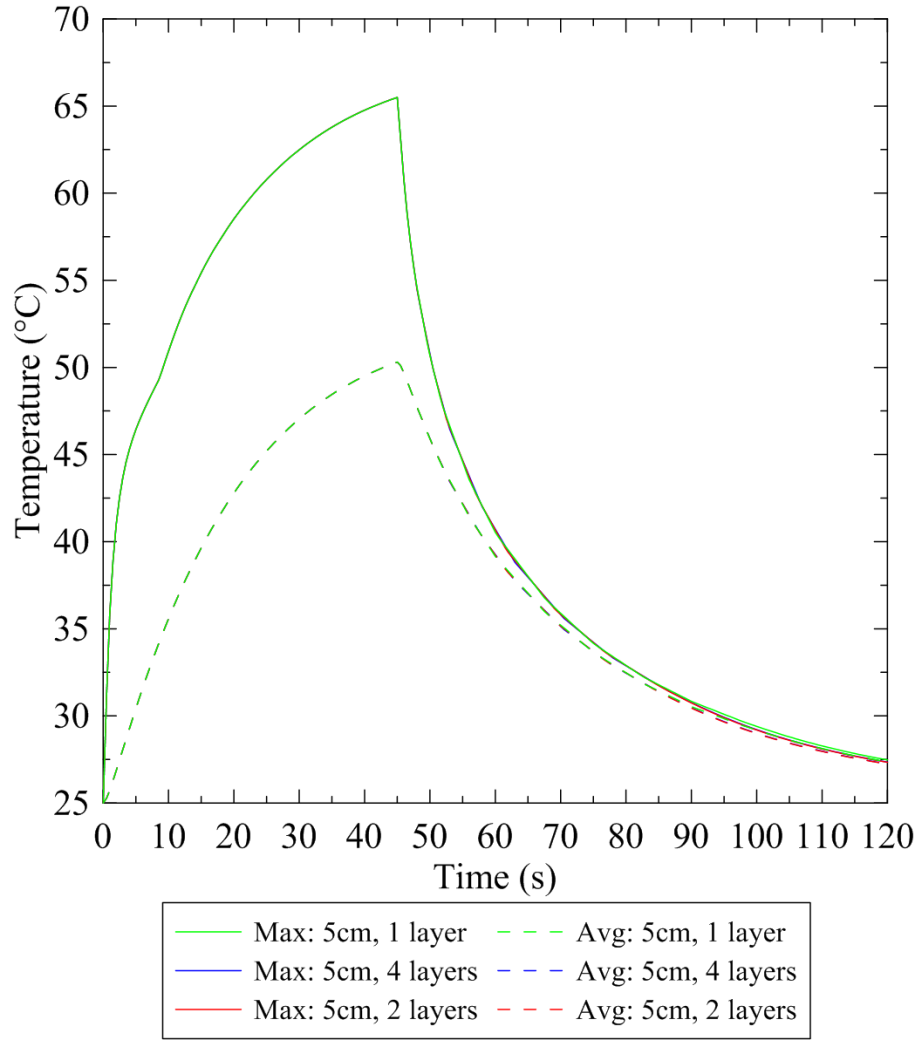
Fig. B.3 Mesh study comparing the Maximum and average temperatures of the front surface for a simulation without PCM

APPENDIX C: DIMENSIONED DRAWING OF EXPERIMENTAL SETUP
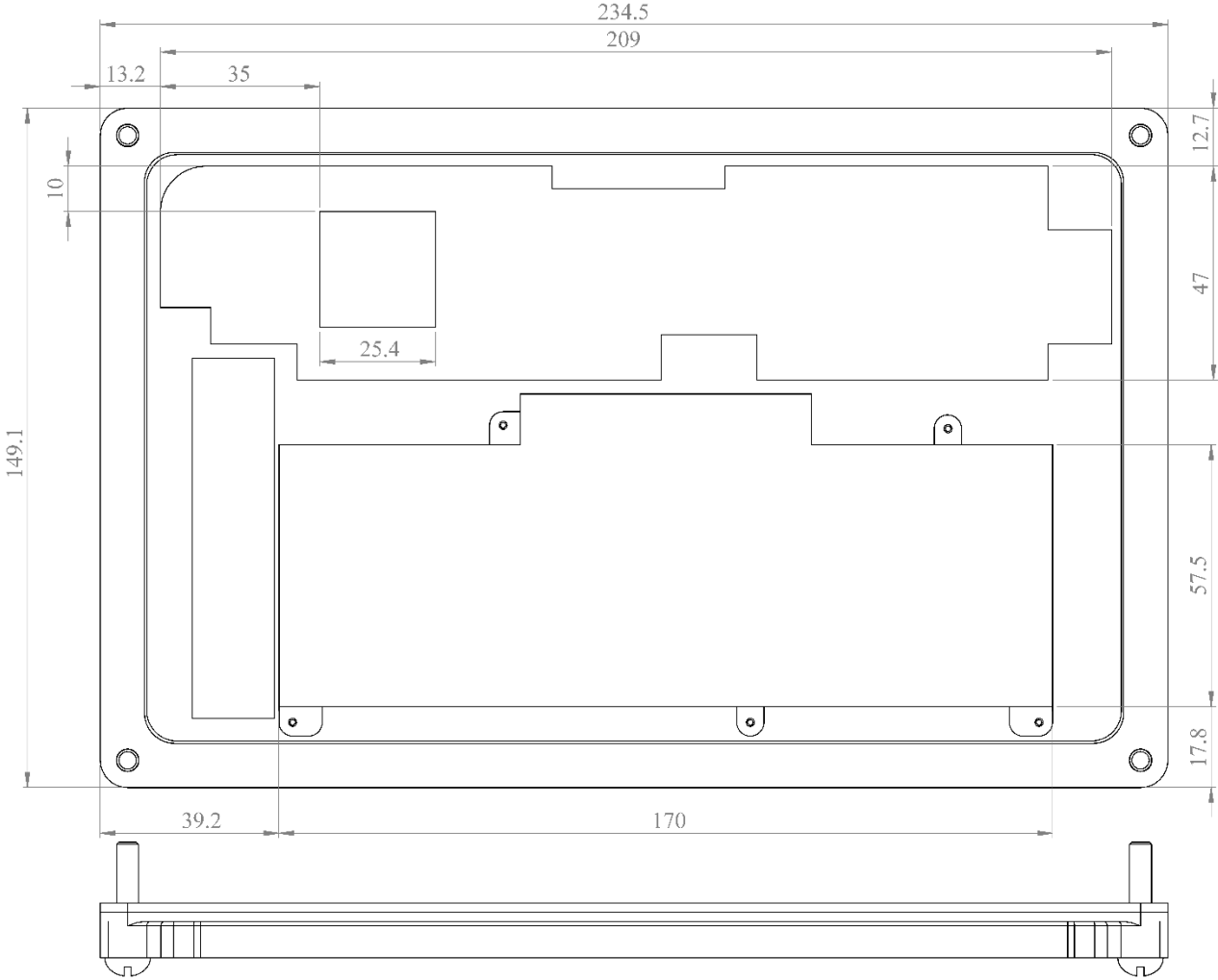
Fig. C.1 Dimensioned drawing of the experimental setup, all dimensions are in mm
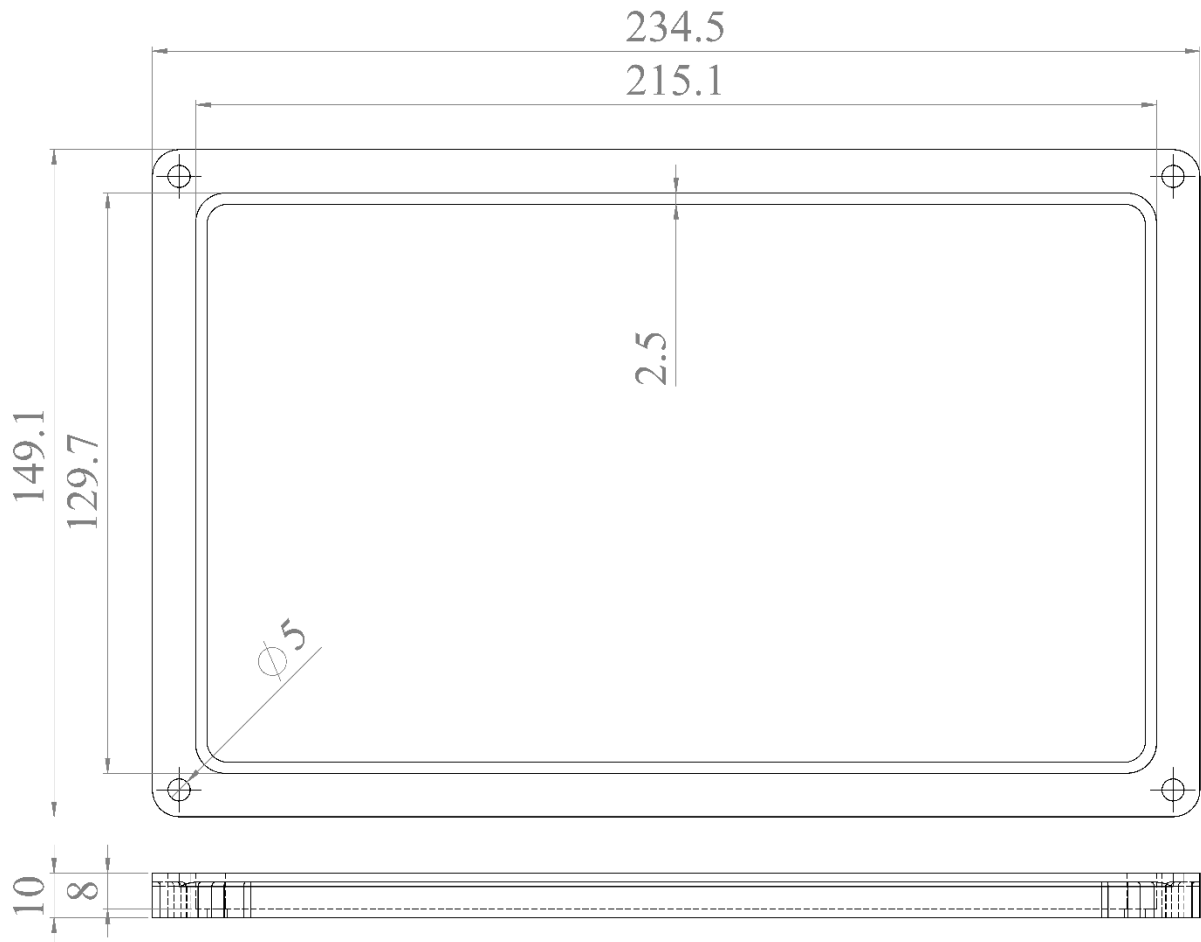
Fig. C.2 Dimensioned drawing of the front frame component, all dimensions are in mm
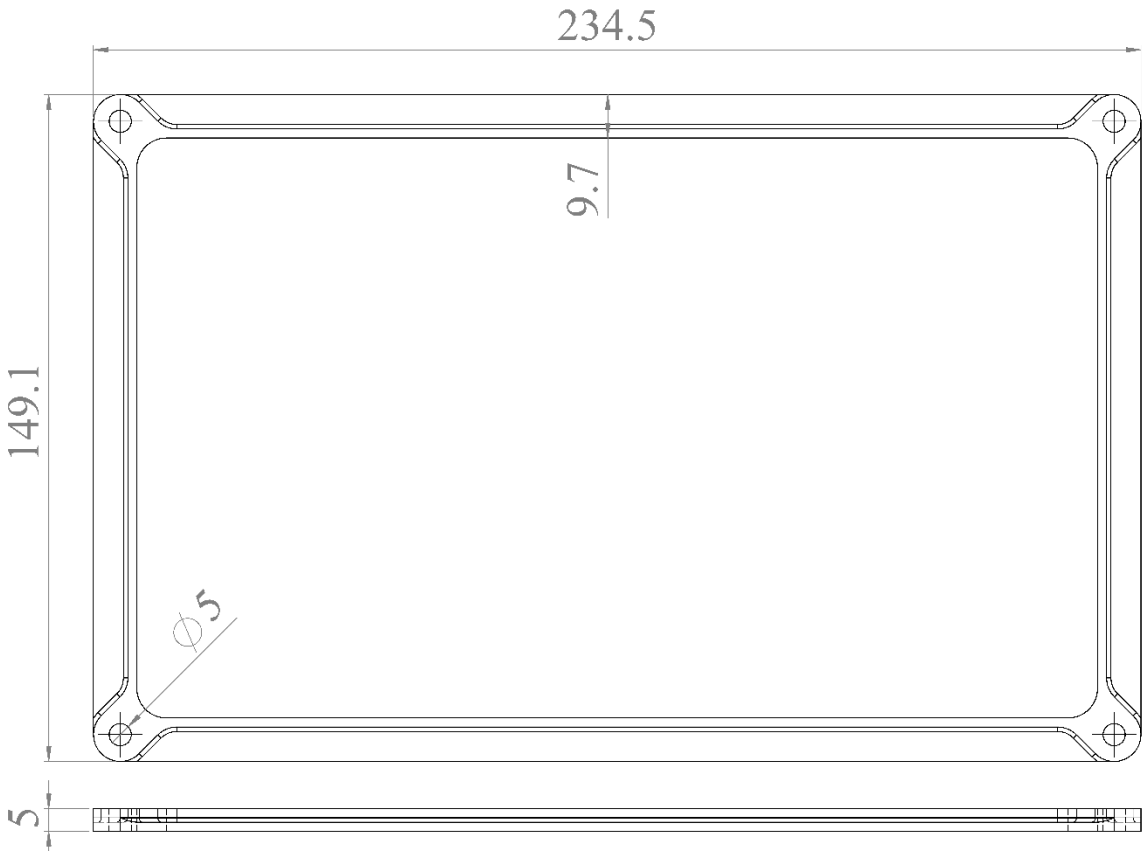
Fig. C.3 Dimensioned drawing of the back frame component, all dimensions are in mm
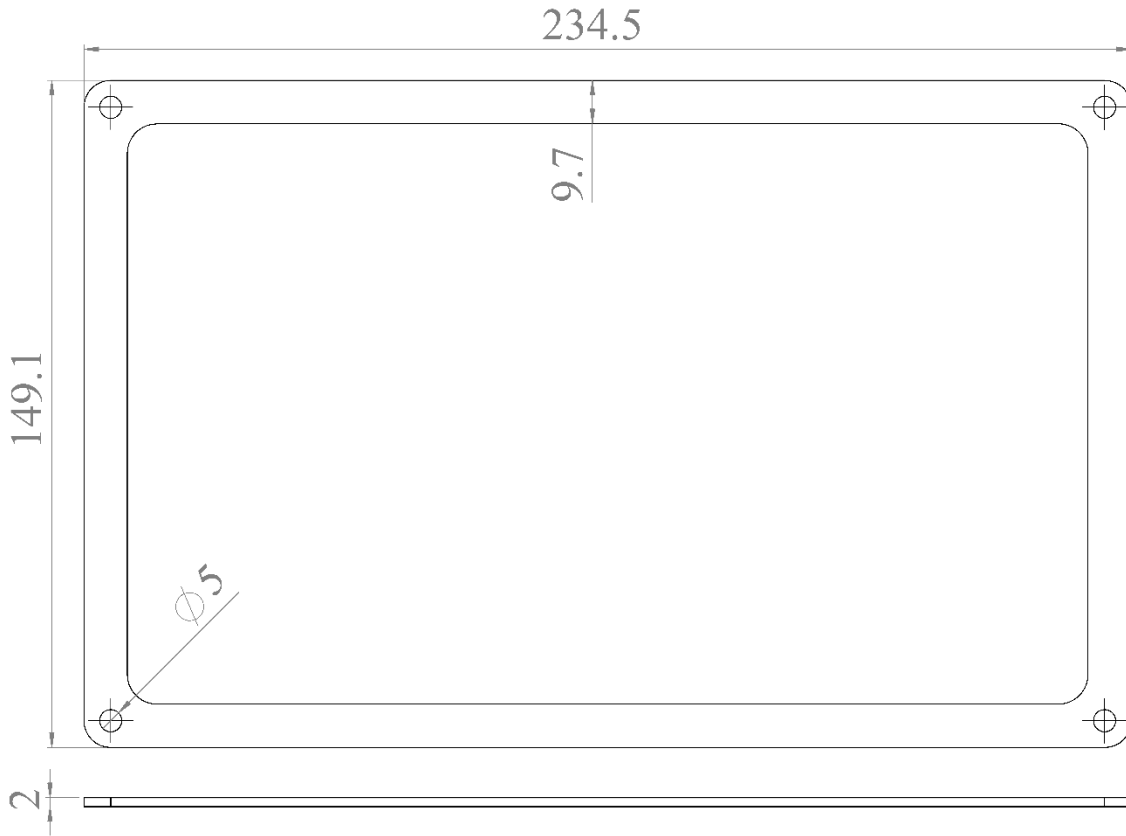
Fig. C.4 Dimensioned drawing of the spacer, all dimensions are in mm

Fig. C.5 Dimensioned drawings of the battery, all dimensions are in mm

178

Fig. C.6 Dimensioned drawing of the nylon cover, all dimensions are in mm

Fig. C.7 Dimensioned drawing of the simulated PCB, all dimensions are in mm

179

APPENDIX D: UNCERTAINTY ANALYSIS OF THE POWER MEASUREMENT SYSTEM

Table D.1 lists the uncertainties in electrical resistance of the resistors and voltage measurements. Table D.2 summarizes the equations used to calculate the heat dissipated by the heater and the uncertainty in this heat dissipation. Using the values and expressions in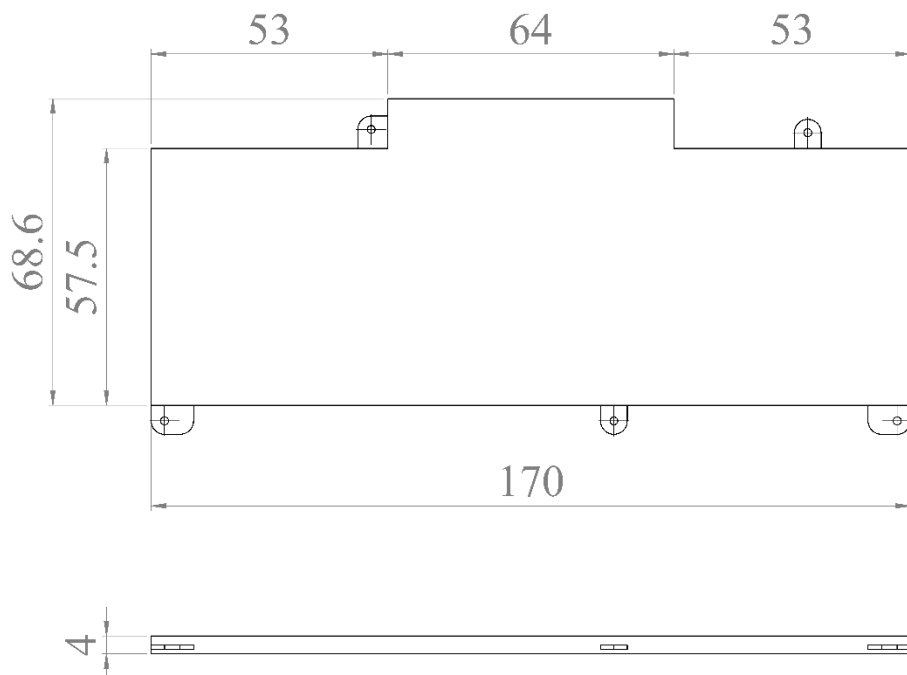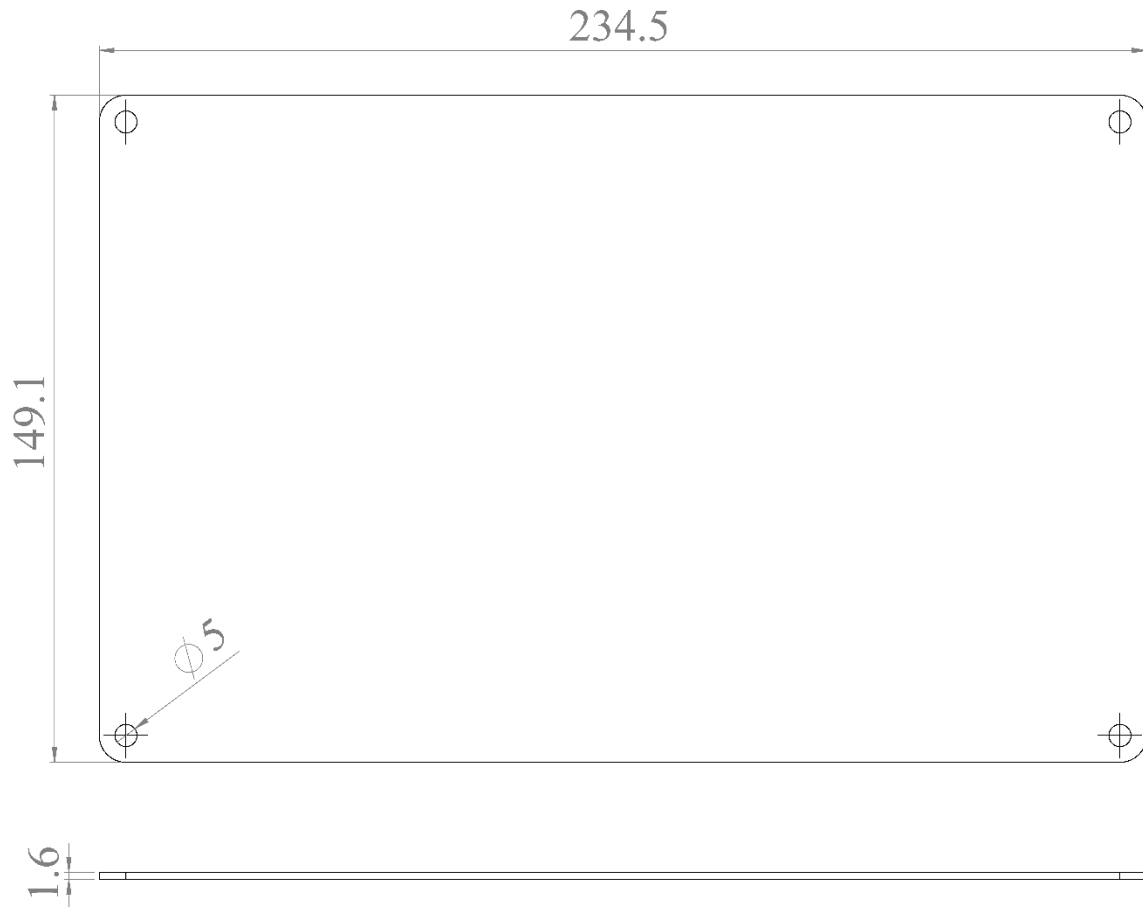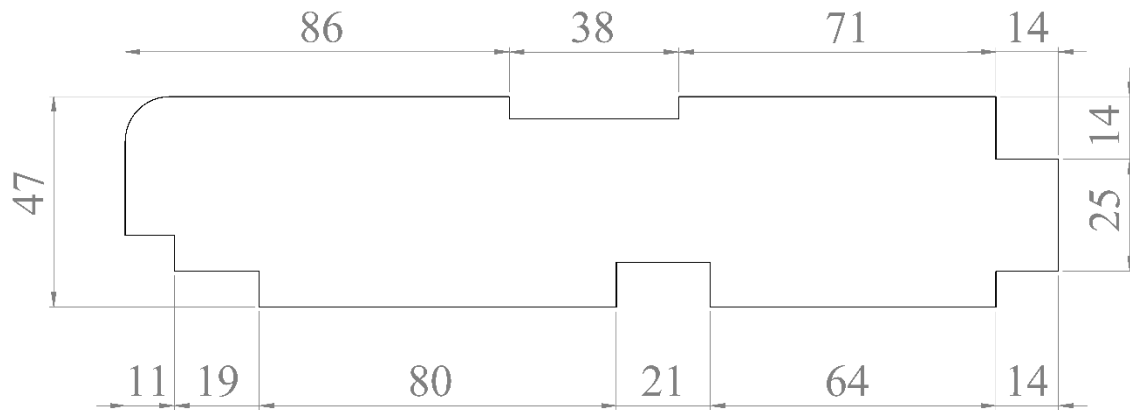 the following tables the uncertainty in the power measurements for 4.5 and 7 W are ±0.33 W and ±0.51 W, respectively. As a percentage of the dissipated power this is an uncertainty of ±7.3%.

Table D.1 uncertainties in electrical resistance of the resistors and voltage measurements

Measured value	Resistance	Measurement uncertainty
V_{R1}	-	$\delta V_{R1} = \pm\, 0.0025 \cdot V_{R1}$
V_{Gain}	-	$\delta V_{R1} = \pm\, 0.0025 \cdot V_{Gain}$
R_1	100 kΩ	$\delta R_1 = \pm\, 0.05 \cdot R_1$
R_2	200 kΩ	$\delta R_2 = \pm\, 0.05 \cdot R_2$
R_3	1 kΩ	$\delta R_3 = \pm\, 0.05 \cdot R_3$
R_{Shunt}	0.05 Ω	$\delta R_{Shunt} = \pm\, 0.025 \cdot R_{Shunt}$

Table D.2 Equations for calculating the heat dissipated and its uncertainty

Calculated value	Measurement uncertainty
$V_{in} = \dfrac{R_1 + R_2}{R_1} V_{R1}$	$\delta V_{in} = \sqrt{\left(\dfrac{\partial V_{in}}{\partial V_{R1}} \delta V_{R1}\right)^2 + \left(\dfrac{\partial V_{in}}{\partial R_1} \delta R_1\right)^2 + \left(\dfrac{\partial V_{in}}{\partial R_2} \delta R_2\right)^2}$
$I_{in} = \dfrac{V_{Shunt}}{R_{Shunt}} = \dfrac{V_{Gain}}{R_{Shunt}} \cdot \dfrac{1}{5 + \dfrac{200\ \text{k}\Omega}{R_3}}$	$\delta I_{in} = \sqrt{\left(\dfrac{\partial I_{in}}{\partial V_{Gain}} \delta V_{Gain}\right)^2 + \left(\dfrac{\partial I_{in}}{\partial R_3} \delta R_3\right)^2 + \left(\dfrac{\partial I_{in}}{\partial R_{Shunt}} \delta R_{Shunt}\right)^2}$
$P = V_{in} \cdot I_{in}$	$\delta P = \sqrt{\left(\dfrac{\partial P}{\partial V_{in}} \delta V_{in}\right)^2 + \left(\dfrac{\partial P}{\partial I_{in}} \delta I_{in}\right)^2}$

APPENDIX E: COPYRIGHT PERMISSION LETTERS

February 6th 2018
Mr. Simon Maranda
Lucerne University of Applied Sciences and Arts
Lucerne, Switzerland

Mr. Maranda

I am preparing my PhD thesis for submission to the Faculty of Graduate Studies at Dalhousie University, Halifax, Nova Scotia, Canada. I am seeking permission to include, from the thesis listed below, figures: 3-1, 3-2, 3-3, 3-5, 3-6, 4-3, 4-6, 4-13, 5-1, and 6-2 into my thesis.

Experimental and numerical investigation of thin PCM packages for thermal management of portable electronic devices, Simon Maranda, 2017.

Canadian graduate theses are reproduced by the Library and Archives of Canada (formerly National Library of Canada) through a non-exclusive, world-wide license to reproduce, loan, distribute, or sell theses. I am also seeking permission for the material described above to be reproduced and distributed by the LAC (NLC). Further details about the LAC (NLC) thesis program are available of the LAC (NLC) website (www.nlc-bnc.ca).

Full publication details and a copy of this permission letter will be included in the thesis.

Yours sincerely,

Benjamin Sponagle

Permission is granted for:

a) the inclusion of the material described above in your thesis

b) for the material described above to be included in the copy of your thesis that is sent to the library and Archives of Canada (formerly National Library of Canada) for reproduction and distribution.

Name: _Simon Maranda_   Title: _____

Signature: ████████████   Date: _14.02.18_

February 12th 2018
Mr. Tousif Ahmed
University of Delaware
Newark, USA

Mr. Ahmed

I am preparing my PhD thesis for submission to the Faculty of Graduate Studies at Dalhousie University, Halifax, Nova Scotia, Canada. I am seeking permission to include, from the thesis listed below, figures: 4-7, 4-8, 4-16, 4-18, 5-3, and 5-10 into my thesis.

Development of a Novel Thermal Management Technology of Tablet Computers using Phase Change Materials, Tousif Ahmed, 2017.

Canadian graduate theses are reproduced by the Library and Archives of Canada (formerly National Library of Canada) through a non-exclusive, world-wide license to reproduce, loan, distribute, or sell theses. I am also seeking permission for the material described above to be reproduced and distributed by the LAC (NLC). Further details about the LAC (NLC) thesis program are available of the LAC (NLC) website (www.nlc-bnc.ca).

Full publication details and a copy of this permission letter will be included in the thesis.

Yours sincerely,

Benjamin Sponagle

Permission is granted for:

a) the inclusion of the material described above in your thesis

b) for the material described above to be included in the copy of your thesis that is sent to the library and Archives of Canada (formerly National Library of Canada) for reproduction and distribution.

Name: _____ Title: _____

Signature: ███████████ Date: 13th Feb, 2018

American Society of Mechanical Engineers ASME LICENSE
TERMS AND CONDITIONS

Mar 07, 2018

This is a License Agreement between Benjamin N Sponagle ("You") and American Society of Mechanical Engineers ASME ("American Society of Mechanical Engineers ASME") provided by Copyright Clearance Center ("CCC"). The license consists of your order details, the terms and conditions provided by American Society of Mechanical Engineers ASME, and the payment terms and conditions.

All payments must be made in full to CCC. For payment instructions, please see information listed at the bottom of this form.

License Number	4303711082405
License date	Feb 24, 2018
Licensed content publisher	American Society of Mechanical Engineers ASME
Licensed content title	Journal of electronic packaging
Licensed content date	Jan 1, 1989
Type of Use	Thesis/Dissertation
Requestor type	Academic institution
Format	Electronic
Portion	chart/graph/table/figure
Number of charts/graphs/tables/figures	1
The requesting person/organization is:	Benjamin Sponagle
Title or numeric reference of the portion(s)	Fig. 9
Title of the article or chapter the portion is from	A Hybrid Thermal Energy Storage Device, Part 1: Design Methodology
Editor of portion(s)	N/A
Author of portion(s)	Zheng, N., & Wirtz, R. A.
Volume of serial or monograph.	126
Issue, if republishing an article from a serial	1
Page range of the portion	5
Publication date of portion	2004
Rights for	Main product
Duration of use	Current edition and up to 5 years
Creation of copies for the disabled	no
With minor editing privileges	no
For distribution to	Canada
In the following language(s)	Original language of publication

183

ELSEVIER LICENSE
TERMS AND CONDITIONS

Feb 06, 2018

This Agreement between Benjamin N Sponagle ("You") and Elsevier ("Elsevier") consists of your license details and the terms and conditions provided by Elsevier and Copyright Clearance Center.

License Number	4283120058507
License date	Feb 06, 2018
Licensed Content Publisher	Elsevier
Licensed Content Publication	Applied Thermal Engineering
Licensed Content Title	Transient cooling of electronics using phase change material (PCM)-based heat sinks
Licensed Content Author	Ravi Kandasamy,Xiang-Qi Wang,Arun S. Mujumdar
Licensed Content Date	Jun 1, 2008
Licensed Content Volume	28
Licensed Content Issue	8-9
Licensed Content Pages	11
Start Page	1047
End Page	1057
Type of Use	reuse in a thesis/dissertation
Portion	figures/tables/illustrations
Number of figures/tables/illustrations	1
Format	both print and electronic
Are you the author of this Elsevier article?	No
Will you be translating?	No
Original figure numbers	Fig. 2
Title of your thesis/dissertation	Temperature Control of Handheld Electronic Devices using Latent Heat Energy Storage
Expected completion date	Feb 2018
Estimated size (number of pages)	180
Requestor Location	Benjamin N Sponagle 318-20 Charlotte Lane
	Halifax, NS b3m 4m1 Canada Attn: Benjamin N Sponagle
Publisher Tax ID	GB 494 6272 12
Total	0.00 CAD
Terms and Conditions	

184